



Investigation of Colour Constancy Using Blind Signal Separation and Physics-based Image Modelling

Waleed Kamal Mohammed Badawi

A thesis submitted in partial fulfilment of the requirements of
Staffordshire University for the degree of Doctor of Philosophy

Staffordshire University,
Faculty of Computing, Engineering, and Technology,
Stafford
United Kingdom

August 2011

To My Family ...

Acknowledgement

Firstly, I would like to thank Almighty Allah for granting me the health, patience, intelligence and support to undertake this programme.

Secondly, I would like to express my sincere thanks and gratitude to my principal supervisor Dr. Claude Chibelushi for his friendship, patient guidance, useful discussion and scientific support throughout my entire research period. I am really proud and glad that I have been fortunate to conduct my research under his exceptional supervision.

I would like to thank my second supervisor Dr. Mohamed Patwary for his valuable inputs, helpful advice and wonderful friendship. Also I would like to thank my third supervisor Prof. Mansour Moniri for his support, kind encouragements and his expert guidance on how to manage my research.

I cannot thank all of them enough for the help, encouragement and the emotional support they have consistently provided me with, during the course of this challenging research period.

I would like to thank Staffordshire University for providing me with the opportunity and all the required resources for my research and special thanks to all my researcher colleagues for giving me support, inspiration and encouragement.

I would like to thank my father in law and my uncle for their support. I cannot mention in words my gratefulness to my parents, my brothers and sisters. And finally, my deepest gratitude goes to my wife 'Marwa' and my children 'Youssef' and 'Malak' for their unconditional love, patience and endless support which have enabled me to undertake and complete the PhD studies.

Waleed K. Badawi

Abstract

Colour is an important property in image and video processing; it is used for the segmentation, classification, and recognition of objects. The observed colour of a surface, as captured by an imaging sensor, can be affected by factors such as specular reflection, illumination variation and shadows which can lead to erroneous colour identification. This creates a need for techniques that are able to extract an illumination invariant descriptor of the surface reflectance of an object, such techniques would enable the development of image and video processing systems which are able to identify the actual colour of an object, independent of illumination variations. Thus achieving what is referred to as colour constancy.

This research aims to investigate the effectiveness of applying blind signal separation integrated with a physical model of image formation into a framework for achieving colour constancy. The particular model considered in this study is the dichromatic reflection model. This model has been used in approaches to colour constancy developed by other researchers. However, most of these approaches use mixed image components (i.e. composed of specular and diffuse components) in order to estimate illumination and consequently achieve colour constancy. In addition, most of these approaches require the segmentation of the image into regions which correspond to different colours on the multi-coloured surfaces, in high specular reflection (highlight) areas of the image. Correct segmentation of multi-coloured surfaces is difficult to achieve. This thesis proposes an alternative approach embodied in a framework which integrates blind signal separation and dichromatic model of image formation. Unlike the conventional approaches, by using blind signal separation, the illumination can be estimated more accurately using the explicitly separated specular image component and colour constancy is achieved by utilising the explicitly separated diffuse image component only. In addition, by using the blind signal separation the multi-coloured surfaces segmentation problem can be avoided. The research questions addressed by this research are “how should blind signal separation be integrated with the dichromatic model?” and “how does the proposed framework perform in the context of achieving colour constancy?”

A novel colour constancy framework is developed in this thesis, and experimental findings about the performance of the framework are reported. Unlike the existing work, the proposed framework includes a new method to estimate the illumination spectral power distribution (ISPD) by using an explicitly extracted specular component of images. Furthermore, the proposed framework includes a new method for estimating the surface spectral reflectance using an explicitly extracted diffuse component, instead of mixed image components which are used by other researchers. The framework consists of three stages which are: the separation of image components, the ISPD estimation and the estimation of surface spectral reflectance.

The methodology exploited to evaluate the performance of the framework involves the development of algorithms, their implementation in software, and their assessment using well-designed experiments anchored on quantitative performance measurement methods. The goodness-of-fit coefficient (GFC) is used to evaluate the performance of the framework, by measuring the degree of similarity between the estimated spectral distribution and a known reference. Values of GFC range between 0 and 1; a higher value representing a higher degree of similarity.

Using an image data set generated by the author, compared to the manufacturer's specifications, the estimated ISPD has an average GFC value equal to 0.9830 and 0.9215 for two light sources with colour temperature of 5500 K and 2900 K, respectively. The average GFC of the estimated ISPD improves significantly by 2.9% when the explicit specular image component is used instead of mixed image components. Furthermore, using Foster et al's image data set (a set of hyperspectral images of natural scenes which was collected by Foster, Nascimento, and Amano), the ISPD is estimated using the mixed image components for other light sources with different colour temperatures. The results show that the estimated ISPD has an average value of the GFC equal to 0.9986 compared to the measured illumination.

Using the data set collected by the author of this thesis, the surface spectral reflectance is estimated at individual pixels of an object illuminated by two alternative light sources with colour temperatures of 5500 K and 2900 K. A comparative assessment shows that the spectral reflectance, estimated for each given surface, has almost the same spectral signature for the two light sources. The comparison between the surface spectral reflectance estimates corresponding to the two light sources gives an average GFC value which ranges from 0.9611 to 0.9887, depending on the type of the blind separation technique that is used (i.e. the spatially constrained FastICA technique and the technique developed by Umeyama and Godin). Given that the surface spectral reflectance is the output of the last stage of the framework, which depends on the output of the previous two stages, therefore the GFC measured for surface spectral reflectance reflects the performance of the whole framework. The high GFC values mean that the estimates of surface reflectance under the two light sources are very similar, despite the differences between the two illuminants. This similarity implies that the extracted surface reflectance is significantly independent of illumination characteristics, hence showing that the proposed framework achieved a significant degree of colour constancy. Moreover, the observed results show a statistically significant improvement in the accuracy of the estimated surface spectral reflectance by 2.6% in terms of average GFC value when the explicitly extracted diffuse image component is used instead of the mixed image components. Compared to the surface spectral reflectance measurements included in Foster et al's image data set, the surface spectral reflectance estimated using the mixed image components has an average GFC value equal to 0.9608.

Table of Contents

Acknowledgement.....	i
Abstract	ii
Table of Contents.....	iv
List of Figures	vii
List of Tables.....	x
1 Introduction.....	1
1.1 Background Concepts	1
1.2 Research Problem and Motivations	2
1.3 Aim and Objectives.....	4
1.4 Methodology	5
1.5 Contribution to Knowledge.....	6
1.6 Thesis Outline	7
2 Survey of Colour Constancy Approaches.....	9
2.1 Introduction.....	9
2.2 Physical Image Formation Model	9
2.2.1 Light Spectral Power Distribution.....	10
2.2.2 Surface Spectral Reflectance.....	11
2.2.3 Specular Reflection	13
2.2.4 Diffuse Reflection	13
2.2.5 Image Formation for the Dichromatic Reflection Model.....	14
2.3 Methods for Separating Light Reflection Components.....	16
2.4 Classification of Illumination Estimation Methods	17
2.4.1 Methods Based on Diffuse Reflection.....	19
2.4.1.1 Gray-World Methods	19
2.4.1.2 Gamut Mapping Methods	20
2.4.1.3 Bayesian Methods	21
2.4.1.4 Colour by Correlation Methods	21
2.4.1.5 Neural Networks Methods	22
2.4.1.6 Retinex Methods	22
2.4.1.7 Combined Methods.....	23
2.4.2 Methods Based on Dichromatic Reflection.....	24
2.4.3 Hybrid Methods.....	27
2.4.4 Related Work on Illumination Estimation for Computer Graphics.....	28
2.5 Illumination-Invariant Colour Descriptor Methods	29
2.5.1 Diagonal Transformation Method	29
2.5.2 Linear Transformation Method	30
2.6 Review of Colour Constancy Frameworks	31
2.7 Summary	32
3 Survey of Blind Signal Separation Techniques.....	34
3.1 Introduction.....	34
3.2 Blind Signal Separation	34
3.2.1 Techniques for Additive Mixed Signals.....	35
3.2.1.1 Techniques Based on Spatial Independence of Sources	35
3.2.1.2 Techniques Based on Temporal Correlation of Sources.....	39
3.2.2 Techniques for Convolutional Mixed Signal.....	40
3.3 Independent Component Analysis (ICA).....	42

3.3.1	Estimation Principle of the ICA model	44
3.3.2	FastICA Technique.....	45
3.3.3	Spatial Constraints on the Mixing Matrix	46
3.3.4	The Spatially Constrained FastICA.....	47
3.4	Summary	48
4	Proposed Colour Constancy Framework	49
4.1	Introduction.....	49
4.2	Description of the Framework	49
4.3	Embodiment of the Framework Evaluated in the Thesis	51
4.3.1	The Image Capture Setting.....	51
4.3.2	Separation of Image Components	52
4.3.3	Estimation of ISPD.....	56
4.3.4	Estimation of Surface Spectral Reflectance	59
4.4	Summary	61
5	Experimental Investigation of the Estimation of the Illumination Spectral Power Distribution	62
5.1	Introduction.....	62
5.2	Creation of the Data set.....	62
5.3	Performance Evaluation of the ISPD Estimation.....	64
5.3.1	The Experimental Setting.....	64
5.3.2	Experimental Procedure, Results, and Discussion	67
5.3.2.1	Experiment 1: Estimation of ISPD from the specular component of images captured under an artificial day light source with colour temperature of 5500 K.....	67
5.3.2.2	Experiment 2: Estimation of ISPD from the specular component of images captured under an artificial light source with colour temperature of 2900 K.....	71
5.3.2.3	Experiment 3: A comparison between the illumination estimation accuracy achieved by using the specular image component and the mixed image components.	74
5.3.2.4	Experiment 4: Estimation of ISPD from mixed image components (i.e highlight area) captured under natural day light sources with different colour temperatures.....	77
5.4	General Discussion	81
5.5	Summary	82
6	Experimental Investigation of the Estimation of the Surface Spectral Reflectance	84
6.1	Introduction.....	84
6.2	Performance Evaluation of the Estimation of Surface Spectral Reflectance	85
6.2.1	The Experimental Setting.....	85
6.2.2	Experimental Procedure, Results and Discussion	87
6.2.2.1	Experiment 1: Comparison between surface spectral reflectance estimated from the diffuse component of images using the estimated illumination and the illumination specifications provided by manufacturer.	87
6.2.2.2	Experiment 2: Comparison between the surface reflectance estimated from the diffuse image component for the same object illuminated by two artificial light sources with different colour temperatures.	93
6.2.2.3	Experiment 3: A comparison between the surface spectral reflectance estimated using the diffuse image component and mixed image components.	96

6.2.2.4	Experiment 4: Estimation of the surface spectral reflectance from mixed image components captured under natural day light sources with different colour temperatures.....	102
6.3	General Discussion	105
6.4	Summary	107
7	Conclusions and Future Work.....	109
7.1	Conclusions.....	109
7.2	Future Work	112
	References	114
Appendix A	Experiment Map	126
Appendix B	Data Set and Illustrative Results on the Separation of Image Components.....	129
Appendix C	Estimates of the Illumination Spectral Power Distribution	139
Appendix D	Estimates of Surface Spectral Reflectance.....	163
Appendix E	Statistical Significance Tests	181
Appendix F	Evaluation Formulas.....	187
Appendix G	List of Publications.....	189

List of Figures

Figure 1.1	General physical image formation model for an inhomogeneous opaque surface of dielectric material [1].	2
Figure 1.2	The image on the left was taken under tungsten illumination. The image on the right is the same scene taken with artificial deep blue sky illumination [4].	3
Figure 2.1	The mean and the first two basis functions of daylight illuminants estimated by Judd [31].	11
Figure 2.2	The first three reflectance basis functions estimated by Parkkinen [33].	12
Figure 2.3	Sensor response of camera DFK 21F04 [40].	16
Figure 2.4	Classification of Illumination Estimation Methods.	18
Figure 3.1	Classification of blind signal separation techniques [111], [112].	36
Figure 4.1	The proposed colour constancy framework	50
Figure 4.2	Separation of the specular and diffuse components for RGB images, using the spatially constrained FastICA algorithm.	55
Figure 4.3	Flowchart of the illumination estimation method.	59
Figure 4.4	Flowchart of the surface reflectance estimation method.	61
Figure 5.1	The four possible illumination estimations using significantly specular pixels selected from the two sets of the specular components (i.e. extracted using the SCFICA and UGICA techniques) using the two corresponding masks (mask-SCFICA and mask-UGICA) interchangeable with each of the two sets, after automatic thresholding for a plastic blue ring illuminated with a light source of colour temperature of 5500 K.	69
Figure 5.2	The four possible illumination estimations using significantly specular pixels selected from the two sets of the specular components (i.e. extracted using SCFICA and UGICA techniques) using the two corresponding masks (mask-SCFICA and mask-UGICA) interchangeable with each of the two sets, after empirical thresholding for a plastic blue ring illuminated with a light source of colour temperature of 5500 K.	69
Figure 5.3	The four possible illumination estimations using significant specular pixels selected from the two sets of the specular components (i.e. extracted using SCFICA and UGICA techniques) using the two corresponding masks (mask-SCFICA and mask-UGICA) interchangeable with each of the two sets, after automatic thresholding for a plastic blue ring illuminated with light source of colour temperature of 2900 K.	73
Figure 5.4	The four possible illumination estimations using significant specular pixels selected from the two sets of the specular components (i.e. extracted using SCFICA and UGICA techniques) using the two corresponding masks (mask-SCFICA and mask-UGICA) interchangeable with each of the two sets, after empirical thresholding for a plastic blue ring illuminated with a light source of colour temperature of 2900 K.	73
Figure 5.5	The illumination estimations from the specular component and mixed image components for a plastic blue ring illuminated with a light source of colour temperature of 5500 K, using empirical thresholding to select the significantly specular pixels.	76

Figure 5.6	The illumination estimations from the specular component and mixed image components for a ceramic violet cup illuminated with a light source of colour temperature of 5500 K, using empirical thresholding to select the significantly specular pixels.....	76
Figure 5.7	The illumination estimation from the first image of Foster et al’s data set [181]. ...	79
Figure 5.8	The illumination estimation from the third image of Foster et al’s data set [181]....	79
Figure 5.9	The illumination estimation from the fourth image of Foster et al’s data set [181]......	80
Figure 5.10	The illumination estimation from the seventh image of Foster et al’s data set [181]......	80
Figure 6.1	Illustrative examples of polarised images, two RGB diffuse image components (i.e extracted using two separation techniques), and surface reflectance estimates. These estimates are obtained from RGB diffuse image components for a pixel located at image position (185, 250) for the plastic blue ring illuminated by a light source which has a colour temperature of 5500 K, using the four possible illumination estimates and light source specifications provided by the manufacturer.	90
Figure 6.2	Illustrative examples of polarised images, two RGB diffuse image components (i.e extracted using two separation techniques), and surface reflectance estimates. These estimates are obtained from RGB diffuse image components for a pixel located at image position (185, 250) for the plastic blue ring illuminated by a light source which has a colour temperature of 2900 K, using the four possible illumination estimates and light source specifications provided by the manufacturer.	91
Figure 6.3	The surface reflectance, for a pixel located at image coordinates (185, 250), estimated from the ‘Diffuse-SCFICA’ image component for a plastic blue ring illuminated by two artificial light sources with colour temperatures of 2900 and 5500 K.....	95
Figure 6.4	The surface reflectance for a pixel located at image coordinates (185, 250), estimated from the ‘Diffuse-UGICA’ image component for a plastic blue ring, and illuminated by two artificial light sources with colour temperatures of 2900 and 5500 K.....	95
Figure 6.5	The surface reflectance (Highlight-Reflectance-1, Highlight-Reflectance-2, Highlight-Reflectance-3) estimated from pixels in image regions which have a strong specular component, shown in comparison to the surface reflectance (reflectance reference-1) estimated from pixels in image regions which have a weak specular component. The test and reference pixels are from images of the plastic blue ring illuminated by a light source with a colour temperature of 5500 K. The reference pixels are from the polarised image, without extracting the diffuse image component.....	99
Figure 6.6	The surface reflectance (Highlight-Reflectance-1, Highlight-Reflectance-2, Highlight-Reflectance-3) estimated from pixels in image regions which have a strong specular component, shown in comparison to the surface reflectance (reflectance reference-2) estimated from pixels in image regions which have a weak specular component. The test and reference pixels are from images of the plastic blue ring illuminated by a light source with a colour temperature of 5500 K. The reference pixels are from the diffuse image component-SCFICA....	99

- Figure 6.7** The surface reflectance (Highlight-Reflectance-1, Highlight-Reflectance-2, Highlight-Reflectance-3) estimated from pixels in image regions which have a strong specular component, shown in comparison to the surface reflectance (reflectance reference-3) estimated from pixels in image regions which have a weak specular component. The test and reference pixels are from images of the plastic blue ring illuminated by a light source with a colour temperature of 5500 K. The reference pixels are from the diffuse image component-UGICA. ... 100
- Figure 6.8** The surface reflectance (Highlight-Reflectance-1, Highlight-Reflectance-2, Highlight-Reflectance-3) estimated from pixels in image regions which have a strong specular component, shown in comparison to the surface reflectance (reflectance reference-1) estimated from pixels in image regions which have a weak specular component. The test and reference pixels are from images of the plastic blue ring illuminated by a light source with a colour temperature of 2900 K. The reference pixels are from the polarised image, without extracting the diffuse image component.100
- Figure 6.9** The surface reflectance (Highlight-Reflectance-1, Highlight-Reflectance-2, Highlight-Reflectance-3) estimated from pixels in image regions which have a strong specular component, shown in comparison to the surface reflectance (reflectance reference-2) estimated from pixels in image regions which have a weak specular component. The test and reference pixels are from images of the plastic blue ring illuminated by a light source with a colour temperature of 2900 K. The reference pixels are from the diffuse image component-SCFICA... 101
- Figure 6.10** The surface reflectance (Highlight-Reflectance-1, Highlight-Reflectance-2, Highlight-Reflectance-3) estimated from pixels in image regions which have a strong specular component, shown in comparison to the surface reflectance (reflectance reference-3) estimated from pixels in image regions which have a weak specular component. The test and reference pixels are from images of the plastic blue ring illuminated by a light source with a colour temperature of 2900 K. The reference pixels are from the diffuse image component-UGICA. ... 101
- Figure 6.11** Illustrative examples for some images of the Foster et al's data set [181], with a white square marker to display the pixel position at which surface reflectance was estimated. The estimated surface reflectance of that pixel is shown in comparison with the measured surface reflectance.104

List of Tables

Table 5.1	Results of the experimental assessment of the effect of: the extraction of the specular image component, and the material of the reflecting object. The table entries represent the similarity between the illumination spectral power distribution estimated in the experiment and the distribution provided by the manufacturer of the light source with colour temperature of 5500 K. The similarity has been calculated using GFC.....	70
Table 5.2	The average and the standard deviation of GFC and error measurements using automatic and empirical thresholds for artificial day light source with colour temperature of 5500 K.....	70
Table 5.3	Results of the experimental assessment of the effect of: the extraction of the specular image component, and the material of the reflecting object. The table entries represent the similarity between the illumination spectral power distribution estimated in the experiment and the distribution provided by the manufacturer of the light source with colour temperature of 2900 K. The similarity has been calculated using GFC.....	74
Table 5.4	The average and standard deviation of the GFC and error measurements using automatic and empirical thresholds for an artificial light source with colour temperature of 2900 K.....	74
Table 5.5	Results of the experimental assessment of the effect of: the extraction of the specular image component, and the material of the reflecting object. The table entries represent the similarity between the illumination spectral power distribution estimated in the experiment and the distribution provided by the manufacturer of the light source with colour temperature of 5500 K. The similarity has been calculated using GFC.	77
Table 5.6	The average and the standard deviation of GFC and error measurements for illumination estimation using specular component and Image 2 (mixed image component).	77
Table 5.7	The GFC measurement, the error measurements, and the threshold value with the corresponding number of pixels for illumination estimation of Foster et al's data set [181].	81
Table 5.8	The average of GFC and error measurements for different day light sources with different colour temperatures.....	81
Table 6.1	The combinations used for estimating the four possible illuminations.	88
Table 6.2	Results of the experimental assessment of the effect of: the extraction of the diffuse image component, the four possible illumination estimates, and the material of the reflecting object. The table entries represent the similarity between the surface reflectance estimates obtained using the four possible illumination estimates and surface reflectance estimate obtained using the illumination specification provided by the manufacturer of the light source with a colour temperature of 5500 K. The spectral similarity has been calculated using the goodness-of-fit coefficient (GFC).....	92
Table 6.3	The average of GFC and other error measurements for the estimated surface reflectance for objects illuminated by artificial day light source with a colour temperature of 5500 K.....	92

Table 6.4	Results of the experimental assessment of the effect of: the extraction of the diffuse image component, the four possible illumination estimates, and the material of the reflecting object. The table entries represent the similarity between the surface reflectance estimates obtained using the four possible illumination estimates and surface reflectance estimate obtained using the illumination specification provided by the manufacturer of the light source with a colour temperature of 2900 K. The spectral similarity has been calculated using the goodness-of-fit coefficient (GFC).....	92
Table 6.5	The average of GFC and other error measurements for the estimated surface reflectance for objects illuminated by artificial day light source with a colour temperature of 2900 K.....	92
Table 6.6	The GFC and error measurements between surface reflectance estimates from pixels of 'Diffuse-SCFICA', at the same pixel coordinate for the same object illuminated by two artificial light sources with colour temperatures of 2900 and 5500 K.....	96
Table 6.7	The GFC and error measurement between surface reflectance estimates for pixels of 'Diffuse-UGICA', at the same pixel coordinate for the same object illuminated by two artificial light sources with colour temperatures of 2900 and 5500 K.....	96
Table 6.8	The three extracted reflectance references and their corresponding images.....	97
Table 6.9	The three extracted highlight-reflectances and their corresponding images.....	97
Table 6.10	The GFC comparison between the surface reflectance (Highlight-Reflectance-1, Highlight-Reflectance-2, and Highlight-Reflectance-3) estimated from pixels in image regions which have a strong specular component, and the surface reflectance (reflectance reference-1, reflectance reference-2, reflectance reference-3) estimated from pixels in image regions which have a weak specular component. The test and reference pixels are from images of different objects illuminated by light sources with colour temperature of 5500 K and 2900 K. The reference pixels are respectively from the polarised image (without extracting the diffuse image component), the 'diffuse image component-SCFICA', and 'diffuse image component-UGICA'	102
Table 6.11	The averaged GFC measurement and other error measurements for surface reflectance estimated on the Foster et al's data set [181].	105

1

Introduction

This chapter aims to present the context of the research, and highlight the research problem, and the contribution to knowledge of the conducted research. The chapter starts with explaining briefly the concepts of blind signal separation and physical model of image formation. The research problem and motivations of this work are then clarified followed by the objectives and methodology of the research. Finally, the contributions of the research are given, followed by a thesis outline.

1.1 Background Concepts

Blind signal separation, which was originally used in the communication area and then was extended to be used in image processing, seeks to separate sources from mixed signals with no knowledge about the mixing and the mixed sources. In the image processing area, blind signal separation has been used to extract watermarks or to separate reflections from the image seen through glass, for example. The process of blind signal separation depends on estimating the mixing matrix that is used to mix the sources. The estimation of the mixing matrix is achieved using a number of observed or mixed signals that are captured by sensors in order to separate the sources. Blind signal separation can be applied for various types of mixtures which have different ways for mixing the sources.

The physical model of image formation explains the relation between an imaging sensor (typically a camera), the light source, and the surface of an object. The image of an object is formed due to the reflection of light from the surface of the object, which is captured by the camera. The light reflected off an object can be described as an interaction of the spectral power distribution of the incident light and the surface

spectral reflectance of an object. According to the dichromatic reflection model [1], the image of an object made of a dielectric material is formed due to two types of reflections which are: specular and diffuse reflection as seen in Figure 1-1. The image produced by the camera is considered to be an additive mixture of two components which are the diffuse and specular components.

Considering the image as a mixture of two components, blind signal separation can be used to separate these components, which are embedded in an image captured by a camera. Each of these components has different spectral characteristics which can be utilised to get information about the characteristics of the spectral power distribution of the light source and the surface spectral reflectance, in order to achieve colour constancy.

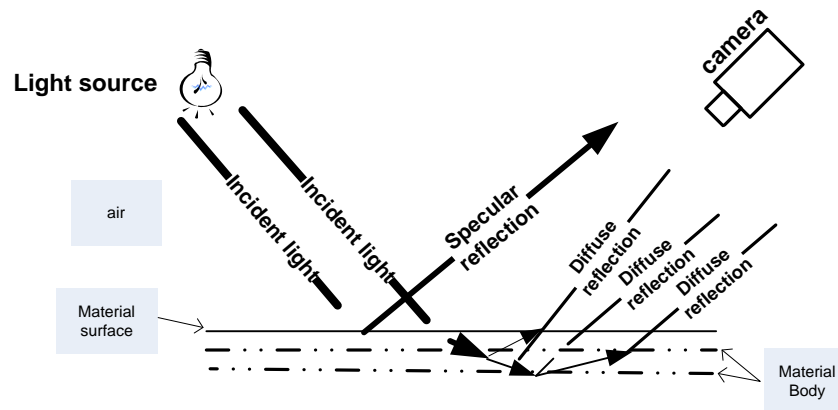


Figure 1-1 General physical image formation model for an inhomogeneous opaque surface of dielectric material [1].

1.2 Research Problem and Motivations

The colour appearance of an object is often not the actual colour of the object. Several factors play significant roles in forming the appearance of the colour of an object, mainly illumination and intrinsic properties or reflectance of an object surface. The effect of illumination can easily be observed in many occasions in daily life, for example, during the evening an outdoor scene may look redder than at midday because of changes to the colour of the illumination emanating from the sun. That is also true for artificial light sources. For example, Figure 1-2 shows how the same ball in front of the green background appears different under two types of illumination. Although the change of illumination can modify the colour appearance of an object or a scene, human beings still have the ability to identify the actual colour of an object or

scene at a certain level of accuracy, whereas a machine or visual system cannot match this ability as yet. This capability, which is known as colour constancy or illumination invariant colour description, is innate in human perception and one of the important aspects of the object recognition processes [2]. The terms ‘colour constancy’ or ‘illumination invariant colour description’ are used interchangeably throughout the thesis to refer to the same meaning. There are two ways reported in the literature [3] by which the visual system can achieve colour constancy. These ways are colour invariant and illumination estimation procedures [3]. In the colour invariant procedures, which is so called by Steven D. Hordley in [3], colour constancy is achieved without explicit estimation of illumination. This is done by generating quantities that are invariant to the scene illumination colour. These quantities are produced by algebraic manipulation of the image data. In some cases this manipulation modifies the spatial structure of the image and the image is represented by few invariant quantities.

On the other hand, in illumination estimation procedures, colour constancy is achieved through two stages. First the scene illumination is estimated using the recorded image data of that scene. Then the estimated illumination is used to correct the recorded image data by discounting the illumination colour of the scene and thus achieve image colour constancy or illumination invariant colour description. The illumination estimation procedures are preferred by many researchers because there is no need for algebraic manipulation which may change the image spatial structure [3]. The work presented in this thesis adopts illumination estimation procedures in order to achieve colour constancy.

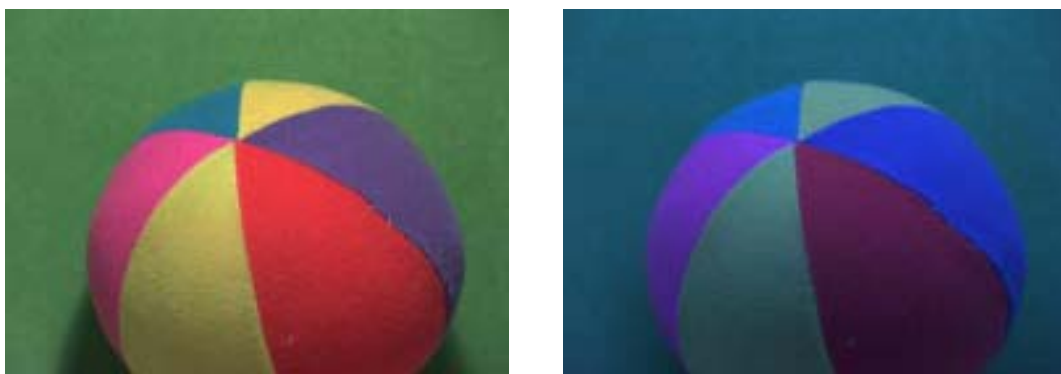


Figure 1-2 The image on the left was taken under tungsten illumination. The image on the right is the same scene taken with artificial deep blue sky illumination [4].

In machine vision, colour constancy is considered as a crucial prerequisite for various applications, which mainly depend on colour, such as colour-based object recognition, colour based-image retrieval [3], colour reproduction [5] and so on. Unfortunately, how humans achieve colour constancy is not yet fully understood. This means that it is not yet possible to replicate human perception of colour constancy in machine vision. This challenge has led to the development of several algorithmic approaches to achieve colour constancy using illumination estimation procedures [6-27]. Although there are many approaches which have been developed to address the problem of obtaining colour constancy, the solution to this problem has still not been fully answered. Some of these approaches are based on the dichromatic reflection model. However, these approaches use mixed image components (i.e. composed of specular and diffuse components) in order to estimate illumination and consequently achieve colour constancy. In addition most of these approaches require segmentation of image regions which correspond to multi-coloured surfaces in high specular reflection (highlight) areas of the image; correct segmentation of multi-coloured surfaces is difficult to achieve.

This thesis proposes an alternative approach embodied in a framework which integrates blind signal separation and the dichromatic model of image formation. By using blind signal separation, the estimation of illumination can be achieved more accurately from the explicitly separated specular component unlike the conventional approaches that use mixed image components. Moreover, the explicitly separated diffuse image can be used to achieve colour constancy instead of mixed image components that is used by conventional approaches. In addition, by using blind signal separation the challenge of segmenting multi-coloured surfaces in images can be avoided. The research questions addressed by this research are “how should blind signal separation be integrated with the dichromatic model?” and “how does the proposed framework perform in the context of achieving colour constancy?”

1.3 Aim and Objectives

The aim of this research is to investigate the effectiveness of applying blind signal separation, integrated with a physical model of image formation into a framework for achieving colour constancy. The particular model considered in this study is the dichromatic reflection model.

The objectives of this research project can be summarised as follows:

- Gain a solid understanding of the dichromatic model of image formation, of illumination estimation methods, of colour constancy frameworks and of illumination invariant colour descriptor methods.
- Review the literature on blind signal separation techniques, and on image component separation methods.
- Devise a blind signal separation technique, coupled to the dichromatic model of image formation, to separate the diffuse and specular components of an image.
- Use the separated specular component of an image to estimate the illumination spectral power distribution.
- Estimate the surface spectral reflectance using the estimated ISPD and the separated diffuse component of an image.
- Evaluate the proposed framework stages and hence evaluate the whole framework.

1.4 Methodology

The investigation presented in this thesis is based on the combination of blind signal separation with the dichromatic model of image formation. The investigation involves the development of algorithms, their implementation in software (using MATLAB and its relevant Toolboxes), and their assessment using well-designed experiments anchored on quantitative performance measurement methods. Methodological details about the experiments are given in the relevant thesis chapters (experiment map is presented in Appendix A). The research phases are as follows:

- The first phase includes gaining a solid understanding of the dichromatic model of image formation, and of the characteristics of the diffuse and specular image components.
- The second phase is a systematic and comprehensive study, based on a literature review, of illumination estimation methods, colour constancy

frameworks, illumination invariant colour descriptors and blind signal separation techniques.

- In the third phase, two blind signal separation techniques are used (one suggested by the author and the other developed by Umeyama and Godin in [28]) to separate the specular and diffuse components.
- In the fourth phase, an appropriate method is implemented to estimate the ISPD using the extracted specular component. Subsequently, the performance of the illumination estimation is evaluated using a suitable error measure.
- In the fifth phase, a technique is developed to estimate the surface reflectance using the previously estimated illumination and the diffuse component extracted from the original image. Then, the performance of the estimation of surface reflectance, for achieving colour constancy, is assessed quantitatively.

The evaluation of the framework is done by evaluating Stage 2 and 3, of the framework, individually. The effect of Stage 1 on Stage 2 and 3 is also considered. The reason for evaluating different stages of the framework independently is to investigate how each stage ultimately affects the overall performance of the framework. The performance of the whole framework can be deduced from integrating the performance evaluation of the framework stages.

1.5 Contribution to Knowledge

The main contribution of this work is the development of a novel colour constancy framework, and experimental findings about the performance of the framework. The novelty of this framework is the coupling of the estimation of surface spectral reflectance to input image data explicitly separated into a specular component and a diffuse component, which are obtained using blind signal separation underpinned by the dichromatic reflection model. The specular image component is used to estimate the spectral power distribution of the illumination, and the diffuse component is used thereafter with the estimated illumination to recover the spectral reflectance of the surface. The framework consists of three stages which include supplementary

contributions to knowledge. The contributions of these stages can be summarised as follows:

- First, a new method to estimate the ISPD using the separated specular component is proposed. Unlike the state of art, this method uses an explicitly extracted specular component to estimate the ISPD while the other researchers [12], [18], [29] use mixed image components, where each pixel is a blend of specular component and diffuse component, to estimate illumination chromaticity.
- Second, the thesis proposes a new method to estimate the surface spectral reflectance from an explicitly extracted diffuse component, with aid of the estimated ISPD (i.e. achieved in first supplementary contribution). Compared to existing methods [26], this method uses an explicitly extracted diffuse component instead of mixed image components.

1.6 Thesis Outline

In this thesis, existing blind signal separation techniques and methods for illumination estimation and illumination invariant colour description are reported. Moreover, the concepts of the physical image formation model are studied. Furthermore, the combination of blind signal separation with the dichromatic model of image formation are investigated to separate the image components and consequently estimate illumination spectral power distribution and ultimately surface spectral reflectance (thereby achieving colour constancy).

The thesis is organised as follows:

Chapter 1 is an introduction to the work including, the statement of the research problem and motivations, the aim and the objectives of the research, the methodology used in the research, and the contribution to knowledge. Finally, the contents of the different chapters are presented.

In **Chapter 2**, an overview of colour constancy related topics is presented including the physical model of image formation, illumination model, and surface reflectance model. Moreover, the methods for separating light reflection components, the illumination estimation methods, the illumination invariant descriptor methods, and the colour constancy frameworks are reviewed.

Chapter 3 includes a literature review of blind signal separation techniques for different types of mixing signals. The definition and the different approaches of independent component analysis are described. Finally, the Fast Independent Component Analysis technique and its modified version are presented.

Chapter 4 starts with presenting the proposed colour constancy framework. After that, the chapter presents the embodiment of the framework which is evaluated in this thesis. The image capture setting, the techniques used for image component separation (first stage of the framework), the proposed method for the estimation of ISPD (second stage of the framework) and the proposed method for the estimation of surface spectral reflectance (third stage of the framework) are described in detail.

In **Chapter 5**, an experimental investigation is carried out, including a series of experiments to evaluate the second stage of the proposed colour constancy framework.

In **Chapter 6**, an experimental investigation is conducted; it consists of a series of experiments to assess the third stage of the developed colour constancy framework.

Finally, **Chapter 7** discusses the conclusions of the present work and offers suggestions for future work.

2

Survey of Colour Constancy Approaches

2.1 Introduction

This chapter presents an overview of colour constancy related topics. In this chapter the physical model of image formation is reviewed, including the illumination model, the surface reflectance model and the dichromatic reflection model. The image component separation methods are then explored. The three categories of existing illumination estimation methods used in approaches to colour constancy are discussed. First, the methods based on diffuse reflection are explored. A comprehensive study of the methods based on dichromatic reflection is then introduced. Moreover hybrid methods are presented which are combinations of diffuse and dichromatic methods. Furthermore, related work for illumination estimation is reviewed. Methods to obtain illumination invariant descriptors of an image captured under unknown illumination are then explored. Finally the existing colour constancy frameworks are presented, and are followed by the chapter summary.

2.2 Physical Image Formation Model

The physical image formation model considers an image as being the result of the interaction between the illumination of the light source, reflectance of the surface, imaging sensor, and the medium between them. The image is formed when light coming from a light source hits a surface and is then reflected in the direction of camera. There are two types of reflected light; they are: interface reflected light (also known as specular reflection) and body reflected light (also called diffuse reflection)

[1]. These two types of reflections will be explained later in this section. Moreover due to the importance of the illumination and the surface reflectance in order to achieve colour constancy, the following subsection will include a review of the illumination model, and the surface reflectance model.

2.2.1 Light Spectral Power Distribution

Light at the atomic scale is formed from packets of energy called photons; it is divided into visible and invisible light spectral power distribution categories. The visible light wavelengths range approximately between 380 nm and 760 nm. In practice, the range used is between 400 nm and 700 nm; this is the range of wavelengths which is considered in calculations in this thesis. The colour of visible light is determined from its spectral power distribution. There are many types of light sources, and they emit dissimilar spectral power distributions [30]. The spectral power distribution of illumination can be expressed as a linear model of illumination basis functions which can be expressed by [9]:

$$E(\lambda) \approx \sum_{i=1}^{\mu} \varepsilon_i b_i(\lambda) \quad (2-1)$$

where $b_i(\lambda)$ is an illumination basis function; λ is wavelength; ε_i is a basis function coefficient; μ is the number of basis functions.

Judd et al [31] show that most of the daylight ISPD can be modelled by using only three basis functions, as seen in Figure 2-1. In [32], Slater et al. claimed that to represent different outdoor illumination spectral power distributions, using seven basis functions is more dependable than using only three basis functions. However, the three basis functions suggested in [31] can still be applied in several colour applications [30].

Alternatively, ISPD can also be modelled by using a blackbody radiator. The blackbody radiator is defined as an object that absorbs all light falling on it, and with no light reflected or transmitted. Hence, the re-radiated energy depends only on the characteristics of the radiating object and not on the incident light. Blackbody radiation can be expressed by using Planck's formula. This formula shows the relation

between the temperature, wavelength and spectral power distribution of emitted light (for a unit solid angle) as follows [17]:

$$E(\lambda) = C_1 \lambda^{-5} [\exp(C_2/\lambda T) - 1]^{-1} \quad (2-2)$$

$$C_1 = 2hc = 3.7418 \times 10^{-16} \text{ Wm}^2 \quad (2-3)$$

$$C_2 = hc/\rho = 1.4388 \times 10^{-2} \text{ mK} \quad (2-4)$$

where h is Planck's constant ($6.62606896 \times 10^{-34}$ Joules. second), c is the speed of light (3×10^8 meter/second), ρ is Boltzmann's constant ($1.3806504 \times 10^{-23}$ Joules/ Kelvin), and T is the colour temperature in Kelvin. Most light sources can be explained by using Planck's formula since they roughly follow the blackbody radiator mechanism.

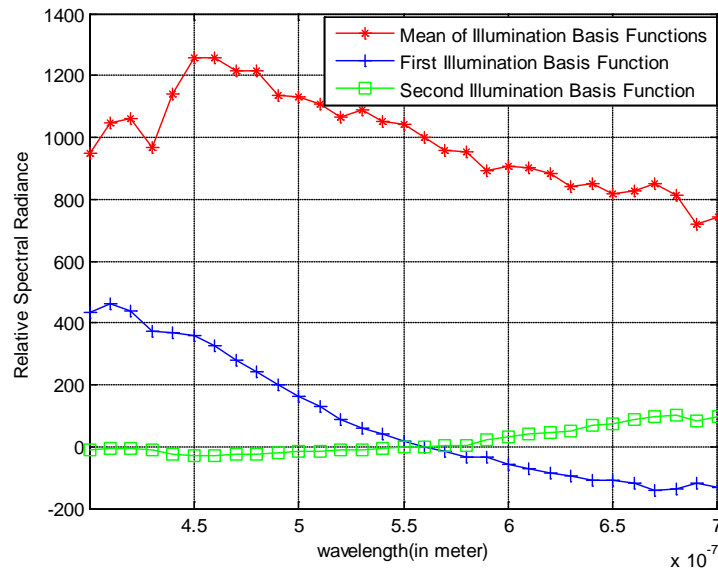


Figure 2-1 The mean and the first two basis functions of daylight illuminants estimated by Judd [31].

2.2.2 Surface Spectral Reflectance

The ability of an object to reflect various spectral distributions when several types of light are incident on its surface is called surface spectral reflectance. Moreover, it is considered as the ratio between the reflected spectral power distributions to the incident spectral power distribution. The spectral reflectance is dissimilar for different surface materials. In the case of a surface, spectral reflectance can be represented by a finite linear model of reflectance basis functions [9], [33]:

$$S(\lambda) \approx \sum_{j=1}^{\alpha} \phi_j \psi_j(\lambda) \quad (2-5)$$

where $\psi_j(\lambda)$ is a reflectance basis function; ϕ_j is a basis function coefficient; α is the number of basis functions. The derivation of the basis functions has been done by using various colours of Munsell chips [33], [34].

To the knowledge of the author, Cohen [34] is the first researcher who calculated reflectance basis from a data set containing 150 measured reflectance curves from various colours of Munsell chips. After that Maloney [33] repeated the same calculation but using a larger number of samples, which are 465 samples. Then Parkkinen et al [33] showed that the 1257 surface spectral reflectance curves in the existing database, which are measured from the Munsell colour chips, can be covered by using eight basis functions.

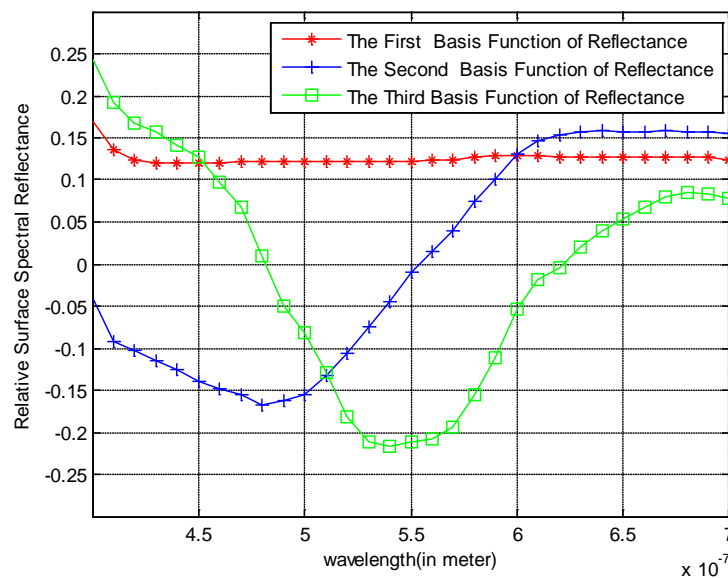


Figure 2-2 The first three reflectance basis functions estimated by Parkkinen [33].

However it is found by Parkkinen et al [33] that the average error will be negligible when only the first three basis functions are used. Compared with other researchers, Parkkinen examined a larger number of samples, with sample interval two times the interval used by others. As a result, Parkkinen's basis functions are considered to be more accurate in representing the surface spectral reflectance. The first three basis functions, which are presented by Parkkinen et al, as seen in Figure 2-2, are useful for several colour constancy applications [30].

2.2.3 Specular Reflection

Specular reflection is a process in which the incident light on a surface is reflected directly at the air-surface interface [1]. This process can be considered as perfect as mirror reflection [28]. Consequently, the characteristics of the specular reflection can be considered as the same as the incident light. The behaviour of the specular reflection can follow the reflection law which states that the angles of the incident and reflected light with respect to the surface normal are equal.

Specular reflection is characterized by a high intensity of light. Moreover it has a high degree of light polarization and it is highly view dependent. The amount of specular reflection depends mainly on the structure and type of the surface material. Optically, most of the objects can be classified in two categories which are: homogenous and non-homogenous objects. Objects which have a uniform refractive index, such as metals, glass and crystals are referred to as homogenous; otherwise they are known as inhomogeneous for example plastics, ceramics, and carpets etc. A homogeneous object (i.e. with smooth or polished surface) reflects only the specular reflection component and a inhomogeneous object reflects diffuse and specular reflection components [35]. In most of the inhomogeneous surfaces the amount of specular reflection on an average surface is small compared to the diffuse reflection. The specular reflection can be modelled by using the Torrance-Sparrow model [36], one of the most popular models of specular reflection in computer vision. This model is based on the assumption that a surface is like the integration of a distribution of randomly oriented mirror-like microfacets.

2.2.4 Diffuse Reflection

Unlike specular reflection, diffuse reflection is generated due to the interaction between the incident light and the surface of the object (inhomogeneous opaque surface with dielectric material). This interaction can occur when the incident light penetrates the surface of the object and refracts and reflects inside the object body and then it reflects back out to the air [36]. Moreover the interaction can occur due to multiple reflection of the incident light caused by surface roughness. Diffuse reflection is view independent and has negligible degree of light polarization [28]. The difference between the specular and diffuse reflections can be explicitly

explained by matte and glossy paint. Although both display a mixture of specular and diffuse reflection, matte paints have a larger amount of diffuse reflection and glossy paints have a higher proportion of specular reflection. In addition, there are various models that represent the diffuse reflection and the most commonly used is the Lambertian model which is described by Lambert's law when the angle of the incident light is not large [28].

2.2.5 Image Formation for the Dichromatic Reflection Model

The reflected light from the surface of an object with different types of material or structure can be formulated mathematically as:

$$R(\lambda) = E(\lambda)S(\lambda) \quad (2-6)$$

Where $R(\lambda)$ is the spectral power distribution of the reflected light; $E(\lambda)$ is the spectral power distribution of the incident light; $S(\lambda)$ is the surface spectral reflectance. Different types of material have different reflection mechanisms such as (specular reflection and diffuse reflection). The reflected light of an inhomogeneous opaque surface with dielectric material can be described by the dichromatic reflection model which is a linear combination of diffuse and specular reflections [1]:

$$R(\lambda, \ell) = w_d(\ell)S_d(\lambda, \ell)E(\lambda, \ell) + w_s(\ell)S_s(\lambda, \ell)E(\lambda, \ell) \quad (2-7)$$

Where $R(\lambda, \ell)$ is the reflected light from the object; ℓ is the position of a surface point; $w_d(\ell)$ is the geometric scale factor for diffuse reflection (depends on the position of light source and camera with respect to location ℓ); $w_s(\ell)$ is the geometric scale factor for specular reflection (depends on the geometric viewing at location ℓ); The value of the geometric scale factor ranges from 0 to 1 [1]; $S_d(\lambda, \ell)$ is the diffuse spectral reflectance function; $S_s(\lambda, \ell)$ is the specular spectral reflectance function; $E(\lambda, \ell)$ is the spectral power distribution of the illumination. Most reflection models assume that the specular reflection component has the same spectral composition as the incident light, whereas the diffuse reflection component has spectral composition which is different from the incident light [30], [37]. This assumption is based on the behaviour of the specular reflection process which is explained in Section 2.2.3. This assumption is known as Neutral Interface Reflection (NIR), which is achieved by setting the specular spectral reflectance function $S_s(\lambda, \ell)$ as constant scalar with respect

to wavelength, i.e. $S_s(\lambda, \ell) = S_s(\ell)$ [37]. The NIR is considered as a fundamental assumption that is used for the dichromatic model [18], [38], [29], so the model equation can be modified as:

$$R(\lambda, \ell) = w_d(\ell)S_d(\lambda, \ell)E(\lambda, \ell) + w_{sn}(\ell)E(\lambda, \ell) \quad (2-8)$$

where $w_{sn}(\ell)$ is modified specular geometrical scale factor which is equal to:

$$w_{sn}(\ell) = w_s(\ell)S_s(\ell) \quad (2-9)$$

In addition, assuming that there is only one light source and its illumination spectral power distribution $E(\lambda, \ell)$ is uniform over the object surface, therefore $E(\lambda, \ell)$ becomes independent of position (ℓ). Thus, the image formation for an inhomogeneous object captured by a camera can be formed as a linear summation of two parts. The first part is the diffuse image component denoted as

$$\mathbf{I}_{d,k}(\ell) = w_d(\ell) \sum_{\lambda=\lambda_L}^{\lambda_H} S(\lambda, \ell)E(\lambda)q_k(\lambda) \quad (2-10)$$

where $k = R, G, \text{ or } B$ is each of the three primary colours, $q_k(\lambda)$ is the imaging sensor response for each colour component, which covers part of the visible light spectrum (i.e. ranging from $\lambda_L = 400\text{nm}$ to $\lambda_H = 700\text{ nm}$), as shown in Figure 2-3, $\mathbf{I}_{d,k}$ is the diffuse component for each of the three primary colours (R, G, B). The second part is the specular image component which can be represented as follows [39]:

$$\mathbf{I}_{s,k}(\ell) = w_{sn}(\ell) \sum_{\lambda=\lambda_L}^{\lambda_H} E(\lambda)q_k(\lambda) \quad (2-11)$$

where $\mathbf{I}_{s,k}$ is the specular image component for each of the three primary colours. So the image formation for the dichromatic reflection model can be simply expressed as:

$$\mathbf{I}_k = \mathbf{I}_{d,k} + \mathbf{I}_{s,k} \quad (2-12)$$

The position of the surface point (ℓ) is removed for simplicity of notation.

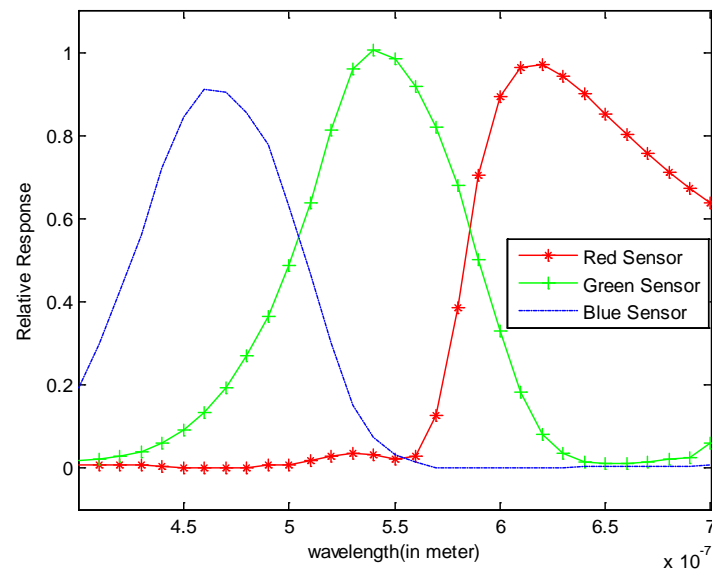


Figure 2-3 Sensor response of camera DFK 21F04 [40].

2.3 Methods for Separating Light Reflection Components

As mentioned previously in Section 2.2.3, the specular reflection is characterised by high intensity. Therefore, in the recorded image, the specular reflection can hide useful information about the object surface such as colour, roughness etc. The existence of the specular reflection in the recorded image can cause problem to machine vision algorithms such as stereo mismatch, false segmentation, and pattern recognition error. Due to these problems the separation of the specular reflection from the diffuse reflection is considered as an important issue for some machine vision algorithms.

Most of the methods used for separating specular reflection from diffuse are based on the dichromatic reflection model which was proposed by Shafer [1]. In this model, the colour of the image pixel can be described as a linear combination of specular reflection colour and the underlying diffuse reflection colour. The methods used for separating specular reflection from the diffuse reflection can be classified into three categories [41]. The first category has methods which use only a single colour image [1], [39], [41-46]. The methods in the first category are more practical compared with methods in the second and third categories, which are explained later in this section. However colour segmentation of different objects is an essential requirement for the success of methods in the first category; effective colour segmentation is a challenge.

The second category involves methods which use more than one input image generated by changing the illumination direction [47], [48] or camera viewpoint [49]. The methods in the second category are considered as less practical than the methods in the first category given that in practice multiple images captured under particular conditions are not always available [44].

The third category consists of methods that utilize a polarizer filter [50-52]. By using the polarizer, the colour segmentation problem that is found in the first category can be solved. However the use of polarizer raises another problem which is finding the minimum and maximum degree of polarization for the same scene. This may make the use of a polarizer impractical [41]. This problem can be reduced and the use of a polarizer can be made more practical if there is no specific need to identify the minimum and maximum degree of polarization for separation purposes. In other word, degrees of polarization other than minimum and maximum can be used to separate the specular and diffuse component from an image. In the following chapter a comprehensive study of other methods that are used for separating different types of signals will be explained. Moreover the following subsection will discuss different methods of illumination estimation.

2.4 Classification of Illumination Estimation Methods

Illumination estimation is considered as an important stage towards obtaining colour constancy. There are several illumination estimation methods; these are categorized by Finlayson [18] into two categories which are: statistics based methods and physics based methods.

In the statistics based method, the illumination is estimated based on statistical assumptions about the distribution of colour in the scene. Conversely, in the physics based methods, the illumination is estimated based on the physical process that provides the relation between the scene and the formed image. In other words, the methods in this category are based on the understanding of the physical process of light reflection. However, since all illumination estimation methods are founded on some kind of physical model of image formation they can be considered, to a certain extent as physics based. Moreover the physics-based method can also make use of statistical knowledge or calculation.

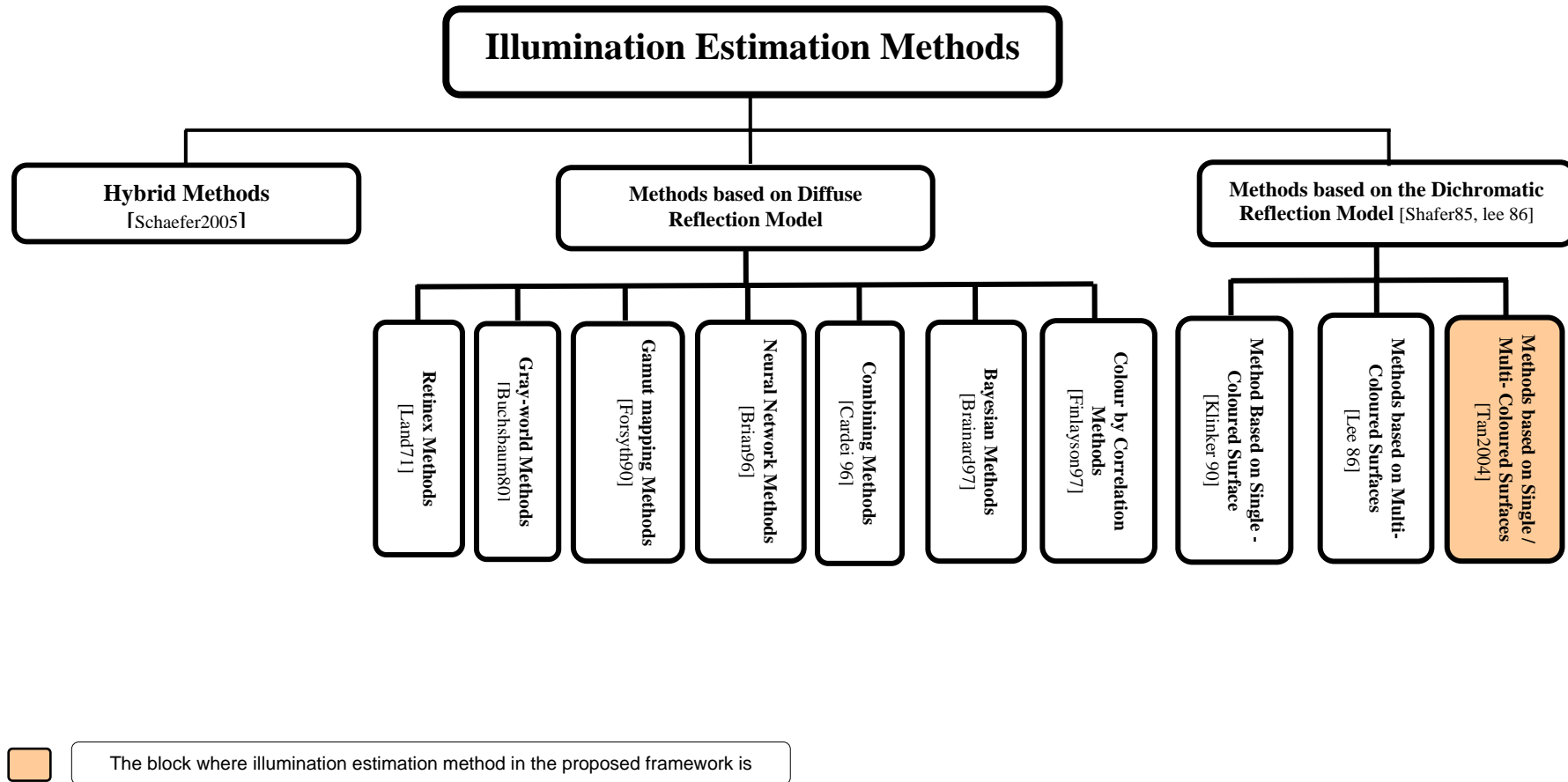


Figure 2-4 Classification of Illumination Estimation Methods

In this chapter, another classification of illumination estimation methods is presented. This classification consists of three categories, based on the reflection model considered in the illumination estimation method. These categories are (see Figure 2-4): methods based on diffuse reflection, methods based on dichromatic reflection, and hybrid methods. The methods based on the diffuse reflection model are founded on the assumption that the input image consists of diffuse reflection only. Conversely, methods based on the dichromatic reflection model are based on the assumption that the input image involves both the specular and the diffuse reflection component. The hybrid methods are a combination of methods based on diffuse and dichromatic reflections.

The research presented in this thesis uses blind signal separation combined with a dichromatic image formation model in order to estimate ISPD, and consequently achieve colour constancy. Therefore, the following sub-sections will highlight the methods based on dichromatic reflection and provide a summary of the methods that relate to the other two categories.

2.4.1 Methods Based on Diffuse Reflection

The main feature of the methods based on diffuse reflection is that they use the diffuse reflection as input for their analysis. This is based on the assumption that the image is formed primarily due to the diffuse reflection [21]. However, the existence of highlights or specularities in the input image can affect the illumination estimation accuracy of these methods. As the amount of the specularities in the input image increases, the accuracy of the estimation decreases. In the following subsections [4], [20] different methods based on the aforementioned assumption are discussed.

2.4.1.1 Gray-World Methods

The gray-world methods are considered the oldest, and simplest, methods in the area of colour constancy [23]. The idea of these methods is to compute a single statistic (mean) of the RGB image components that is used to estimate illumination (which is assumed to be uniform over the scene). This is achieved based on the assumption that the spatial average of surface reflectance in the scene is achromatic, which is referred to as gray. An achromatic surface changes the reflected light equally over the entire wavelength. As a result, the colour of the incident light is equal to the spatial average

of the reflected light [16]. Based on the gray-world assumption, different methods have been proposed by various authors in different forms.

Buchsbaum [6] was the first to make use of the gray-world assumption with low dimensional linear models which describe the lights and surface in order to estimate the ISPD [16]. In this method, the estimation of illumination is achieved using a fixed spatial average of the surface reflectance (standard) as gray colour reference.

Gershon et al [26] improved Buchsbaum's method [6] by calculating the reflectance basis functions from a real reflectance database, and using the average from a real reflectance database as the reference gray colour. Moreover, they realized that a segmentation of the image pixels into different groups corresponding to different object materials should be considered. This is because the performance of the method reduces when segmentation is inaccurate [23].

Gijsenij in [27] proposed a method based on low level image features (such as the mean value of image pixels) using image regions to avoid the effect of biased pixel values (e.g a large portion of blue sky) which may decrease the performance of illumination estimation. Most of the gray-world methods, which have been stated previously, identify the achromatic surface by averaging the surface reflectance in the scene. However there are some methods, for example max-RGB, gray-edge, higher order gray-edge [53], [54] and shade of gray [22], which use a different hypothesis to identify the achromatic surface (for more details about the different hypotheses, see [53]).

2.4.1.2 Gamut Mapping Methods

The first gamut mapping illumination estimation method was proposed by Forsyth [55] and improved by Finlayson [56]. The estimation in this method is achieved through two stages. First, the set of all possible illumination is recovered. This set corresponds to a set of mapping matrices which take the image colours (image gamut) captured under an unknown illumination to the gamut of all colours observed under a known canonic illumination (canonic colour gamut). Second, one illumination is selected as an estimate of the unknown scene.

The first form of gamut mapping, which was introduced by Forsyth [55], was implemented using the three dimensional (3-D) RGB space. Although this form of gamut mapping produced good results, it has a number of problems. For instance, it

cannot handle images containing specularities. Furthermore it is difficult to implement and it is computationally intensive [15].

Finlayson [56] improved the Forsyth method by proposing a new version working in the two dimensional (2-D) chromaticity space. The reasons for using chromaticity space are to discard the effect of specularities on the illumination estimation method and to reduce the computational complexity. However, it was found that by comparing the performance of the 3-D and 2-D methods, the 3-D method delivered a better estimate of illumination [15]. Moreover, Finlayson combined a helpful constraint related to the set of feasible illumination with the basic 2-D gamut mapping. The idea is based on the fact that some of the illumination is not found in the real world so these should be excluded when estimating illumination.

In addition, Arjanin *et al* in [57] tried to improve the performance of gamut mapping for estimating the illumination of the scene by proposing a gamut mapping method which used image derivative structures instead of pixel values.

2.4.1.3 Bayesian Methods

The Bayesian decision theory was initially used by Freeman and Brainard [14] and extended by others [58], [59] in order to solve the illumination estimation problem. The Bayesian methods are based on the assumption that prior knowledge about the probability of occurrence of particular illuminations and surfaces in reality are known. The estimation of illumination in these methods can be achieved using Maximum *a posteriori* [58], Minimum Mean-Squared-Error estimation [60], or Minimum Local Mass estimator [14].

2.4.1.4 Colour by Correlation Methods

The first version of colour by correlation methods was introduced by Finlayson [61] as an improvement for the gamut mapping method in [56]. The main idea of colour by correlation is to pre-calculate a correlation matrix that is used to estimate illumination colour of the scene. The pre-calculation of the correlation matrix is based on information that consists of the probability of occurrence of the surfaces and illuminations and how their interaction affects the occurrence probability of the observed camera responses. In [16], [56] the correlation matrix describes the relation between the suggested illuminations and the occurrence of the image chromaticity using (r-g chromaticity space). On the other hand, Barnard [62] modifies the colour by

correlation approach to work in three dimensional colour space. The argument for doing this modification is that the information about the pixel intensity is ignored in chromaticity space. Moreover the intensity of the pixel is useful even if only the illumination chromaticity is considered.

2.4.1.5 Neural Networks Methods

By using neural networks in the area of colour constancy, a good estimation of the illumination chromaticity has been obtained [63-65]. The authors in these works trained the neural network on synthetic images generated randomly from a database of illumination and reflectance. Moreover, the neural network shows good results when applied to estimate illumination of images when the origin of the images is unavailable and when it has no knowledge about the illumination [66], [67]. Furthermore, Cardei *et al* in [68] present a novel neural network method which used the image chromaticity information. This method estimates the unknown illumination of the scene by learning the relationship between image colour appearance and the scene illumination. A good performance is achieved by testing this method on real images and the error is lower than that obtained by gray-world and retinex methods. Chin *et al* [69] proposed a method to estimate the illumination of an image using a chromaticity histogram and a neural network. The neural network is trained by the back propagation method to identify the relationship between the chromaticity histogram and the coefficients of illumination basis functions. After that, the trained neural network is used to estimate the illumination spectral power distribution. However it is difficult to generalize the neural network and make it able to estimate scene illumination in previously unseen images. In addition to the neural network there are other machine learning methods that are used for illumination chromaticity estimation such as support vector regression [70], ridge regression, and kernel regression [71].

2.4.1.6 Retinex Methods

A great contribution was added to the colour constancy area when Land proposed [72], [73] the retinex or lightness method to estimate the illumination colour. The retinex method is based on the assumption that small spatial variations in pixels values on an object surface are caused only by changes in illumination, while large changes are related to surfaces changes [23]. The aim of retinex is to calculate the

lightness of a surface by applying a logarithmic-differentiation operation for pixel values. The calculation of lightness eliminates the effect of the illumination colour on the object surface and consequently the colour of the surface is extracted. The retinex work of Land is developed and extended by Land and others [8], [74-76]. All the published versions of the retinex method share the same basic principle which is lightness computation, but they are different in computation methods of the lightness [74], [77]. The Max-rgb or white patch is the most famous version of these methods; this is due to its simplicity in implementation.

2.4.1.7 Combined Methods

In the combined methods, researchers try to combine different methods based on diffuse reflection or these methods with other theories in order to improve the illumination estimation accuracy.

Cardei [66] presents the committee method which combines different methods based on diffuse reflection. The goal of this combination is to achieve more accurate estimates of illumination chromaticity than any of the methods taken individually. The test for the committee of gray-world, retinex (white patch), and neural network is done; the committee gives better results than any of these methods provides separately.

In [24], Finlayson et al proposed a method that combines the chromagenic approach with the conventional gamut mapping method. In this method, a chromagenic colour filter is used to capture two images for the same scene with and without a filter. This method exploits the relation between unfiltered and filtered image as additional information for gamut mapping to estimate the illumination. This means that the filtered and unfiltered RGBs change with and depend strongly on illumination. This method performs significantly better than gray-world, retinex, and colour by correlation using real and synthetic images.

For the sake of improving the illumination estimation accuracy, recently some researchers proposed different approaches for automatic selection and combination of illumination estimation methods. These approaches are mainly based on image content which is used to extract features. These features are then used by a classifier to do the selection and the combination decision. Different approaches use various classifiers such as Classification And Regression Tree [78], [79], Mixture of

Gaussians [80], Ridge Regression [81] (other approaches and more detail about these approaches can be found in [78], [80], [82]).

It was reported [21], [30] that most of the methods based on the diffuse reflection have some drawbacks. For achieving efficient estimation of illumination, these methods require many colour observations on the surface of an object and complex computation [21]. Moreover, in most of the methods, the existence of the specular reflection can reduce accuracy of illumination estimation. According to the nature of problems that afflict the methods based on the diffuse reflection model, in reality, these problems are difficult to control and it remains as an open question to be solved. In the following section, methods which use less surface colours, have less computational complexity and are robust against the specular reflections are highlighted.

2.4.2 Methods Based on Dichromatic Reflection

The colour image responses of an object surface captured under uniform illumination will fall in a plane in RGB colour space if the surface follows a dichromatic reflection model [1]. This is because the colour responses are a combination of two reflection colours which are diffuse reflection, and specular reflection. In most dielectric materials, the interface reflectance function is constant, so this means that the colour of the incident illumination is the same as specular reflection. On the other hand, the diffuse reflection depends on the colour of the object surface and incident illumination; as a result, different surfaces can be identified by different diffuse reflection. Many researchers [12], [18], [21], [29], [83], [84] have proposed methods for estimating illumination that depend on the dichromatic reflection model and most of these methods utilize specular reflection as the main part to be analyzed in order to extract information about incident illumination. Most of them use the original image which is a mixture of specular and diffuse image components to estimate illumination by analyzing the mixed components in different colour spaces. In this thesis the original image is referred to as 'mixed image components' to clearly distinguish the methods that operate on both components.

The idea of using colour space to estimate illumination chromaticity is that the RGB components of different surfaces will fall into different planes and the intersection of these planes will be a good indication about the illumination characteristics. A number

of researchers [12], [18], [29], [83], [84] proposed methods using these ideas to estimate the illumination chromaticity.

Klinker et al in [12] proposed a method to estimate illumination chromaticity from a uniform coloured surface using RGB space. It was found that in this space, the uniformly coloured surfaces with highlight form a T-shape distribution. Then the colour of the illumination and body reflection can be found by extraction and decomposition of this T-shape. Unfortunately, due to the noise which is commonly present in real images, the extraction of the T-shape becomes quite difficult. As a result, the final estimation of the colour of illumination and body reflection become undependable.

By using the highlight of at least two surface colours, Lee [29] proposed a method to estimate illumination chromaticity. This is achieved by determining the intersection of dichromatic lines of the surface colours in r-g chromaticity space. This method has some limitations [30]. First, the segmentation of the surface colour underneath the highlight is required to generate a dichromatic line for each surface colour. Furthermore, the colour segmentation of highly textured objects is a complex process. Second, surfaces with the same colour will form nearly parallel dichromatic lines and this makes the intersection sensitive to noise. As a result, the estimation for similar surface colours becomes unsteady in real images where noise is commonly found. Finally, the method is not applicable to uniformly coloured surfaces. Other researchers have extended and developed upon Lee's method [18], [83], [84].

In [83], a robust method to create dichromatic lines in chromaticity space is proposed. This method makes the assumption that the colour surface in the highlight is uniform. Unfortunately, this method fails when it is applied to multipart textured surfaces which include more than one surface colour in the highlighted regions.

Researchers in [84-86] tackle the second limitation of Lee's method, which is instability in obtaining the intersection of dichromatic lines. In [84], and [85] it is obtained by imposing constraints on colours of illumination using the statistics of natural illumination colours. In [86] the second limitation of Lee's method is addressed by applying pre-processing for highlight pixels to avoid the noise generated by the CCD camera using a method based on Mahalanobis distance.

In addition, Finlayson et al [18] proposed a method to estimate illumination from a uniform surface colour using Planck's locus as a constraint on the illumination chromaticity. This method is more robust in estimating the illumination particularly for real images and this occurred due to the use of the Planckian constraint. Nevertheless, this method suffers from the requirement of colour segmentation for multicolour surfaces in the highlight area [30].

One of the limitations of the previous dichromatic methods [84], [85], [18] is that it is difficult to classify image pixels in terms of scene materials. In order to overcome this problem, Javier and Brian [87] proposed a multi-linear constraint on the illumination colour of the scene.

Tan [21] proposed a new method to estimate illumination colour without using colour segmentation of image regions which correspond to multi-coloured surfaces in the highlight areas. This method estimates illumination from single- or multi-coloured surface. The method uses highlights as the main source to be processed and analyzed in a new colour space. This space is called inverse intensity colour space. The space describes the correlation between image chromaticity and illumination chromaticity. The proposed method has many advantages over the previous dichromatic based methods. The colour segmentation which is needed in the previous methods is not required at all in this method. As a result, this method can be applied even for highly textured surfaces. Moreover, accurate estimation of the highlight regions is not required for this method. The highlight regions can be achieved by simple thresholding of the intensity values. Furthermore, as no assumptions are made about the illumination chromaticity, the method is applicable for all possible illumination colours. Moreover, in this method, the intrinsic camera characteristics are not needed. However this method is very complex and time consuming on detecting highlight area and on calculating intersections by the Hough transform [88].

Li in [88] tried to reduce the complexity of Tan's method by using a voting method to detect the highlight areas. Then the pixels in highlight areas are projected to the Inverse-Intensity colour space, which was proposed by Tan [21]. Finally by applying a line fitting method to all projected pixels in Inverse-Intensity colour space, illumination chromaticity can be estimated. In [89] Javier proposed a method to estimate illumination without a need for pre-segmentation of the highlight area in an

image into a region of uniform surface reflectance. In this method, the colour of the illumination is obtained based on optimizing a cost function.

Long Yang et al [90] proposed a method to estimate spectral power distribution based on the dichromatic reflection model and a finite dimensional linear model. In this method, the illumination chromaticity is estimated from the intersection of two-colour signals of two inhomogeneous surfaces. Then from the illumination chromaticity the ISPD is estimated adopting Judd's illumination basis functions and assuming that the surface reflectance is 1. This method gives suitable results when it is tested on colour chip images. However this method may not give the same result if it is applied to a real image because it will require colour segmentation of image regions which correspond to multi-coloured surfaces in the highlight areas, which is a problem for most of the methods which are based on the dichromatic model

In summary, from the above survey, it can be noticed that the methods based on the dichromatic model utilize the original image which is a mixture of specular and diffuse components and try to estimate illumination chromaticity by analyzing it in different colour spaces. Moreover, most of the methods in this category suffer from either the problem of segmenting image regions which correspond to multi-coloured surfaces in the highlight areas or face the problem of computational complexity. However, the estimation of illumination using an explicitly separated specular image component has not been reported in the literature and one way to extract the specular image component is to use blind signal separation as it will be discussed in Chapter 3. As the spectral characteristics of specular reflection component are similar to spectral characteristics of illumination, estimating illumination based on this component is likely to give more accurate results. Moreover work in separated specular image component has potential to avoid the complicated segmentation that is needed in the conventional methods.

2.4.3 Hybrid Methods

In the hybrid methods, researchers try to combine methods based on diffuse reflection with methods based on dichromatic reflection to improve the performance of illumination estimation.

To the knowledge of the author, Schaefer et al [91] present the first method which combines a method based on diffuse reflection and a method based on the dichromatic reflection. The aim of this combination is to integrate the advantages of the colour by correlation method with those of methods based on the dichromatic reflection model. The combined method outperforms the methods based purely on diffuse or dichromatic reflection. The illumination estimation in the combined method is achieved by combining the estimation results for two combining methods (correlation and dichromatic).

The estimation of the illumination is a very important factor not only for colour constancy but also for other research areas. In the following section, a summary of related illumination estimation methods is reviewed.

2.4.4 Related Work on Illumination Estimation for Computer Graphics

Parallel to colour constancy research, the problem of illumination estimation, which is considered as an ill posed problem, is important for computer graphics applications such as augmented reality and lighting reproduction. In these applications, researchers [92-95] deal with the illumination estimation problem in a different manner, using various types of additional information as a guide for the estimation process. The additional information can be given by shading, shadows, or specular reflection.

Some researchers exploit the specular reflection cue that is obtained by inserting a calibration device such as a mirrored ball [96] or sphere [97], [98], [92] into the scene in order to estimate illumination locations and intensity. There are many methods which use the shading cue to estimate the illumination of a single light source or multiple light sources. Most of these methods use the shading cue to estimate the illumination of a single light source [95], [99]. However, in order to estimate multiple light sources, several methods have been proposed [100], [101], [93]. The cast shadow is useful information which can be used to recover the light directions and intensities. Sato et al [102], [94] proposed methods to estimate complex illumination distribution in a real scene by utilizing the brightness values within shadows cast on an object.

Although, the illumination estimation methods which are based on using the shading, shadow, or specular reflection provide some success, they have limitations. For example, they have difficulties in detecting the critical points for shading, frontal illumination for shadow, and the need for using a special calibration device for specular reflection. To overcome these limitations, some researchers have proposed methods which combine the use of shading and shadow [103], while others integrate the use of shading, shadow and specular reflection [95] cues.

2.5 Illumination-Invariant Colour Descriptor Methods

As explained earlier in this thesis, the aim of computational colour constancy techniques is to obtain illumination invariant colour descriptors of a scene from an image captured under unknown illumination. This is typically achieved through two stages. In the first stage the estimation of the illumination parameters are obtained using one of the illumination estimation methods which are reviewed in the previous sections (2.4.1 and 2.4.2). Then the estimated illumination parameters are used to calculate illumination invariant colour descriptors; colour constancy is thus achieved. The illumination invariant colour descriptors can be represented by an image of a scene as if it is captured under known illumination, or by the spectral reflectance of the object surfaces in the scene. The two forms of the illumination invariant colour descriptors can be obtained by two methods of transformation mapping. These methods are diagonal mapping and linear (general) mapping which will be explained in the following subsections.

2.5.1 Diagonal Transformation Method

The diagonal transformation method is mainly based on the assumption that the camera sensor sensitivity is narrowband and follows Dirac delta function. Most of the illumination estimation methods reviewed in this chapter are combined with the diagonal transformation method in order to produce illumination invariant colour descriptors. This is due to the simplicity of this transformation method. By using this transformation method, the illumination invariant colour descriptors are obtained by taking the dot product of the diagonal matrix and the image captured under unknown illumination. The diagonal matrix consists of values which represent the ratio between known and unknown (estimated) illumination. However, the assumption that this

method is based on can be quite poor for certain cameras which have broad-band sensor sensitivity. As a result, to improve the computational colour constancy based on the diagonal transformation, Finlayson [104] and Barnard [105] proposed a method called “sensor sharpening”. The idea behind this method is to use an appropriate linear transformation to map the data into a new space where the narrow-band sensor sensitivity assumption can reliably apply. After that, the diagonal transformation is applied to the new data (new space). Then the result of the diagonal transformation is mapped back to the original RGB space using the inverse of the linear transformation. The sensor sharpening method improves some of the computational colour constancy techniques which are based on diagonal transformation but it has a negative effect on others [105]. Moreover, identifying the appropriate linear transformation is not a clear task because it requires some knowledge about the illumination and scene surfaces.

2.5.2 Linear Transformation Method

In this transformation method, most of the researchers consider 3×3 matrices for linear mapping of image pixels values. Moreover, a finite dimensional linear model is used to represent the illumination spectral power distribution and the spectral surface reflectance. To the knowledge of the author, Buchsbaum [6] is one of the early researchers to use linear transformation to extract spectral surface reflectance. Moreover, to improve the accuracy of the surface reflectance estimation of Buchsbaum’s method, Gershon [26] proposed another method to estimate the spectral surface reflectance based on the linear transformation. The common element in these two methods is that the illumination is estimated based on the gray world assumption (explained in Section 2.4.1.1).

Furthermore, Maloney and Wandell [9] proposed a method for estimating the surface spectral reflectance of objects in a scene based on a linear transformation. This method includes two different limitations on the recovery of the surface reflectance. First, if the ISPD is known, then the surface reflectance can be estimated only under the condition that the number of surface reflectance basis functions is equal to the number of image sensors. Second, if the ISPD is unknown, the surface reflectance can be obtained if and only if the number of surface reflectance basis functions is less than the number of image sensors (which is commonly equal to 3) [30]. Theoretically, the previous assumption is correct, but this method performs badly when it is applied to

real images because the failure of this assumption will decrease the surface spectral accuracy [19], [60], [106].

To increase the efficiency of the Maloney-Wandell method, Drew et al [11] use the RGB values in the mutual reflection region due to the combination of the reflected lights from each surface. These values are used as extra information, as well as sensor measurement from each surface separately, to recover the surface reflectance.

2.6 Review of Colour Constancy Frameworks

To the knowledge of the author, the first colour constancy framework was proposed by Finlayson and et al [16].

Finlayson et al [16] proposed a general correlation framework. This framework allows many of the illumination estimation methods (i.e. methods based on the diffuse reflection which are previously stated in Section 2.4.1) such as gray-world, gamut mapping, Bayesian, and neural network to be used within the framework. In this framework, the illumination is estimated through three steps. First, the generation of the correlation matrix is obtained by the determination of the image colours which can occur under each set of possible lights. Then the colour information which is provided by a particular image (i.e. the image from which it is required to estimate the illumination) is correlated with the previously generated information (correlation matrix). The result of this operation gives the probability that each of the possible lights was the scene illuminant. Finally, an estimate of the scene illumination is recovered using these probabilities. Although the framework is able to achieve reasonable colour constancy accuracy, it has some drawbacks. The framework is based on complex methods with high computational cost. The framework needs a large image data set with known illuminations, for more accurate illumination estimation [53].

Van de Weijer et al [53] developed a framework which allows the use of some of the existing illumination estimation methods which are less complex compared to the methods used in the framework developed by Finlayson et al in [16]. The methods used by Joost et al in [53], which are based on low level image features, are gray-world, max -RGB, shade of the gray, gray-edge, and higher order gray-edge (Section 2.4.1.1). Although the framework is simple and fast in computation, it requires a high

number of observed colour surfaces in a scene, for more accurate colour constancy estimation.

Rei [107] proposed a framework to estimate surface colour based on changing the colour of the illumination. In this framework, two images of the same scene are captured under two different illuminations with different colour temperatures. Then the illumination chromaticity and the surface colour of the scene objects are calculated in the chromaticity space using pixels values of the two images. Moreover, in [108] the shadow and non-shadow regions in images are used in the framework (i.e. proposed in [107]) to estimate the illumination and colour of the surface.

A common limitation which is deduced from the frameworks, which are mentioned in this section, is that these frameworks base their analysis on the assumption of no specular reflection content within the images. However, in reality the presence of specular reflection within the images cannot be neglected in some cases. Specular reflection can cause the failure of the process or reduce the accuracy of these frameworks to achieve colour constancy.

The frameworks which are mentioned in this section use the approach in which the illumination is explicitly estimated in order to be used to achieve colour constancy. On the other hand, there are some frameworks which achieve colour constancy without explicit estimation of illumination [109].

2.7 Summary

In this chapter, a survey of colour constancy related topics is discussed. The survey highlighted that illumination estimation methods have been used in approaches to colour constancy developed by other researchers. The illumination estimation methods are considered as a key stage towards achieving illumination invariant colour descriptors or colour constancy. Then invariant colour descriptor methods are reviewed, followed by colour constancy frameworks.

Most of the methods based on the dichromatic reflection model utilize the original image which is a mixture of specular and diffuse components and try to estimate illumination chromaticity by analyzing it in different colour spaces. Moreover, most of the methods based on the dichromatic reflection model suffer from the problem of segmenting image regions which correspond to multi-coloured surfaces in the highlight areas while the others face the problem of computational complexity. The

estimation of illumination using an explicitly separated specular image component has not been reported in the literature and one way to extract the specular image component is to use blind signal separation as it will be discussed in Chapter 3. As the spectral characteristics of the specular reflection component are similar to the spectral characteristics of illumination, estimating illumination based on this component is likely to give more accurate results. Moreover, work with an explicitly separated specular image component has the potential to avoid the complicated segmentation which is needed in the conventional methods.

The next chapter presents a survey of blind signal separation techniques, which are combined with the physical model of image formation (i.e. which assumes dichromatic reflection) in the colour constancy framework proposed in this thesis.

3

Survey of Blind Signal Separation Techniques

3.1 Introduction

This chapter presents a survey of the blind signal separation techniques which are pertinent to this research on colour constancy. The chapter discusses blind signal separation techniques for additive mixed signals and convolutive mixed signals. The survey includes a comprehensive study of Independent Component Analysis (ICA) which is used to solve the problem of blind signal separation. A description of ICA is given; it includes the ICA model, the assumptions, and the ambiguities of the model, and the principle of estimating the ICA model. Subsequently, one of the least complex and efficient ICA techniques, which is named FastICA, is explored. Finally, the spatially constrained FastICA, which is a modified version of FastICA, is presented, followed by the chapter summary.

3.2 Blind Signal Separation

Blind signal separation is the ability to extract the unobserved signals or sources from several observed mixtures. The observed mixtures are obtained at the output of a set of sensors and each sensor output is a combination of the sources or signals. This process is called ‘blind’ because the separation of the sources occurs without knowledge about the sources or signals and the corresponding mixtures. Blind signal separation is used for various types of applications, with different types of mixing processes. The possible types of mixtures are the additive and the convolutive

mixtures [110]. In the additive mixing, the mixtures are generated as a weighted sum of the individual sources or signals without time delay. This means that the sources reach the sensor at the same time. However, in the convolutive mixing, the mixture contains a time delay due to the fact that the sources reach the sensor at the different times [111]. According to the mixing condition, blind signal separation techniques can be classified into two categories which are: techniques for additive mixed signals and techniques for convolutive mixed signals, as seen in Figure 3-1.

The mixed signals that are considered in this research project are images, which are created mainly based on the dichromatic reflection model. This model assumes that the image is formed due to two components which are additively mixed. Due to this assumption, the survey will focus on the additive mixed signals techniques including a brief summary of techniques for convolutive mixed signals.

3.2.1 Techniques for Additive Mixed Signals

Blind signal separation can be achieved using two types of separating methods which are linear and nonlinear. The linear separating method is used when the number of sources is less than or equal to the number of mixed signals and the nonlinear separating method is used when the number of sources is greater than the number of mixed signals [112]. Moreover, using nonlinear separating method requires assumptions such as sparseness of the sources, which is not found in the sources considered within the context of this research. This chapter is mainly concerned with techniques that use a linear separating method, and it gives some examples of techniques that use the nonlinear separating method. The procedures of the blind separation process in the additive mixed signals techniques depend on what is assumed about the sources [113]. According to the assumptions made about the sources, there are two types of procedures, one type uses the spatial independence and non-Gaussianity of the sources, and the other uses the spatial decorrelation and temporal correlation assumption [113].

3.2.1.1 Techniques Based on Spatial Independence of Sources

In this class of blind signal separation techniques, each source is assumed to be statistically independent of the other sources. Moreover, the probability density

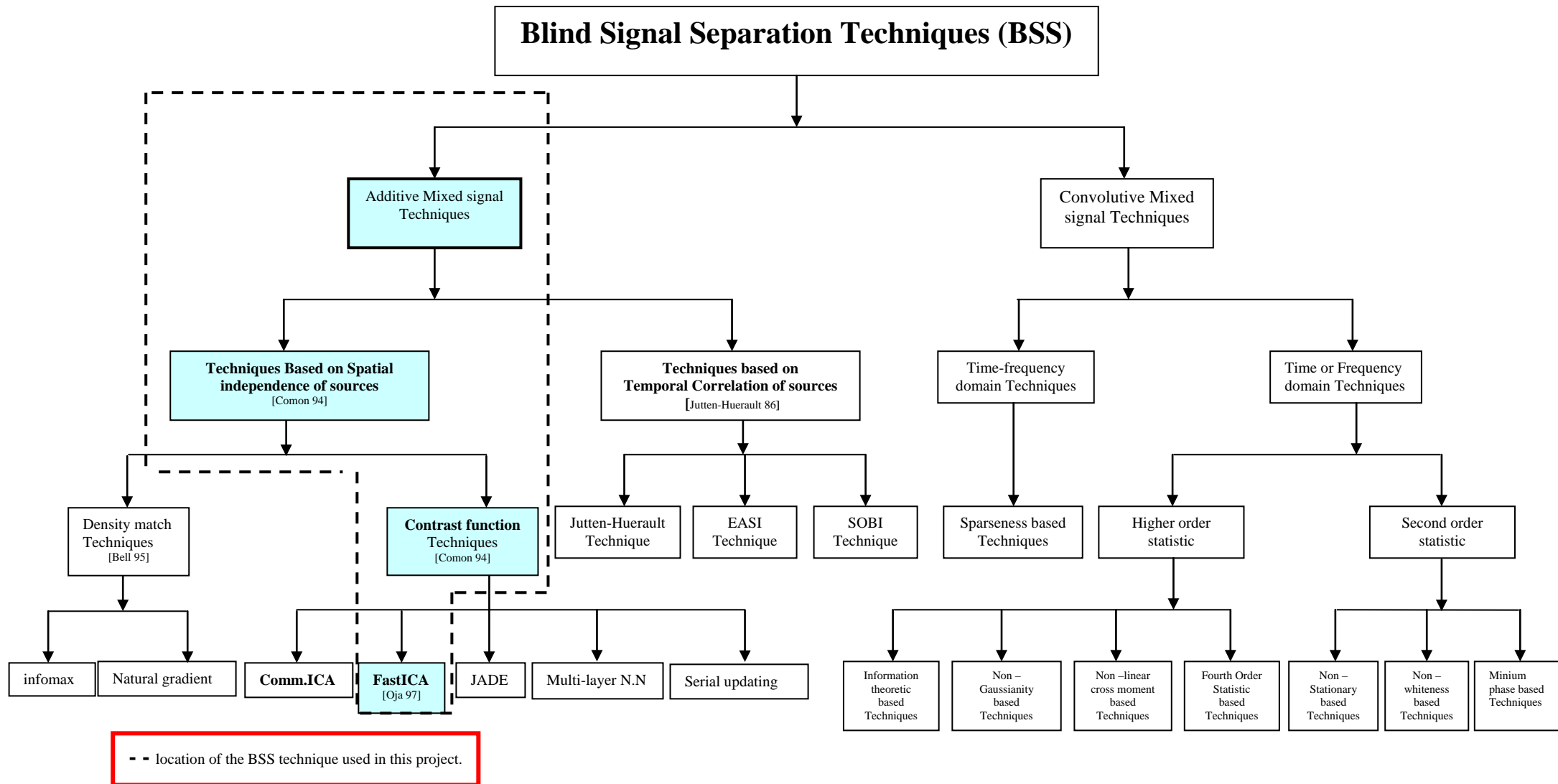


Figure 3-1 Classification of blind signal separation techniques [111], [113].

functions of all sources must be non-Gaussian except that one at most must be Gaussian. The separation in this class of techniques relies on some knowledge of the higher-order or lower-order statistics of the source signals. Blind signal separation techniques which assume spatial independence can follow two different approaches which use the density matching of sources or the contrast function optimization [110].

The density matching blind signal separation techniques are based mostly on concepts from information theory. These techniques mainly include entropy maximization for each source and mutual information minimization between sources. Information theory supports these techniques by the amount of information that is shared in a set of signals. The separation of sources in this class of techniques occurs when no common information can be found between any two output sources. Researchers formulate the density-matching techniques in different ways [110] for sharing information from various signals.

Bell and Sejnowski are the first researchers who used information theory to perform blind signal separation [114]. They developed an information maximization technique which is called the 'infomax technique'. The proposed technique is an adaptive learning technique which works by maximizing the information passed through a neural network. This technique shows how the neural network is capable of separating independent components in the input, which means that the neural network can perform independent component analysis. The technique proves that the minimization of mutual information among the output components can be approximately achieved by maximizing the joint entropy of the output of the neural network. Although the technique was shown to be able to separate up to ten sources, it is limited to separate sources with super-Gaussian distribution [115].

In order to separate the sources with variant distributions, [116] extends the infomax technique. The extended technique provides a simple and general learning rule with fixed nonlinearity to separate sources with either sub- or super-Gaussian distributions.

Although Amari et al [117] proposed a different technique; the learning rule outcome was the same as the Bell and Sejnowski learning rule. The technique was then extended by performing a descent on the natural gradient. As the starting point in this

technique derivation, the Kullback-Leibler distance was used to measure the similarity of the probability density functions. The output components are independent if the joint entropy of the outputs is the same as the product of the individual entropies. This is achieved by minimizing the Kullback-Leibler distance between the probability density function of the output components and the product of the probability density function of the individual output components.

In the contrast function optimization blind signal separation techniques, an introductory concept of contrast function for blind signal separation was initially presented by Comon [118]. The contrast function can be applied directly because it is non quadratic and mainly depends on a single extracted output source. Such functions are used as constraints over the demixing matrix elements to separate independent sources from their linear mixture. The common characteristics between density matching techniques and the contrast function techniques is that they both depend on the spatial independence and non-Gaussianity of the source signals to perform the separation. However, density matching techniques entail a significant knowledge about the nature of the source signal, the probability density functions, in order to perform separation which is different to the contrast function techniques. There are different techniques in this class which differ in the definition of the contrast function.

Comon [118] proposed a technique which provides a precise definition of the independent component analysis problem within an applicable mathematical framework based on the contrast function. It was shown that, in Comon's ICA technique, the sources are separated from their mixture when the contrast function is maximized. The main feature of this technique is that the contrast function is mainly dependent on the fourth order cumulant of the source. The principles of ICA and further detail about it will be explained in detail later in this chapter (Section 3.3).

Burel presented in [119] a technique based on the multilayer neural network which is used to construct the contrast function. Such a contrast function is designed to make each output source to have zero mean and unity variance and make sources independent. The source separation in this technique is achieved due to minimizing the contrast function by updating the neural network weights. Subsequently, by using the natural gradient method, an information backpropagation technique by Burel was developed [120]. Moreover, Yang et al in [121] proposed a radial basis function

neural network described by a contrast function which is defined by the mutual information.

Cardoso proposed a technique which was closely related to Comon's technique, called serial updating [115]. Like Comon's technique, the update of the serial updating technique is derived in two steps which are: whitening of the observed signal, and the rotation until the contrast function is minimized (the case of the serial updating technique) or maximized (the case of the Comon's technique). On the other hand, the serial updating technique used the fourth-order moments of the output signal to define the contrast function while Comon's technique uses fourth-order-cumulants.

Moreover Cardoso proposed another important technique which is known as joint approximate diagonalization of eigenmatrices (JADE) [122]. The main feature of this technique is that the cumulant tensor eigenvalue decomposition is considered as pre-processing. The contrast function of JADE effectively measures the mutual information between the cross cumulants. The separation of sources is found when the mutual information or contrast function is minimized.

In [123] the fixed-point technique, named FastICA, was introduced using kurtosis and then it was modified for a general contrast function using negentropy approximation [124]. The FastICA technique has many advantages over the other contrast function techniques, which make it a good candidate to be combined with the physical image formation model (i.e. assumed to be dichromatic model) in order to achieve colour constancy (the framework proposed in this thesis). These advantages and further details of the FastICA technique will be discussed later in this chapter (Section 3.3.2) [124].

3.2.1.2 Techniques Based on Temporal Correlation of Sources

The techniques of this class depend on a set of source properties such as spatial and temporal properties. Unlike the previous techniques, the spatial independence of the sources is not needed. However, the sources need to be spatially uncorrelated and temporally correlated. The main advantage of blind signal separation techniques which use temporal correlation is that the source separation is achieved by using second-order statistics. Much research has been done using the temporal properties of the sources for blind signal separation [110].

Jutten and Huerault found the earliest solution for blind signal separation using a neural network that was based on the temporal correlation of sources [115]. The separation of sources is achieved by cancelling the non-linear cross-correlation of the sources, which means obtaining independent sources. The disadvantage of this technique, known as the Jutten-Huerault technique, is that it converges slowly under a severe restriction due to computation of matrix inversion [125].

Moreover, researchers in [126] proposed another technique based on cancelling the non-linear cross-correlation, which is called the equivariant adaptive separation via independence (EASI) technique. In this technique, the researchers try to overcome the disadvantages of Jutten-Huerault's technique by decreasing the calculation process which is achieved by avoiding any matrix inversion and improving the stability of the technique.

Furthermore, [127] presented a new blind signal separation technique for temporally correlated sources, known as second order blind identification (SOBI). This technique uses joint diagonalization of an arbitrary set of covariance matrices [128]. Unlike the higher order cumulant technique, this technique allows for separation of sources with Gaussian distribution and also depends only on the second-order statistics of the received signals.

3.2.2 Techniques for Convolutional Mixed Signal

There are several techniques which are proposed to separate sources from a convolutional mixture. Based on the separation domain, these techniques can be grouped into three categories, which are: time based techniques, frequency based techniques, and time–frequency based techniques [129]. The separation in these categories is achieved based on the assumption that the sources are statistically independent or at least decorrelated. Moreover, the separation criteria in both the time-based technique and frequency-based technique can be divided into methods based on higher-order statistics, and second-order statistics (SOS) [111].

In the higher order statistics based techniques; there are many researchers who dealt with the problem of separation using different categories of techniques.

- The first category, which is known as the techniques based on fourth order statistics, is based on minimizing the second and fourth order dependence between the sources. In this category, researchers tackled the problem of separation by using fourth order cumulant [129-133], second and third order cumulants [134], kurtosis [135-137], and negentropy [138].
- In the second category, which is the set of techniques based on non-linear cross moments, researchers indirectly applied higher-order statistics to solve the problem of the convolutive mixture separation by using odd non-linear functions [111], [115], [139].
- In the third category, the techniques based on information theory, probability density functions are used as an indication of the statistical independence of the sources. Based on information theory, there are many techniques derived using the maximization of entropy [140], [141] the Maximum Likelihood, Maximum a Posteriori [111], Bayesian formulation, and Hidden Markov Model [111], [142], [143].

On the other hand, the techniques based on second-order statistics need only non-correlated sources instead of higher-order statistical independence [127]. Unlike the higher-order statistical techniques, these techniques make alternative assumptions such as the non-stationarity of the source [144-146] or a minimum phase mixing system, and non whiteness [111]. The separation using these techniques depends mainly on minimizing the cross correlation of separated sources. The main advantages of the techniques based on the SOS are that they are less sensitive to noise and outliers, and consequently require less data for their estimation [147].

As declared previously in Section 3.2.1, it is difficult to extract more sources than there are sensors with a linear separating system. Researchers try to address this problem, of extracting more sources than sensors, using the sparseness assumption [112], a nonlinear system, and a Bayesian formulation [111]. The sparse assumption is considered when the source signals are not overlapped in the time-frequency domain, which increases the possibility of separating the sources [112].

3.3 Independent Component Analysis (ICA)

ICA is one of the blind signal processing techniques used to represent random variables as linear combinations of statistically independent components. The simple model of ICA can be defined by a linear relationship between the observed random variables and the unknown independent components in matrix form as follows:

$$\mathbf{X} = \mathbf{AS} \quad (3-1)$$

where \mathbf{X} represents the matrix of the observed random variables (e.g observed image data) and each row in the matrix contains the random variable vector, $\mathbf{X} = (\mathbf{x}_1, \mathbf{x}_2, \dots, \mathbf{x}_p)^T$; \mathbf{S} is an independent component matrix (e.g specular and diffuse image components) and each row includes an independent component, $\mathbf{S} = (\mathbf{s}_1, \mathbf{s}_2, \dots, \mathbf{s}_n)^T$; \mathbf{A} is an unknown ($p \times n$) matrix of full rank, which is known as the mixing matrix. The ICA model is considered as a generative model which describes how the observed signals are generated from the mixing matrix and components [118].

For example, in the work presented in this thesis, different instance images (\mathbf{X}) are created. ICA techniques are then applied to these images in order to extract the image sources or the components (\mathbf{S}) that contribute in the reconstruction of these images. The number of the created images depends on the number of components which need to be extracted.

The main issue of the ICA technique is to estimate the original independent components or the mixing matrix, which are equivalent, from observed variables (signals). This estimation is based on some assumptions about the observed signals and the independent components. These assumptions can be listed as follows [113]:

- The number of observed signals is greater than or equal to the number of the independent components ($p \geq n$).
- The independent components must be mutually statistically independent, with a zero mean.
- All independent components must have a non-Gaussian distribution with an exception of one component which can have a Gaussian distribution; otherwise the estimation of components will fail.

- The mixing matrix must be full column rank.

After the estimation of the mixing matrix \mathbf{A} is obtained, the demixing matrix $\mathbf{W}=(\mathbf{w}_1,\dots,\mathbf{w}_n)^T$ which is the inverse of \mathbf{A} , is calculated. Where \mathbf{w}_i are the rows of the inverse of the mixing matrix (\mathbf{A}) and also are equal to the columns of the mixing matrix according to the property of an orthogonal matrix: $\mathbf{A}^{-1} = \mathbf{A}^T$. Then the independent components \mathbf{S} can be simply computed by the following formula [148].

$$\mathbf{S} = \mathbf{W}\mathbf{X} \quad (3-2)$$

There are uncertainties in the ICA model. These uncertainties are:

- The energies (variance) and the sign of the independent components cannot be identified. This is due to the fact that, both independent components(\mathbf{S}) and mixing matrix (\mathbf{A}) are unknown.
- The order of the independent components cannot be defined. This is also because no knowledge about the \mathbf{S} and \mathbf{A} is used and the estimation is randomly obtained [125].

ICA has been selected for the proposed project because it has been shown to give good results for recovering scenes degraded by reflections off a semi-reflecting medium such as a glass window, by decomposing the image which contains a mixture of the original image and the reflected scene image [149-151]. This is similar in principle to the problem of separating additive mixed components of the image, which are specular and diffuse components. Furthermore, ICA achieved good results on blind signal separation tasks [149-157].

ICA is mostly used for blind source separation and it achieves good results on this task. Moreover, ICA has been used in different applications of image and signal processing, such as embedding [158-160] and extracting watermarks [161, 162], image retrieval [163-165], pattern recognition (face [166-170], iris [171], fingerprint pre-processing [172]), image restoration and enhancement [173], medical imaging [152], [174], signal processing [153], [155], [175], speech recognition [176], removal of reflections from an image [149-151] and separating the image components [28]. ICA has been successfully implemented in different applications as mentioned above [149-157], and especially for separating components of an additive mixture of signals.

The image formation in the framework presented in this thesis is based on the dichromatic reflection model which means that the image is formed due to an additive mixture of the diffuse and specular components. Hence, ICA techniques are suggested to be used for the separation of the diffuse and specular components of an image in this framework.

3.3.1 Estimation Principle of the ICA model

Non-Gaussianity is considered as a key issue for estimating the ICA model and the estimation will be impossible without it. The estimation principle of the ICA model is based on the central limit theorem. The central limit theorem states that the sum of independent random variables has a distribution which is closer to the Gaussian distribution than any of the original random variables [148]. The principle of the ICA model is to determine the vector \mathbf{w} , which maximizes non-Gaussianity of the linear combination which is denoted by $\mathbf{y} = \mathbf{w}^T \mathbf{x} = \sum_i w_i x_i$. This linear combination actually equals one of the independent components. There are different techniques for ICA estimation based on several criteria such as: maximization of non-Gaussianity, minimization of mutual information, and maximization of likelihood. The technique that is used in this project, to estimate the ICA model, is based on the maximization of the non-Gaussianity of the independent components. This is because this technique does not require additional information about the nature of the separated source, while the others need such information.

In most of the ICA techniques, the preprocessing of the data is considered as an important and useful stage. The preprocessing makes the estimation of the ICA model simpler in computational terms and makes it perform better in estimating the independent components. In ICA, the preprocessing is done by two procedures which are data centring or ‘sphering’ and whitening. The data centring is achieved by removing the mean of the data vector which sets the mean of the variable to zero. The whitening is achieved by using the eigenvalue decomposition of the covariance matrix of the centred observed data [177]. The goal of whitening is to transform the observed vector linearly to the new vector where its components are uncorrelated and have unit variance. This means that the new vector covariance matrix is an identity matrix. Moreover, the whitening transforms the mixing matrix \mathbf{A} into a new mixing matrix which is orthogonal. The effect of the whitening is to reduce the complexity of the

ICA model by decreasing the number of parameters to be estimated. The following section explains an efficient and simple ICA technique which uses a contrast function; its estimation is based on maximization of non-Gaussianity.

3.3.2 FastICA Technique

This technique is based on a very simple and efficient fixed-point iteration scheme to estimate the non Gaussian independent components using the kurtosis contrast function. The kurtosis, which is also called as the fourth-order cumulant, is the classical measure of non-Gaussianity. Although kurtosis calculation is computationally simple, it is not robust for non-Gaussianity measurement. The estimated value for the kurtosis is sensitive to outliers; this is due to the degree of the kurtosis equation.

On the other hand, the negentropy is considered as the optimal estimator of non-Gaussianity in some sense. However, the drawback of using negentropy is the difficulty of its computation. This difficulty is due to the need to estimate the density function of the random variable. Therefore, simpler approximations of negentropy are introduced [125], [148]. These approximations, which are considered as one-unit contrast functions, are characterised by simplicity, speed of computation, and addressing the problem of robustness. These approximations of negentropy provide FastICA with a general contrast function.

Also, the FastICA is considered as a general technique because it is used to optimize one-unit or multi-unit contrast function. The one-unit FastICA is used to estimate only one of the independent components. However multi-unit FastICA is used to estimate several independent components. This is achieved by running the one-unit FastICA technique using several units with the weight vectors $\mathbf{w}_1, \dots, \mathbf{w}_n$. The estimation of these components can be achieved in two different ways. These ways are a sequential (one by one), which is called a deflation scheme, or a parallel (all at the same time), which is known as a symmetric scheme.

Compared with current techniques for ICA, the FastICA technique and the fundamental contrast functions have a number of essential properties.

- The FastICA convergence is very fast because its convergence is cubic (or at least quadratic) under the assumption of the ICA data model. In gradient descent methods the convergence is just linear.
- The FastICA is easy to use because it does not require selecting proper step size parameters while the gradient-based techniques do.
- In the FastICA technique, the independent component of any non-Gaussian distribution can be estimated directly using any nonlinearity functions. However in many ICA techniques, the nonlinearity function is selected corresponding to the estimated probability distribution.
- By selecting a suitable nonlinearity function, the performance of the FastICA in terms of robustness can be optimized.
- The FastICA has most of the advantages of the neural-network techniques such as simplicity in computation and little memory space requirements.

3.3.3 Spatial Constraints on the Mixing Matrix

In blind signal separation and ICA, there are different types of generic mixing matrix constraints, such as orthonormality, orthogonality, non-negativity, sparsity, and symmetry which are commonly used [177]. These types of constraints control the mixing matrix to satisfy certain conditions without specific prior knowledge of the mixing matrix coefficients. On the other hand, the spatial constraints on the mixing matrix consider specific prior knowledge or assumptions about the coefficients of certain columns of the mixing matrix. There are two types of spatial constraints on the mixing matrix. The first one is the parametric constraint in which the space of the component coefficients is restricted by a generative model which imitates geometrical and physical properties of the source (component) mixing and the signal generating process [178]. The second one, which is called reference or constraint topographies, considers that some component coefficients (mixing matrix columns) are approximately known. Constraint topographies can be manually determined by the selection of components extracted from previous data using an unconstrained ICA model, or generated from a mathematical model of the signal mixing process [178]. Moreover, the way of determining constraint topographies depends on the application.

For constraint topographies, the spatially constrained mixing matrix \mathbf{A} contains two types of columns as follow:

$$\mathbf{A} = [\mathbf{a}_c \quad \mathbf{a}_u] \quad (3-3)$$

Where \mathbf{a}_c are the spatially constrained columns and \mathbf{a}_u are the spatially unconstrained columns. For various accuracies of the predetermined constraint topographies, there are different spatial constraints severities which are defined as hard, soft, and weak spatial constraints. Determination of the spatial constraint severity depends on the degree of confidence about the constraint topographies [179]. In the following section, the spatially constrained FastICA will be explained.

3.3.4 The Spatially Constrained FastICA

This technique is considered as a modified version of conventional FastICA. This modification is achieved by using spatial constraints on the mixing matrix of the conventional FastICA [179]. The goal of this technique is to estimate the mixing matrix coefficients and a set of sources including both independent components and spatial components. This is achieved by maximizing the statistical independence of unconstrained sources while minimizing the divergence between the spatially constrained source projections and their corresponding reference topographies [178]. Similar to the conventional FastICA, the preprocessing of the observed signals and the selection of an appropriate non-linearity function for the FastICA contrast function are necessary for the spatially constrained FastICA. However the ICA and the conventional FastICA are not able to differentiate between the separated components. On the other hand, the spatially constrained FastICA is able to make the differentiation between the components clearer and easier than the conventional FastICA. In the proposed colour constancy framework, the differentiation of separated components (specular and diffuse components) is necessary in order to achieve an accurate estimation of illumination and surface reflectance. For this reason, the spatially constrained FastICA becomes a good candidate to be used for blind signal separation within the proposed colour constancy framework. The steps of the separation process of the specular and diffuse components from an image, using the spatially constrained FastICA, are explained in detail in Chapter 4. Moreover, a brief description of the ICA technique, which was developed by Umeyama and Godin [28]

for separating the specular and diffuse image is provided in Chapter 4. The technique developed by Umeyama and Godin [28] and the spatially constrained FastICA are used for testing the colour constancy framework proposed in this thesis.

3.4 Summary

In this chapter, a survey of blind signal separation techniques for two types of mixed signals is presented. A critical study of these techniques is conducted. This study reflects that the spatially constrained FastICA technique is characterised by some properties. These properties support the selection of the spatially constrained FastICA technique to be used for blind image separation within the colour constancy framework proposed in this thesis. Further justification for choosing the spatially constrained FastICA technique is given in Section 4.3.2. Moreover, the ICA technique which was developed by Umeyama and Godin [28], for separating the specular and diffuse image, is used within the colour constancy framework proposed in this thesis. The next chapter explains in detail the proposed colour constancy framework and the methods used for each of its stages.

4

Proposed Colour Constancy Framework

4.1 Introduction

This chapter presents a novel framework to address the challenge of achieving colour constancy. The proposed framework is based on the combination of blind signal separation and a physical model of image formation, chosen to be a dichromatic reflection model. The chapter starts with presenting the proposed colour constancy framework. After that, the chapter presents the embodiment of the framework which is evaluated in this thesis. The image capture setting is also explained, and then the methods used within the framework are described in detail. The chapter concludes with a summary.

4.2 Description of the Framework

In the colour constancy framework proposed in this thesis, the image is assumed to be formed by an imaging process which can be represented by the dichromatic reflection model. This model represents the light reflected by an object as a linear combination of diffuse and specular reflections, as explained in Section 2.2.5. The framework is designed to achieve colour constancy by recovering the spectral reflectance of surfaces from the diffuse component, with the help of characteristics of the illumination which are estimated from the specular reflection component. This surface colour recovery process requires the separation of images into specular and diffuse components. The proposed colour constancy framework thus consists of three significant stages, as shown in Figure 4-1.

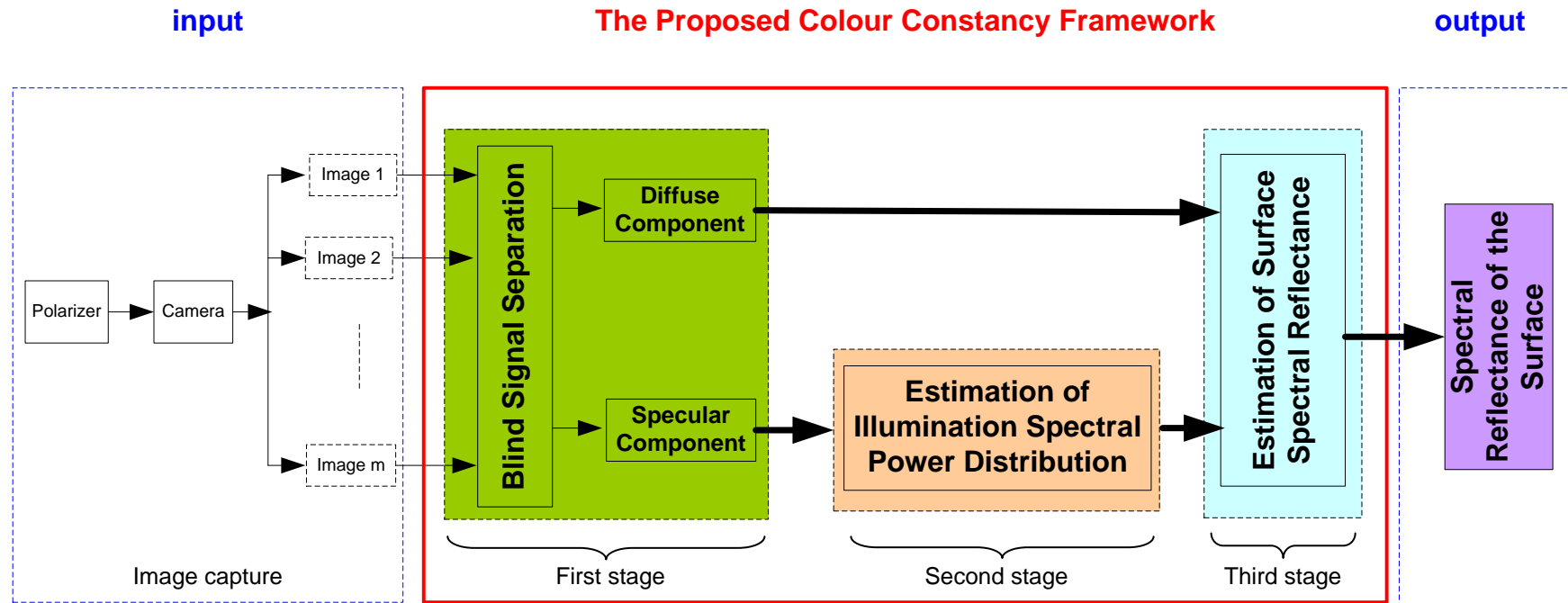


Figure 4-1 The proposed colour constancy framework

The three stages respectively perform: (i) the extraction (using blind signal separation) of separate specular and diffuse components of the pictured scene, (ii) the estimation of the spectral power distribution of the illumination incident onto the scene, and (iii) the estimation of the spectral reflectance of surfaces which make up the scene. There are many possible choices of techniques and algorithms which can be used for implementing this generic framework. The particular embodiment of the framework which is evaluated in this thesis is presented in the next section. The section begins by presenting the image capture setting, which explains how the set of images that have been used as input for the evaluated embodiment of the proposed framework were generated.

Moreover, the stages of the proposed framework, implemented for experimental evaluation, are explained in detail individually, including the input data and methods used for each stage.

4.3 Embodiment of the Framework Evaluated in the Thesis

4.3.1 The Image Capture Setting

The image capture setting, which is used in the embodiment of the framework evaluated in this research, uses a polarizer in front of the camera and assumes free air as the medium between the light source, object surface, and camera. The polarizer has a significant effect on polarized light whereas it has no impact on unpolarized light. This means that the amount of polarized light which passes through the polarizer varies according to the rotation angle of the polarizer, but the amount of unpolarized light is constant.

The specular reflected light is highly polarized; hence, the intensity of specular reflection which reaches the camera changes with different polarizer angles. In contrast, diffuse reflection has a small amount of polarization; hence, the polarizer has a negligible effect on the diffuse reflection which reaches the camera. As a result, it can be assumed that the polarizer has a significant effect only on the specular reflected light. The polarizer has previously been used, by other researchers, to separate the specular and the diffuse components [28], and it has been used to achieve colour constancy by representing the specular and the diffuse components in colour space [52]. In this research, based on the dichromatic reflection model, the first stage of the framework uses the effect of a polarizer on the captured images in order to separate the specular and diffuse image components. The separation of these components is achieved using a blind signal separation technique. These components have special characteristics which are used in this research to estimate the ISPD

and subsequently the surface reflectance, in order to achieve colour constancy. In the image capture model used in the implemented framework, the impact of the polarizer on the observed images for different polarizer orientation angles can be expressed by extending Equation (2-12) into:

$$\begin{bmatrix} \mathbf{I}_{1,k} \\ \mathbf{I}_{2,k} \\ \vdots \\ \mathbf{I}_{p,k} \end{bmatrix} = \begin{bmatrix} \mathbf{I}_{d,k} + \Phi(\tau_1)\mathbf{I}_{s,k} \\ \mathbf{I}_{d,k} + \Phi(\tau_2)\mathbf{I}_{s,k} \\ \vdots \\ \mathbf{I}_{d,k} + \Phi(\tau_p)\mathbf{I}_{s,k} \end{bmatrix} = \begin{bmatrix} 1 & \Phi(\tau_1) \\ 1 & \Phi(\tau_2) \\ \vdots & \vdots \\ 1 & \Phi(\tau_p) \end{bmatrix} \begin{bmatrix} \mathbf{I}_{d,k} \\ \mathbf{I}_{s,k} \end{bmatrix} \quad (4-1)$$

where p is the number of observed images which corresponds to the number of polarizer orientation angles; $\Phi(\tau)$ is a function that depends on the orientation angle of the polarizer and the relative specific geometrical configuration of the light source, object surface, and camera; τ is the angle between the specular reflection plane and the orientation of the polarizer. When the light source is far away from an object, the local angle (incident angle) of the incident light is almost equal for all image pixels. Consequently, specular planes of all pixels are nearly parallel to each other, and the polarizer has approximately the same effect on the specular reflection corresponding to these pixels [28]. As it can be noticed in Equation (4-1), all the images observed through a polarizer are linear combination of approximately the same diffuse component and different specular components which depend on the orientation angle of the polarizer.

4.3.2 Separation of Image Components

In the first stage of the framework, after capturing the same scene with different angles of polarization to produce p observed images ($\mathbf{I}_{p,k}$), the separation of specular and diffuse components of an image is achieved using the spatially constrained FastICA technique, as one of the options. The choice of this technique is mainly based on the number and the characteristics of the sources of the mixed signals that are considered in this research. The number of sources, which are considered in this research, is two. These sources are the specular component and the diffuse component. For simplicity and accuracy of applying the linear separation method, the number of mixed signals used in this research can be increased using a polarizer (Section 3.2.1). The probability density functions of specular and diffuse components, which represent the sources that are considered in this research, are unknown. This means that density matching techniques are not suitable to perform the separation in the

framework proposed in this research (Section 3.2.1.1). In real images, there is some spatial correlation between the specular and the diffuse component [28]. This means that the properties of the sources which need to be separated in this research do not satisfy the requirements (i.e the sources have to be spatially uncorrelated and temporally correlated) of the techniques based on temporal correlation of sources (Section 3.2.1.2). On the other hand, signal separation by techniques based on the contrast function optimization (e.g. ICA techniques) depends on the spatial independence and non-Gaussianity of the sources. ICA techniques have been used successfully to solve a kind of separation problem that is similar to the one dealt with in this research. One of the common ICA techniques is the spatially constrained FastICA. The spatially constrained FastICA technique can be explained as follows:

The p observed images ($\mathbf{I}_{p,k}$) are converted to row vectors ($\mathbf{i}_{p,k}$).

$$\mathbf{X} = \begin{bmatrix} \mathbf{i}_{1,k} \\ \vdots \\ \mathbf{i}_{p,k} \end{bmatrix} = \mathbf{A}\mathbf{S} \quad (4-2)$$

Then, centring the image row vectors and generating the whitening matrix (\mathbf{V}), using eigenvalue decomposition of the data covariance matrix [177], are performed. The whitened image rows (\mathbf{Z}) (which have unit variance) are calculated using the following equation.

$$\mathbf{Z} = \mathbf{V}\mathbf{X} \quad (4-3)$$

After that, the constrained mixing matrix (\mathbf{A}), which contains constrained and unconstrained columns ($\mathbf{a}_c, \mathbf{a}_u$), is constructed. Constrained column refers to coefficients that do not change significantly for different observations. These coefficients can therefore be determined and are therefore known. Unconstrained column refers to coefficients that can change for different observations and therefore need to be estimated. According to the behaviour of the polarizer on the diffuse and specular reflection components, the constrained column (\mathbf{a}_c) is related to the coefficients of the diffuse component. These coefficients are set to 1 (as seen in Equation (4-1)). The unconstrained column (\mathbf{a}_u) is related to the coefficients of the specular component which are initialized randomly for all experiments that are performed in this research using this technique.

$$\mathbf{A} = [\mathbf{1} \quad \mathbf{a}_u] \quad (4-4)$$

Then, the whitened constrained mixing matrix (\mathbf{H}), which is an orthogonal matrix, is calculated using

$$\mathbf{H} = \mathbf{V}\mathbf{A} = [\mathbf{h}_c \quad \mathbf{h}_u] \quad (4-5)$$

Gram-Schmidt orthonormalization is applied to the whitened constrained mixing matrix, followed by updating and normalizing \mathbf{h}_u , using

$$\mathbf{h}_{u,i} = E_x \{ \mathbf{Z}g(\mathbf{h}_{u,i-1}^T \mathbf{Z}) \} - E_x \{ g'(\mathbf{h}_{u,i-1}^T \mathbf{Z}) \} \mathbf{h}_{u,i-1}^T \quad (4-6)$$

and

$$\mathbf{h}_{u,i} = \frac{\mathbf{h}_{u,i}}{\|\mathbf{h}_{u,i}\|} \quad (4-7)$$

where E_x , g , i , and g' are the expectation, nonlinear function, iterative index, and derivative of a nonlinear function; g can be formulated as (for further details about g see [123]):

$$g(u) = \tanh(u), \quad g(u) = u^3, \text{ or } g(u) = u \exp(-u^2 / 2) \quad (4-8)$$

The updating and normalizing of \mathbf{h}_u are iterative until convergence occurs as specified by

$$\mathbf{h}_{u,i-1}^T \mathbf{h}_{u,i} \cong \mathbf{1} \quad (4-9)$$

At that time, the separation of the specular and diffuse components can be achieved by

$$\mathbf{S} = \mathbf{H}^T \mathbf{Z} = \begin{bmatrix} \mathbf{i}_{d,k} \\ \mathbf{i}_{s,k} \end{bmatrix} \quad (4-10)$$

and the mean of the observed image row vectors is added to each of the separated components. The spatially constrained FastICA technique is repeated for the R, G and B image components to separate the specular and diffuse components for each of them. The process of image component separation is applied for the whole image. The flowchart in

Figure 4-2 summarizes the steps of the separation of the specular and diffuse components for RGB images, using the spatially constrained FastICA technique.

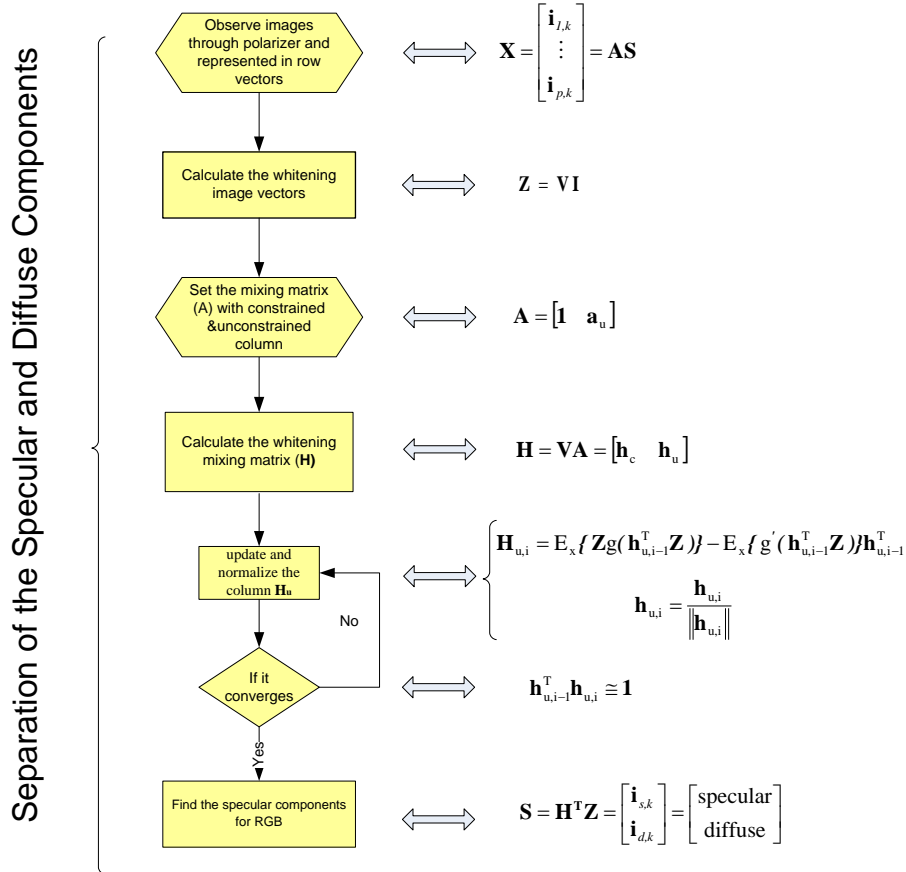


Figure 4-2 Separation of the specular and diffuse components for RGB images, using the spatially constrained FastICA algorithm.

As an alternative to the spatially constrained FastICA technique, the technique developed by Umeyama and Godin [28] is used for separating the specular and diffuse image in the proposed colour constancy framework in this thesis. To the author's knowledge, the technique developed by Umeyama and Godin in [28] is the only one which used blind signal separation for specular and diffuse components. In brief, this technique is also applied to two images produced by a polarizer. The estimation of the mixing matrix and the separated components in the technique reported in [28] is found by using singular value decomposition of the observed images with an arbitrary matrix. The task of the arbitrary matrix is to guide the separation process; different arbitrary matrices give different separated components. The arbitrary matrix values are controlled by one parameter varied in the range from 0 to π (in radians). The desired arbitrary matrix is the matrix that gives separated components which have minimum mutual information (for more detail about the technique see [28]).

4.3.3 Estimation of ISPD

The method proposed for estimating the ISPD in the second stage of the framework is based on the dichromatic reflection model, in order to utilize the specular image component to estimate the illumination. In the proposed method, the ISPD is estimated using an explicitly extracted specular component instead of mixed image components (i.e. composed of specular and diffuse components) which are used by other researchers [12], [18], [29]. Moreover, in the illumination estimation method used in the developed framework, the illumination is modelled by a linear model of basis functions. The estimation of the ISPD is achieved by calculating the linear combination coefficients of the illumination basis functions. The calculation of these coefficients is done by using the specular component, some illumination basis functions, and the spectral sensitivities of camera sensors, for each of the RGB image channels, as follows. The specular component of the RGB channels, which are represented by Equation (2-11), can be expressed as:

$$\mathbf{I}_{s,k} = w_{sn} (\mathbf{E} \cdot \mathbf{q}_k) \quad (4-11)$$

where (\cdot) is dot product operation, $k=R, G, B$ is the subscript of RGB imaging sensor response and w_{sn} is a modified specular geometrical scale factor, its value is in the interval (0-1) but for simplicity it is assumed to be 1. Note that the illumination spectral power distribution (\mathbf{E}) and the imaging sensor response (\mathbf{q}_k) are functions of wavelength which is omitted for simplicity of notation, in the rest of this chapter. Equation (4-11) can be formulated by modelling the illumination spectral power distribution as a linear model of basis functions using Equation (2-1) as:

$$\mathbf{I}_{s,k} = \sum_{i=1}^3 \varepsilon_i \mathbf{Q}_{k,i} \quad (4-12)$$

where

$$\mathbf{Q}_{k,i} = \mathbf{b}_i \cdot \mathbf{q}_k \quad (4-13)$$

where \mathbf{b}_i are the illumination basis functions, ε_i are the illumination basis function coefficients, $i=1, 2, 3$ is the subscript of the illumination basis functions. Note that the illumination basis functions are functions of wavelength which is omitted for simplicity of notation, in the rest of this chapter. It was reported in [30] that the last value of the index ‘ i ’

can be set to 3 because, if 'i' is greater than 3, the complexity of the estimation increases and also the accuracy of the estimation increases negligibly (See Section 2.2.1). Hence, the specular component for RGB channels can be represented in matrix form as:

$$\begin{bmatrix} \mathbf{I}_{s,R} \\ \mathbf{I}_{s,G} \\ \mathbf{I}_{s,B} \end{bmatrix} = \begin{bmatrix} Q_{R,1} & Q_{R,2} & Q_{R,3} \\ Q_{G,1} & Q_{G,2} & Q_{G,3} \\ Q_{B,1} & Q_{B,2} & Q_{B,3} \end{bmatrix} \begin{bmatrix} \varepsilon_1 \\ \varepsilon_2 \\ \varepsilon_3 \end{bmatrix} \quad (4-14)$$

Then by applying matrix inversion to the previous formula, the illumination basis function coefficients can be calculated as:

$$\begin{bmatrix} \varepsilon_1 \\ \varepsilon_2 \\ \varepsilon_3 \end{bmatrix} = \begin{bmatrix} Q_{R,1} & Q_{R,2} & Q_{R,3} \\ Q_{G,1} & Q_{G,2} & Q_{G,3} \\ Q_{B,1} & Q_{B,2} & Q_{B,3} \end{bmatrix}^{-1} \begin{bmatrix} \mathbf{I}_{s,R} \\ \mathbf{I}_{s,G} \\ \mathbf{I}_{s,B} \end{bmatrix} \quad (4-15)$$

In the illumination estimation method used within the implemented framework and used for all experiments in this thesis, the illumination is modelled by using Judd's basis functions which are shown in Figure 2-1. By using Judd's basis functions most of the daylight illumination can be reconstructed from a mean of daylight illuminations and two basis functions which are derived from a data set of daylight illuminations. Judd's basis functions are pertinent to be applied in several colour applications [30]. A further justification of the choice of these basis functions is given in Sections 2.2.1. The spectral range of these basis functions is from 400nm to 700 nm, with spectral step of 1nm as seen in Figure 2-1.

By using Judd's basis functions the specular component represented by Equation (4-11) is modified by

$$\mathbf{I}_{s,k} = (\mathbf{m} + \varepsilon_1 \mathbf{b}_1 + \varepsilon_2 \mathbf{b}_2) \cdot \mathbf{q}_k \quad (4-16)$$

where \mathbf{m} is the mean of the Judd's basis functions; \mathbf{b}_1 and \mathbf{b}_2 are first two Judd's basis functions; ε_1 and ε_2 are the coefficients of these basis functions. Note that the mean (\mathbf{m}), and the basis functions (\mathbf{b}_1 , \mathbf{b}_2) are functions of wavelength which is omitted for simplicity of notation. Equation (4-16) implies that two coefficients need to be estimated instead of three. The coefficients will be estimated from specular pixels. Pixels considered as predominantly specular will be selected by applying a suitable threshold to the specular component extracted from the input image by blind signal separation. The calculation of the coefficients is performed as follows.

$$\begin{bmatrix} \varepsilon_1 \\ \varepsilon_2 \end{bmatrix} = \begin{bmatrix} Q_{R,1} & Q_{R,2} \\ Q_{G,1} & Q_{G,2} \\ Q_{B,1} & Q_{B,2} \end{bmatrix}^+ \begin{bmatrix} \mathbf{I}_{s,R} - \mathbf{m} \cdot \mathbf{q}_R \\ \mathbf{I}_{s,G} - \mathbf{m} \cdot \mathbf{q}_G \\ \mathbf{I}_{s,B} - \mathbf{m} \cdot \mathbf{q}_B \end{bmatrix} \quad (4-17)$$

or

$$\begin{bmatrix} \varepsilon_1 \\ \varepsilon_2 \end{bmatrix} = \begin{bmatrix} Q_{R,1} & Q_{R,2} \\ Q_{G,1} & Q_{G,2} \end{bmatrix}^{-1} \begin{bmatrix} \mathbf{I}_{s,R} - \mathbf{m} \cdot \mathbf{q}_R \\ \mathbf{I}_{s,G} - \mathbf{m} \cdot \mathbf{q}_G \end{bmatrix}$$

where

$$Q_{k,1} = \mathbf{b}_1 \cdot \mathbf{q}_k, \quad Q_{k,2} = \mathbf{b}_2 \cdot \mathbf{q}_k, \quad (4-18)$$

(+) and (-) respectively represent pseudo-inverse and inverse operation. The estimation of the coefficients can be achieved using the pseudo-inverse of the $Q_{k,i}$ matrix for the R, G and B colour components, or the inverse $Q_{k,i}$ matrix for (any two of R, G, and B) colour components. Then two coefficients ($\varepsilon_1, \varepsilon_2$) from each selected specular pixel are calculated using Equation (4-17). The coefficient ' ε_1 ' from all selected specular pixels are averaged; similarly ' ε_2 ' is also averaged. The spectral power distribution of the illumination can then be calculated using the mean and the other two illumination basis functions, together with the estimated average coefficients, in Equation (4-19).

$$\mathbf{E} = \mathbf{m} + \varepsilon_{av1} \mathbf{b}_1 + \varepsilon_{av2} \mathbf{b}_2$$

where

$$\varepsilon_{av1} = \text{mean}(\varepsilon_{1,f}), \varepsilon_{av2} = \text{mean}(\varepsilon_{2,f}) \quad (4-19)$$

f is the number of specular pixels used to calculate the average coefficients.

The derivation of the full spectrum of the illumination from only 3 or 2 values (i.e. R, G, and B or any two of R, G, and B) per pixel is thus achieved with aid of the basis functions. The basis functions are considered as additional information in order to achieve the estimation of more than 3 values from only 3 or 2 input values (under the constraints of the estimation problem). The flowchart in Figure 4-3 summarises the illumination estimation method used within the implemented framework.

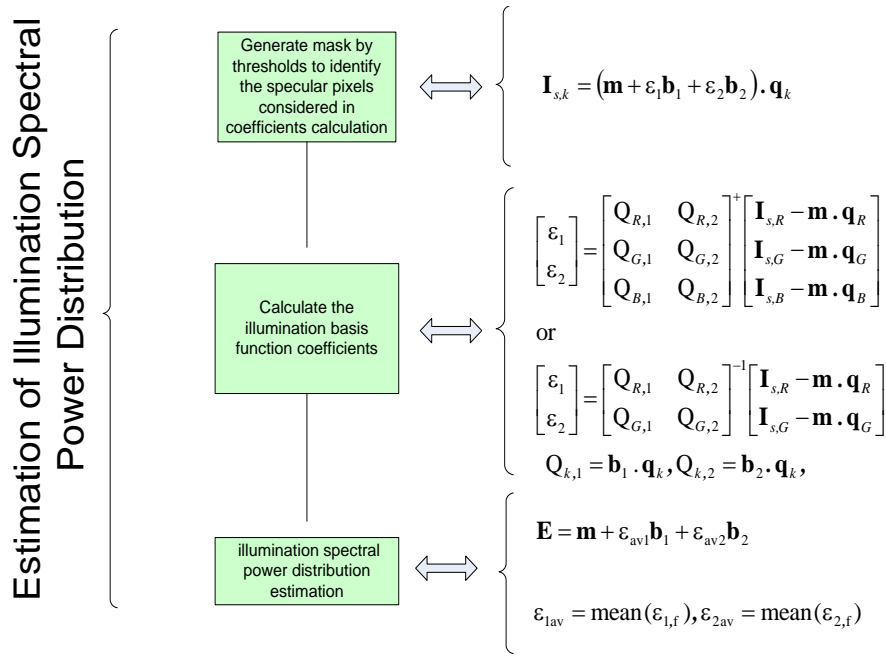


Figure 4-3 Flowchart of the illumination estimation method.

4.3.4 Estimation of Surface Spectral Reflectance

The proposed method used for estimating the surface spectral reflectance in the third stage of the developed framework is based on a linear mapping of the pixels values of the diffuse image component (see Section 2.5.2). In the proposed method, the surface spectral reflectance is estimated using an explicitly extracted diffuse component, instead of mixed image components which are used by other researchers [26]. Moreover, in the surface reflectance estimation method used in the implemented framework, the surface reflectance is modelled by a linear model of basis functions.

The estimation of the surface spectral reflectance is performed by calculating the coefficients of the surface reflectance basis functions. The calculation of these coefficients is done by using the RGB diffuse components, the illumination spectral power distribution, the surface reflectance basis functions, and camera sensor sensitivities, for each of the RGB image channels, as follows. The diffuse component of the RGB channels, which are represented by Equation (2-10), can be formulated

$$\mathbf{I}_{d,k} = \mathbf{w}_d ((\mathbf{S} \mathbf{E}) \cdot \mathbf{q}_k) \quad (4-20)$$

where w_d is diffuse geometrical scale and its value is in the interval (0-1) but for simplicity it is assumed to be 1. The surface spectral reflectance (\mathbf{S}) is a function of wavelength which is omitted for simplicity of notation, in the rest of this chapter. Equation (4-20) can be formulated by modelling the surface reflectance as a linear combination of basis functions using Equation (2-5) as

$$\mathbf{I}_{d,k} = \sum_{j=1}^3 \varphi_j P_{k,j} \quad (4-21)$$

where

$$P_{k,j} = (\boldsymbol{\psi}_j \mathbf{E}) \cdot \mathbf{q}_k \quad (4-22)$$

φ_j are the reflectance basis function coefficients, $j=1, 2, 3$ is the subscript of the reflectance basis functions. $\boldsymbol{\psi}_j$ represents the surface reflectance basis functions. The surface reflectance basis functions are functions of wavelength which is omitted for simplicity of notation, in the rest of this chapter. It was reported in [33] that the last value of the index 'j' can be set to 3 because, if 'j' is greater than 3, the complexity of the estimation will increase with negligible decrease of the average error of the estimation (see Section 2.2.2). The diffuse components for RGB channels can be represented in matrix form as

$$\begin{bmatrix} \mathbf{I}_{d,R} \\ \mathbf{I}_{d,G} \\ \mathbf{I}_{d,B} \end{bmatrix} = \begin{bmatrix} \mathbf{P}_{R,1} & \mathbf{P}_{R,2} & \mathbf{P}_{R,3} \\ \mathbf{P}_{G,1} & \mathbf{P}_{G,2} & \mathbf{P}_{G,3} \\ \mathbf{P}_{B,1} & \mathbf{P}_{B,2} & \mathbf{P}_{B,3} \end{bmatrix} \begin{bmatrix} \varphi_1 \\ \varphi_2 \\ \varphi_3 \end{bmatrix} \quad (4-23)$$

Then by applying matrix inversion to the previous formula, the coefficient for each surface reflectance basis function can be calculated. Hence, the coefficients of the surface reflectance basis functions are found using the following equation.

$$\begin{bmatrix} \varphi_1 \\ \varphi_2 \\ \varphi_3 \end{bmatrix} = \begin{bmatrix} \mathbf{P}_{R,1} & \mathbf{P}_{R,2} & \mathbf{P}_{R,3} \\ \mathbf{P}_{G,1} & \mathbf{P}_{G,2} & \mathbf{P}_{G,3} \\ \mathbf{P}_{B,1} & \mathbf{P}_{B,2} & \mathbf{P}_{B,3} \end{bmatrix}^{-1} \begin{bmatrix} \mathbf{I}_{d,R} \\ \mathbf{I}_{d,G} \\ \mathbf{I}_{d,B} \end{bmatrix} \quad (4-24)$$

Then, after the surface reflectance basis function coefficients are calculated, the spectral surface reflectance is calculated using the linear model of surface reflectance which is represented by Equation (2-5). The flowchart in Figure 4-4 summarises the surface reflectance estimation method which is used within the implemented framework.

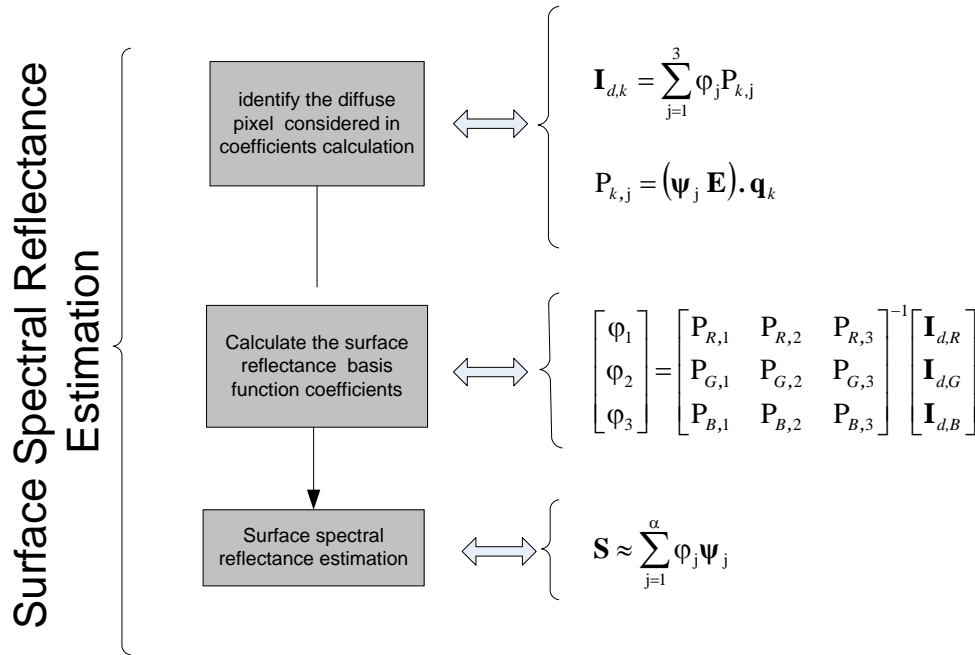


Figure 4-4 Flowchart of the surface reflectance estimation method

4.4 Summary

This chapter presents the colour constancy framework developed in the research reported in the thesis. The framework consists of 3 stages; it is based on the combination of a blind signal separation technique with a physical model of image formation (assumed to be the dichromatic model).

In the first stage of the framework, the spatially constrained FastICA technique and the technique developed by Umeyama and Godin [28] are used as individual alternatives to separate the input images into specular and diffuse components. In the second stage of the framework, the proposed illumination estimation method is based on the dichromatic reflection model, in order to use the explicitly extracted specular image component to estimate the spectral power distribution of the illumination. In the third stage of the framework, the proposed method for estimating surface spectral reflectance is based on a linear mapping of the diffuse image component pixels values (Section 2.5.2).

The next chapter presents the experimental investigation of the second stage of the colour constancy framework; this stage performs the estimation of the spectral power distribution of the illumination. Moreover, this investigation assesses how two different separation techniques, which are used in first stage of the framework for extracting the specular component, affect the estimation accuracy of the ISPD.

5

Experimental Investigation of the Estimation of the Illumination Spectral Power Distribution

5.1 Introduction

The aim of this chapter is to investigate and explore how the proposed method for estimating the illumination spectral power distribution (ISPD) in the second stage of the developed framework performs in terms of the goodness-of-fit coefficient (GFC). The reason for investigating the second stage separately is to explore how the different separation results (i.e. achieved in first stage of the developed framework) and other factors (i.e the thresholding method used for selecting the significantly specular pixels and the chosen illumination basis functions) affect the performance of the illumination estimation method in terms of GFC. The experimental investigation in this chapter is conducted by estimating ISPD for different light sources with different colour temperatures. Then the estimated ISPD for these different light sources are compared either with manufacturer's specifications or the measured ISPD of these light sources. This chapter starts with a section on the creation of a test data set. Then it presents a section on the performance evaluation for the ISPD estimation; the section includes a description of the experimental method, and the presentation and discussion of the results. The chapter concludes with a summary.

5.2 Creation of the Data set

To the knowledge of the author, no other public domain image data set is available which consists of pairs of images of the same scene captured using a polarizer (as required by the ICA model used for signal separation) and a camera with known sensor sensitivity (as

required for estimating parameters of the physical model). Hence the need to create a data set which can be used to test the framework is required.

The equipment used by the author to create the data set of RGB colour images are two artificial light sources, a CCD camera, a light polarizer, and objects of different materials (see Appendix B). The two light sources used to create the author's image data set have two types of lamps: a 55W Kino KF55 Compact and a 55W Kino KF29 Compact [180]. The colour temperatures of these lamps are 5500 and 2900 Kelvin, respectively. There are two reasons for using these two lamps. The first reason is to determine the effect of the different light sources, which emit different colours of illumination, on the performance of the developed framework. Second, the spectral distribution curves for these lamps have been released by the respective manufacturer [180]; these curves will be used for the evaluation of the illumination estimation stage within the developed framework (see Sections 5.3.2.1 and 5.3.2.2).

The type of camera which was used for creating the data set is a FireWire camera (DFK 21F04) with known sensor characteristics (see Section 2.2.5) [40]. Gamma correction was set to 'off' for all captured images in the data set. This was done to ensure the linearity between the flux of the incident light and the camera output. Furthermore, a linear polarizer (1.25 inch-PR032-30.5) was used to create the data set. The images in the data set were captured for different scenes consisting of various objects of different materials such as plastic, ceramic and fruits. These types of materials were selected because their atomic structure allows specular and diffuse reflections (see Section 2.2.3). These two types of reflection are required for the validation of the developed framework. Particularly, images without a specular component are not considered for the validation of illumination estimation and consequently surface reflectance estimation.

The data set generated by the author consists of two sets of image pairs of the same object captured under two artificial light sources with different colour temperature (2900 K and 5500 K). Each pair contains two images for the same scene but with different polarization angles. In order to capture the two images of different polarization angle, the two orientation angles, which give an amount of specular reflection between its maximum and minimum, are chosen. The reason for creating pairs of images for the same scene with different polarization angles is that two images are required to separate two components, which is one of the assumptions of the ICA model (see Section 3.3). Appendix B shows some examples of the created data set and the corresponding results of the separation of diffuse and specular components, using the

two ICA techniques (i.e the spatially constrained FastICA technique and the technique developed by Umeyama and Godin [28]). The pixel value range for each R, G and B colour component of the images is between 0 and 1, for all experiments throughout this thesis.

The images are stored in uncompressed raw data format, using a double precision (32-bit) number representation of the pixel value. Compression is avoided in order to preserve the full information content.

5.3 Performance Evaluation of the ISPD Estimation

In this section, the performance of the ISPD estimation (second stage of the developed colour constancy framework) is evaluated in four experiments. The aims of these experiments are to investigate the performance of the proposed method for estimating ISPD and to explore the factors which affect its estimation performance in terms of GFC and error values (formulas are given in Appendix F), within the colour constancy framework. The ISPD is estimated using the specular components of images which are captured under artificial light sources with colour temperature of 5500 K and 2900 K, respectively in Experiment 1 and Experiment 2. The estimated illumination is then compared with the manufacturer's specifications of the artificial light source. Experiment 3 compares the illumination estimated using an explicit specular image component and the illumination estimated using mixed image components (where each pixel is a blend of a specular component and a diffuse component). Experiment 4 uses a public-domain set of hyperspectral images (i.e. Foster et al's data set [181]); the illumination is estimated using mixed image components captured under different natural day light sources with different colour temperatures. Experiment 4 is conducted to validate the proposed method for estimating ISPD of different light sources. The estimated illumination is then compared with the illumination measurements provided with the hyperspectral images by Foster et al [181]. In Experiment 4, the ISPD is estimated without utilizing the output of the first stage. In the following sub-sections, the experimental settings are stated, followed by the experimental procedure, results and a discussion.

5.3.1 The Experimental Setting

This section discusses the experimental setting for all experiments in this chapter including the data set, camera sensor sensitivity, thresholding technique, normalization process, matrix inversion operation, nonlinear function (i.e. used in SCFICA separation technique) and statistical significance test which have been used.

1) Experiments 1, 2, and 3 use the image data set, described in Section 5.2. The reason for using this data set is that it is suitable for applying blind signal separation (the first stage of the framework) in order to extract the specular component, which is used in the estimation of the ISPD. Foster et al's data set is used in Experiment 4, it contains 8 images of various scenes captured under different natural day light sources with different colour temperatures [181]. The reason for using Foster et al's data set in this experiment is the availability of the measured ISPD for each image, which can be used to evaluate the proposed method for estimating ISPD.

2) The manufacturer sensor spectral sensitivity curves which are used in Experiments 1, 2, 3 and 4 are shown in Figure 2-3 [40]. The curves have spectral range from 400 nm to 700nm with spectral step of 1nm. These curves represent the sensor responses of the camera which captured the image data set used in Experiments 1, 2 and 3. However, they are not the sensor responses of the camera used to capture the data set used in Experiment 4. The sensor response curves of the camera used to capture Foster et al's data set were not available.

3) In Experiments 1 and 2, the estimation of ISPD is achieved using selected pixels of the specular component which are considered as predominantly specular. The illumination estimation depends upon the selection of an optimal threshold for identifying these pixels. The threshold is used to generate the mask for extracting the significantly specular pixels, which are assumed to contain most of the characteristics of the light source. Although the automatic selection of the threshold is not the focus of this research, an automatic selection process has been tested based upon two methods (maximum likelihood and intermodes threshold [182]) from which the maximum value of the two threshold values is chosen. However, the automatic selection of the threshold does not provide a suitable threshold value for all the test images. In these cases, an empirical threshold determination is used whereby the automatic threshold is increased or decreased until the estimated illumination curve is the best approximation of the measured illumination curve. In Experiments 3 and 4, the empirical threshold determination is used directly (without an automatic threshold selection pass) to identify the threshold which gives the best illumination estimation. In Experiment 4, the threshold is used to identify the high intensity pixels which are assumed to be mostly composed of specular reflection, with a negligible amount of diffuse reflection.

4) In Experiments 1, 2, 3 and 4, the estimation of the illumination coefficients is obtained from the normalised version of Equation (4-16); the normalisation makes the ranges for both sides of the equation between 0 and 1. The formula used for normalisation is expressed as:

$$\mathbf{IM}_{s,k} = \frac{(\mathbf{m} + \varepsilon_1 \mathbf{b}_1 + \varepsilon_2 \mathbf{b}_2) \cdot \mathbf{q}_k}{\max(\mathbf{E} \cdot \mathbf{q}_k)} \quad (5-1)$$

The left hand side of Equation (5-1) represents the specular image component. This component is normalised (0-1) assuming that the maximum value of $(I_{s,R}, I_{s,G}, I_{s,B})$ represents the pixel reflecting the highest illumination intensity in the image. The formula used for normalisation is expressed as:

$$\mathbf{IM}_{s,k} = \frac{(I_{s,k} - \min(I_{s,R}, I_{s,G}, I_{s,B}))}{\max(I_{s,R}, I_{s,G}, I_{s,B}) - \min(I_{s,R}, I_{s,G}, I_{s,B})}, k = R, G, B \quad (5-2)$$

The right handside of Equation (5-1) represents the specular component estimated using the dichromatic image formation model and normalised against the maximum of the camera response for different daylight sources, where $\max(\mathbf{E} \cdot \mathbf{q}_k)$ is a normalised factor which is represented as:

$$\max(\mathbf{E} \cdot \mathbf{q}_k) = \max(\mathbf{E}_1 \cdot \mathbf{q}_k, \dots, \mathbf{E}_5 \cdot \mathbf{q}_k) \quad (5-3)$$

where $\mathbf{E}_1, \dots, \mathbf{E}_5$ are the ISPD for light sources with colour temperatures of 4800 K, 5500 K, 6500 K, 7500 K and 10000 K, respectively. The normalisation factor represents the maximum value of the dot product of the camera sensor responses and different natural day light sources with different colour temperatures. The reason for using only these day light sources with these colour temperatures is that these are the light sources with known coefficients as provided by Judd[31]. Hence, by using these coefficients with the mean and the two basis functions, the spectral characteristics of these light sources are recovered and used in the normalisation as in Equation (5-3). Moreover, in line with other researchers [31], the estimated illumination spectrum is normalised by dividing its values by the value at the wavelength of 560 nm.

5) In all experiments in this chapter, it was noticed that using the inverse operation gives better estimation results than using pseudo-inverse operation (Section 4.3.3, Equation (4-17)). There is no clear reason for this observation. Moreover, no difference was observed between

the estimation results obtained from any pair of R, G, and B colour components. In all experiments in this chapter the inverse of the $\mathbf{Q}_{k,i}$ matrix for the R and G colour components is used to estimate the illumination coefficients.

6) For applying SCFICA separation technique, all nonlinear functions (g) (Section 4.3.2, Equation (4-8)) are tested but there is no significant difference in the separation results. For all experiments in this thesis $g(u) = u^3$ is considered.

7) The results of Experiments 1, 2 and 3 have been tested to be statistically significant at confidence level of 95% using the independent two-sample t-test (Appendix E).

The implementation of the software used in all experiments in this thesis is done by using Matlab version 7.2 and the Image Processing Toolbox.

5.3.2 Experimental Procedure, Results, and Discussion

This section consists of the procedure, results and discussion for each individual experiment.

5.3.2.1 Experiment 1: Estimation of ISPD from the specular component of images captured under an artificial day light source with colour temperature of 5500 K.

a) Procedure

The aim of this experiment is to investigate how the proposed illumination estimation method, used within the developed colour constancy framework, performs for estimating the illumination of the artificial day light source with colour temperature of 5500 K, when the method is coupled to one of two alternative blind signal separation techniques. These techniques are the Spatially Constrained FastICA (SCFICA) and the technique developed by Umeyama and Godin (UGICA) in [28], each separation technique provided a set of RGB specular components.

Each set of RGB specular components corresponding to the separation technique, is used separately to estimate the illumination spectral power distribution. Moreover, for each set, a different threshold has been selected to generate a pixel mask used to identify the significantly specular pixels. These pixels are then used to estimate the coefficients of the illumination basis functions. In order to determine the effect of the separation techniques and the pixel masks on the illumination estimation accuracy, the pixel mask generated for each set of RGB specular components is used on both sets of RGB specular components (i.e. achieved using

blind signal separation techniques (SCFICA and UGICA in [28])). Four different significant pixel sets have been constructed from the two pixel masks (Mask-UGICA and Mask-SCFICA) and two sets of RGB specular components (Specular-SCFICA, Specular-UGICA). These four sets of significantly specular pixels are used to estimate four possible illuminations.

Moreover, to observe the effect of the automatic and empirical threshold, this experiment is repeated twice for the two different thresholds. The GFC measurement and other errors (Root Mean Square (RMS), median, mean, and angular error) measurements, which are commonly used by other researchers [3], [183], [184], are calculated between the four possible illumination estimation and the manufacturer's specifications. The advantage of the GFC measurement over the other errors measurements is that it is not affected by amplitude scaling [184]. Because of this advantage, it has been selected as base measurement to be used for all comparison in this thesis. GFC is a measure of the degree of similarity between an estimated and a known reference. The value of GFC ranges between 0 and 1; a higher value representing higher degree of similarity.

b) Results and discussion

The results for the four possible illumination estimations of artificial day light source with colour temperature of 5500 K using automatic and empirical threshold are shown in Figure 5-1 and Figure 5-2. These figures represent illumination estimation for one example of the tested images. Appendix C (Figures C.1 to C.6) shows the illumination estimation for more examples. Figures C.7 to C.14 in Appendix C illustrate the selected pixels used for illumination estimation, by showing the two sets of RGB specular components and the corresponding mask using the automatic and empirical threshold for all tested images in this experiment. The automatic and corresponding empirical threshold values that are selected for each set of RGB specular components of each test image are shown in Table C.1 in Appendix C. The values of the GFC for automatic and empirical threshold for all tested images in this experiment are summarised in Table 5-1, while the other error measurements are shown in Appendix C (Tables C.2 to C.5). The average and standard deviation of the GFC values and the error measurements using two types of thresholds (i.e. automatic and empirical) are calculated and summarised in Table 5-2. These calculations are based on the values found in Table 5-1 and Tables C.2 to C.5 in Appendix C.

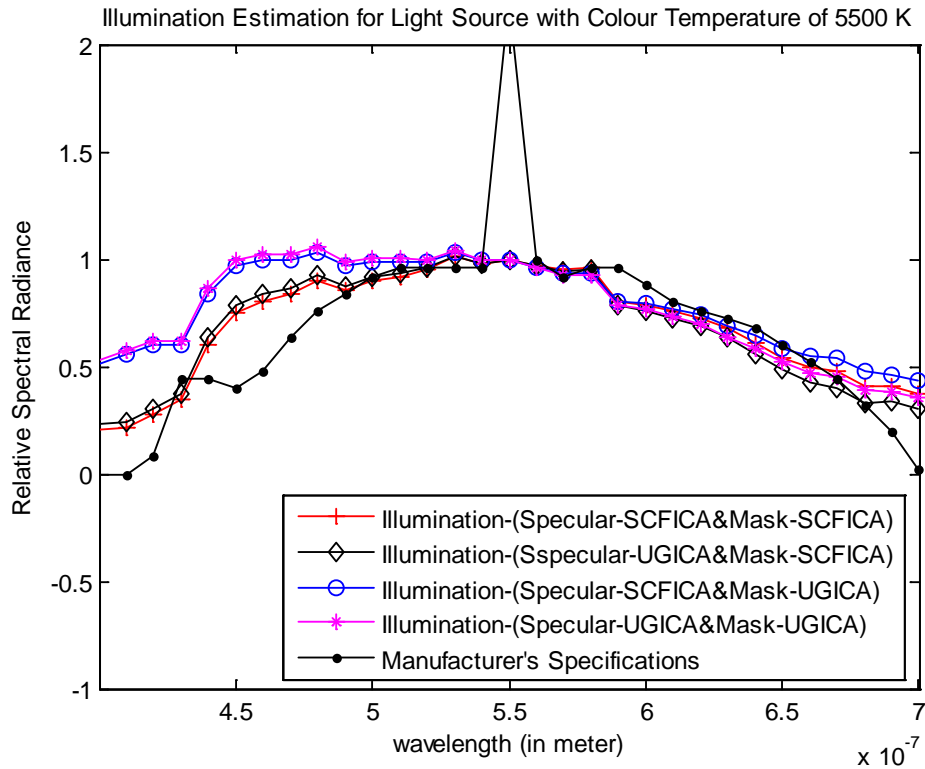


Figure 5-1 The four possible illumination estimations using significantly specular pixels selected from the two sets of the specular components (i.e. extracted using the SCFICA and UGICA techniques) using the two corresponding masks (mask-SCFICA and mask-UGICA) interchangeable with each of the two sets, after *automatic* thresholding for a plastic blue ring illuminated with a light source of colour temperature of 5500 K.

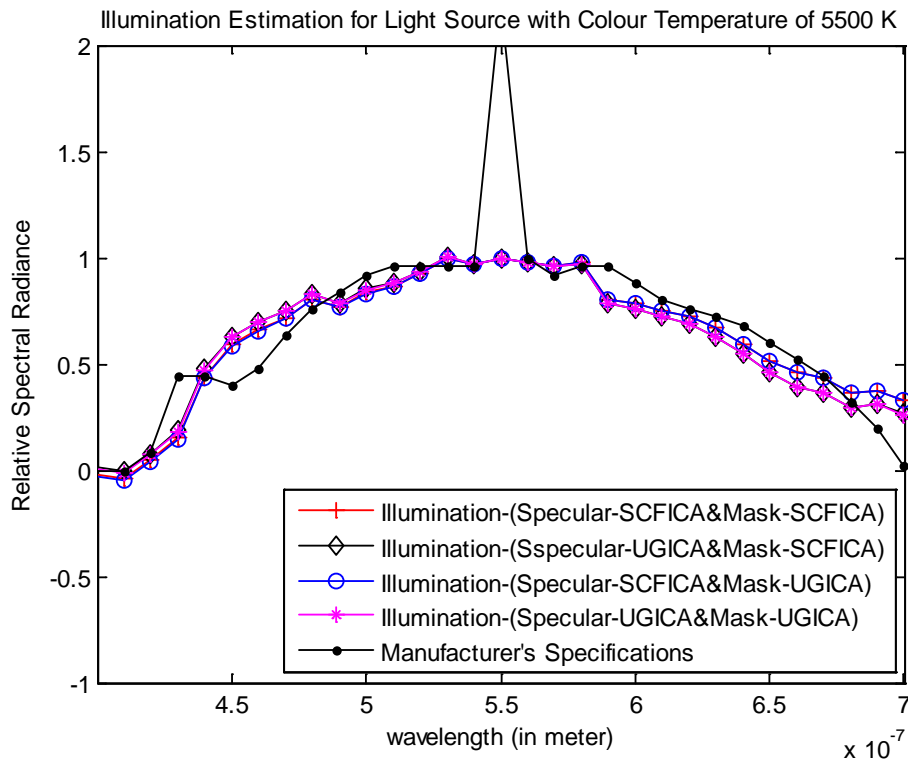


Figure 5-2 The four possible illumination estimations using significantly specular pixels selected from the two sets of the specular components (i.e. extracted using SCFICA and UGICA techniques) using the two corresponding masks (mask-SCFICA and mask-UGICA) interchangeable with each of the two sets, after *empirical* thresholding for a plastic blue ring illuminated with a light source of colour temperature of 5500 K.

In Figure 5-1 and Figure 5-2, it is found that the illumination estimation is achieved with some difference in spectral characteristics compared with manufacturer’s specification. Table 5-2 shows that the illumination is estimated with an average GFC value of 0.9830 when the empirical threshold is used (i.e. to select significantly specular pixels which are used in the estimation) and with a GFC value of 0.9447 when the automatic threshold is used. This means that the illumination estimation accuracy is improved by 3.8% when the empirical threshold is used instead of the automatic threshold. This improvement is statistically significant, with confidence level of 95%. The statistical test is based on the GFC values given in Table 5-1 and the results of the test are reported in Appendix E, Table E.1.

Table 5-1 Results of the experimental assessment of the effect of: the extraction of the specular image component, and the material of the reflecting object. The table entries represent the similarity between the illumination spectral power distribution estimated in the experiment and the distribution provided by the manufacturer of the light source with colour temperature of 5500 K. The similarity has been calculated using GFC.

Illumination source	Extraction of specular image component		Material of the reflecting object				
	Signal separation	Selection of significantly specular pixels	Plastic blue ring	Ceramic violet cup	Plastic green ring	Red apple	
Colour temperature: 5500 K	Spatially constrained FastICA Technique (SCFICA)	Automatic selection	Mask-SCFICA	0.9758	0.9824	0.8836	0.9739
			Mask-UGICA	0.9480	0.9796	0.9434	0.9688
		Empirical selection	Mask-SCFICA	0.9880	0.9839	0.9845	0.9879
			Mask-UGICA	0.9879	0.9829	0.9676	0.9759
	Umeyama and Godin ICA Techniques (UGICA)	Automatic selection	Mask-SCFICA	0.9723	0.9847	0.7545	0.9877
			Mask-UGICA	0.9435	0.9847	0.8462	0.9865
		Empirical selection	Mask-SCFICA	0.9874	0.9872	0.9653	0.9786
			Mask-UGICA	0.9874	0.9878	0.9880	0.9880

Table 5-2 The average and the standard deviation of GFC and error measurements using automatic and empirical thresholds for artificial day light source with colour temperature of 5500 K.

		GFC	RMS error	Median error	Mean error	Angular error (in degree)
Automatic threshold	Average	0.9447	21.58×10^{-2}	4.26×10^{-2}	10.12×10^{-2}	7.87
	Standard deviation	± 0.0644	$\pm 11.02 \times 10^{-2}$	$\pm 6.45 \times 10^{-2}$	$\pm 8.97 \times 10^{-2}$	± 5.88
Empirical threshold	Average	0.9830	13.15×10^{-2}	3.09×10^{-2}	3.61×10^{-2}	2.70
	Standard deviation	± 0.0074	$\pm 2.96 \times 10^{-2}$	$\pm 2.40 \times 10^{-2}$	$\pm 3.80 \times 10^{-2}$	± 1.67

The results show that there is no statistically significant difference in the estimation accuracy of the ISPD using the specular components extracted by each of the two blind signal separation techniques (SCFICA and UGICA in [28]) compared to the manufacturer’s specifications. This statement is supported by the statistical significance test based on the

GFC values which correspond to the two blind signal separation techniques (Table 5-1). The results of the statistical significance test are reported in Appendix E (Table E.2).

As it is observed in all figures in this experiment and also in Experiment 2 (Section 5.3.2.2), the manufacturer's illumination specification curves include some spikes. To the knowledge of the author, these spikes are due to the nature of materials used to produce this type of artificial light source [185]. These spikes cannot be achieved in the estimated illumination. This is because the basis functions used in the estimation are smooth and generated from natural day light sources samples. The peak values of these spikes reach maximum amplitude of 2.25 and 5.5 for the two lights (i.e with with colour temperature of 5500 K and 2900 K respectively) as shown in this experiment (Figure 5-1 and Figure 5-2) and in Experiment 2 (Figure 5-3 and Figure 5-4).

5.3.2.2 Experiment 2: Estimation of ISPD from the specular component of images captured under an artificial light source with colour temperature of 2900 K.

a) Procedure

The aim of this experiment is to investigate how the proposed illumination estimation method, used within the colour constancy framework, performs for estimating the illumination of the artificial source with colour temperature of 2900 K, when the estimation is coupled to two alternative blind signal separation techniques. In Experiment 2, the illumination is estimated using the specular components of the pair of images captured under an artificial light source with colour temperature of 2900 K. The same steps and calculation used in Experiment 1 (Section 5.3.2.1) are followed in Experiment 2.

b) Results and discussion

The results for the four possible illumination estimations of artificial light source with colour temperature of 2900 K using automatic and empirical threshold are shown in Figure 5-3 and Figure 5-4. These figures show the illumination estimation results for one example of the tested images (illumination estimation results for more examples are shown in Appendix C (Figures C.15 to C.20)). Figures C.21 to C.28 in Appendix C demonstrate the selected pixels used for illumination estimation by showing the two sets of RGB specular components and the corresponding mask using the automatic and empirical threshold for all tested images in this experiment. The automatic and corresponding empirical threshold values which are selected for each set of RGB specular components of each test image are shown in Table C.6 (Appendix C). The values of the GFC for automatic and empirical threshold for all tested

images in this experiment are summarised in Table 5-3 while the other error measurements are shown in Appendix C (Tables C.7 to C.10). The average and standard deviation of the GFC values and the error measurements using two types of thresholds (i.e. automatic and empirical) are calculated and summarised in Table 5-4. These calculations are based on the values found in Table 5-3 and Tables C.7 to C.10 in Appendix C.

The results in Table 5-4 show that the illumination is estimated with an average GFC value of 0.9215 when the empirical threshold is used (i.e. to select significantly specular pixels, which are used in the estimation) and with an average GFC value 0.8921 when the automatic threshold is used. This means that the illumination estimation accuracy is improved by 2.9% when the empirical threshold is used instead of the automatic threshold. The observed improvement is statistically significant with a confidence level of 95%. The statistical test is based on the GFC values given in Table 5-3 and the results of the test are reported in (Appendix E, Table E.3).

Although there is an improvement in the results by the use of an empirical threshold, the curves of the estimated illumination are not close to the manufacturer's specifications curve as compared with the results from Experiment 1 (Section 5.3.2.1). In Experiment 2, the average GFC and the average of error measurements (Table 5-4) are respectively less and greater than the corresponding values found in Experiment 1 (Section 5.3.2.1, Table 5-2). The reason for the performance degradation observed in Experiment 2, compared to Experiment 1, can possibly be deduced from the use of Judd's basis functions to estimate the illumination of the artificial light source with colour temperature of 2900 K. More specifically, these illumination basis functions are not able to capture the characteristics of this light source. This is because these basis functions are generated from daylight source samples with colour temperatures, which do not include the colour temperature of the light source used in this experiment. Therefore, it is concluded that the performance of the illumination estimation method measured in terms of GFC and curve-difference error can possibly be affected by the selection of suitable illumination basis functions.

Compared to the manufacturer's specifications, the results show that there is no statistically significant difference in the estimation accuracy of the ISPD using the specular components extracted by each of the two blind separation techniques (SCFICA and UGICA in [28]). This statement is supported by the statistical significance test based on the GFC values which correspond to the two blind signal separation techniques (Table 5-3). The results of the statistical significance test are reported in Appendix E (Table E.4).

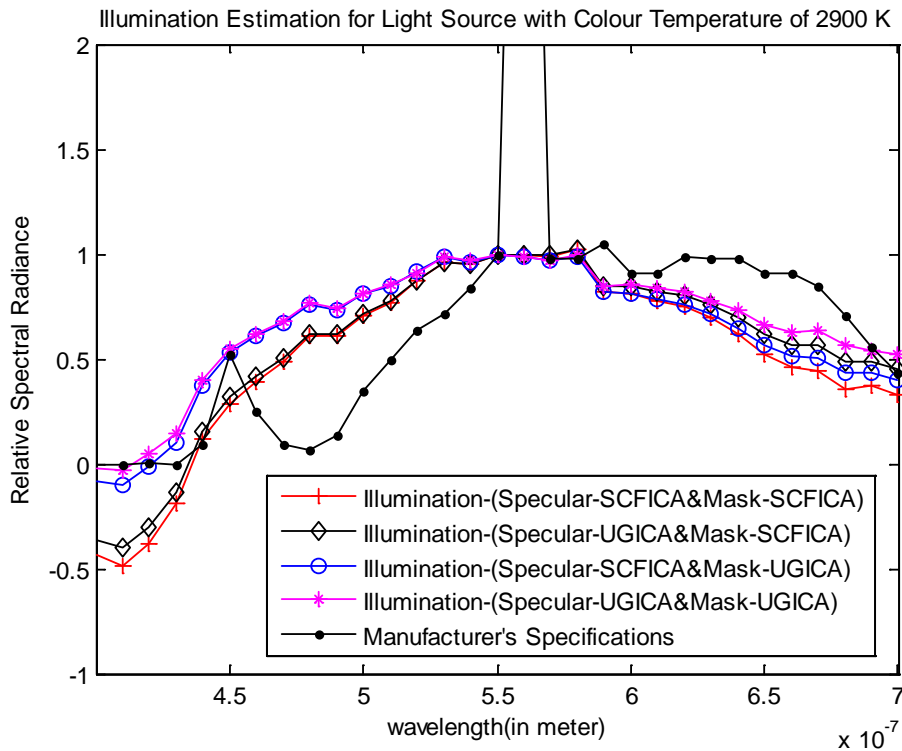


Figure 5-3 The four possible illumination estimations using significant specular pixels selected from the two sets of the specular components (i.e. extracted using SCFICA and UGICA techniques) using the two corresponding masks (mask-SCFICA and mask-UGICA) interchangeable with each of the two sets, after *automatic* thresholding for a plastic blue ring illuminated with light source of colour temperature of 2900 K.

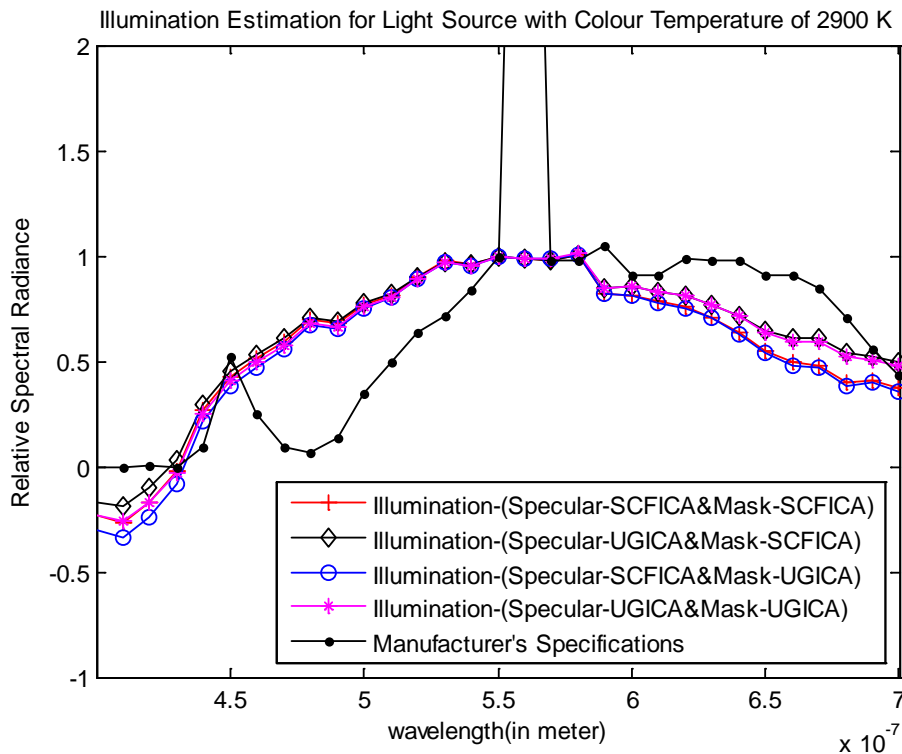


Figure 5-4 The four possible illumination estimations using significant specular pixels selected from the two sets of the specular components (i.e. extracted using SCFICA and UGICA techniques) using the two corresponding masks (mask-SCFICA and mask-UGICA) interchangeable with each of the two sets, after *empirical* thresholding for a plastic blue ring illuminated with a light source of colour temperature of 2900 K.

Table 5-3 Results of the experimental assessment of the effect of: the extraction of the specular image component, and the material of the reflecting object. The table entries represent the similarity between the illumination spectral power distribution estimated in the experiment and the distribution provided by the manufacturer of the light source with colour temperature of 2900 K. The similarity has been calculated using GFC.

Illumination source	Extraction of specular image component		Material of the reflecting object				
	Signal separation	Selection of significantly specular pixels	Plastic blue ring	Ceramic violet cup	Plastic green ring	Green apple	
Colour temperature: 2900 K	Spatially constrained FastICA Technique (SCFICA)	Automatic selection	Mask-SCFICA	0.9060	0.9105	0.8557	0.8785
			Mask-UGICA	0.9091	0.9371	0.8483	0.8649
		Empirical selection	Mask-SCFICA	0.9139	0.9402	0.9010	0.9006
			Mask-UGICA	0.9131	0.9416	0.9109	0.9122
	Umeyama and Godin ICA Techniques (UGICA)	Automatic selection	Mask-SCFICA	0.9310	0.9001	0.8749	0.8750
			Mask-UGICA	0.9259	0.9277	0.8676	0.8614
		Empirical selection	Mask-SCFICA	0.9332	0.9309	0.9185	0.9131
			Mask-UGICA	0.9341	0.9323	0.9282	0.9201

Table 5-4 The average and standard deviation of the GFC and error measurements using automatic and empirical thresholds for an artificial light source with colour temperature of 2900 K.

		GFC	RMS error	Median error	Mean error	Angular error (in degree)
Automatic threshold	Average	0.8921	34.06×10^{-2}	8.78×10^{-2}	15.83×10^{-2}	18.19
	Standard deviation	± 0.0296	$\pm 6.77 \times 10^{-2}$	$\pm 6.16 \times 10^{-2}$	$\pm 10.72 \times 10^{-2}$	± 5.73
Empirical threshold	Average	0.9215	26.89×10^{-2}	3.42×10^{-2}	5.58×10^{-2}	13.87
	Standard deviation	± 0.0131	$\pm 1.35 \times 10^{-2}$	$\pm 2.65 \times 10^{-2}$	$\pm 3.54 \times 10^{-2}$	± 1.49

5.3.2.3 Experiment 3: A comparison between the illumination estimation accuracy achieved by using the specular image component and the mixed image components.

a) Procedure

The aim of this experiment is to measure the improvement in the illumination estimation accuracy arising from using an explicitly extracted specular image component compared to using the original image which can be seen as a mixture of specular and diffuse image components.

This experiment uses the same images and the same empirical threshold values (i.e. used to generate pixels masks (Mask-SCFICA and Mask-UGICA), which were used in Experiment 1. In Experiment 3, the illumination is estimated from the specular component of the significantly specular pixels and from the corresponding mixed pixels (i.e. high intensity pixels) of the polarised Image 2 (or mixed image components). The reason for using polarised

Image 2 instead of Image 1 is that polarised Image 2 consists of higher intensity pixels (i.e. more information about the characteristics of the illumination) than image1.

b) Results and discussion

The results of the illumination estimation using the two alternative sets of the RGB specular components (i.e. achieved using the blind separation techniques SCFICA and UGICA in [28]) and polarised Image 2 are shown in Figure 5-5 and Figure 5-6. These figures show the illumination estimation results for two examples of the tested images (illumination estimation results for more examples are shown in Appendix C (Figure C.29 and Figure C.30)).

Compared to the manufacturer's specification, the GFC values of the estimated illumination (i.e using specular component and mixed image component) for all tested images in this experiment are summarised in Table 5-5, while the others error measurements are shown in Appendix C (Tables C.2 to C.5). The average and the standard deviation of the GFC values and the error measurements for illumination estimation (i.e using specular component and mixed image component) are calculated and summarised in Table 5-6. These calculations are based on the values found in Table 5-5 and Tables C.2 to C.5 in Appendix C.

The results show that there is a statistically significant difference between the illumination estimation accuracy (measured using the GFC) arising from using the specular image component and the accuracy obtained for mixed image components (Table 5-6). This statement is supported by the t-test for statistical significance applied to the GFC values shown in Table 5-5. The results of the statistical significance test are reported in Appendix E (Table E.5).

To conclude, the average GFC value of the estimated illumination is significantly improved by 2.9% when the specular component is used instead of mixed image components.

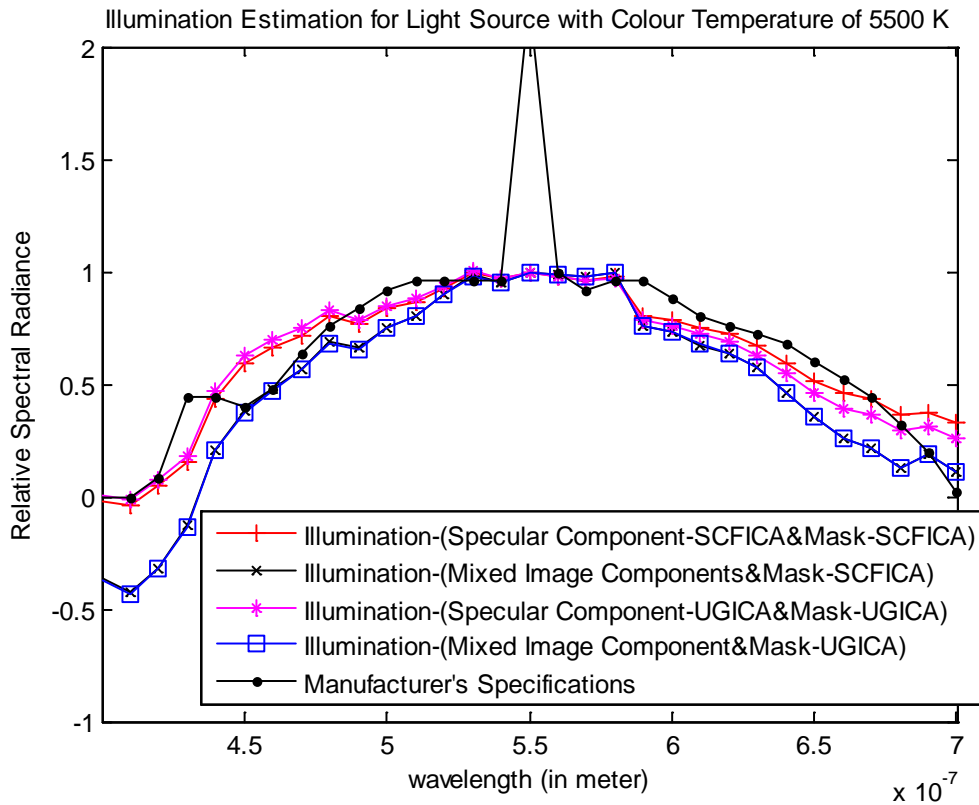


Figure 5-5 The illumination estimations from the specular component and mixed image components for a plastic blue ring illuminated with a light source of colour temperature of 5500 K, using empirical thresholding to select the significantly specular pixels.

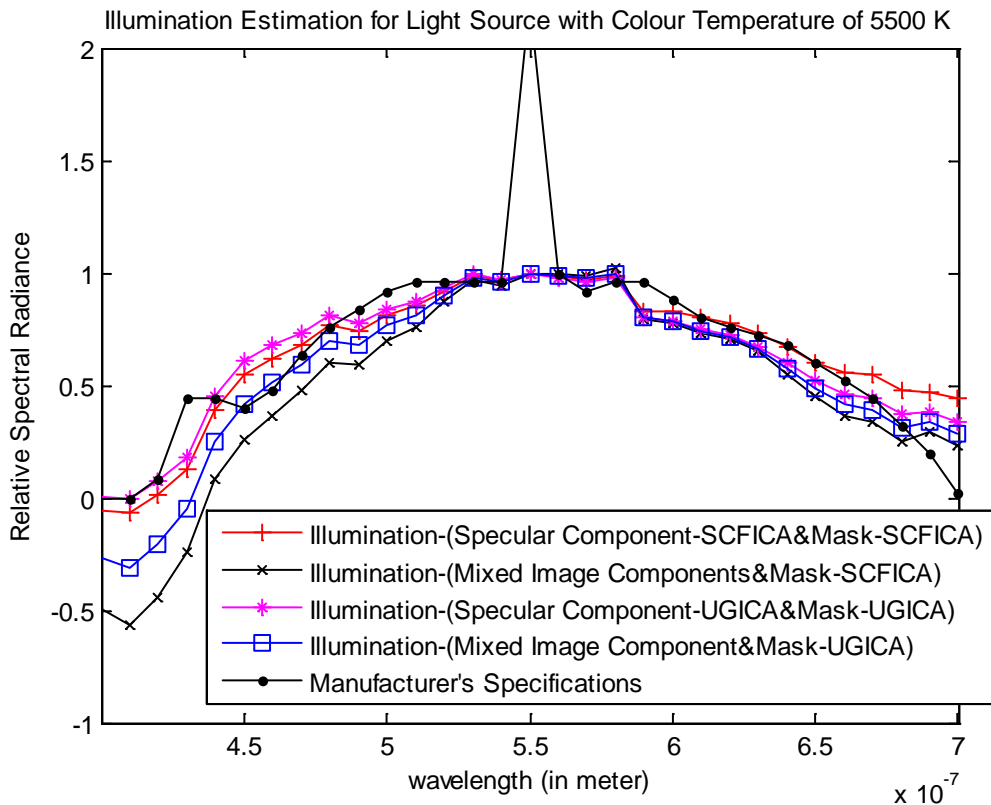


Figure 5-6 The illumination estimations from the specular component and mixed image components for a ceramic violet cup illuminated with a light source of colour temperature of 5500 K, using empirical thresholding to select the significantly specular pixels.

Table 5-5 Results of the experimental assessment of the effect of: the extraction of the specular image component, and the material of the reflecting object. The table entries represent the similarity between the illumination spectral power distribution estimated in the experiment and the distribution provided by the manufacturer of the light source with colour temperature of 5500 K. The similarity has been calculated using GFC.

Illumination source	Extraction of specular image component			Material of the reflecting object			
	Signal separation	Selection of significantly specular pixels		Plastic blue ring	Ceramic violet cup	Plastic green ring	Red apple
Colour temperature: 5500 K	Spatially constrained FastICA Technique (SCFICA)	Empirical selection	Mask-SCFICA	0.9880	0.9839	0.9845	0.9879
			Mask-UGICA	0.9879	0.9829	0.9676	0.9759
	Umeyama and Godin ICA Techniques (UGICA)	Empirical selection	Mask-SCFICA	0.9874	0.9872	0.9653	0.9786
			Mask-UGICA	0.9874	0.9878	0.9880	0.9880
	None	Empirical selection	Mask-SCFICA	0.9582	0.9394	0.9605	0.9434
			Mask-UGICA	0.9574	0.9756	0.9288	0.9662

Table 5-6 The average and the standard deviation of GFC and error measurements for illumination estimation using specular component and Image 2 (mixed image component).

		GFC	RMS error	Median error	Mean error	Angular error (in degree)
Specular Image Component	Average	0.9830	13.15×10^{-2}	3.09×10^{-2}	3.61×10^{-2}	2.70
	Standard deviation	± 0.0074	$\pm 2.96 \times 10^{-2}$	$\pm 2.40 \times 10^{-2}$	$\pm 3.80 \times 10^{-2}$	± 1.67
Mixed Image Component	Average	0.9537	22.02×10^{-2}	6.62×10^{-2}	9.45×10^{-2}	8.52
	Standard deviation	± 0.0153	$\pm 4.23 \times 10^{-2}$	$\pm 5.93 \times 10^{-2}$	$\pm 5.28 \times 10^{-2}$	± 3.22

5.3.2.4 Experiment 4: Estimation of ISPD from mixed image components (i.e highlight area) captured under natural day light sources with different colour temperatures.

a) Procedure

The aim of this experiment is to investigate how the method used in the second stage of the implemented framework performs for estimating ISPD for different natural day light sources with different colour temperatures in comparison with measured illumination.

This experiment used the same illumination estimation method as in Experiments 1, 2 and 3 in this chapter. The test is performed on Foster et al’s data set [181]. The blind signal separation techniques (i.e. used in the first stage of developed framework) are not applicable to this data set because these techniques require a pair of images for the same scene in order to separate the specular and diffuse components of the image. Therefore, the specular components of these images (Foster et al’s data set [181]) cannot be obtained as output of the first stage of the developed framework. However, this experiment is not about testing the

effect of the separation techniques on the performance of the illumination estimation method; hence, the estimation of illumination is done without applying signal separation techniques. This means that the output of the first stage of the developed framework is not used in this experiment.

The investigation is done based on the assumption that the selected mixed pixels (i.e. high intensity pixels), which are used for illumination estimation, consist predominantly of a specular component and a negligible diffuse component. The selection of predominantly specular pixels is done by empirical thresholding because it gives better results than automatic thresholding in the previous three experiments (Sections 5.3.2.1, 5.3.2.2, and 5.3.2.3); moreover, defining an optimum automatic threshold is not the focus of this research.

b) Results and discussion

The results of the illumination estimation for some examples of images in this data set are shown in Figure 5-7 to Figure 5-10. Moreover, to show the selected mixed pixels used in the illumination estimation, these figures also show the masks used to extract the predominantly specular pixels. The results of the illumination estimation for more examples of images in Foster et al's data set are shown in Appendix C (Figures C.31 to C.34).

Furthermore, the illumination estimated from each image is compared to the measured illumination which is provided with the Foster et al's data set [181]. This comparison is achieved by calculating the GFC and others curve-matching error measurements which are given in Table 5-7. Table 5-7 also contains the threshold values used to generate the pixel masks, and the corresponding number of pixels extracted by this mask for each image in Foster et al's data set [181]. The average and standard deviation of the GFC values and the error measurements are calculated and summarised in Table 5-8. These calculations are based on the values obtained in Table 5-7. All figures in this experiment show that the estimated illumination results are very similar to the illumination measured by Foster et al [181].

Compared with average GFC values and error measurements for the illumination estimated in Experiments 1 and 2 (5.3.2.1 and 5.3.2.2), it is found that the average GFC is better, and the average errors are less, in Experiment 4 (Table 5-8). However, this comparison is not valid because the data set used in Experiment 4 is different from the data sets used in Experiments 1 and 2. The ISPD estimated from mixed image components for different natural day light sources with different colour temperatures has an average GFC value equal to 0.9986, measured over Foster et al's data set.

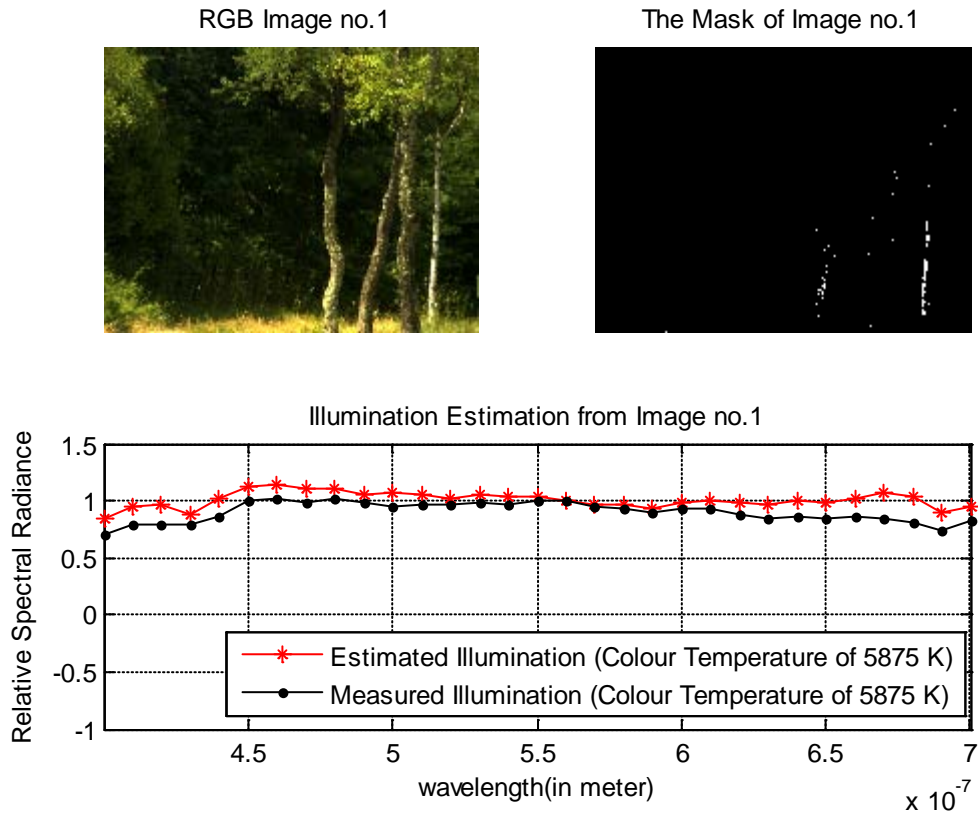


Figure 5-7 The illumination estimation from the first image of Foster et al’s data set [181].

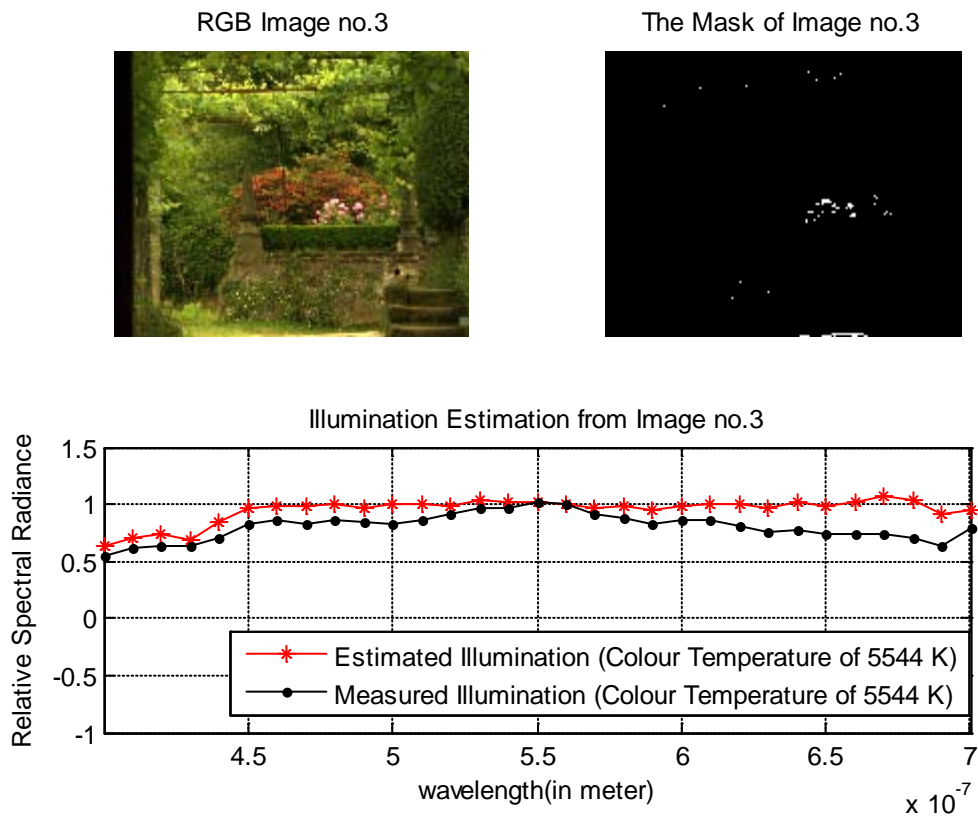


Figure 5-8 The illumination estimation from the third image of Foster et al’s data set [181].

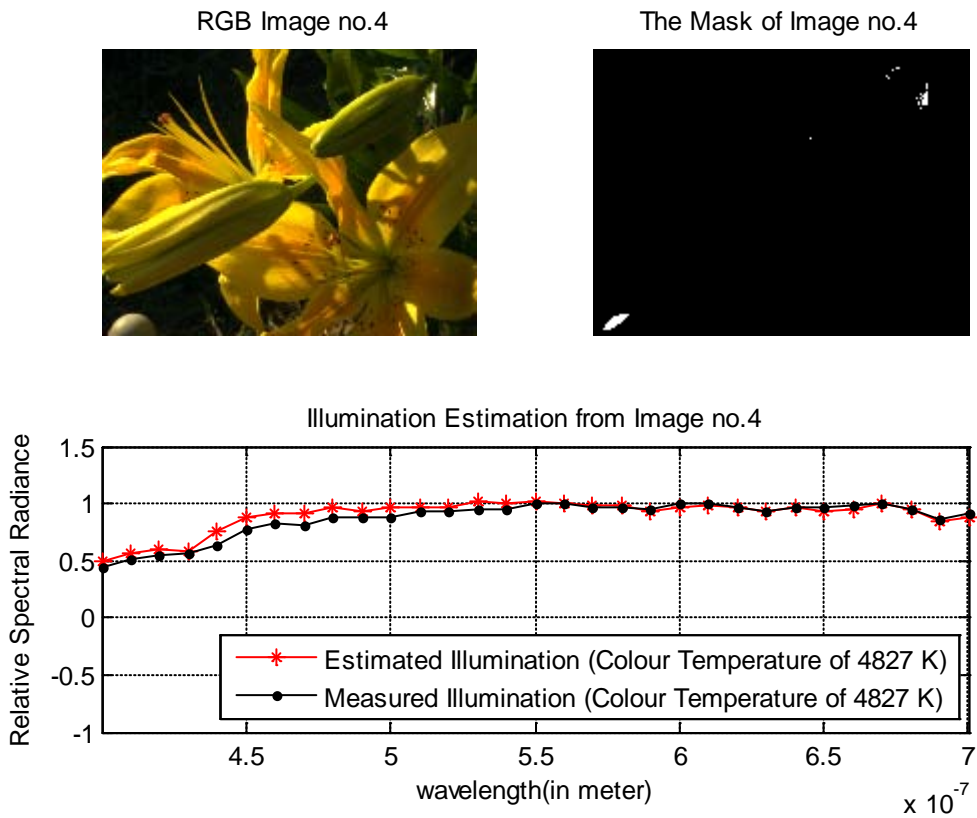


Figure 5-9 The illumination estimation from the fourth image of Foster et al’s data set [181].

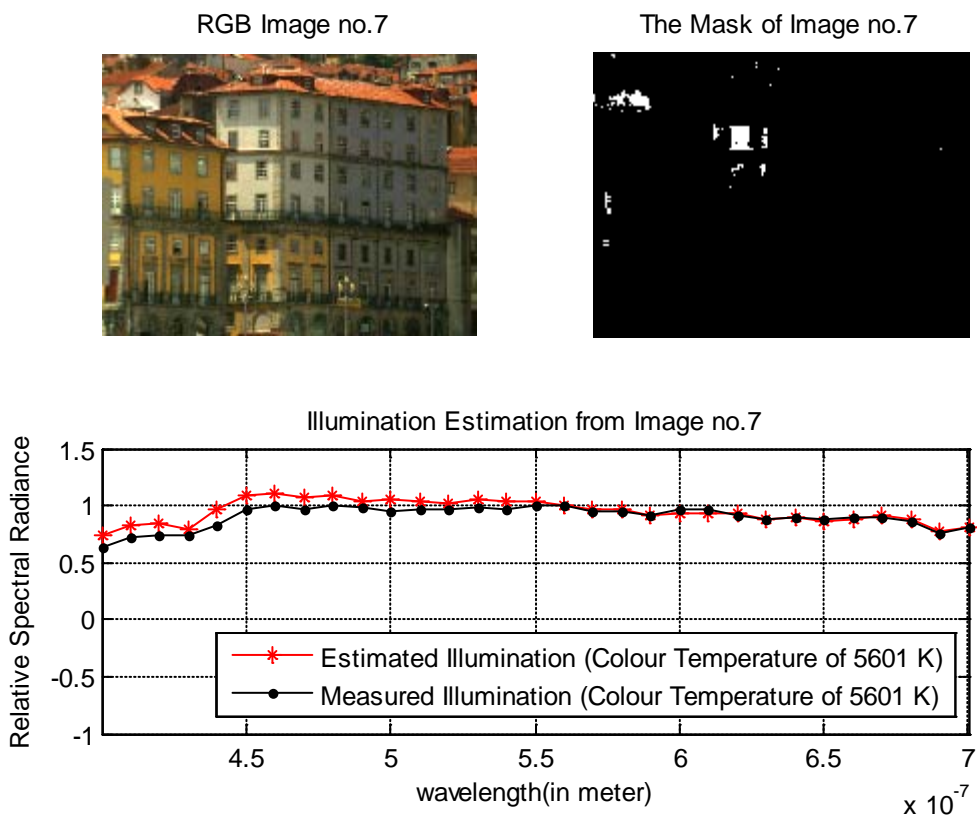


Figure 5-10 The illumination estimation from the seventh image of Foster et al’s data set [181].

Table 5-7 The GFC measurement, the error measurements, and the threshold value with the corresponding number of pixels for illumination estimation of Foster et al’s data set [181].

Image	GFC	RMS error	Median error	Mean error	Angular error	Threshold (number of pixel)
The first image	0.9982	11.94×10^{-2}	10.95×10^{-2}	10.67×10^{-2}	1.44	0.55 (4039)
the second image	0.9994	4.20×10^{-2}	3.35×10^{-2}	2.54×10^{-2}	0.06	0.55 (3713)
the third image	0.9951	16.62×10^{-2}	12.88×10^{-2}	14.35×10^{-2}	1.60	0.50 (4436)
the fourth image	0.9986	5.30×10^{-2}	2.10×10^{-2}	2.74×10^{-2}	1.50	0.42 (4273)
the fifth image	0.9996	3.41×10^{-2}	2.48×10^{-2}	2.18×10^{-2}	0.27	0.50 (2581)
the sixth image	0.9996	3.55×10^{-2}	2.47×10^{-2}	2.34×10^{-2}	0.25	0.60 (14437)
the seventh image	0.9987	6.56×10^{-2}	3.53×10^{-2}	4.47×10^{-2}	1.44	0.65 (15883)
the eighth image	0.9992	4.28×10^{-2}	2.25×10^{-2}	1.90×10^{-2}	0.61	0.55 (12248)

Table 5-8 The average of GFC and error measurements for different day light sources with different colour temperatures.

	GFC	RMS error	Median error	Mean error	Angular error (in degree)
Average	0.9986	6.98×10^{-2}	5.00×10^{-2}	5.15×10^{-2}	0.90
Standard deviation	± 0.0015	$\pm 4.78 \times 10^{-2}$	$\pm 4.33 \times 10^{-2}$	$\pm 4.71 \times 10^{-2}$	± 0.66

5.4 General Discussion

The GFC values obtained in all experiments in this chapter as shown in tables (Table 5-2, Table 5-4 and Table 5-8) demonstrate that the proposed illumination estimation method provides a reasonably accurate estimation, even when compared with measured values. It should be noted that in these experiments the proposed illumination estimation methods include some sources of error. These sources are the normalisation process, the specular geometrical scale factor (w_{sn}) (Equation (4-11)), and the use of camera sensor sensitivity characteristics for estimating illumination from image which is captured with different camera sensor sensitivity characteristics. The effects of these errors are discussed as follows.

- The normalisation process, which introduces loss of information, is required in these experiments to find a common reference as explained in Section 5.3.1. However, in these experiments, the double precision (32 bit number representation) of pixel values was used in order to minimise the effect of this error. Furthermore, this error predominantly affects the absolute value of the estimated illumination and has an insignificant effect on the accuracy of the estimation of the relative illumination spectral power distribution, which is estimated by the proposed illumination estimation method.

- Due to the difficulty in calculating the specular geometrical scale factor (w_{sn}) for each pixel in the image [1], in these experiments this factor is considered to be 1 for simplicity. This assumption will affect the absolute value of the estimated illumination; however it will not affect the relative illumination spectral power distribution. The proposed method estimates the relative spectral power distribution; hence the value of the geometrical scale factor does not significantly affect the accuracy of the estimation process.
- The same camera sensor sensitivity characteristics are used for all experiments. Although these camera characteristics are not the ones used to create Foster et al's data set however, the results in Experiment 4 (Section 5.3.2.4), in which the illumination is estimated from Foster et al's data set, show reasonable estimation accuracy with an average GFC value of 0.9986. This could be due to the similarity between different camera sensitivity characteristics which can be inferred from the observation that the sensor sensitivity characteristics have minimum effect on the estimation process.

The proposed method for illumination estimation requires simple two-level thresholding, which can be done empirically or automatically, to identify the significant specular pixels that are used in the estimation. The illumination estimation proposed method, however, avoids multi-coloured surface segmentation, the problem that is being faced by the existing illumination methods (Section 2.4.2).

5.5 Summary

This chapter presents an experimental assessment of factors which affect the performance of the second stage of the proposed colour constancy framework. This stage estimates the spectral power distribution of the illumination, using the specular component of the images which display the scene under observation. The performance of the proposed illumination estimation method is evaluated quantitatively in two ways. The evaluation consists of four experiments. The aim of these experiments is to investigate the performance of the proposed method for estimating ISPD and to explore the factors which affect the estimation performance, measured in terms of GFC, within the proposed colour constancy framework.

Experiments 1 and 2 investigate the performance of the proposed illumination estimation method when estimating the illumination of artificial light sources with colour temperatures of 5500 K and 2900 K, respectively for Experiments 1 and 2. The investigation is done for

two blind signal separation techniques. The results for each of the two light sources show no significant difference in the accuracy of estimation using the specular components extracted by each of the two blind separation techniques (SCFICA and UGICA in [28]). When compared to the manufacturer's specification, the illumination estimated for the 5500 K light source has average GFC values equal to 0.9447 and 0.9830, using automatic and empirical thresholding (i.e. used for the selection of the significant specular pixels that have been used for illumination estimation) respectively. The corresponding GFC values for the 2900 K light source are 0.8921 and 0.9215. There is a statistically significant improvement in the illumination estimation accuracy (measured in terms of average of GFC) by 3.8% and 2.9% when the empirical threshold is used instead of the automatic threshold for the 5500 K light source and the 2900 K light source respectively. The selection of illumination basis functions has an impact on the accuracy of the illumination estimation method used within the colour constancy architecture, measured in terms of GFC value.

Experiment 3 measures the improvement in the illumination estimation accuracy, measured in terms of GFC value, arising from using an explicitly extracted specular image component instead of mixed image components (i.e. composed of unseparated specular and diffuse components). It is found that there is a statistically significant improvement by 2.9% in the average GFC value of the estimated ISPD when the specular component is used instead of mixed image components.

Experiment 4 compares illumination measurements, which are provided with a public-domain set of hyperspectral images (i.e. Foster et al's data set), with the illumination estimated by the proposed method. It is shown that the ISPD estimation for natural day light sources with different colour temperature is achieved with average GFC value equal to 0.9986 compared with the measured illumination.

The next chapter presents the experimental evaluation of the estimation of the surface spectral reflectance (which represents the last stage of the framework) using the estimated ISPD. In particular, the chapter explores to what extent the image component separation results achieved by using two different separation techniques (in the first stage of the framework) and the estimated ISPD (in the second stage of the framework) affect the accuracy of the surface spectral reflectance estimation.

6

Experimental Investigation of the Estimation of the Surface Spectral Reflectance

6.1 Introduction

The aim of this chapter is to investigate the performance of the method proposed for estimating the surface spectral reflectance in the third stage of the framework. The investigation of the third stage will explore how the different separation results (i.e. achieved in the first stage of the framework) and the estimated illumination (i.e. achieved in the second stage of the framework) influence the estimation of the surface spectral reflectance. The investigation in this chapter is done by estimating the surface spectral reflectance from images of different objects captured under different light sources with different colour temperatures. The evaluation of the estimated surface spectral reflectance is conducted in three ways. First, the evaluation is performed by comparing the two surface reflectance estimates which are obtained using the estimated illumination and the illumination specifications given by the light source manufacturer, for the same object illuminated by the same light source. Second, the evaluation is performed by comparing the two surface reflectance estimates for the same object illuminated by two different light sources. Third, the evaluation is performed by comparing the estimated surface reflectance with either the measured surface reflectance or a reference produced by the author from the diffuse-only pixels. This chapter is organised as follows. First, it presents a performance evaluation for surface spectral reflectance estimation; including the experimental method, results and discussion. This is followed by a summary.

6.2 Performance Evaluation of the Estimation of Surface Spectral Reflectance

In this section, the performance of the surface spectral reflectance estimation (the third stage of the colour constancy framework) is evaluated in four experiments. The aims of these experiments are to investigate the performance of the proposed method for estimating surface reflectance and to explore the factors which affect its estimation accuracy in terms of GFC and error, within the colour constancy framework.

In Experiment 1, the surface spectral reflectance is estimated from the diffuse components of images which are captured under two different artificial light sources with two colour temperatures (5500 K and 2900 K). The estimation of the surface spectral reflectance from the diffuse pixel is obtained using the four possible illuminations estimated in the second stage (see Sections 5.3.2.1 and 5.3.2.2). Then the surface reflectance, estimated using the four possible estimated illuminations, is compared with the surface reflectance estimated using the specification of illumination for each light source as given by its manufacturer. In Experiment 2, the comparison between surface reflectance estimated from the diffuse component for the same object illuminated by two different artificial lights with two different colour temperatures (5500 K and 2900 K), is executed. Experiment 3 carries out a comparison between the surface spectral reflectance estimated using the explicitly extracted diffuse component and mixed image components (where each pixel is a blend of a specular component and a diffuse component). In Experiment 4, the surface spectral reflectance is estimated using mixed image components (i.e. Foster et al's data set [181]) captured under different natural day light sources with different colour temperatures. Then the estimated surface reflectance is compared with the reflectance which was measured by Foster et al [181]. In Experiment 4, the surface reflectance estimation method does not utilise the output of the first stage of the developed framework. In the following sub-sections, the experimental settings are stated followed by the experimental procedure, results and discussion.

6.2.1 The Experimental Setting

This section discusses the experimental setting for all experiments in this chapter including the data set, camera sensor sensitivity, surface reflectance basis functions, normalization process, and statistical significance test which have been used.

1) The first three experiments reported in this chapter use the data set collected by the author. More details about the data set are found in Section 5.2. The reason for using this data set in the first three experiments is that it is suitable (as described in Section 5.2) for applying blind signal separation (the first stage of the developed framework), in order to extract the diffuse component, which is used in the estimation of the surface spectral reflectance in these experiments. The data set used in Experiment 4 was collected by Foster et al [181] (more details are found in Section 5.3.1). The reason for using Foster et al's data set in Experiment 4 is the availability of the measured surface spectral reflectance for each pixel, which can be used in evaluating the method proposed for estimating surface spectral reflectance.

2) The sensor spectral sensitivity curves which are used in all experiments in this chapter are shown in Figure 2-3. More details about these sensor spectral sensitivity curves are found in Section 5.3.1.

3) In all experiments in this chapter, the reflectance basis functions, which are used for surface spectral reflectance estimation, are Parkkinen's basis functions [33] which are shown in Figure 2-2. An explanation of the choice of these basis functions is given in Section 2.2.2. The spectral range of these basis functions is from 400 nm to 700 nm with spectral step of 1nm, as seen in Figure 2-2.

4) In all experiments in this chapter, the estimation of the surface reflectance coefficients is obtained from the normalised version of Equation (4-21), to make the ranges for both sides of the equation between 0 and 1, which is expressed as:

$$\mathbf{IM}_{d,k} = \frac{\sum_{j=1}^3 \varphi_j \mathbf{P}_{k,j}}{N_k} \quad (6-1)$$

The left hand side of Equation (6-1) ($\mathbf{IM}_{d,k}$) represents the diffuse image component which is normalized (0-1) assuming that the maximum value of ($\mathbf{I}_{d,R}$, $\mathbf{I}_{d,G}$, $\mathbf{I}_{d,B}$) represents a white object on the scene which is expressed as:

$$\mathbf{IM}_{d,k} = \frac{(\mathbf{I}_{d,k} - \min(\mathbf{I}_{d,R}, \mathbf{I}_{d,G}, \mathbf{I}_{d,B}))}{\max(\mathbf{I}_{d,R}, \mathbf{I}_{d,G}, \mathbf{I}_{d,B}) - \min(\mathbf{I}_{d,R}, \mathbf{I}_{d,G}, \mathbf{I}_{d,B})}, k = R, G, B \quad (6-2)$$

The right handside of equation equation (6-1) represents the diffuse component estimated using the dichromatic image formation model and normalised against a white object (i.e. the

surface spectral reflectance (S) is equal to 1). N_k is a normalisation factor which is represented as:

$$N_k = \mathbf{E} \cdot \mathbf{q}_k \quad (6-3)$$

5) The results of Experiments 2 and 3 have been tested to be statistically significant at confidence level of 95% using the independent two-sample t-test (Appendix E).

6.2.2 Experimental Procedure, Results and Discussion

This section provides the procedure, results, and discussion for each individual experiment.

6.2.2.1 Experiment 1: Comparison between surface spectral reflectance estimated from the diffuse component of images using the estimated illumination and the illumination specifications provided by manufacturer.

a) Procedure

The aim of this experiment is to investigate how the estimated illumination (i.e. extracted in the second stage of the framework) affects the performance of the proposed method for estimating surface spectral reflectance, in comparison with the estimate derived from illumination specifications given by the manufacturer of the light source.

In this experiment, the estimation of surface reflectance is achieved from the RGB diffuse components. The RGB diffuse components are extracted by one of two alternative separation techniques, which are the SCFICA technique and the UGICA technique [28], used in the first stage of the framework. Each separation technique provides a set of RGB diffuse components. The estimation of the surface reflectance is found by first estimating the linear combination coefficients of surface reflectance basis functions from each random selected pixel of the diffuse components. The surface spectral reflectance is then calculated by the addition of the multiplication of the estimated coefficients and the corresponding basis functions.

The aim of this experiment is achieved by comparing, for the same diffuse pixel, the estimate of surface reflectance obtained using the estimated illumination against the surface reflectance estimate obtained using the illumination specification provided by the manufacturer of the light source. This comparison is done using the four possible illumination estimations for each of the two light sources with colour temperatures of 5500 K and 2900 K (i.e. achieved using empirical thresholding in Experiments 1, and 2 (Section 5.3.2.1, and Section 5.3.2.2)). Table 6-1 shows which set of RGB specular components and masks are used to estimate the four

possible illuminations. To make it easy for the reader the four possible illumination estimations are labelled as ‘illumination-1’, ‘illumination-2’, ‘illumination-3’, and ‘illumination-4’.

Moreover, the comparison is conducted for the two sets of RGB diffuse components extracted using the two separation techniques (first stage of the framework). For simplicity of understanding the figures, each set of RGB diffuse components is called by its corresponding techniques as ‘Diffuse-SCFICA’ and ‘Diffuse-UGICA’. The GFC measurement and other error (RMS, median, mean, and angular error) measurements, which are commonly used by other researchers [3], [183], [184], are calculated between the estimated surface reflectance using the four possible estimated illuminations and the reflectance estimated using the illumination measured by the manufacturer. The GFC and the error measurements are calculated for each object considering a randomly selected set of pixels, which were empirically chosen to be 100 after performing a number of exploratory experiments.

Table 6-1 The combinations used for estimating the four possible illuminations.

Estimated illumination	Combination used for estimation	
Illumination-1	Specular-SCFICA	Mask-SCFICA
Illumination-2	Specular-UGICA	Mask-SCFICA
Illumination-3	Specular-SCFICA	Mask-UGICA
Illumination-4	Specular-UGICA	Mask-UGICA

b) Results and discussion

Figure 6.1 shows illustrative examples of polarized images, the two sets of RGB diffuse image components (i.e extracted using two separation techniques), and surface reflectance estimates using the four possible estimated illumination and the specification provided by the light source manufacturer. In this figure, the surface reflectance estimate has been calculated using the same pixel (with same coordinate) for each set of RGB diffuse components for the plastic blue ring illuminated by a light source which has a colour temperature of 5500 K. The same examples have been repeated with the light source of colour temperature of 2900 K, as shown in Figure 6.2. Further illustrative examples using different objects illuminated with light sources of colour temperatures of 5500 K and 2900 K are shown in Appendix D (Figures D.1 to D.4).

The calculation of the GFC using the two separation techniques for the artificial light sources with colour temperature of 5500 and 2900 K are summarised in Table 6-2 and Table 6-4 respectively, for all test images in this experiment. The other error measurements are shown in Appendix D (Tables D.1 to D.8). The average and standard deviation of GFC and the other error measurements, over all test images in this experiment, for the two artificial light sources with two colour temperatures (i.e. 5500 K and 2900 K) are calculated and summarised in Table 6-3 and Table 6-5. These calculations are based on the values found in Table 6-2, Table 6-4 and Tables D.1 to D.8.

The average GFC values for the two light sources show that the surface reflectance estimated using the estimated illumination and using the manufacturer's illumination specifications are almost the same. Based on these averages, it can be said that the illumination is estimated with accuracy corresponding to an average GFC equal to 0.9830 (Experiment 1 in Section 5.3.2.1, Table 5-2) gave a surface reflectance estimate with accuracy corresponding to an average GFC equal to 0.9974. Moreover, illumination estimation with accuracy corresponding to an average GFC equal to 0.9215 (Experiment 2 in Section 5.3.2.2, Table 5-4) gave a surface reflectance estimation with accuracy corresponding to an average GFC equal to 0.9942. These observations give evidence that the surface reflectance estimation method evaluated within the framework is significantly tolerant of illumination estimation error. It can therefore be concluded from this experiment that the illumination estimated in the second stage of the framework is appropriate to be used for estimating surface spectral reflectance within the proposed framework. This conclusion is based on the observation that the difference between the surface reflectance estimated using the estimated illumination and using the manufacturer's illumination specifications is not significant.

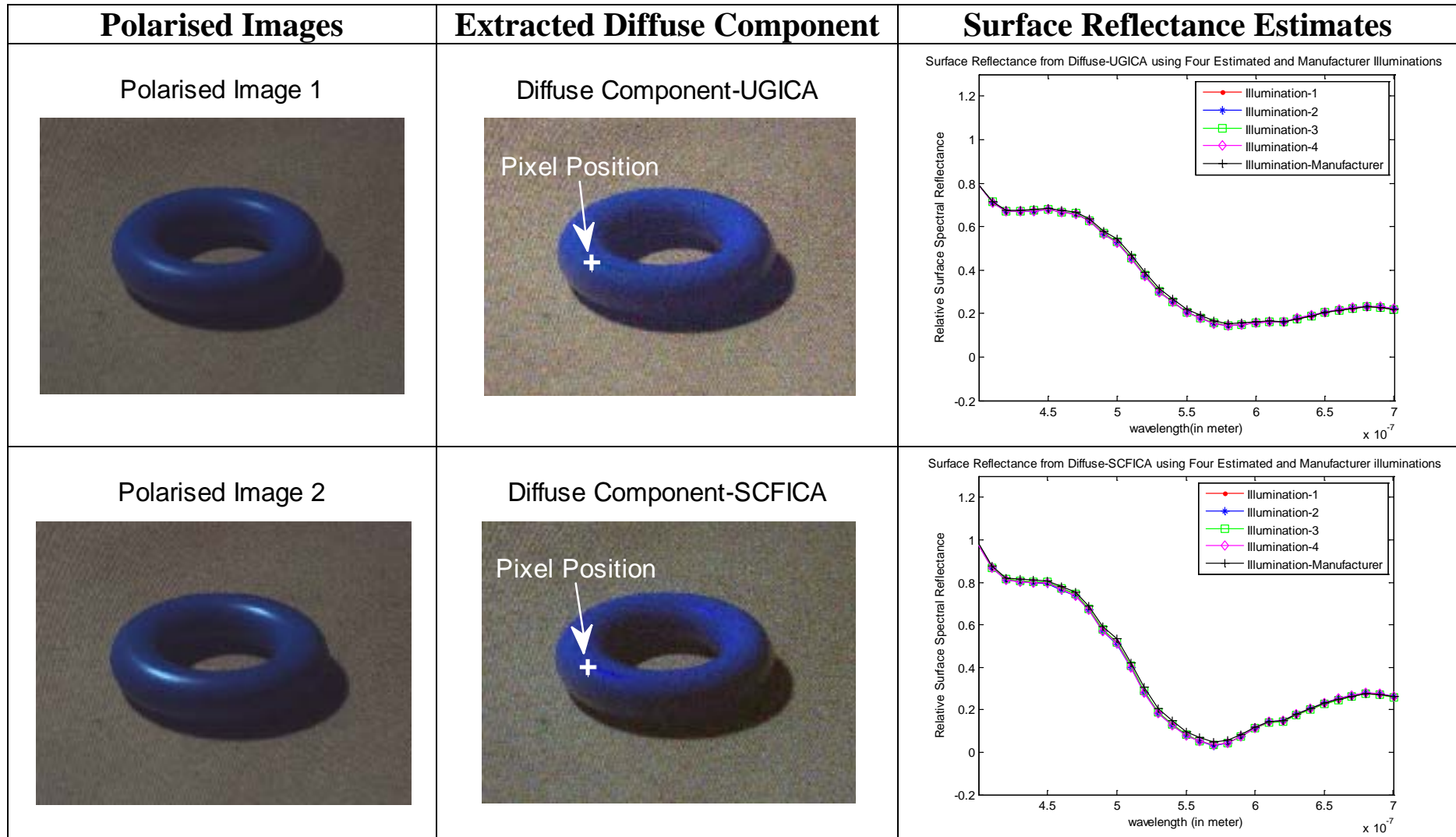


Figure 6-1 Illustrative examples of polarised images, two RGB diffuse image components (i.e extracted using two separation techniques), and surface reflectance estimates. These estimates are obtained from RGB diffuse image components for a pixel located at image position (185, 250) for the plastic blue ring illuminated by a light source which has a colour temperature of 5500 K, using the four possible illumination estimates and light source specifications provided by the manufacturer.

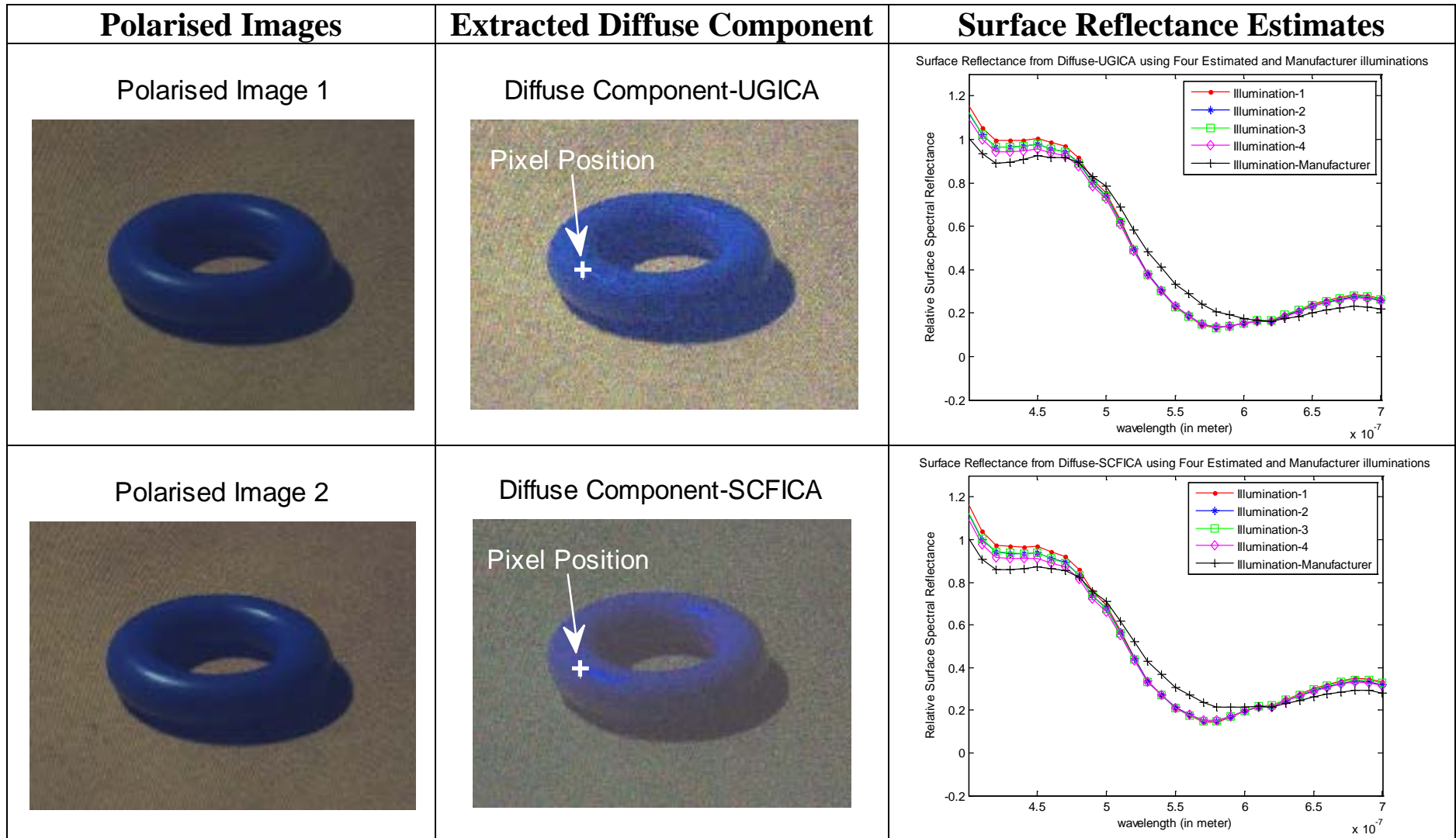


Figure 6-2 Illustrative examples of polarised images, two RGB diffuse image components (i.e extracted using two separation techniques), and surface reflectance estimates. These estimates are obtained from RGB diffuse image components for a pixel located at image position (185, 250) for the plastic blue ring illuminated by a light source which has a colour temperature of 2900 K, using the four possible illumination estimates and light source specifications provided by the manufacturer.

Table 6-2 Results of the experimental assessment of the effect of: the extraction of the diffuse image component, the four possible illumination estimates, and the material of the reflecting object. The table entries represent the similarity between the surface reflectance estimates obtained using the four possible illumination estimates and surface reflectance estimate obtained using the illumination specification provided by the manufacturer of the light source with a colour temperature of 5500 K. The spectral similarity has been calculated using the goodness-of-fit coefficient (GFC).

Extraction of diffuse image component Signal separation	The four possible illumination estimates	Material of the reflecting object		
		Plastic blue ring	Ceramic violet cup	Plastic green ring
Spatially constrained FastICA technique (Diffuse -SCFICA)	Illumination-1	0.9999	1.0	0.9992
	Illumination 2	0.9998	0.9886	0.9861
	Illumination-3	0.9999	0.9999	0.9955
	Illumination-4	0.9998	1.0	1.0
Umeyama and Godin ICA technique (Diffuse-UGICA)	Illumination-1	0.9999	0.9999	0.9992
	Illumination 2	0.9998	0.9881	0.9867
	Illumination-3	0.9999	0.9998	0.9956
	Illumination-4	0.9998	0.9999	1.0

Table 6-3 The average of GFC and other error measurements for the estimated surface reflectance for objects illuminated by artificial day light source with a colour temperature of 5500 K.

	GFC	RMS error	Median error	Mean error	Angular error (in degree)
Average	0.9974	3.07×10^{-2}	1.64×10^{-2}	2.17×10^{-2}	2.02
Standard deviation	± 0.0048	$\pm 4.22 \times 10^{-2}$	$\pm 1.55 \times 10^{-2}$	$\pm 2.65 \times 10^{-2}$	± 2.41

Table 6-4 Results of the experimental assessment of the effect of: the extraction of the diffuse image component, the four possible illumination estimates, and the material of the reflecting object. The table entries represent the similarity between the surface reflectance estimates obtained using the four possible illumination estimates and surface reflectance estimate obtained using the illumination specification provided by the manufacturer of the light source with a colour temperature of 2900 K. The spectral similarity has been calculated using the goodness-of-fit coefficient (GFC).

Extraction of diffuse image component Signal separation	The four possible illumination estimates	Material of the reflecting object		
		Plastic blue ring	Ceramic violet cup	Plastic green ring
Spatially constrained FastICA technique (Diffuse -SCFICA)	Illumination-1	0.9949	0.9919	0.9959
	Illumination 2	0.9962	0.9919	0.9955
	Illumination-3	0.9967	0.9962	0.9993
	Illumination-4	0.9973	0.9961	0.9993
Umeyama and Godin ICA technique (Diffuse-UGICA)	Illumination-1	0.9938	0.9915	0.9813
	Illumination 2	0.9949	0.9916	0.9803
	Illumination-3	0.9950	0.9960	0.9968
	Illumination-4	0.9957	0.9960	0.9968

Table 6-5 The average of GFC and other error measurements for the estimated surface reflectance for objects illuminated by artificial day light source with a colour temperature of 2900 K.

	GFC	RMS error	Median error	Mean error	Angular error (in degree)
Average	0.9942	6.07×10^{-2}	2.22×10^{-2}	2.88×10^{-2}	4.01
Standard deviation	± 0.0046	$\pm 2.81 \times 10^{-2}$	$\pm 1.35 \times 10^{-2}$	$\pm 1.13 \times 10^{-2}$	± 1.51

6.2.2.2 Experiment 2: Comparison between the surface reflectance estimated from the diffuse image component for the same object illuminated by two artificial light sources with different colour temperatures.

a) Procedure

The aim of this experiment is to investigate how the proposed method for estimating surface spectral reflectance performs, within the proposed colour constancy framework, in terms of the similarity (measured using the GFC) between two spectral reflectance curves obtained for the same object illuminated alternatively by two artificial light sources with different colour temperatures.

This experiment uses the same test images, same number of pixels and estimated illumination for each light source, as in Experiment 1 (Section 6.2.2.1). In this experiment, the measured GFC of the estimated surface spectral reflectance indicates the performance of the last stage of the framework. The results of last stage depend on the extracted diffuse component and estimated illumination from the previous two stages. This means that the GFC measured in this experiment reflects the performance of the whole framework. The GFC and error measurements, between the surface spectral reflectance estimates correspond to the two light sources, are calculated for each object considering a randomly selected set of pixels, which are empirically chosen to be 100 after performing a number of exploratory experiments.

The aim of this experiment is achieved by comparing the surface reflectance estimated for the same object illuminated by two different artificial light sources. The experiment compares the surface reflectance calculated from two estimates of the diffuse component extracted by the same signal separation technique, at the same pixels coordinates, for the same object captured under two different artificial light sources.

b) Results and discussion

The results for this comparison are shown in Figure 6-3 and Figure 6-4. These figures show the comparison for one object (plastic blue ring) while more comparison results for different objects are given in Appendix D (Figures D.5 to D.8). Ideally the surface spectral reflectances for the same pixel of an object illuminated by different light sources have to be similar. However, in this experiment, the comparison of the surface spectral reflectance, estimated for the same pixel of an object illuminated by two light sources with colour temperatures of 5500 K and 2900 K, shows that the estimated curves have almost the same spectral signature for the two light sources but there is a shift in amplitude between them.

This shift represents change in the amplitude ratio between the two surface spectral reflectances and it does not represent change in spectral characteristics (i.e. identified the material colour). This means that the surface reflectance estimation method used within the developed framework is able to extract from images the same material colour for an object illuminated by different light sources. For example, as seen in Figure 6-3 and Figure 6-4, the blue component (ranges from 400 nm to 500 nm) in the surface spectral reflectance estimates is dominant; this reflects the colour of the object under investigation (plastic blue ring).

The GFC and error measurements, between the surface spectral reflectance estimates corresponding to the two light sources for all the test images, are given in Table 6-6 and Table 6-7. From these tables, it is found that the comparison between the surface spectral reflectance estimates corresponding to the two light sources gives an average GFC value (over all test images) equal to 0.9887 by using the UGICA separation technique and 0.9611 by using the SCFICA separation technique. This means that the performance (in terms of GFC) of the proposed method for estimating surface spectral reflectance depends on the type of blind separation technique that is used. The results show that there is an improvement in the performance of the proposed surface reflectance method by 2.8% in terms of average GFC value when the UGICA separation technique is used instead of SCFICA. This improvement is statistically significant, with a significance level of 95%. The results of the statistical significance test are reported in Appendix E (Table E.6). The high GFC value means that the estimates of surface reflectance under the two light sources are very similar, despite the differences between the two illuminants. This similarity implies that the extracted surface reflectance is significantly independent of illumination characteristics, hence showing that the proposed framework achieved colour constancy.

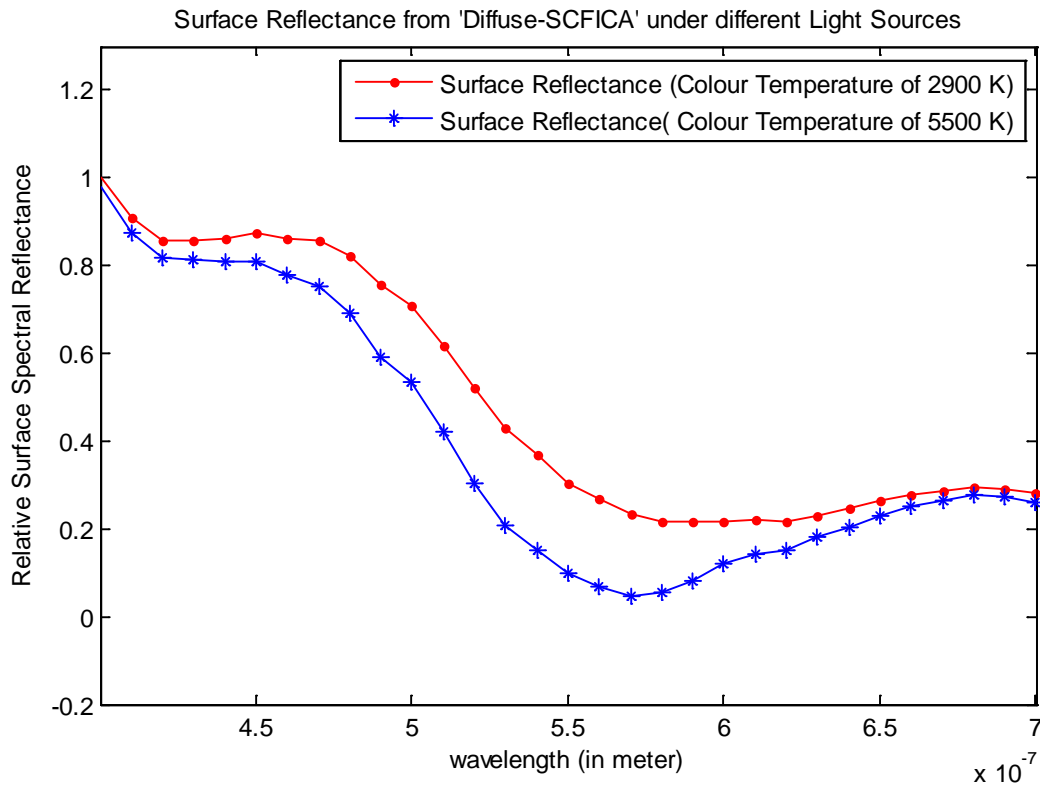


Figure 6-3 The surface reflectance, for a pixel located at image coordinates (185, 250), estimated from the 'Diffuse-SCFICA' image component for a plastic blue ring illuminated by two artificial light sources with colour temperatures of 2900 and 5500 K.

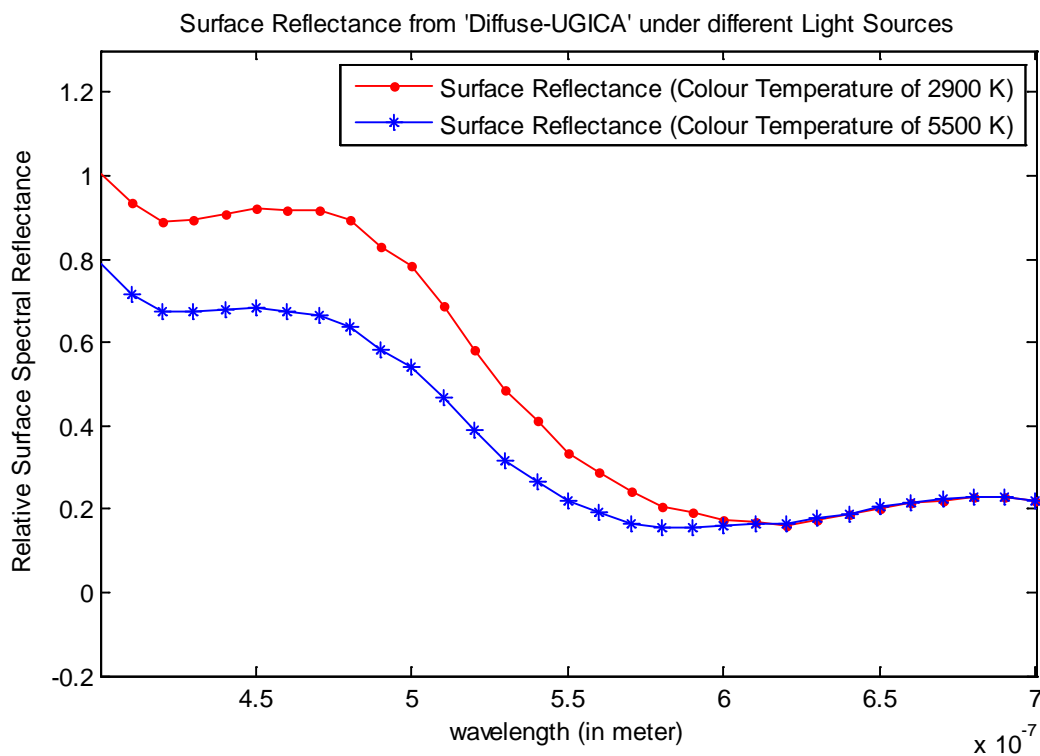


Figure 6-4 The surface reflectance for a pixel located at image coordinates (185, 250), estimated from the 'Diffuse-UGICA' image component for a plastic blue ring, and illuminated by two artificial light sources with colour temperatures of 2900 and 5500 K.

Table 6-6 The GFC and error measurements between surface reflectance estimates from pixels of ‘Diffuse-SCFICA’, at the same pixel coordinate for the same object illuminated by two artificial light sources with colour temperatures of 2900 and 5500 K.

Object	GFC	RMS error	Median error	Mean error	Angular error (in degree)
Plastic blue ring	0.9808	11.33×10^{-2}	10.89×10^{-2}	8.82×10^{-2}	11.22
Ceramic violet cup	0.9799	18.94×10^{-2}	9.72×10^{-2}	14.71×10^{-2}	8.99
Plastic green ring	0.9227	18.70×10^{-2}	0.7×10^{-3}	5.34×10^{-2}	13.18
Average	0.9611	16.32×10^{-2}	6.89×10^{-2}	9.62×10^{-2}	11.13
Standard deviation	± 0.0333	$\pm 4.33 \times 10^{-2}$	$\pm 5.94 \times 10^{-2}$	$\pm 4.74 \times 10^{-2}$	± 2.09

Table 6-7 The GFC and error measurement between surface reflectance estimates for pixels of ‘Diffuse-UGICA’, at the same pixel coordinate for the same object illuminated by two artificial light sources with colour temperatures of 2900 and 5500 K.

Object	GFC	RMS error	Median error	Mean error	Angular error (in degree)
Plastic blue ring	0.9939	8.47×10^{-2}	3.33×10^{-2}	3.98×10^{-2}	5.03
Ceramic violet cup	0.9972	17.72×10^{-2}	13.21×10^{-2}	15.90×10^{-2}	3.32
Plastic green ring	0.9749	14.15×10^{-2}	1.19×10^{-2}	3.87×10^{-2}	7.61
Average	0.9887	13.45×10^{-2}	5.91×10^{-2}	7.92×10^{-2}	5.32
Standard deviation	± 0.0120	$\pm 4.66 \times 10^{-2}$	$\pm 6.41 \times 10^{-2}$	$\pm 6.91 \times 10^{-2}$	± 2.16

6.2.2.3 Experiment 3: A comparison between the surface spectral reflectance estimated using the diffuse image component and mixed image components.

a) Procedure

The aim of this experiment is to measure the improvement in the surface reflectance estimation accuracy (measured using the GFC) arising from using an explicitly extracted diffuse image component instead of the original image which is effectively a mixture of specular and diffuse image components.

Due to the lack of a reference for the surface spectral reflectance of the material in high specular reflection areas (i.e. highlight areas) of images, the surface spectral reflectance of neighbouring pixels (slightly or not affected by specular reflections) will be taken as a reference. This reference is then compared with surface spectral reflectance estimates of pixels located in the high specular reflection areas of the mixed image components and the corresponding pixels in the diffuse image component. In this experiment, a set of randomly selected pixels (i.e. assumed to be diffuse-only pixels) has been chosen to create three spectral reflectance references. The number of pixels in this set is 100 and this number was chosen empirically after performing a number of exploratory experiments. To rely on one reference, a set of 100% diffuse-only pixels is required. However, this set is unavailable and therefore three different references are created from three sets of pixels with different accuracy of diffuse-only pixels. The locations of the selected pixels (reference pixels) are chosen from the pixels neighbouring the high specular reflection areas. The three spectral reflectance

references are estimated from the mixed image components and the two diffuse image components, which are extracted using the two separation techniques (SCFICA and UGICA) considered in the experiments. The creation of the spectral reflectance references is based on the assumption that these references represent the invariant characteristic colour of the material in the test image. Each surface spectral reflectance reference is obtained by averaging the surface spectral reflectance estimates, which are estimated from the selected pixels corresponding to each image component. In this experiment, to make it easy for the reader the three reflectance references are labelled as ‘reflectance reference-1’, ‘reflectance reference-2’, and ‘reflectance reference-3’. Table 6-8 shows which image component is used to generate the corresponding reflectance reference.

Table 6-8 The three extracted reflectance references and their corresponding images.

Surface reflectance Reference (pixels neighbouring the high specular reflection areas)	Image component
Reflectance Reference-1	Mixed image components- polarised image2
Reflectance Reference-2	Diffuse image component-SCFICA
Reflectance Reference-3	Diffuse image component-UGICA

The test pixels are from another set of pixels which is selected from the high specular reflection area of the mixed image components, and the corresponding two diffuse image components which are extracted using the two separation techniques (SCFICA and UGICA). The number of pixels in this set is 20 which is also been chosen empirically after performing a number of exploratory experiments. The pixels corresponding to each image component are used to estimate surface spectral reflectances. The surface spectral reflectance estimates from pixels corresponding to each image component are then averaged. The resulting three spectral reflectances of the surface under the specular reflection area are labelled as ‘highlight-reflectance-1’, ‘highlight reflectance-2’, and ‘highlight reflectance-3’. Table 6-9 shows which image component is used to generate the corresponding surface spectral reflectance of the surface under the specular reflection areas.

Table 6-9 The three extracted highlight-reflectances and their corresponding images.

Highlight-Surface Reflectance (pixels in specular reflection areas or highlight areas)	Image component
Highlight-Reflectance-1	Mixed image components-polarized image2
Highlight-Reflectance-2	Diffuse image component -SCFICA
Highlight-Reflectance-3	Diffuse image component -UGICA

The aim of this experiment is achieved by comparing the three highlight-reflectances (Table 6-9) with each spectral reflectance reference (Table 6-8). The number of pixels considered in creating the highlight-reflectance has to be equal to the number of pixels considered in

creating reflectance references to ensure robust comparison. However, in this experiment the number of pixels in the highlight area is small. To avoid this limitation and to ensure the validity of comparison, the pixels in highlight area are selected randomly and the experiment is repeated a number of times. All these comparisons gave similar results.

The experiment uses the same images and the two light sources with colour temperatures of 5500 K and 2900 K as used in Experiments 1 and 2, in this chapter. The illumination specifications given by light source manufacturers are used in estimating the reflectance reference and the highlight reflectance. This is because it has been shown in Experiment 1 (Section 6.2.2.1) that the difference between the estimated surface reflectance using the manufacturer's illumination specifications and the estimated illumination is not significant. Moreover, the effect of the estimated illumination in the estimation of the surface reflectance is not a target in this experiment.

b) Results and discussion

The results of the comparison of the highlight-reflectance for each image component with each reflectance reference are shown in Figure 6-5 to Figure 6-10, for the two light sources. These Figures show the comparison results for one example of the test images while more comparison results for other test images are shown in Appendix D (Figures D.9 to D.20). Compared to all reflectance references, highlight-reflectance-2 and highlight-reflectance-3 (i.e. estimated using diffuse image components) show, on average, better similarity than highlight-reflectance-1 (i.e. estimated using mixed image component). This is shown by the GFC value between each highlight-reflectance and each reflectance reference, which is given in Table 6-10, for the two light sources. The higher GFC value means higher similarity, shown by the results of comparing either highlight-reflectance-3 (i.e. diffuse image component–UGICA) or highlight-reflectance-2 (i.e. Diffuse Image Component–SCFICA) with all reflectance references. The average GFC value of the estimated surface spectral reflectance is improved by 1.1 % when the 'Diffuse Image Component–SCFICA' is used and by 4.1 % when 'Diffuse Image Component–UGICA' is used instead of the 'Mixed Image component'(Table 6-10). To conclude, the average GFC value of the estimated surface spectral reflectance is improved by 2.6 % when the diffuse image component is used instead of the mixed image component. This improvement is statistically significant, with a confidence level of 95%. The results of the statistical significance test are reported in Appendix E (Table E.7).

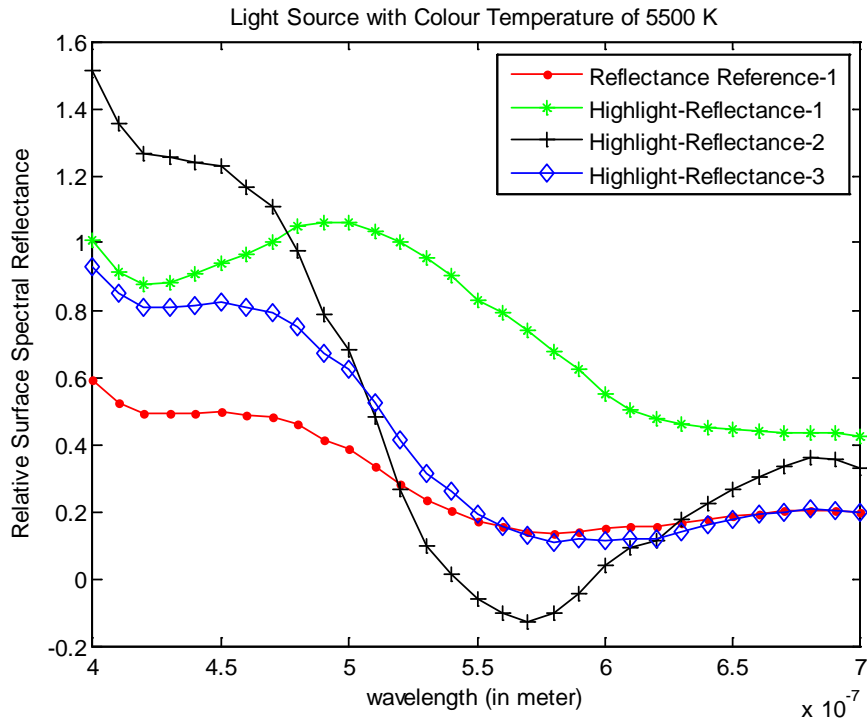


Figure 6-5 The surface reflectance (Highlight-Reflectance-1, Highlight-Reflectance-2, Highlight-Reflectance-3) estimated from pixels in image regions which have a strong specular component, shown in comparison to the surface reflectance (reflectance reference-1) estimated from pixels in image regions which have a weak specular component. The test and reference pixels are from images of the plastic blue ring illuminated by a light source with a colour temperature of 5500 K. The reference pixels are from the polarised image, without extracting the diffuse image component.

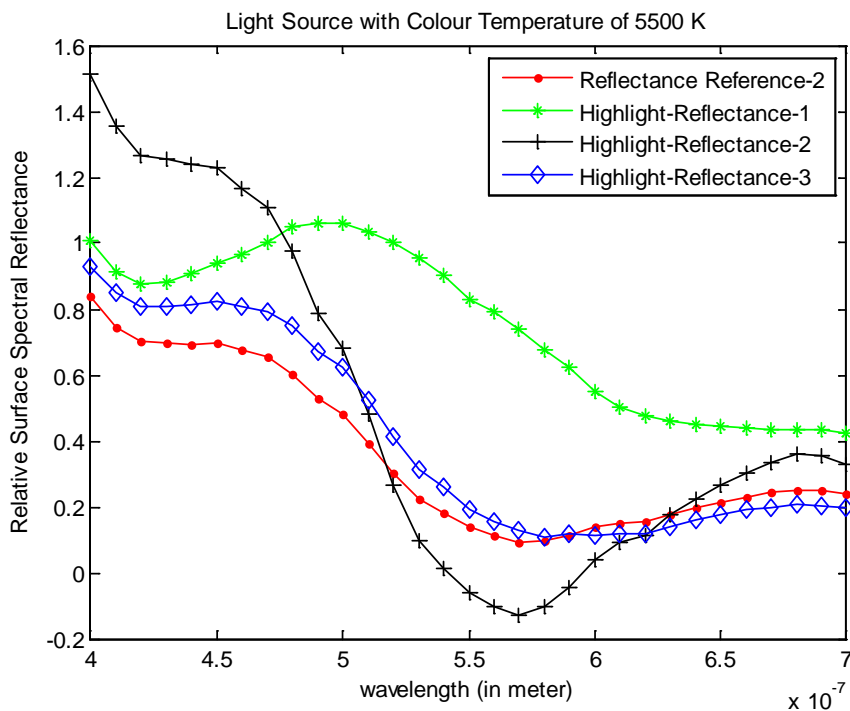


Figure 6-6 The surface reflectance (Highlight-Reflectance-1, Highlight-Reflectance-2, Highlight-Reflectance-3) estimated from pixels in image regions which have a strong specular component, shown in comparison to the surface reflectance (reflectance reference-2) estimated from pixels in image regions which have a weak specular component. The test and reference pixels are from images of the plastic blue ring illuminated by a light source with a colour temperature of 5500 K. The reference pixels are from the diffuse image component-SCFICA.

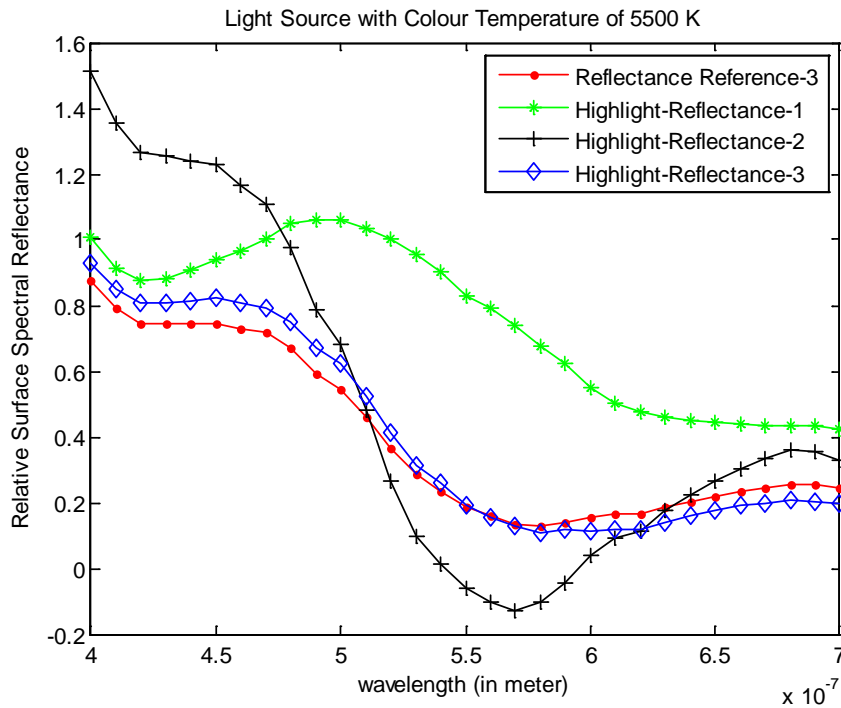


Figure 6-7 The surface reflectance (Highlight-Reflectance-1, Highlight-Reflectance-2, Highlight-Reflectance-3) estimated from pixels in image regions which have a strong specular component, shown in comparison to the surface reflectance (reflectance reference-3) estimated from pixels in image regions which have a weak specular component. The test and reference pixels are from images of the plastic blue ring illuminated by a light source with a colour temperature of 5500 K. The reference pixels are from the diffuse image component-UGICA.

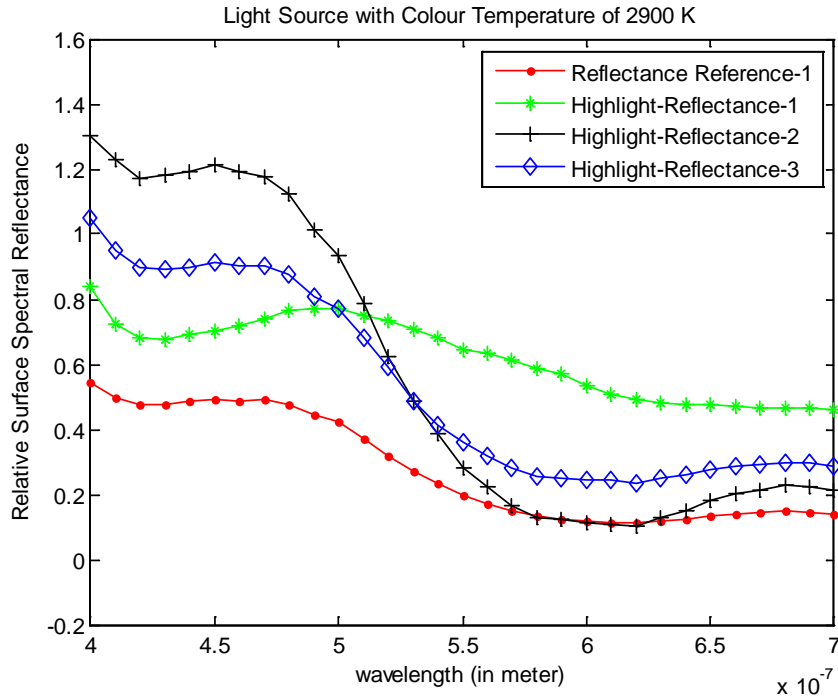


Figure 6-8 The surface reflectance (Highlight-Reflectance-1, Highlight-Reflectance-2, Highlight-Reflectance-3) estimated from pixels in image regions which have a strong specular component, shown in comparison to the surface reflectance (reflectance reference-1) estimated from pixels in image regions which have a weak specular component. The test and reference pixels are from images of the plastic blue ring illuminated by a light source with a colour temperature of 2900 K. The reference pixels are from the polarised image, without extracting the diffuse image component.

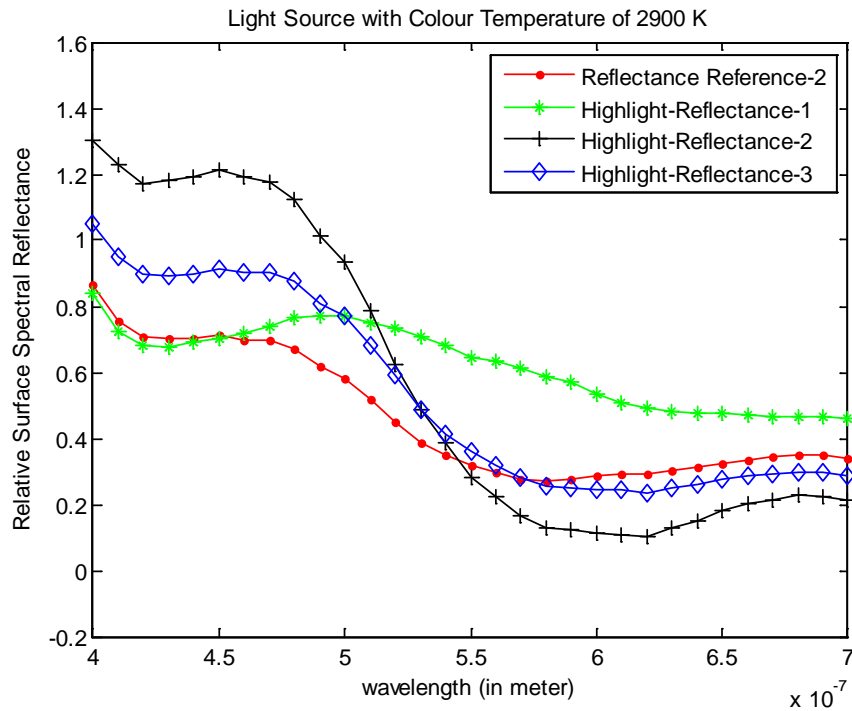


Figure 6-9 The surface reflectance (Highlight-Reflectance-1, Highlight-Reflectance-2, Highlight-Reflectance-3) estimated from pixels in image regions which have a strong specular component, shown in comparison to the surface reflectance (reflectance reference-2) estimated from pixels in image regions which have a weak specular component. The test and reference pixels are from images of the plastic blue ring illuminated by a light source with a colour temperature of 2900 K. The reference pixels are from the diffuse image component-SCFICA.

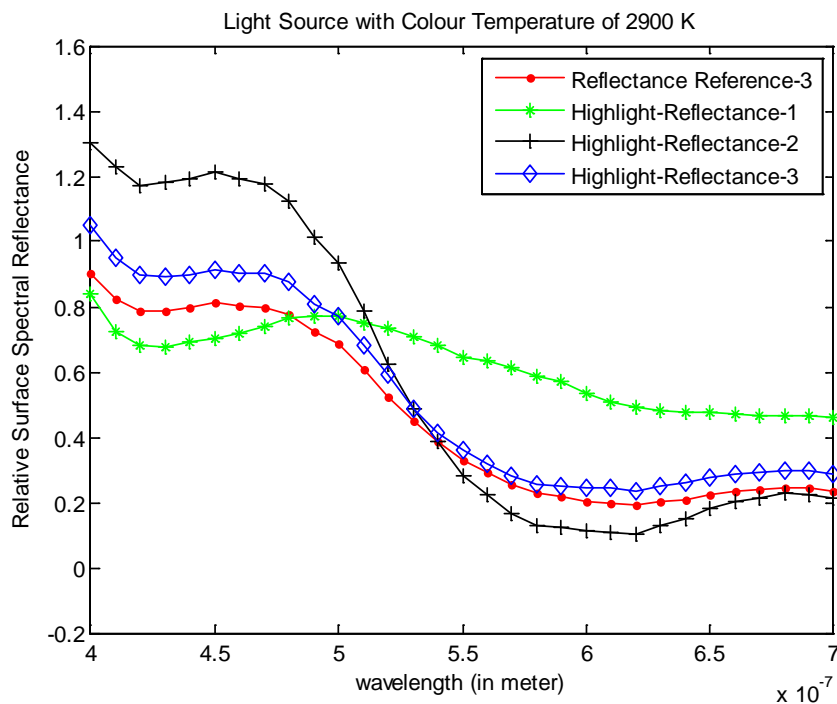


Figure 6-10 The surface reflectance (Highlight-Reflectance-1, Highlight-Reflectance-2, Highlight-Reflectance-3) estimated from pixels in image regions which have a strong specular component, shown in comparison to the surface reflectance (reflectance reference-3) estimated from pixels in image regions which have a weak specular component. The test and reference pixels are from images of the plastic blue ring illuminated by a light source with a colour temperature of 2900 K. The reference pixels are from the diffuse image component-UGICA.

Table 6-10 The GFC comparison between the surface reflectance (Highlight-Reflectance-1, Highlight-Reflectance-2, and Highlight-Reflectance-3) estimated from pixels in image regions which have a strong specular component, and the surface reflectance (reflectance reference-1, reflectance reference-2, reflectance reference-3) estimated from pixels in image regions which have a weak specular component. The test and reference pixels are from images of different objects illuminated by light sources with colour temperature of 5500 K and 2900 K. The reference pixels are respectively from the polarised image (without extracting the diffuse image component), the 'diffuse image component-SCFICA', and 'diffuse image component-UGICA'.

Light source	Object		Highlight-Reflectance-1	Highlight-reflectance-2	Highlight-reflectance-3
Colour Temperature 5500 K	Plastic blue ring	Reflectance Reference-1	0.9481	0.9388	0.9872
		Reflectance Reference-2	0.9031	0.9740	0.9944
		Reflectance Reference-3	0.9199	0.9643	0.9967
	Ceramic violet cup	Reflectance Reference-1	0.9730	0.9998	0.9829
		Reflectance Reference-2	0.9701	0.9988	0.9821
		Reflectance Reference-3	0.9487	0.9961	0.9948
	Plastic green ring	Reflectance Reference-1	0.9754	0.9965	0.9911
		Reflectance Reference-2	0.8987	0.9546	0.9738
		Reflectance Reference-3	0.9249	0.9714	0.9904
Colour Temperature 2900 K	Plastic blue ring	Reflectance Reference-1	0.9330	0.9868	0.9995
		Reflectance Reference-2	0.9649	0.9546	0.9909
		Reflectance Reference-3	0.9357	0.9856	0.9997
	Ceramic violet cup	Reflectance Reference-1	0.9818	0.9265	0.9947
		Reflectance Reference-2	0.9504	0.9718	0.9971
		Reflectance Reference-3	0.9674	0.9499	0.9993
	Plastic green ring	Reflectance Reference-1	0.9601	0.9098	0.9822
		Reflectance Reference-2	0.9897	0.9003	0.9980
		Reflectance Reference-3	0.9625	0.9204	0.9876
Average			0.9504	0.9611	0.9912
Standard Deviation			±0.0264	±0.0316	±0.0074

6.2.2.4 Experiment 4: Estimation of the surface spectral reflectance from mixed image components captured under natural day light sources with different colour temperatures.

a) Procedure

The aim of this experiment is to investigate how the proposed method for the third stage of the framework performs for estimating the surface spectral reflectance of different objects illuminated by natural day light sources with different colour temperatures, in terms of

similarity (measured as a GFC value) between the estimated and measured spectral reflectance curves.

The investigation in Experiment 4 is done based on the assumption that the selected pixels are mostly composed of diffuse reflection with a negligible amount of specular reflection. The selection of these pixels is done by the author based on empirical observation. In Experiment 4, the same surface reflectance estimation method used in previous experiments in this chapter is tested on Foster et al's data set [181].

b) Results and discussion

Figure 6-11 shows illustrative examples for some images of the Foster et al's data set [181], it also displays the pixel position (white square marker) for each image at which surface reflectance was estimated. In this Figure, the surface reflectance estimated at these pixels is shown in comparison with the measured surface reflectance. More illustrative examples for other images of Foster et al's data set are shown in Appendix D (Figure D.21).

As seen in Figure 6-11, the surface spectral reflectance is estimated well from the non-specular pixels for different images illuminated by natural day light illuminations with different colour temperatures. The estimated surface spectral reflectance has almost the same signature as the reflectance measured by Foster et al [181], which means the estimated reflectance effectively captures the colour of the surface material, but with a shift in amplitude. As explained in Experiment 2 (Section 6.2.2.2), this shift represents a change in the amplitude ratio between the two surface spectral reflectances, and it does not represent a change in the spectral characteristics which identify the colour of the material.

Furthermore, the surface reflectance estimates from a set of randomly selected pixels for each image are compared to the measured surface reflectances which are provided by Foster et al [181]. The number of pixels in this set is 100 and this number was chosen empirically after performing a number of exploratory experiments. This comparison is achieved by calculating the GFC and other error measurements which are shown in Table 6-11. The entries of Table 6-11 consist of the average of GFC and other error measurements over the set of pixels considered for each image in Foster et al's data set. This table also includes the average of the GFC value and of the other error measurements, for all images considered in the experiment.

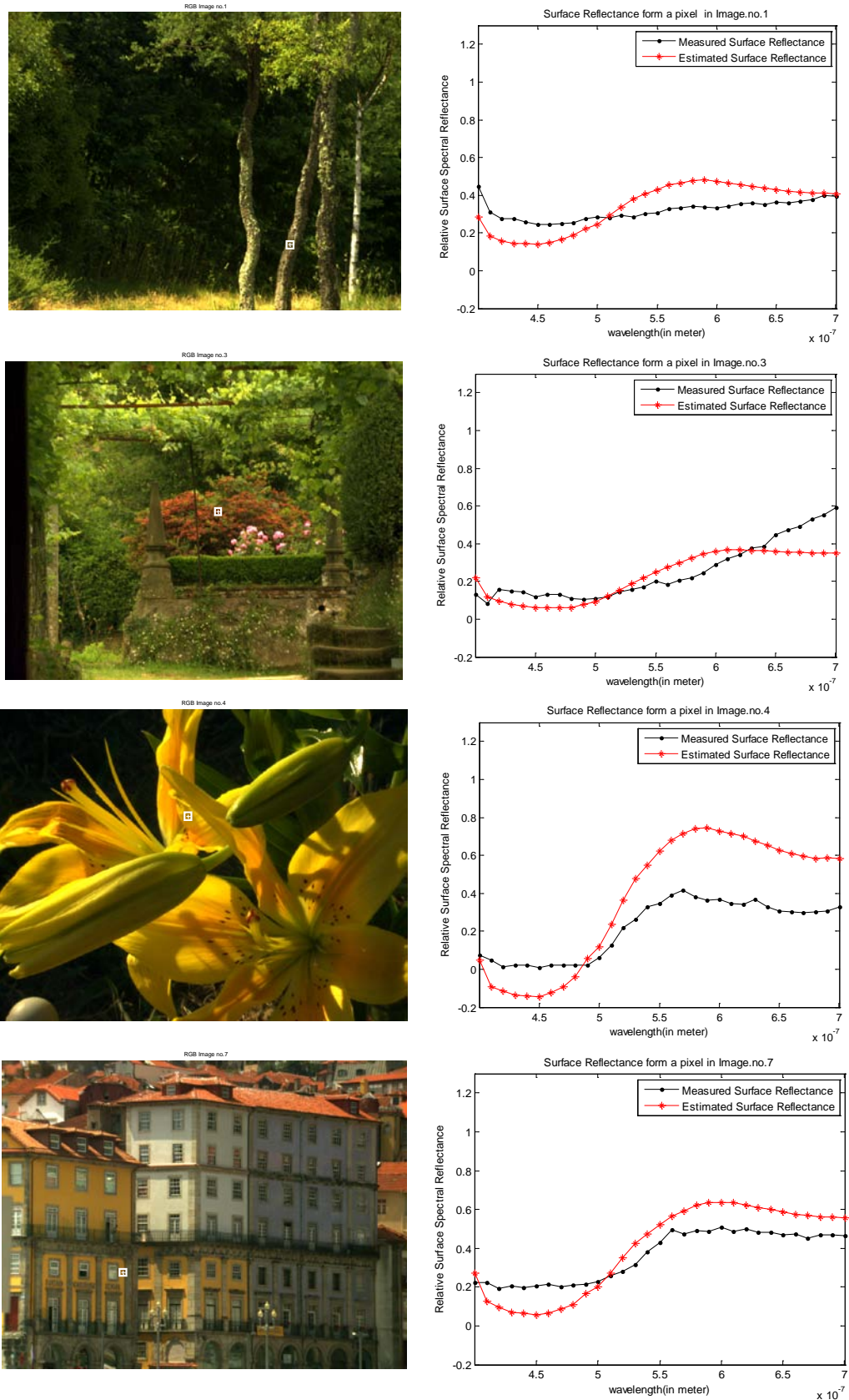


Figure 6-11 Illustrative examples for some images of the Foster et al's data set [181], with a white square marker to display the pixel position at which surface reflectance was estimated. The estimated surface reflectance of that pixel is shown in comparison with the measured surface reflectance.

In conclusion, compared to the measured surface reflectance, the estimated surface reflectance for different objects illuminated by different natural day light sources with different colour temperatures is obtained with an average GFC of 0.9608. This shows a close similarity between the estimated and the measured surface reflectances for different objects illuminated by natural day light sources with different colour temperatures. This average GFC cannot be compared to the ones achieved in Experiment 2 (Section 6.2.2.2). This is because different data sets are used in these two experiments.

Table 6-11 The averaged GFC measurement and other error measurements for surface reflectance estimated on the Foster et al's data set [181].

Image	GFC	RMS error	Median error	Mean error	Angular error (in degree)
The first image	0.9701	9.96×10^{-2}	5.03×10^{-2}	1.82×10^{-2}	8.74
The second image	0.9095	37.81×10^{-2}	39.97×10^{-2}	27.86×10^{-2}	5.40
The third image	0.9519	13.19×10^{-2}	3.49×10^{-2}	6.22×10^{-2}	8.31
The fourth image	0.9850	24.83×10^{-2}	24.22×10^{-2}	15.56×10^{-2}	6.35
The fifth image	0.9326	34.11×10^{-2}	34.51×10^{-2}	28.04×10^{-2}	7.54
The sixth image	0.9775	24.38×10^{-2}	23.38×10^{-2}	19.88×10^{-2}	8.66
The seventh image	0.9810	10.62×10^{-2}	8.27×10^{-2}	2.98×10^{-2}	8.04
The eighth image	0.9788	17.79×10^{-2}	13.94×10^{-2}	13.50×10^{-2}	5.65
Average	0.9608	21.59×10^{-2}	19.10×10^{-2}	14.48×10^{-2}	7.34
Standard Deviation	± 0.0272	$\pm 10.55 \times 10^{-2}$	$\pm 13.64 \times 10^{-2}$	$\pm 10.39 \times 10^{-2}$	± 1.35

6.3 General Discussion

The GFC values obtained in all experiments in this chapter, as given in tables (Table 6-6, Table 6-7, Table 6-10, and Table 6-11), show that the proposed surface reflectance estimation method provides reasonably accurate estimates. Noting that in these experiments the proposed surface reflectance estimation method includes some sources of error. These sources are the normalisation process, the diffuse geometrical scale factor (w_d) (Equation (4-20)), and the use of camera sensor sensitivity characteristics for estimating surface reflectance from image which is captured with different camera sensor sensitivity characteristics. The effects of these errors are discussed below.

- The normalisation process, which introduces loss of information, is required in these experiments to produce a common reference as explained in Section 6.2.1. However, in these experiments, the double precision (32-bit number representation) of pixel values was used in order to minimise the effect of this error. Furthermore, this error predominantly affects the absolute value of the estimated surface reflectance and have insignificant effect on the accuracy of the estimation of the relative spectral

surface reflectance, which is estimated by the proposed surface reflectance estimation method.

- Due to the difficulty in calculating the diffuse geometrical scale factor (w_d) for each pixel in the image [1], in these experiments this factor is considered to be 1 for simplicity. This assumption will affect the absolute value of the estimated surface reflectance; however it will not affect the relative spectral surface reflectance. The proposed method estimates the relative spectral surface reflectance, hence the value of the geometrical scale factor does not significantly affect the accuracy of the estimation process.
- The same camera sensor sensitivity characteristics are used for all experiments. Although these camera characteristics are not the ones used to create Foster et al's data set however, the results in Experiment 4 (Section 6.2.2.4), in which the surface reflectance estimated from Foster et al's data set, show reasonable estimation accuracy, yielding an average GFC value of 0.9608. This could be due to a fortunate similarity between camera sensitivity characteristics, which can be inferred from the results of Experiment 4 which show that the sensor sensitivity characteristics have a minimal effect on the estimation.

In addition, some of the test images look grainy which means that random noise is included in the pixel values. As seen in the results which correspond to these images in Chapters 5 and 6, this noise does not affect the estimation process. This is because the estimates of the illumination and the surface reflectance are calculated separately from a number of pixels and then averaged. Hence the averaging process reduces the effect of the noise.

The proposed framework has been tested initially using an in-house data set of 16 images containing two light sources and 4 objects, all images were taken using camera sensor sensitivity characteristics shown in Figure 2-3. In order to test whether the framework can be extended to be used for more lights sources and objects, the experiments for illumination estimation and surface reflectance estimation have been repeated using Foster et al's data set (Experiment 4 (Section 5.3.2.4) and Experiment 4 (Section 6.2.2.4)). The results obtained in these experiments confirm this proposition as shown in Table 5-8 and Table 6-11.

Moreover, the performance assessment of the proposed framework is based on the embodiments (i.e specific implementations) which are considered in this thesis (Chapter 4).

Nevertheless, it is possible to use other embodiments of the proposed framework. Further research is required in order to find the optimum embodiments for the framework.

Moreover, the use of blind signal separation and the dichromatic reflection model in the proposed framework give two advantages compared to existing colour constancy frameworks. Firstly, the achievement of colour constancy does not depend on the number of observed colour surfaces in the scene; it therefore can deal robustly with real images. Secondly, the proposed framework does not require computationally expensive operations such as generating a correlation or gamut matrix and a training process, which are needed in existing frameworks.

The results show that colour constancy is achieved with reasonable accuracy. The data set required for the evaluation of the proposed framework is not standard data set as polarised images are needed. However, the results were evaluated on its own as it has been compared with manufacturer's specifications and measured values. While the inspection and discussion of the results reported in the relevant literature is used to gain an insight into how the proposed framework performs relative to others, a side-by-side comparison is not possible due to inavailability of a common data set and lack of a common reference.

6.4 Summary

This chapter assesses the performance of the estimation of the surface spectral reflectance using the extracted diffuse image component. This estimation is performed by the last stage of the framework. The performance is evaluated quantitatively in three ways. The evaluation is conducted through four experiments. These experiments aim to investigate the performance of the proposed method to estimate surface reflectance and to explore the factors which affect its estimation accuracy, measured in terms of GFC value, within the colour constancy framework.

Experiment 1 investigates how the estimated illumination affects the performance of the proposed method for estimating surface spectral reflectance, in comparison to the reflectance estimated using the illumination specification provided by the manufacturer. It is shown that there is no significant difference between the surface reflectance estimated using the estimated illumination or using the manufacturer's illumination specification. Hence, the estimated illumination is a valid input for estimating surface spectral reflectance within the framework.

Experiment 2 further assesses the proposed method for estimating surface spectral reflectance by comparing the surface spectral reflectance estimated for the same pixel of an object illuminated by two alternative light sources, one with colour temperature of 5500 K and the other with colour temperature of 2900 K. It is observed that the estimated surface spectral reflectance has almost the same spectral signature for the two light sources. The comparison between the surface spectral reflectance estimates corresponding to each of the two light sources gives an average GFC value which ranges from 0.9611 to 0.9887, depending on the type of blind separation technique that is used. The results show that there is a statistically significant improvement in the performance of the proposed surface reflectance method by 2.8%, in terms of the average GFC value, when the UGICA separation technique is used instead of SCFICA. Given that the surface spectral reflectance is the output of the last stage of the framework, which depends on the output of the previous two stages, it follows that the measured GFC indicates the performance of the whole framework. The observed high GFC value means that the estimates of surface reflectance under the two light sources are very similar, despite the differences between the two illuminants. This similarity implies that the extracted surface reflectance is significantly independent of illumination characteristics, hence showing that the proposed framework achieves colour constancy.

In Experiment 3, the improvement in the estimation accuracy for surface reflectance is measured in terms of GFC value between the surface reflectance obtained by using an explicitly extracted diffuse image component instead of the mixed image components (i.e. composed of blended specular and diffuse components). Depending on the type of the blind separation technique which is used to extract the diffuse component, the average GFC value of the estimated surface spectral reflectance improves in the range from 1.1 % to 4.1 % when the diffuse component is used instead of the mixed image component. The observed results show a statistically significant improvement in the accuracy of the estimated surface spectral reflectance by 2.6% in terms of average GFC value when the diffuse image component is used instead of the mixed image component.

Experiment 4 investigates the performance of the proposed method for estimating the surface spectral reflectance of different objects illuminated by natural day light sources with different colour temperatures. It is shown that an average GFC of 0.9608 is obtained when comparing the surface reflectance measured for a set of hyperspectral images (i.e. Foster et al's data set) to the estimated surface reflectance for different objects illuminated by natural day light sources with different colour temperatures.

7

Conclusions and Future Work

7.1 Conclusions

Colour constancy is considered as one of the most important requirements for various applications, which use colour as the main feature in image or video processing. Achieving colour constancy is a challenge which has been addressed by other researchers and has also been addressed in this thesis. The research presented in this thesis aims to investigate the effectiveness of applying blind signal separation integrated with a physical model of image formation into a framework for achieving colour constancy. The particular model considered in this study is the dichromatic reflection model. The research questions addressed by this research are “how should blind signal separation be integrated with the dichromatic model?” and “how does the proposed framework perform in the context of achieving colour constancy?”

The colour constancy survey revealed that most illumination estimation methods based on the dichromatic model (as used in approaches to colour constancy) utilise the mixed image components which is a mixture of specular and diffuse components and try to estimate illumination chromaticity by analyzing it in different colour spaces. Moreover, most of the methods based on dichromatic reflection suffer from the problem of segmenting image regions which correspond to multi-coloured surfaces in the highlight areas. This thesis proposed an alternative approach embodied in a framework which integrates blind signal separation and the dichromatic model of image formation. By using blind signal separation the estimation of illumination can be achieved more accurately from the explicitly separated specular component unlike the conventional approaches that use mixed image components. Moreover, the explicitly separated diffuse image can be used to achieve colour constancy instead of mixed image components that are used by conventional approaches. In addition, by

using blind signal separation the challenge of segmenting multi-coloured surfaces in images can be avoided. Two suitable blind signal separation techniques have been proposed within the developed framework. These two techniques are the spatially constrained FastICA technique, which is characterised by its simplicity, efficiency, and ability to differentiate between the separated specular and diffuse components and the technique developed by Umeyama and Godin, which has successfully been used for separating specular and diffuse components in other image processing applications. Moreover, the use of blind signal separation and the dichromatic reflection model give two advantages to the proposed framework compared to existing colour constancy frameworks. Firstly, the achievement of colour constancy does not depend on the number of observed colour surfaces in the scene; it therefore can deal robustly with real images. Secondly, the proposed framework does not require computationally expensive operations such as generating a correlation or gamut matrix and a training process, which are needed in existing frameworks. The developed framework consists of three stages, which are: separation of image components (specular and diffuse components), estimation of ISPD, and estimation of surface spectral reflectance.

The methodology used for evaluating the performance of the framework involves the development of algorithms, their implementation in software, and their assessment using well-designed experiments anchored on quantitative performance measurement methods. The GFC is used to evaluate the performance of the framework. GFC is a measure of degree of similarity between the estimated spectral distribution and a known reference. GFC values range between 0 and 1; a higher value representing a higher degree of similarity. The following observations were made in the evaluation of the proposed framework stages, from which the performance of the whole framework was deduced.

Using the image data set generated by the author, the comparison of the manufacturer's specifications of the ISPD, for two light sources with colour temperature of 5500 K and 2900 K, with the ISPD estimated using the explicitly extracted specular image component, has an average GFC value equal to 0.9830 and 0.9215, respectively after empirical thresholding. The results also show a statistically significant improvement in the illumination estimation accuracy (measured in terms of average of GFC) by 3.8% and 2.9% when the empirical threshold is used instead of the automatic threshold for the 5500 K light source and the 2900 K light source respectively. Moreover, there is no significant difference in the estimation accuracy of the ISPD obtained using the specular components extracted by the SCFICA and UGICA [28] blind separation techniques, for the images of scenes illuminated with the

artificial light sources with colour temperature of 5500 K and 2900 K. The selection of illumination basis functions has an impact on the accuracy of the illumination estimation method used within the colour constancy framework, measured in terms of the GFC value. Furthermore, it is found that there is a statistically significant improvement by 2.9% in the average GFC value of the estimated ISPD when the specular component is used instead of mixed image components. In addition, experiments using Foster et al's image data set yielded an average GFC of 0.9986 between the illumination measured by Foster et al and the ISPD estimated, for different natural day light sources with different colour temperatures, using the mixed image components.

By using the author's data set, it was found that the illumination, estimated in the second stage of the developed framework, is a valid input for estimating surface spectral reflectance within the framework. Comparison of the surface spectral reflectance, estimated for the same pixel of an object illuminated by two light sources with colour temperatures of 5500 K and 2900 K, shows that the estimated surface spectral reflectance has almost the same spectral signature for the two light sources. The comparison between the surface spectral reflectance estimates corresponding to each of the two light sources gives an average GFC value which ranges from 0.9611 to 0.9887, depending on the type of the blind separation technique that is used. The results show that there is a statistically significant improvement in the performance of the proposed surface reflectance method by 2.8% in terms of average GFC value when the UGICA separation technique is used instead of SCFICA. Given that the surface spectral reflectance is the output of the last stage of the framework, which depends on the output of the previous two stages, it follows that the measured GFC indicates the performance of the whole framework. The observed high GFC value means that the estimates of surface reflectance under the two light sources are very similar, despite the differences between the two illuminants. This similarity implies that the extracted surface reflectance is significantly independent of illumination characteristics, hence showing that the proposed framework achieves a significant degree of colour constancy. Moreover, the observed results show a statistically significant improvement in the accuracy of the estimated surface spectral reflectance by 2.6% in terms of average GFC value when the diffuse image component is used instead of the mixed image component. Furthermore, compared to the measured surface spectral reflectance and using Foster et al's image data set, the surface spectral reflectance estimated using the mixed image components has an average value of the GFC equal to 0.9608.

This thesis shows the applicability of blind signal separation integrated with the dichromatic model of image formation into a framework for achieving colour constancy. The proposed framework is valid for inhomogeneous opaque surfaces with dielectric materials, whose atomic structure follow the dichromatic reflection model. However the proposed framework is not valid for the transparent or translucent materials, whose atomic structure does not follow the dichromatic reflection model [1]. The proposed framework requires a pair of images for same scene, acquired with different polarisation angles. In the proposed framework, suitable illumination and surface reflectance basis functions need to be known.

The ability to obtain an accurate estimate of surface spectral reflectance allows the determination of an object actual colour, independent of illumination. This is very useful in a wide range of practical applications. In machine vision applications, the work presented in this thesis offers a new way for detecting material colour with improved accuracy. In colour matching applications such as cinematography and film making, the proposed approach will offer a more accurate colour identification capability. In colour reproduction applications such as realistic 3-D computer graphics and animation, the proposed approach is likely to help improve the realism of computer-generated objects. The accurate estimation of colour presented in this thesis has the potential to improve the accuracy of automated object detection. This is practically useful in video analytics and intelligent surveillance systems. Further, the contribution towards improving object detection and segmentation is expected to facilitate content-based coding of real images.

The main contribution of this thesis is the development of a novel colour constancy framework, and experimental findings about the performance of the framework. The proposed framework consists of a new method to estimate the ISPD by using an explicitly extracted specular component instead of mixed image components. Other researchers use a composite image representation where each pixel is a blend of a specular component and a diffuse component. Furthermore, the proposed framework includes a new method for estimating the surface spectral reflectance using an explicitly extracted diffuse component instead of mixed image components which are used by other researchers.

7.2 Future Work

Although the developed colour constancy framework is able to identify the colour of the material (i.e. achieve a significant degree of colour constancy) with accuracy ranging between 0.9611 and 0.9887 in terms of average GFC value, and the performance of all stages within

this framework have been examined individually, the following issues require further investigation.

- To find out a method that identifies the optimal threshold value automatically, in order to avoid the use of empirical selection of the threshold value (i.e. used to extract the significant specular pixels that are used in the illumination estimation). The motivation of this is to increase the degree of automation of the framework.
- There is a need to discover the possibility of estimating the sensor response of the camera from the specular component with a known ISPD. This is because most of camera manufacturers do not release the sensor response of their cameras. By using the specular component instead of the diffuse component less number of parameters is required to be known in order to estimate the sensor response of the camera.
- To create a comprehensive standard data set which contains many pairs of images captured under more than two different (artificial and natural) light sources, including the measured illumination of these lights source, the measured surface reflectance of the captured objects, and the sensor response of the camera used to capture images is required. The generation of this data set will enable researchers to test and improve each stage of the developed framework. Moreover, a robust and trustable reference (diffuse or specular component) for these pairs of image is needed, to be made available, in order to measure the accuracy of the separation techniques.
- To generate trustable global illumination basis functions which are valid for most type of light sources, together with the values of illumination basis function coefficients which correspond to these light sources. The reason for this suggested further work is also to increase the degree of automation of the framework.
- To find out an optimum method to be used in each stage of the framework, in order to achieve the best colour constancy.
- In the evaluation of the proposed framework, uncompressed raw images are used in order to avoid any information loss. Now after the hypothesis has been verified, it would be useful to investigate the effect of different compression techniques on the accuracy of the proposed framework.

References

- [1] S. Shafer, "Using Color to Separate Reflection Components," *Color Research and Applications*, vol. 10, no. 4, pp. 210-218, 1985.
- [2] S. Tominaga and B. A. Wandell, "Natural Scene-Illuminant Estimation using the Sensor Correlation," *Proceedings of IEEE*, vol. 90, no. 1, pp. 42-56, 2002.
- [3] S. D. Hordley, "Scene Illuminant Estimation: Past, Present, and Future," *Color Research & Application*, vol. 31, no. 4, pp. 303-314, 2006.
- [4] K. Barnard, "Modeling Scene Illumination Colour for Computer Vision and Image Reproduction: A Survey of Computational Approaches" Technical report, Simon Fraser University, 1998.
- [5] R. W. G. Hunt, *The Reproduction of Colour*, 6th ed: John Wiley & Sons, Ltd, 2004.
- [6] G. Buchsbaum, "A Spatial Processor Model for Object Colour Perception," *Journal of the Franklin Institute*, vol. 310, pp. 1-26, 1980.
- [7] J. J. McCann and K. Houston, "Calculating Color Sensations from Arrays of Physical Stimuli," *IEEE Transaction on Systems Man Cybern*, vol. 13, pp. 1000-1007, 1983.
- [8] E. H. Land, "Recent Advances in Retinex Theory and Some Implications for Cortical Computations: Color Vision and the Natural Image," *Proceedings of the National Academy of Sciences of the United States of America*, vol. 80, pp. 5163-5169, 1983.
- [9] L. T. Maloney and B. A. Wandell, "Color Constancy: A Method for Recovering Surface Spectral Reflectance," *Journal of Optical Society of America A. (JOSAA)*, vol. 3, no. 1, pp. 29-33, 1986.
- [10] M. D'Zmura and P. Lennie, "Mechanisms of Color Constancy," *Journal of Optical Society of America A. (JOSAA)*, vol. 3, no. 1, pp. 1662-1672, 1986.
- [11] M. S. Drew and B. V. Funt, "Calculating Surface Reflectance using A Single-Bounce Model of Mutual Reflection," *Proceedings of the Third International Conference on Computer Vision*, pp. 394-399, 1990.
- [12] G. J. Klinker, S. A. Shafer, and T. Kanade, "A Physical Approach to Color Image Understanding," *International Journal of Computer Vision*, vol. 4, no. 1, pp. 7-38, 1990.
- [13] B. V. Funt and M. S. Drew, "Color Space Analysis of Mutual Illumination," *IEEE Transactions on Pattern Analysis and Machine Intelligence*, vol. 15, no. 12, pp. 1319-1326, 1993.
- [14] W. T. Freeman and D. H. Brainard, "Bayesian Decision Theory, the Maximum local Mass Estimate, and Color Constancy," *Proceedings of IEEE International Conference on Computer Vision*, pp. 210-217, 1995.
- [15] G. D. Finlayson and S. Hordley, "Improving Gamut Mapping Color Constancy," *IEEE Transaction on Image Processing*, vol. 9, no. 10, pp. 1774-1783, 2000.
- [16] G. D. Finlayson, S. D. Hordley, and P. M. Hubel, "Color by Correlation: A Simple, Unifying Framework for Color Constancy," *IEEE Transactions on Pattern Analysis and Machine Intelligence*, vol. 23, no. 11, pp. 1209-1221, 2001.

-
- [17] G. D. Finlayson and S. D. Hordley, "Color Constancy at A Pixel," *Journal of Optical Society of America A.(JOSAA)*, vol. 2, no. 18, pp. 253-264, 2001.
- [18] G. D. Finlayson and G. Schaefer, "Solving for Color Constancy Using a Constrained Dichromatic Reflection Model," *International Journal of Computer Vision and Pattern Recognition*, vol. 42, no. 3, pp. 127-144, 2001.
- [19] K. Barnard, V. Cardei, and B. Funt, "A Comparison of Computational Color Constancy Algorithms—Part I: Methodology and Experiments with Synthesized Data," *IEEE Transaction on Image Processing*, vol. 11, no. 9, pp. 972-983, 2002.
- [20] K. Barnard, L. Martin, A. Coath, and B. Funt, "A Comparison of Computational Color Constancy Algorithms—Part II: Experiments with Image Data," *IEEE Transaction on Image Processing*, vol. 11, no. 9, pp. 985-996, 2002.
- [21] R. T. Tan, K. Nishino, and K. Ikeuchi, "Color Constancy through Inverse Intensity Chromaticity Space," *Journal of the Optical Society of America A. (JOSAA)*, vol. 3, no. 21, pp. 321-334, 2004.
- [22] G. D. Finlayson and E. Trezzi, "Shades of Gray and Colour Constancy," Proceedings of Color Imaging Conference, Scottsdale, Arizona, USA, pp. 37-41, 2004.
- [23] J. Verges, "Color Constancy and Image Segmentation Techniques for Applications to Mobile Robotics" PhD Thesis, Technical University of Catalonia, 2005.
- [24] G. D. Finlayson, S. D. Hordley, and P. Morovic, "Colour Constancy using the Chromagenic Constraint," Proceedings of IEEE Computer Society Conference on Computer Vision and Pattern Recognition, vol. 1, pp. 1079-1086, 2005.
- [25] G. Finlayson, S. Hordley, and I. Tastl, "Gamut Constrained Illuminant Estimation," *International Journal of Computer Vision*, vol. 67, no. 1, pp. 93-109, 2006.
- [26] R. Gershon, A. D. Jepson, and J. K. Tsotsos, "From [R,G,B] to Surface Reflectance: Computing Color Constant Descriptors in Images," *Perception*, pp. 755-758, 1988.
- [27] A. Gijsenij and T. Gevers, "Color Constancy using Image Regions," Proceedings of IEEE International Conference on Image Processing, vol. 3, pp. 501-504, 2007.
- [28] S. Umeyam and G. Godin, "Separation of Diffuse and Specular Components of Surface Reflection by Use of Polarization and Statistical Analysis of Images," *IEEE Transactions on Pattern Analysis and Machine Intelligence*, vol. 26, no. 5, pp. 639-647, 2004.
- [29] H. C. Lee, "Method for Computing the Scene-Illuminant chromaticity from Specular Highlights," *Journal of Optical Society of America A. (JOSAA)*, vol. 3, no. 10, pp. 1694-1699, 1986.
- [30] R. T. Tan, "Illumination Color and Intrinsic Surface Properties-Physics-Based Color Analyses from A Single Image" PhD Thesis, The University of Tokyo, 2003.
- [31] D. B. Judd, D. L. MacAdam, G. Wyszecki, H. W. Budde, H. R. Condit, S. T. Henderson, and J. L. Simonds, "Spectral Distribution of Typical Daylight as A Function of Correlated Color Temperature," *Journal of the Optical Society of America*, vol. 54, no. 8, pp. 1031-1040, 1964.
- [32] D. Slater and G. Healey, "What is the Spectral Dimensionality of Illumination Functions in Outdoor Scenes," Proceedings of IEEE Computer Society Conference on Computer Vision and Pattern Recognition, pp. 105-110, 1998.
- [33] J. P. S. Parkkinen, J. Hallikainen, and T. Jasskelainen, "Characteristic Spectra of Munsell Colors," *Journal of Optical Society of America A. (JOSAA)*, vol. 6, no. 2, pp. 318-322, 1989.
- [34] J. Cohen, "Dependence of the Spectral Reflectance Curves of the Munsell Color Chips," *Psychon. Sci*, vol. 1, pp. 369-370, 1964.

- [35] G. Healey, "Using Color for Geometry-Insensitive Segmentation," *Journal of Optics Society of America A. (JOSAA)*, vol. 6, no. 6, pp. 920-937, 1989.
- [36] S. K. Nayar, K. Ikeuchi, and T. Kanade, "Surface Reflection: Physical and Geometrical Perspectives," *IEEE Transactions on Pattern Analysis and Machine Intelligence*, vol. 13, no. 7, pp. 611-634, 1991.
- [37] H. C. Lee, E. J. Breneman, and C.P.Schulte, "Modeling Light Reflection for Computer Color Vision," *IEEE Transactions on Pattern Analysis and Machine Intelligence*, vol. 12, pp. 402-409, 1990.
- [38] S. Tominaga and B. A. Wandell, "Standard Surface-Reflectance Model and Illumination Estimation," *Journal of Optical Society of America A. (JOSAA)*, vol. 6, no. 4, pp. 576-584, 1989.
- [39] R. T. Tan and K. Ikeuchi, "Separating Reflection Components of Textured Surfaces Using a Single Image," *IEEE Transactions on Pattern Analysis and Machine Intelligence*, vol. 27, no. 2, pp. 178-193, 2005.
- [40] The Imaging Source, "Spectral Sensitivity and Color Formats", http://www.theimagingsource.com/downloads/fwcamspecwp.en_US.pdf, Last accessed: August 2010.
- [41] R. T. Tan and K. Ikeuchi, "Reflection Components Decomposition of Textured Surfaces using Linear Basis Functions," Proceedings of IEEE Computer Society Conference on Computer Vision and Pattern Recognition, vol. 1, pp. 125-131, 2005.
- [42] G. J. Klinker, S. A. Shafer, and T. Kanade, "The Measurement of Highlights in Color Images," *International Journal of Computer Vision*, vol. 2, no. 1, pp. 7-32, 1988.
- [43] P. Tan, L. S, L. Quan, and H.-Y. Shum, "Highlight Removal by Illumination-Constrained Inpainting," Proceedings of the Ninth IEEE International Conference on Computer Vision, vol. 1, pp. 164-169, 2003.
- [44] P. Tan, L. Quan, and L. S, "Separation of Highlight Reflections on Textured Surfaces," Proceedings of IEEE Computer Society Conference on Computer Vision and Pattern Recognition, vol. 2, pp. 1855-1860, 2006.
- [45] R. T. Tan, K. Nishino, and K. Ikeuchi, "Separating Reflection Components Based on Chromaticity and Noise Analysis," *IEEE Transactions on Pattern Analysis and Machine Intelligence*, vol. 26, no. 10, pp. 1373-1379, 2004.
- [46] Z.-H. Wang, H.-M. Liu, and X. Xue, "HSICT: A Method for Removing Highlight and Shading in Color Image," Proceedings of International Conference on Wavelet Analysis and Pattern Recognition, pp. 51-56, 2009.
- [47] Y. Sato and K. Ikeuchi, "Temporal-Color Space Analysis of Reflection," *Journal of Optical Society of America A. (JOSAA)*, vol. 11, no. 11, pp. 2990-3002, 1994.
- [48] S. Lin and H.-Y. Shump, "Separation of Diffuse and Specular Reflection in Color Images," Proceedings of IEEE Computer Society Conference on Computer Vision and Pattern Recognition, vol. 1, pp. 341-346, 2001.
- [49] S. Lin, Y. Li, S. Kang, X. Tong, and H.-. Y.Shum, "Diffuse-Specular Separation and Depth Recovery from Image Sequences," Proceedings of European Conference on Computer Vision, pp. 210-224, 2002.
- [50] L. B. Wolff, "Polarization-Based Material Classification from Specular Reflection," *IEEE Transactions on Pattern Analysis and Machine Intelligence*, vol. 12, no. 11, pp. 1059-1071, 1990.

-
- [51] S. K. Nayar, X.-S. Fang, and T. Boult, "Removal of Specularities using Color and Polarization," Proceedings of IEEE Computer Society Conference on Computer Vision and Pattern Recognition, New York, USA, pp. 583-590, 1993.
- [52] S. K. Nayar, X.-S. Fang, and T. Boult, "Separation of Reflection Components Using Color and Polarization," *International Journal of Computer Vision*, vol. 21, no. 3, pp. 163-186, 1997.
- [53] J. van de Weijer, T. Gevers, and A. Gijsenij, "Edge-Based Color Constancy," *IEEE Transactions on Image Processing*, vol. 16, no. 9, pp. 2207-2213, 2007.
- [54] J.-z. Yuan, L.-y. Tian, H. Bao, J.-h. Huang, and R.-z. Zhang, "Illumination Estimation Combining Physical and Statistical Approaches," Proceedings of the Third International Symposium on Intelligent Information Technology Application, vol. 1, pp. 365-368, 2009.
- [55] D. A. Forsyth, "A Novel Approach To Colour Constancy," Proceedings of the Second International Conference on Computer Vision., pp. 9-18, 1988.
- [56] G. D. Finlayson, "Color in Perspective," *IEEE Transactions on Pattern Analysis and Machine Intelligence*, vol. 18, no. 10, pp. 1034-1038, 1996.
- [57] A. Gijsenij, T. Gevers, and J. v. d. Weijer, "Generalized Gamut Mapping Using Image Derivative Structures for Color Constancy," *International Journal of Computer Vision*, vol. 86, no. (2-3), pp. 127-139, 2010.
- [58] S. Skaff, T. Arbel, and J. J. Clark, "Active Bayesian Color Constancy with Non-Uniform Sensors," Proceedings of the 16th International Conference on Pattern Recognition, vol. 2, pp. 681-684, 2002.
- [59] P. V. Gehler, C. Rother, A. Blake, T. Minka, and T. Sharp, "Bayesian Color Constancy Revisited," Proceedings of IEEE Conference on Computer Vision and Pattern Recognition, pp. 1-8, 2008.
- [60] D. H. Brainard and W. T. Freeman, "Bayesian Color Constancy," *Journal of Optical Society of America A. (JOSAA)*, vol. 14, no. 7, pp. 1393-1411, 1997.
- [61] G. D. Finlayson, P. M. Hubel, and S. D. Hordley, "Color by Correlation," Proceedings of the 5th Color Imaging Conference, pp. 6-11, 1997.
- [62] K. Barnard, L. Martin, and B. Funt, "Colour by Correlation in a Three Dimensional Colour Space," Proceedings of the 6th European Conference on Computer Vision, pp. 275-289, 2000.
- [63] B. Funt, V. Cardei, and K. Barnard, "Neural Network Color Constancy and Specularly Reflecting Surfaces," Proceedings of AIC Color 97, Kyoto, Japan, pp. 25-30, 1997.
- [64] B. V. Funt, "Color Constancy in Digital Imagery," Proceedings of the International Conference on Image Processing, vol. 3, pp. 55-59, 1999.
- [65] B. Funt, V. Cardei, and K. Barnard, "Learning Color Constancy," Proceedings of the Fourth Color Imaging Conference, pp. 58-60, 1996.
- [66] V. Cardei and B. Funt, "Committee-Based Color Constancy," Proceedings of the Seventh Color Imaging Conference, pp. 311-313, 1999.
- [67] V. Cardei, B. Funt, and K. Barnard, "White Point Estimation for Uncalibrated Images," Proceedings of the Seventh Color Imaging Conference, pp. 97-100, 1999.
- [68] V. Cardei, B. Funt, and K. Barnard, "Estimating the Scene Illumination Chromaticity by Using A Neural Network," *Journal of Optical Society of America A. (JOSAA)*, vol. 19, no. 12, pp. 2374-2386, 2002.

- [69] C.-T. Lin, K.-W. Fan, and W.-C. Cheng, "An Illumination Estimation Scheme for Color Constancy Based on Chromaticity Histogram and Neural Network," *Proceedings of IEEE International Conference on Systems, Man and Cybernetics*, vol. 3, pp. 2488-2494, 2005.
- [70] B. Funt and W. Xiong, "Estimating Illumination Chromaticity via Support Vector Regression," *Proceedings of Color Imaging Conference, Scottsdale, Arizona, USA*, pp. 47-52, 2004.
- [71] A. Vivek, G. Andrei, K. Andreas, R. A. Besma, and A. A. Mongi, "Illumination Chromaticity Estimation Using Linear Learning Methods," *Journal of Pattern Recognition Research*, vol. 4, no. 1, pp. 92-109, 2009.
- [72] E. H. Land and J. J. McCann, "Lightness and Retinex Theory," *Journal of Optical Society of America*, vol. 61, no. 1, pp. 1-11, 1971.
- [73] E. H. Land and J. J. McCann, "The Retinex Theory of Color Vision," *Scientific American*, vol. 237, no. 6, pp. 108-128, 1977.
- [74] E. H. Land, "An Alternative Technique for the Computation of the Designator in the Retinex Theory of Color Vision," *Proceedings of the National Academy Science of the United States of America*, vol. 83, pp. 3078-3080, 1986.
- [75] B. K. P. Horn, "Determining Lightness from An Image," *Proceedings of Computer Vision, Graphics and Image Processing*, vol. 3, pp. 277-299, 1974.
- [76] B. V. Funt, M. S. Drew, and M. Brockington, "Recovering Shading from Color Images," *Proceedings of the Second European Conference on Computer Vision*, pp. 124-132, 1992.
- [77] D. H. Brainard and B. A. Wandell, "Analysis of the Retinex Theory of Color Vision," *Journal of Optical Society of America A. (JOSAA)*, vol. 3, no. 10, pp. 1651-1661, 1986.
- [78] S. Bianco, G. Ciocca, C. Cusano, and R. Schettini, "Automatic Color Constancy Algorithm Selection and Combination," *Pattern Recogn.*, vol. 43, no. 3, pp. 695-705, 2010.
- [79] S. Bianco, G. Ciocca, C. Cusano, and R. Schettini, "Improving Color Constancy Using Indoor-Outdoor Image Classification," *IEEE Transactions on Image Processing*, vol. 17, no. 12, pp. 2381-2392, 2008.
- [80] A. Gijsenij and T. Gevers, "Color Constancy using Natural Image Statistics and Scene Semantics," *IEEE Transactions on Pattern Analysis and Machine Intelligence*, vol. 33, no. 4, pp. 687-698, 2011.
- [81] R. Lu, D. Xu, and B. Li, "Color Constancy Using Ridge Regression," *Journal of Information Science and Engineering*, vol. 26, no. 1, pp. 119-130, 2010.
- [82] S. Bianco, F. Gasparini, and R. Schettini, "Combining Strategies for Automatic White Estimation in Real Images," *Proceedings of the 14th International Conference on Image Analysis and Processing Workshops*, pp. 175-178, 2007.
- [83] T. M. Lehmann and C. Palm., "Color line Search for Illuminant Estimation in Real-World Scene," *Journal of Optical Society of America A. (JOSAA)*, vol. 18, no. 11, pp. 2679-2691, 2001.
- [84] G. D. Finlayson and G. Schaefer, "Convex and Non-Convex Illuminant Constraints for Dichromatic Color Constancy," *Proceedings of IEEE Conference on Computer Vision and Pattern Recognition*, vol. 1, pp. 598-604, 2001.
- [85] G. Schaefer, "Robust Dichromatic Colour Constancy," *Proceedings of the International Conference on Image Analysis Recognition*, vol. 3212, pp. 257-264, 2004.
- [86] K. Oh-Seol, C. Yang-Ho, K. Yun-Tae, and H. Yeong-Ho, "Illumination Estimation Based on Valid Pixel Selection in Highlight Region," *Proceedings of the International Conference on Image Processing*, vol. 4, pp. 2419-2422, 2004.

-
- [87] J. Toro and B. Funt, "A Multilinear Constraint on Dichromatic Planes for Illumination Estimation," *IEEE Transactions on Image Processing*, vol. 16, no. 1, pp. 92-97, 2007.
- [88] Y. Li, "Estimation Illumination Chromaticity," Proceedings of the Second International Symposium on Intelligent Information Technology Application, vol. 3, pp. 756-760, 2008.
- [89] J. Toro, "Dichromatic Illumination Estimation without Pre-Segmentation," *Pattern Recognition Letters*, vol. 29, no. 7, pp. 871-877, 2008.
- [90] Y. Long, H. Luo, and A. Yi, "Color Recovering Based on Dichromatic Reflection Model and Finite Dimensional Linear Model," Proceedings of the International Conference on Measuring Technology and Mechatronics Automation, vol. 1, pp. 441-444, 2009.
- [91] G. Schaefer, S. Hordley, and G. D. Finlayson, "A Combined Physical and Statistical Approach to Colour Constancy," Proceedings of IEEE Computer Society Conference on Computer Vision and Pattern Recognition, vol. 1, pp. 148-153, 2005.
- [92] W. Zhou and C. Kambhampati, "A Unified Framework for Scene Illuminant Estimation," *Image and Vision Computing*, vol. 26, no. 3, pp. 415-429, 2008.
- [93] Y. Wang and D. Samaras, "Estimation of Multiple Illuminants from A Single Image of Arbitrary Known Geometry," Proceedings of the European Conference on Computer Vision, pp. 272-288, 2002.
- [94] I. Sato, Y. Sato, and K. Ikeuchi, "Stability Issues in Recovering Illumination Distribution from Brightness in Shadows," Proceedings of IEEE Computer Society Conference on Computer Vision and Pattern Recognition, vol. 2, pp. 400-407, 2001.
- [95] L. Yuanzhen, S. Lin, L. Hanqing, and S. Heung-Yeung, "Multiple-Cue Illumination Estimation in Textured Scenes," Proceedings of the Ninth IEEE International Conference on Computer Vision, vol. 2, pp. 1366-1373, 2003.
- [96] P. Debevec, "Rendering Synthetic Objects into Real Scenes: Bridging Traditional and Image-Based Graphics with Global Illumination and High Dynamic Range Photography," Proceedings of ACM SIGGRAPH, pp. 189-198, 1998.
- [97] M. W. Powell, S. Sarkar, and D. Goldgof, "A Simple Strategy for Calibrating the Geometry of Light Sources," *IEEE Transactions on Pattern Analysis and Machine Intelligence*, vol. 23, no. 9, pp. 1022-1027, 2001.
- [98] W. Zhou and C. Kambhampati, "Estimation of Illuminant Direction and Intensity of Multiple Light Sources," Proceedings of the 7th European Conference on Computer Vision, vol. 2353, pp. 206-220, 2002.
- [99] Q. Zheng and R. Chellappa, "Estimation of Illuminant Direction, Albedo, and Shape from Shading," *IEEE Transactions on Pattern Analysis and Machine Intelligence*, vol. 13, no. 7, pp. 680-702, 1991.
- [100] Y. Zhang and Y. H. Yang, "Multiple Illuminant Direction Detection with Application to Image Synthesis," *IEEE Transactions on Pattern Analysis and Machine Intelligence*, vol. 23, no. 8, pp. 915-920, 2001.
- [101] Y. Yang and A. Yuille, "Sources from Shading," Proceedings of IEEE Computer Society Conference on Computer Vision and Pattern Recognition, pp. 534-539, 1991.
- [102] I. Sato, Y. Sato, and K. Ikeuchi, "Illumination Distribution from Shadows," Proceedings of IEEE Computer Society Conference on Computer Vision and Pattern Recognition, vol. 1, pp. 306-312, 1999.
- [103] K. Hara, K. Nishino, and K. Ikeuchi, "Light Source Position and Reflectance Estimation from a Single View without the Distant Illumination Assumption," *IEEE Transactions on Pattern Analysis and Machine Intelligence*, vol. 27, no. 4, pp. 493-505, 2005.

-
- [104] G. D. Finlayson, M. S. Drew, and B. V. Funt, "Spectral Sharpening Sensor Transformations for Improved Color Constancy," *Journal of Optical Society of America A. (JOSAA)*, vol. 11, no. 5, pp. 1553-1563, 1994.
- [105] K. Barnard, F. Ciurea, and B. Funt, "Sensor Sharpening for Computational Color Constancy," *Journal of Optical Society of America A. (JOSAA)*, vol. 18, no. 11, pp. 2728-2743, 2001.
- [106] G. D. Finlayson, B. V. Funt, and K. Barnard, "Color Constancy under Varying Illumination," *Proceedings of the Fifth International Conference on Computer Vision*, pp. 720-725, 1995.
- [107] R. Kawakami, R. T. Tan, and K. Ikeuchi, "A Robust Framework to Estimate Surface Color from Changing Illumination," *Proceedings of Asian Conference on Computer Vision*, vol. 2, pp. 1026-1031, 2004.
- [108] R. Kawakami, K. Ikeuchi, and R. T. Tan, "Consistent Surface Color for Texturing Large Objects in Outdoor Scenes," *Proceedings of Tenth IEEE International Conference on Computer Vision*, vol. 2, pp. 1200-1207, 2005.
- [109] J. M. Geusebroek, R. Boomgaard, S. Smeulders, and a. H. Geert., "Color Invariance," *IEEE Transactions on Pattern Analysis and Machine Intelligence*, vol. 12, no. 23, pp. 1338-1350, 2001.
- [110] S. C. Douglas, "Blind Signal Separation and Blind Deconvolution," in *Handbook of Neural Network Signal Processing, Electrical Engineering and Applied Signal Processing Series*, Y. H. Hu and J.-N. Hwang, Eds.: CRC Press LLC, 2002, pp. 169-199.
- [111] M. S. Pedersen, J. Larsen, U. Kjems, and L. C. Parra, "A Survey of Convolutional Blind Source Separation Methods," in *Springer Handbook of Speech Processing and Speech Communication*, J. Benesty, M. M. Sondhi, and Y. Huang, Eds. New York: Springer Press, 2007.
- [112] P. D. O'Grady, B. A. Pearlmutter, and S. T. Rickard, "Survey of Sparse and Non-Sparse Methods in Source Separation," *the International Journal of Imaging Systems and Technology*, vol. 15, no. 1, pp. 18-33, 2005.
- [113] N. Das, A. Routray, and P. K. Dash, "ICA Methods for Blind Source Separation of Instantaneous Mixtures: A Case Study," *Neural Information Processing - Letters and Reviews*, vol. 11, no. 11, pp. 225-246, 2007.
- [114] A. J. Bell and T. J. Sejnowski, "An information-Maximization Approach to Blind Separation and Blind Deconvolution," *Neural Computation*, vol. 7, no. 6, pp. 1129-1159, 1995.
- [115] Y. Li, P. Wen, and D. Powers, "Methods for the Blind Signal Separation Problem," *Proceedings of IEEE International Conference on Neural Networks and Signal Processing*, Nanjing, China, vol. 2, pp. 14-17, 2003.
- [116] T.-W. Lee and T. J. Sejnowski, "Independent Component Analysis for Mixed Sub-Gaussian and Super-Gaussian Sources," *Proceedings of the Fourth Joint Symposium on Neural Computation Proceedings*, pp. 132-139, 1997.
- [117] S. Amari, S. C. Douglas, A. Cichocki, and H. H. Yang, "Multichannel Blind Deconvolution and Equalization using the Natural Gradient," *Proceedings of the First IEEE Signal Processing Workshop on Signal Processing Advances in Wireless Communications*, pp. 101-104, 1997.
- [118] P. Comon, "Independent Component Analysis, A new Concept?" *Signal Processing*, vol. 36, no. 3, pp. 278-314, 1994.
- [119] G. Burel, "Blind Separation of Sources: A nonlinear Neural Algorithm," *Neural Networks*, vol. 5, pp. 937-947, 1992.

- [120] H. H. Yang, S. I. Amari, and A. Cichocki, "Information Backpropagation for Blind Separation of Sources in Nonlinear Mixture," *Proceedings of the International Conference on Neural Networks*, vol. 4, pp. 2141-2146, 1997.
- [121] Y. Tan, J. Wang, and J. M. Zurada, "Nonlinear Blind Source Separation Using a Radial Basis Function Network," *IEEE Transactions on Neural Networks*, vol. 12, no. 1, pp. 124-134, 2001.
- [122] J. F. Cardoso and A. Souloumiac, "Blind Beamforming for Non-Gaussian Signals," *IEE Proceedings-F Radar and Signal Processing*, vol. 140, no. 6, pp. 362-370, 1993.
- [123] A. Hyvärinen and E. Oja, "A Fast Fixed-Point Algorithm for Independent Component Analysis," *Neural Computation*, vol. 9, no. 7, pp. 1483-1492, 1997.
- [124] A. Hyvarinen, "Fast and Robust Fixed-Point Algorithms for Independent Component Analysis," *IEEE Transaction on Neural Networks*, vol. 10, no. 3, pp. 626-634, 1999.
- [125] A. Hyvarinen, "Survey on Independent Component Analysis," *Neural Computing Surveys*, vol. 2, pp. 94-128, 1999.
- [126] A. Cichocki, R. E. Bogner, L. Moszczynski, and K. Pope, "Modified Herault-Jutten Algorithms for Blind Separation of Sources," *Digital Signal Processing*, vol. 7, no. 14, pp. 80-93, 1997.
- [127] A. Belouchrani, K. Abed-Meraim, J.-F. Cardoso, and E. Moulines, "A Blind Source Separation Technique Using Second-Order Statistics," *IEEE Transactions on Signal Processing*, vol. 45, no. 2, pp. 434-444, 1997.
- [128] S. Choi, A. Cichocki, H.-M. Park, and S.-Y. Lee, "Blind Source Separation and Independent Component Analysis: A Review," *Neural Information Processing-Letters and Reviews*, vol. 6, no. 1, pp. 1-57, 2005.
- [129] J. K. Tugnait, "On Blind Separation of Convolutional Mixtures of Independent Linear Signals in Unknown Additive Noise," *IEEE Transactions on Signal Processing*, vol. 46, no. 11, pp. 3117-3123, 1998.
- [130] D. Yellin and E. Weinstein, "Criteria for Multichannel Signal Separation," *IEEE Transactions on Signal Processing*, vol. 42, no. 8, pp. 2158-2168, 1994.
- [131] D. Kolossa and R. Orglmeister, "Nonlinear Postprocessing for Blind Speech Separation," *Proceedings of the International Conference on Independent Component Analysis and Blind Source Separation*, pp. 832-839, 2004.
- [132] P. Comon, E. Moreau, and L. Rota, "Blind Separation of Convolutional Mixtures: A Contrast-Based Joint Diagonalization Approach," *Proceedings of the Third International Conference on Independent Component Analysis*, San Diego, pp. 686-691, 2001.
- [133] M. Ito, M. Kawamoto, N. Ohnishi, and Y. Inouye, "Eigenvector Algorithms with Reference Signals for Frequency Domain BSS," *Proceedings of the Sixth International Conference on Independent Component Analysis and Blind Source Separation*, Charleston, USA, pp. 123-131, 2006.
- [134] Y. Zhongfu, C. Chunqi, W. Chen, Z. Jian, and F. H. Y. Chan, "Blind Separation of Convolutional Mixtures Based on Second Order and Third Order Statistics," *Proceedings of IEEE International Conference on Acoustics, Speech, and Signal Processing*, vol. 5, pp. 305-308, 2003.
- [135] R. K. Prasad, H. Saruwatari, and K. Shikano, "Problems in Blind Separation of Convolutional Speech Mixtures by Negentropy Maximization," *Proceedings of the International Workshop on Acoustic Echo and Noise Control*, Kyoto, Japan, pp. 287-290, 2003.

- [136] R. Prasad, "Fixed-Point ICA based Speech Signal Separation and Enhancement with Generalized Gaussian Model" PhD Thesis, Nara Institute of Science and Technology, 2005.
- [137] J. Thomas, Y. Deville, and S. Hosseini, "Time-Domain Fast Fixed-Point Algorithms for Convolutive ICA," *IEEE Signal Processing Letters*, vol. 13, no. 4, pp. 228-231, 2006.
- [138] R. Prasad, H. Saruwatari, and K. Shikano, "An ICA Algorithm for Separation of Convolutive Mixture of Speech Signals," *International Journal of Information Technology*, vol. 2, no. 4, pp. 273-283, 2004.
- [139] M. Stanacevic, M. Cohen, and G. Cauwenberghs, "Blind Separation of Linear Convolutive Mixtures using Orthogonal Filter Banks," Proceedings of the Third International Conference on Independent Component Analysis, pp. 260-265, 2001.
- [140] J. P. Reilly and L. C. Mendoza, "Blind Signal Separation for Convolutive Mixing Environments using Spatial-Temporal Processing," Proceedings of IEEE International Conference on Acoustics, Speech, and Signal Processing, vol. 3, pp. 1437-1440, 1999.
- [141] K. Torkkola, "Blind Separation Of Convolved Sources Based On Information Maximization," Proceedings of IEEE Workshop on Neural Networks for Signal Processing, pp. 423-432, 1996.
- [142] S. C. Douglas, H. Sawada, and S. Makino, "Natural Gradient MultiChannel Blind Deconvolution and Speech Separation using Causal FIR Filters," *IEEE Transactions on Speech and Audio Processing*, vol. 13, no. 1, pp. 92-104, 2005.
- [143] X. Sun and S. C. Douglas, "Adaptive Paraunitary Filter Banks for Contrast-Based Multichannel Blind Deconvolution," Proceedings of IEEE International Conference on Acoustics, Speech, and Signal Processing, vol. 5, pp. 2753-2756, 2001.
- [144] L. Parra and C. Spence, "Convolutive Blind Separation of Non-Stationary Sources," *IEEE Transactions on Speech and Audio Processing*, vol. 8, no. 3, pp. 320-327, 2000.
- [145] R. Aichner, S. Araki, S. Makino, T. Nishikawa, and H. Saruwatari, "Time Domain Blind Source Separation of Non-Stationary Convolved Signals by Utilizing Geometric Beamforming," Proceedings of the 12th IEEE Workshop on Neural Networks for Signal Processing, pp. 445-454, 2002.
- [146] H. Buchner, R. Aichner, and W. Kellermann, "A Generalization of Blind Source Separation Algorithms for Convolutive Mixtures Based on Second-Order Statistics," *IEEE Transactions on Speech and Audio Processing*, vol. 13, no. 1, pp. 120-134, 2005.
- [147] K. Rahbar and James P. Reilly, "A Frequency Domain Method for Blind Source Separation of Convolutive Audio Mixtures," *IEEE Transactions on Speech and Audio Processing*, vol. 13, no. 5, pp. 832-844, 2005.
- [148] A. Hyvarinen and E. Oja, "Independent Component Analysis: Algorithms and Applications," *Neural Network*, vol. 13, no. 4-5, pp. 411-430, 2000.
- [149] M. Yamazaki, Y.-W. Chen, and G. Xu, "Separating Reflections from Images Using Kernel Independent Component Analysis," Proceedings of the 18th International Conference on Pattern Recognition, vol. 3, pp. 194-197, 2006.
- [150] H. Farid and E. Adelson, "Separating Reflection and Lighting Using Independent Component Analysis," Proceedings of IEEE Conference on Computer Vision and Pattern Recognition, pp. 262-267, 1999.
- [151] M. M. Bronstein, A. M. Bronstein, M. Zibulevsky, and Y. Y. Zeevi, "Separation of Reflections via Sparse ICA," Proceedings of the International Conference on Image Processing, vol. 1, pp. 313-316, 2003.

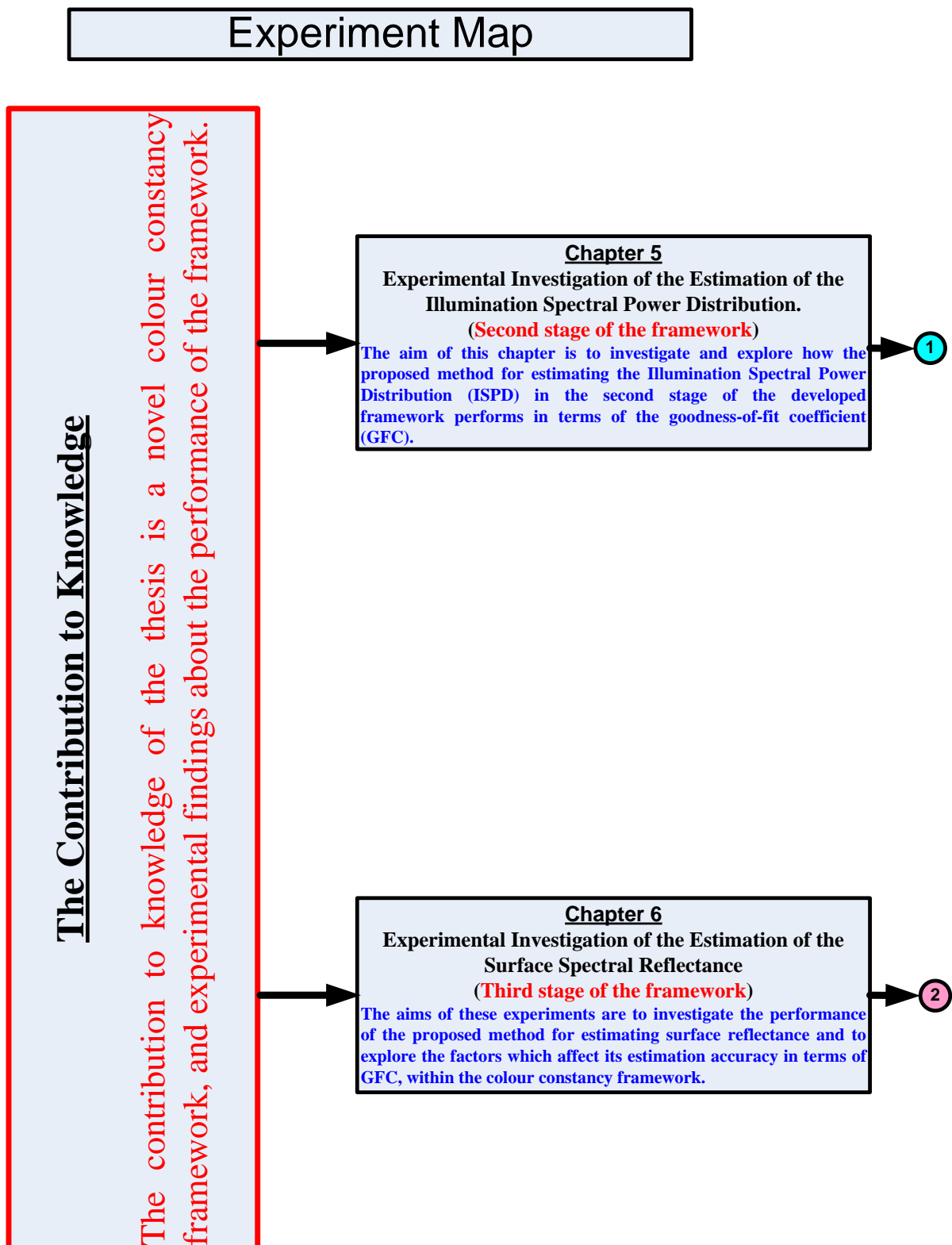
- [152] S. Umeyama, "Blind Deconvolution of Images Using Gabor Filters and Independent Component Analysis," Proceedings of the Fourth International Symposium on Independent Component Analysis and Blind Signal Separation, pp. 319-324, 2003.
- [153] L. D. Lathauwer, B. D. Moor, and J. Vandewalle, "Fetal Electrocardiogram Extraction by Blind Source Subspace Separation," *IEEE Transactions on Biomedical Engineering*, vol. 47, no. 5, pp. 567-572, 2000.
- [154] T.-P. Jung, S. Makeig, M. J. McKeown, A. Bell, T.-W. Lee, and T. Sejnowski, "Imaging Brain Dynamics Using Independent Component Analysis," *Proceedings of the IEEE*, vol. 89, no. 7, pp. 1107-1122, 2001.
- [155] C. Melissanta, A. Ypmaa, E. E. E. Frietmana, and C. J. Stamb, "A Method for Detection of Alzheimer's Disease Using ICA-Enhanced EEG Measurements," Proceedings of Artificial Intelligence in Medicine, vol. 33, pp. 209-222, 2005.
- [156] S. Y. Low and S. Nordholm, "A Hybrid Speech Enhancement System Employing Blind Source Separation and Adaptive Noise Cancellation," Proceedings of the Sixth Nordic Signal Processing Symposium, Espoo, Finland, pp. 204-207, 2004.
- [157] N. Kosaka and Y. Kosugi, "ICA Aided Linear Spectral Mixture Analysis of Agricultural Remote Sensing Images," Proceedings of the Fourth International Symposium on Independent Component Analysis and Blind Signal Separation, Nara Japan, pp. 221-226, 2003.
- [158] M. Shen, X. Zhang, L. Sun, P. J. Beadle, and F. H. YChan, "A Method for Digital Image Watermarking using ICA," Proceedings of The Fourth International Symposium on Independent Component Analysis and Blind Signal Separation, Nara, Japan, pp. 209-214, 2003.
- [159] M. Shen, J. Huang, and P. J. Beadle, "Application of ICA to the Digital Image Watermarking," Proceedings of IEEE International Conference on Neural Network and Signal Processing, Nanjing China, vol. 2, pp. 1485-1488, 2003.
- [160] J. Liu, X. Zhang, M. Najar, and M. A. Lagunas, "A Robust Digital Watermarking Scheme Based on ICA," Proceedings of IEEE International Conference on Neural Networks & Signal Processing, Nanjing, China, pp. 1481-1484, 2003.
- [161] S. Sener and B. Günsel, "Blind Audio Watermark Decoding Using Independent Component Analysis," Proceedings of the 17th International Conference on Pattern Recognition, vol. 2, pp. 875-878, 2004.
- [162] D. Yu, F. Sattar, and K.-K. Ma, "Watermark Detection and Extraction Using Independent Component Analysis Method," *Journal on Applied Signal Processing*, vol. 2002, no. 1, pp. 92-104, 2002.
- [163] T. Kolenda, L. K. Hansen, J. Larsen, and O. Winther, "Independent Component Analysis for Understanding Multimedia Content," Proceedings of the 12th IEEE Workshop on Neural Networks for Signal Processing, pp. 757-766, 2002.
- [164] S. Dubnov and A. Ben-Shalom, "Review of ICA and HOS Methods for Retrieval of Natural Sounds and Sound Effects," Proceedings of the Fourth International Symposium on Independent Component Analysis and Blind Signal Separation, Nara, Japan, pp. 703-708, 2003.
- [165] A. Vinokourov, D. R. Hardoon, and J. S. Taylor, "Learning the Semantics of Multimedia Content with Application to Web Image Retrieval and Classification," Proceedings of the Fourth International Symposium on Independent Component Analysis and Blind Signal Separation, 2003.

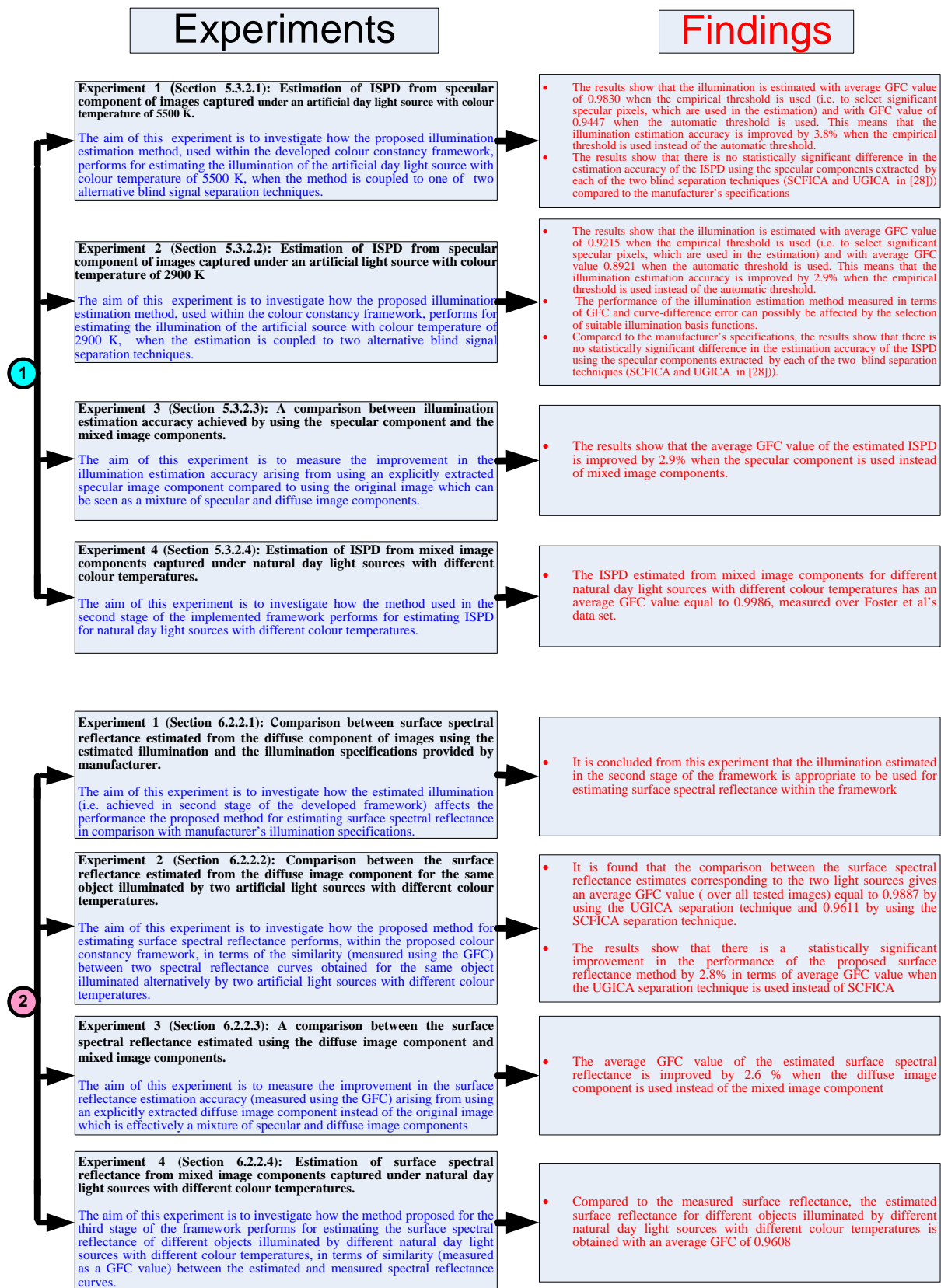
- [166] C. Havran, L. Hupet, J. Czyz, J. Lee, L. Vandendorpe, and M. Verleysen, "Independent Component Analysis for Face Authentication," *Proceedings of Knowledge-Based Intelligent Information and Engineering Systems*, Crema, Italy, pp. 1207-1211, 2002.
- [167] C. Liu and H. Wechsler, "Comparative Assessment of Independent Component Analysis (ICA) for Face Recognition," *Proceedings of The Second International Conference on Audio- and Video-based Biometric Person Authentication*, USA, 1999.
- [168] M. S. Bartlett, J. R. Movellan, and T. J. Sejnowski, "Face Recognition by Independent Component Analysis," *IEEE Transactions on Neural Networks*, vol. 13, no. 6, pp. 1450-1464, 2002.
- [169] J. Fortuna and D. Capson, "ICA Filters for Lighting Invariant Face Recognition," *Proceedings of the 17th International Conference on Pattern Recognition*, vol. 2, pp. 334-337, 2004.
- [170] W. Zha, R. Chellappa, P. J. Phillips, and A. Rosenfeld, "Face Recognition: A Literature Survey," *ACM Computing Surveys*, vol. 35, pp. 399-458, 2003.
- [171] Y. Wang and J.-Q. Han, "Iris Recognition Using Independent Component Analysis," *Proceedings of The Fourth International Conference on Machine Learning and Cybernetics*, vol. 7, pp. 4487-4492, 2005.
- [172] F. Long and B. Kong, "Independent Component Analysis and Its Application in the Fingerprint Image Preprocessing," *Proceedings of the International Conference on Information Acquisition*, pp. 365-368, 2004.
- [173] C. H. Chen and X. Wang, "A Novel Theory of SAR Image Restoration and Enhancement with ICA," *Proceedings of the International Geoscience and Remote Sensing Symposium*, vol. 6, pp. 3911-3914, 2004.
- [174] V. D. Calhoun, T. Adali, L. K. Hansen, J. Larsen, and J. J. Pekar, "ICA of Functional MRI Data: An Overview," *Proceedings of the International Workshop on Independent Component Analysis and Blind Signal Separation*, Nara, Japan, pp. 281-288, 2003.
- [175] V. Zarzoso and A. K. Nandi, "Noninvasive Fetal Electrocardiogram Extraction: Blind Separation Versus Adaptive Noise Cancellation," *IEEE Transactions on Biomedical Engineering*, vol. 48, no. 1, pp. 12-18, 2001.
- [176] T.-W. Leung, C.-W. Ngo, and R. W. H. Lau, "ICA-FX Features for Classification of Singing Voice and Instrumental Sound," *Proceedings of the 17th International Conference on Pattern Recognition*, vol. 2, pp. 367-370, 2004.
- [177] A. Cichocki and S.-i. Amari, *Adaptive Blind Signal and Image Processing: Learning Algorithm and Applications*. New York: John Wiley & Sons., 2003.
- [178] C. W. Hesse and C. J. James, "On Semi-Blind Source Separation Using Spatial Constraints With Applications in EEG Analysis," *IEEE Transactions on Biomedical Engineering*, vol. 53, no. 12, pp. 2525-2534, 2006.
- [179] C. W. Hesse and C. J. James, "The FastICA Algorithm with Spatial Constraints," *IEEE Signal Processing Letters*, vol. 12, no. 11, pp. 792-795, 2005.
- [180] Kino Flo Lighting systems, "True Match Lamps Spectral Charts", <http://www.kinoflo.com/Kino%20Flo%20lamps/True%20Match/True%20Match.htm>, Last accessed: August 2010.
- [181] D. H. Foster, S. Nascimento, Eacute, M. C. Rgio, and K. Amano, "Information limits on Neural Identification of Colored Surfaces in Natural Scenes," *Visual Neuroscience*, vol. 21, no. 3, pp. 331-336, 2004.
- [182] C. A. Glasbey, "An Analysis of Histogram-Based Thresholding Algorithms," *Graphical Models and Image Processing*, vol. 55, no. 6, pp. 532-537, 1993.

- [183] S. D. Hordley and G. D. Finlayson, "Re-evaluating Colour Constancy Algorithms," *Proceedings of the 17th International Conference on Pattern Recognition*, vol. 1, pp. 76-79, 2004.
- [184] J. L. Nieves, C. Plata, E. M. Valero, and J. Romero, "Unsupervised Illuminant Estimation from Natural Scenes: an RGB Digital Camera Suffices," *Applied Optics*, vol. 47, no. 20, pp. 3574-3584, 2008.
- [185] A. M. Srivastava and C. R. Ronda, "Phosphors," *Electrochemical Society Interface*, vol. 12, no. 2, pp. 48-51, 2003.
- [186] E. Huizingh, *Applied Statistics with SPSS*: SAGE Publications Ltd, 2007.
- [187] M. R. Spiegel, *Schuam's Outline Series Theory and Problems of Statistics*, 2 ed: McGraw-Hill, Inc, 1990.

Appendix **A**

Experiment Map





Appendix **B**

Data Set and Illustrative Results on the
Separation of Image Components

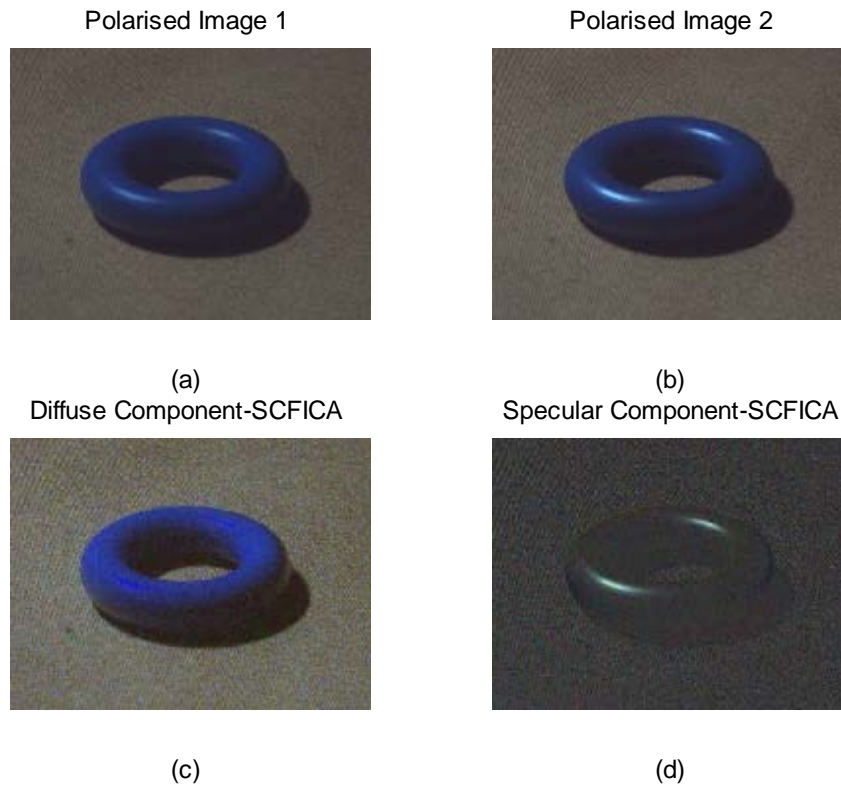


Figure B.1 The specular and the diffuse components extracted from an RGB colour image for a plastic blue ring illuminated with a light source with a colour temperature of 5500 K using the SCFICA technique.

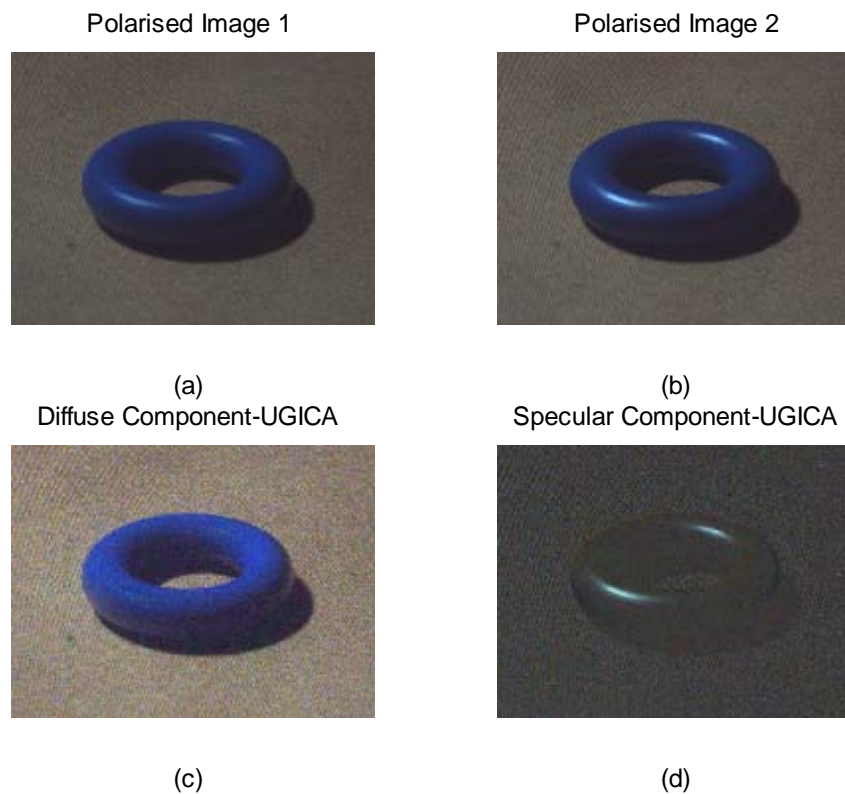


Figure B.2 The specular and the diffuse components extracted from an RGB colour image for a plastic blue ring illuminated with a light source with a colour temperature of 5500 K using the UGICA technique [28].

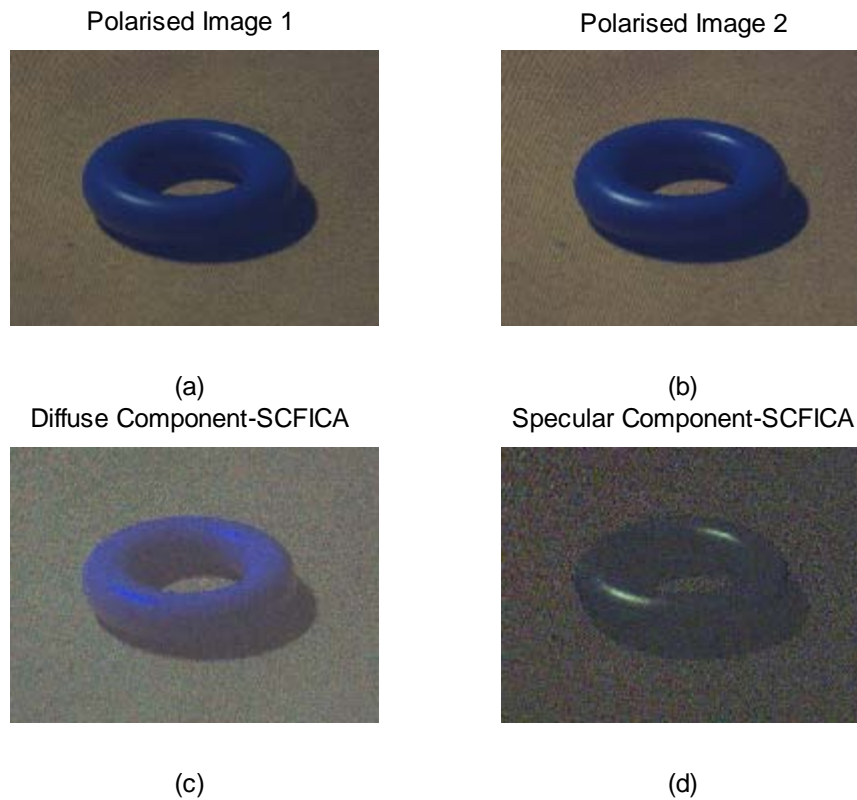


Figure B.3 The specular and the diffuse components extracted from an RGB colour image for a plastic blue ring illuminated with a light source with a colour temperature of 2900 K using the SCFICA technique.

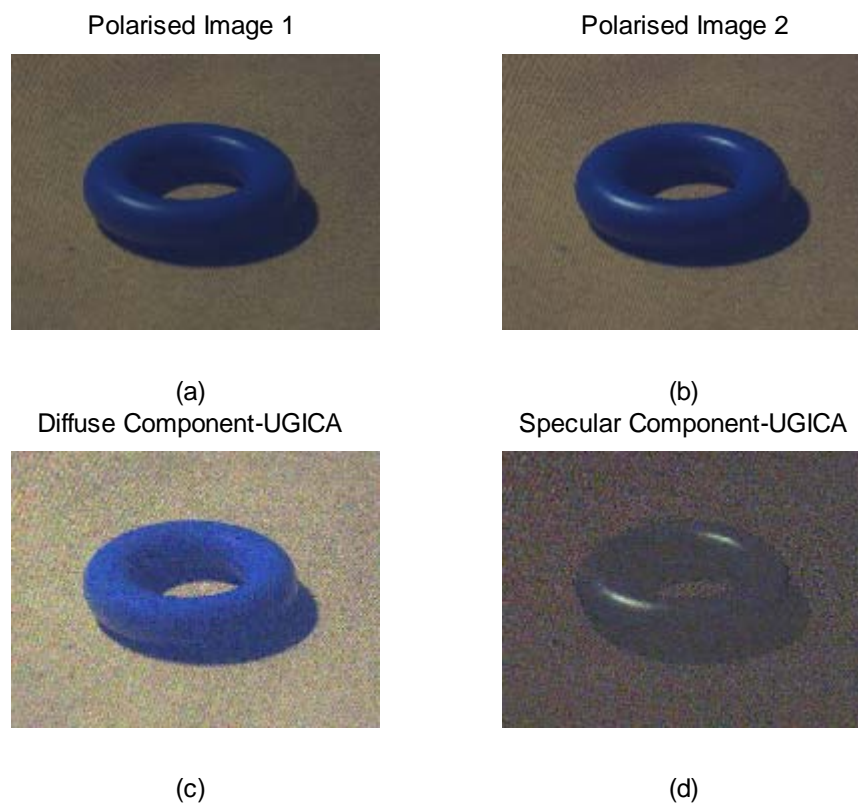


Figure B.4 The specular and the diffuse components extracted from an RGB colour image for a plastic blue ring illuminated with a light source with a colour temperature of 2900 K using the UGICA technique [28].

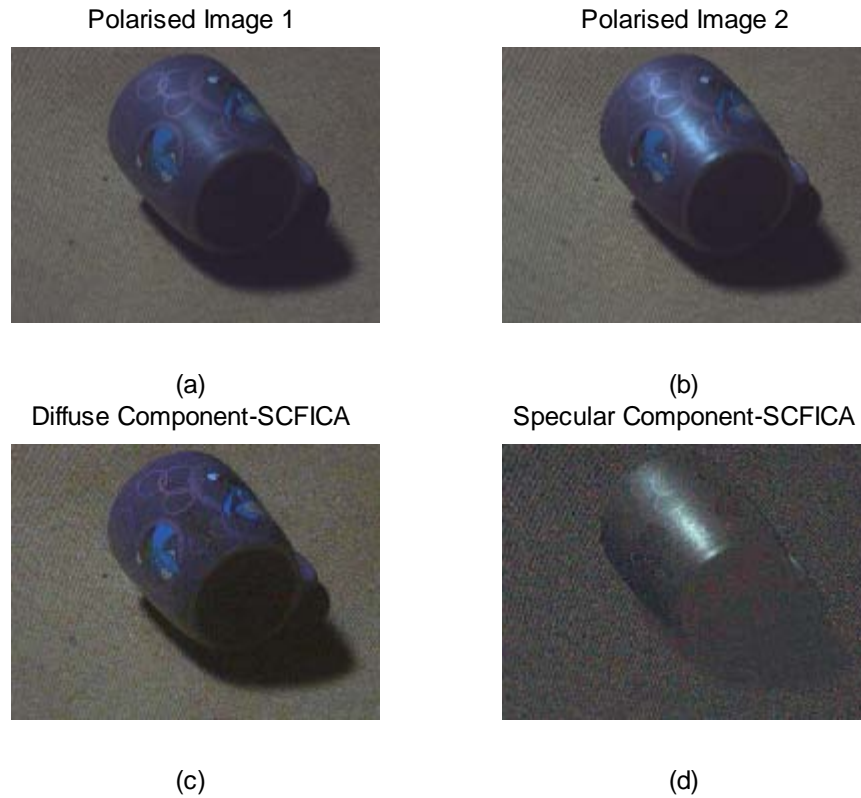


Figure B.5 The specular and the diffuse components extracted from an RGB colour image for the ceramic violet cup illuminated with a light source with a colour temperature of 5500 K using the SCFICA technique.

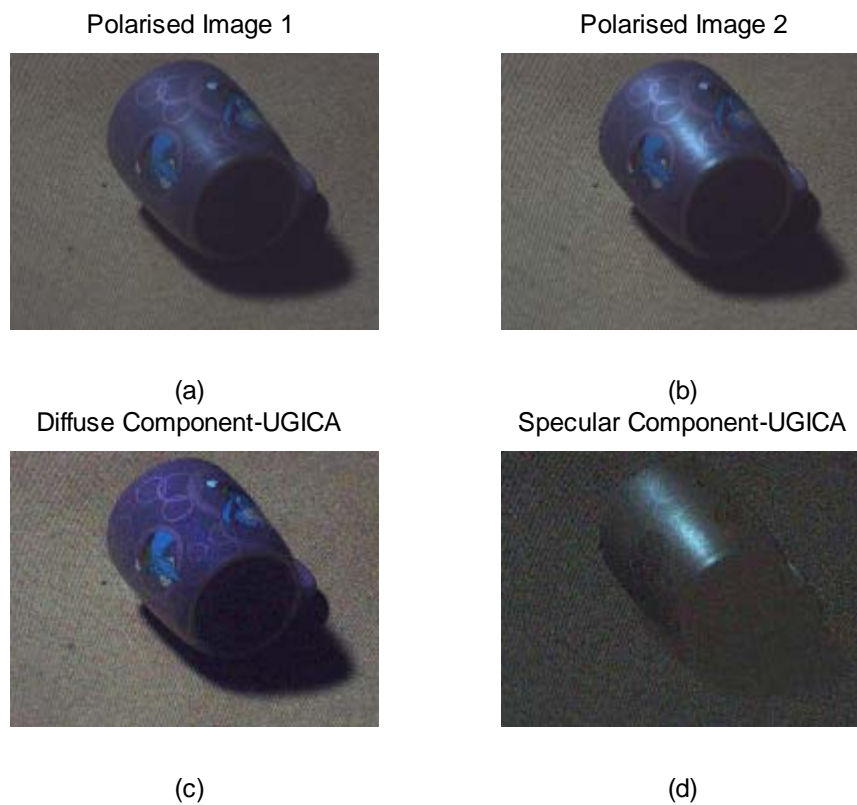


Figure B.6 The specular and the diffuse components extracted from an RGB colour image for the ceramic violet cup illuminated with a light source with a colour temperature of 5500 K using the UGICA technique [28].

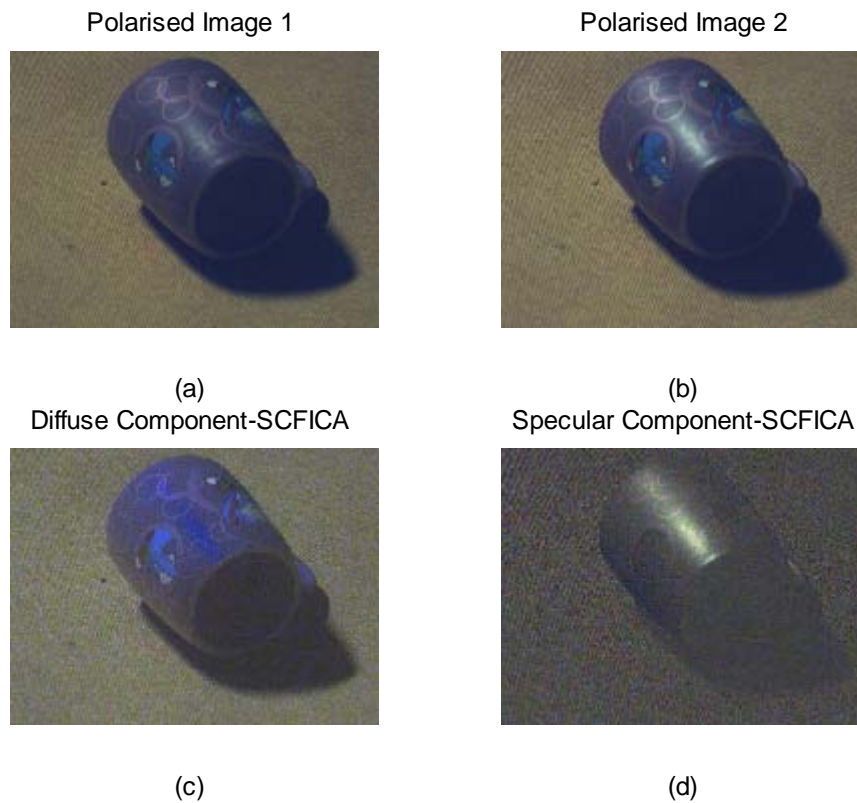


Figure B.7 The specular and the diffuse components extracted from an RGB colour image for the ceramic violet cup illuminated with a light source with a colour temperature of 2900 K using the SCFICA technique.

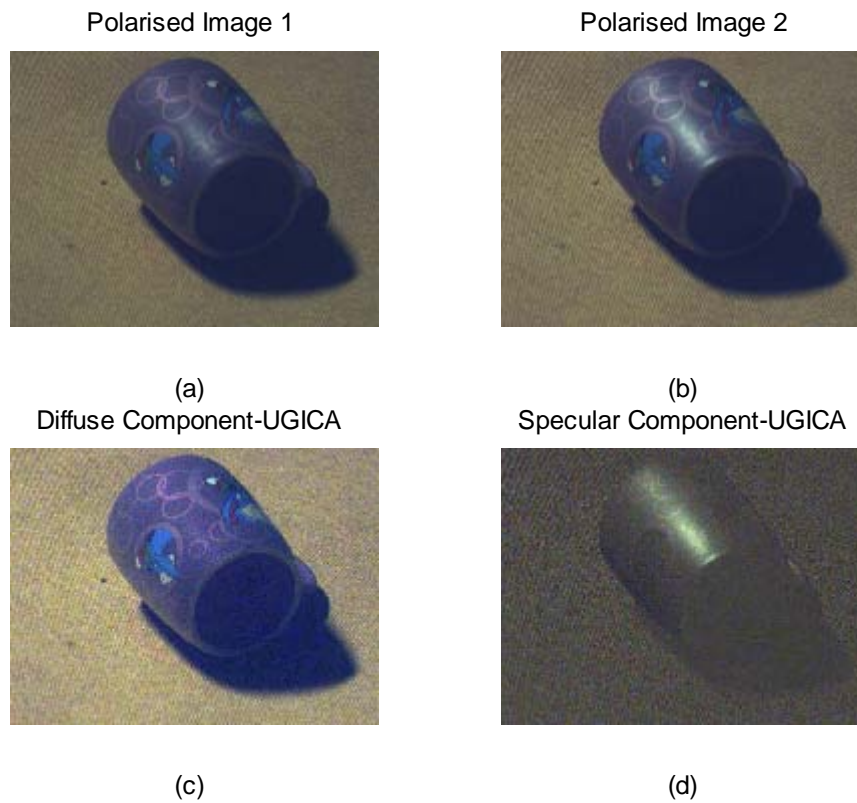


Figure B.8 The specular and the diffuse components extracted from an RGB colour image for the ceramic violet cup illuminated with a light source with a colour temperature of 2900 K using the UGICA technique [28].

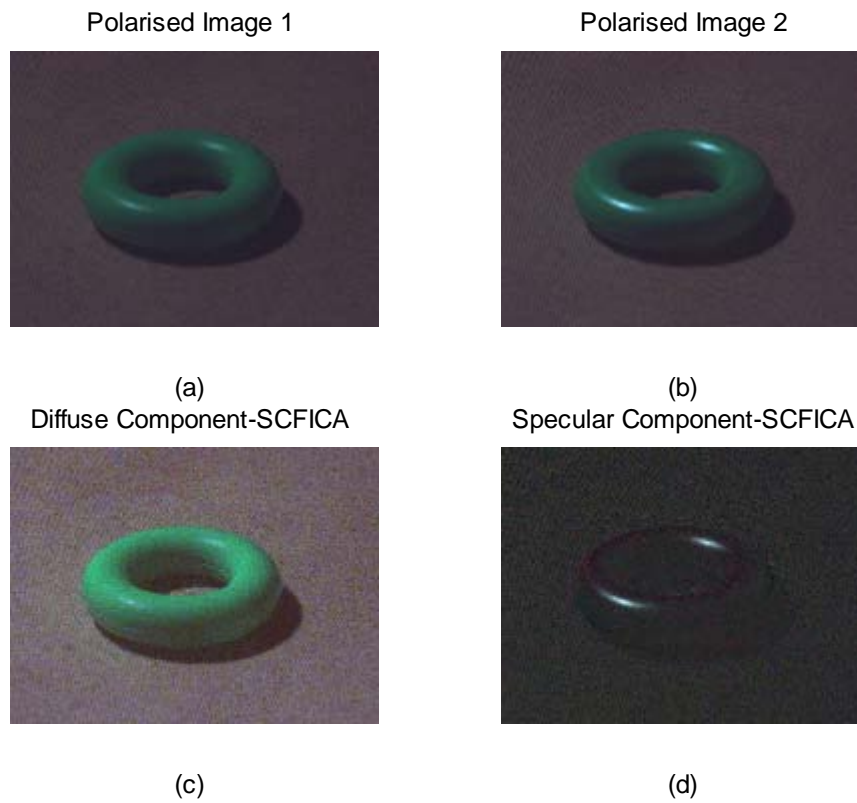


Figure B.9 The specular and the diffuse components extracted from an RGB colour image for the plastic green ring illuminated with a light source with a colour temperature of 5500 K using the SCFICA technique.

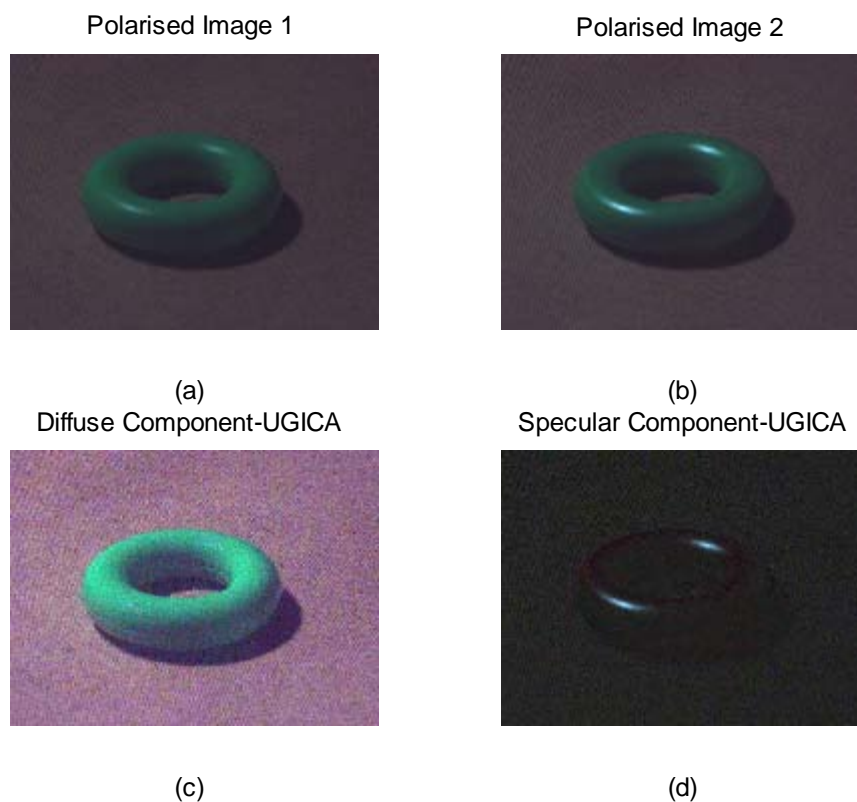


Figure B.10 The specular and the diffuse components extracted from an RGB colour image for the plastic green ring illuminated with a light source with a colour temperature of 5500 K using the UGICA technique [28].

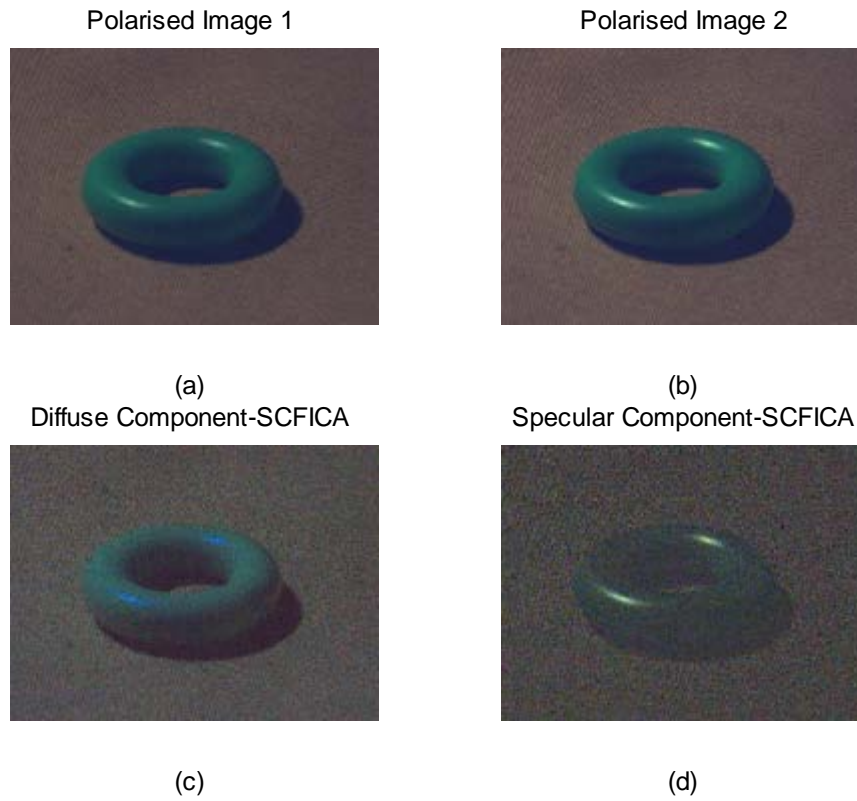


Figure B.11 The specular and the diffuse components extracted from an RGB colour image for the plastic green ring illuminated with a light source with a colour temperature of 2900 K using the SCFICA technique.

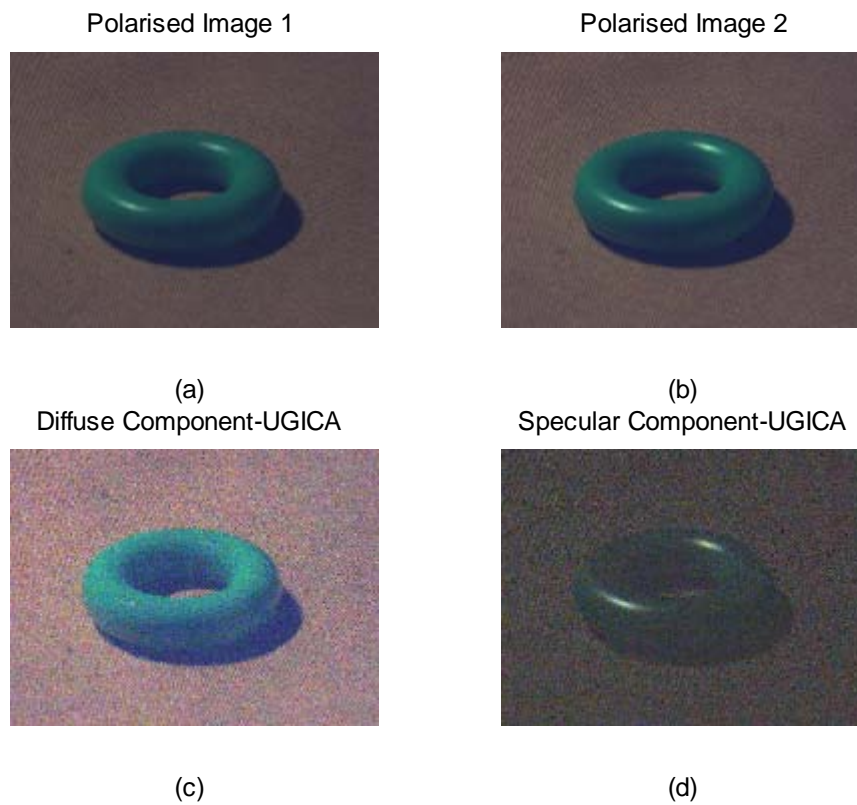


Figure B.12 The specular and the diffuse components extracted from an RGB colour image for the plastic green ring illuminated with a light source with a colour temperature of 2900 K using the UGICA technique [28].

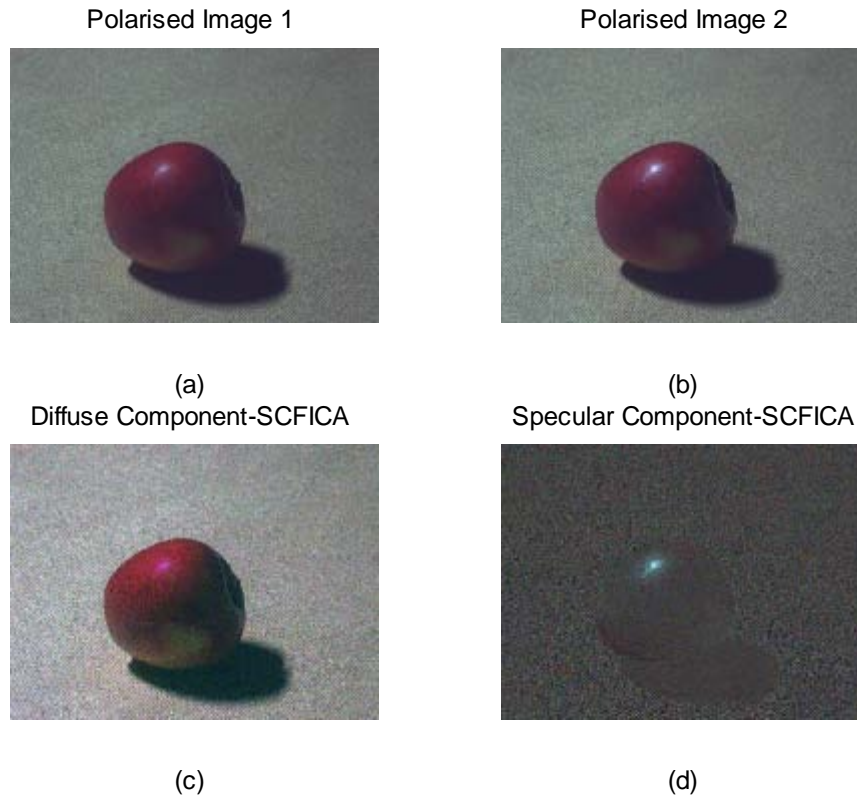


Figure B.13 The specular and the diffuse components extracted from an RGB colour image for the red apple illuminated with a light source with a colour temperature of 5500 K using the SCFICA technique.

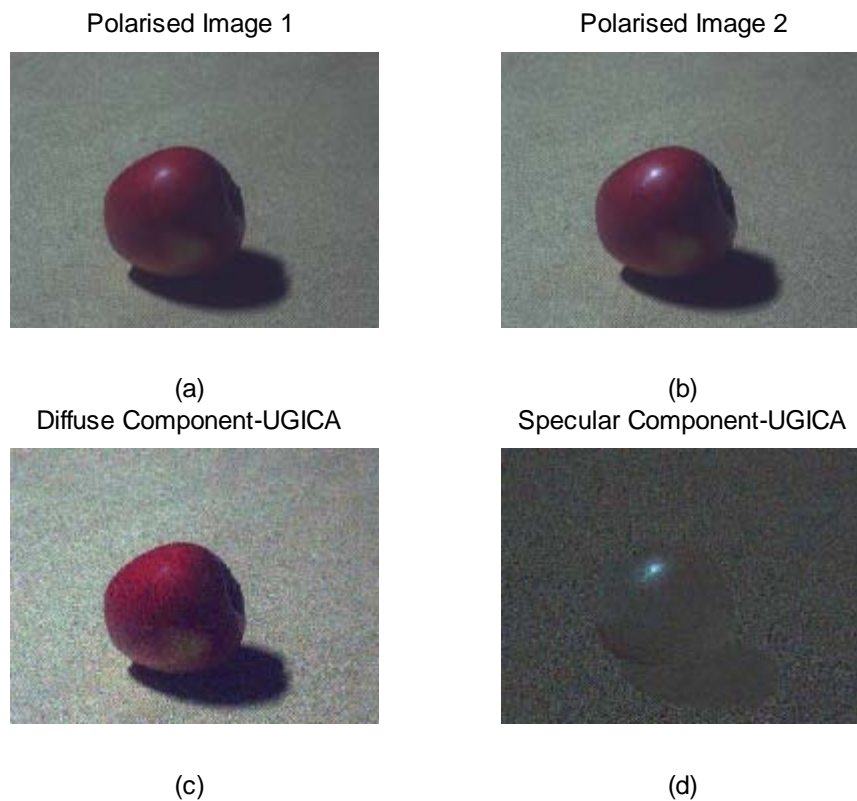


Figure B.14 The specular and the diffuse components extracted from an RGB colour image for the red apple illuminated with a light source with a colour temperature of 5500 K using the UGICA technique [28].

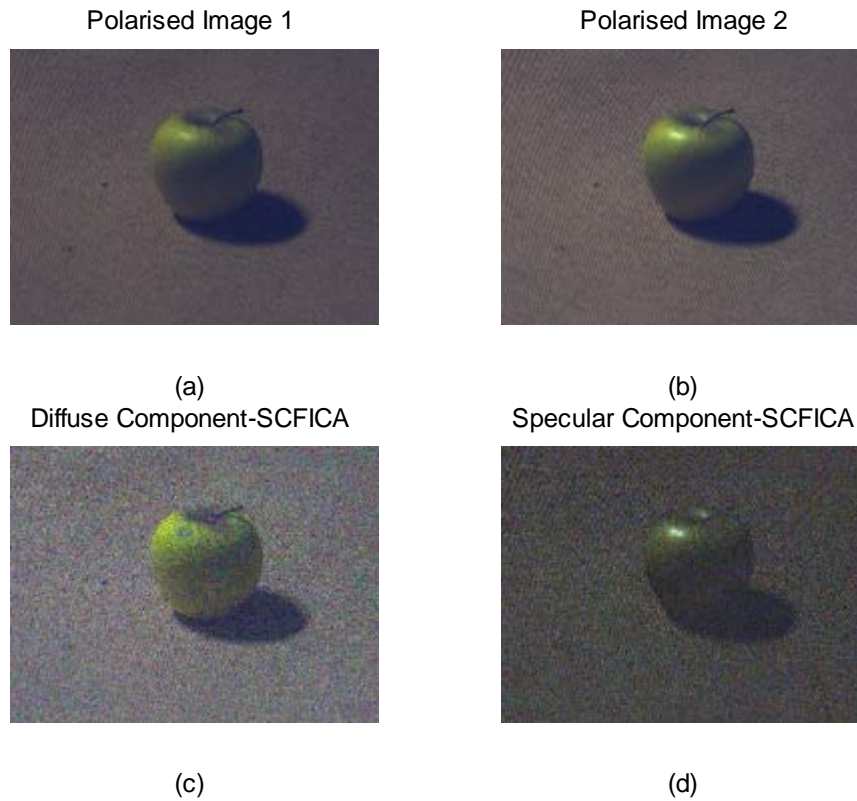


Figure B.15 The specular and the diffuse components extracted from an RGB colour image for the green apple illuminated with a light source with a colour temperature of 2900 K using the SCFICA technique.

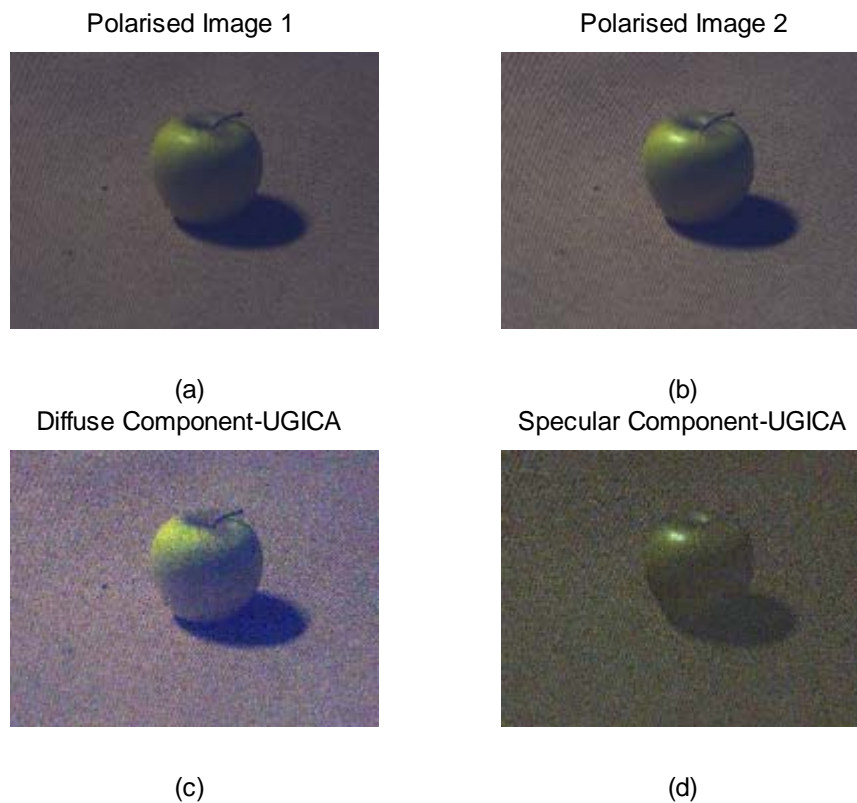


Figure B.16 The specular and the diffuse components extracted from an RGB colour image for the green apple illuminated with a light source with a colour temperature of 2900 K using the UGICA technique [28].

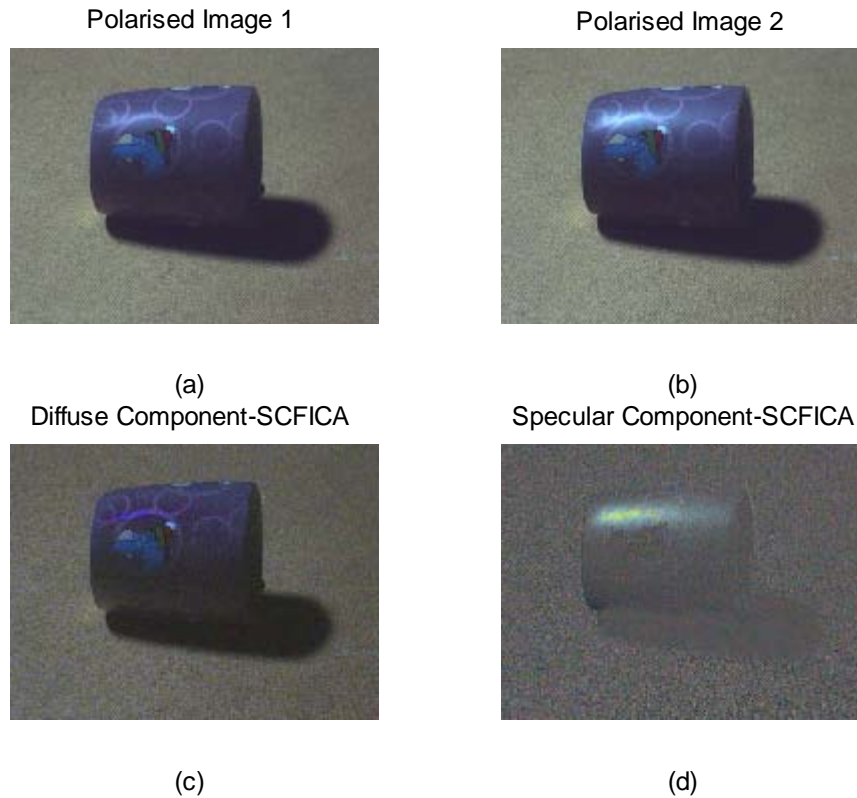


Figure B.17 The specular and the diffuse components extracted from an RGB colour image for the ceramic violet cup illuminated with a light source with a colour temperature of 5500 K using the SCFICA technique.

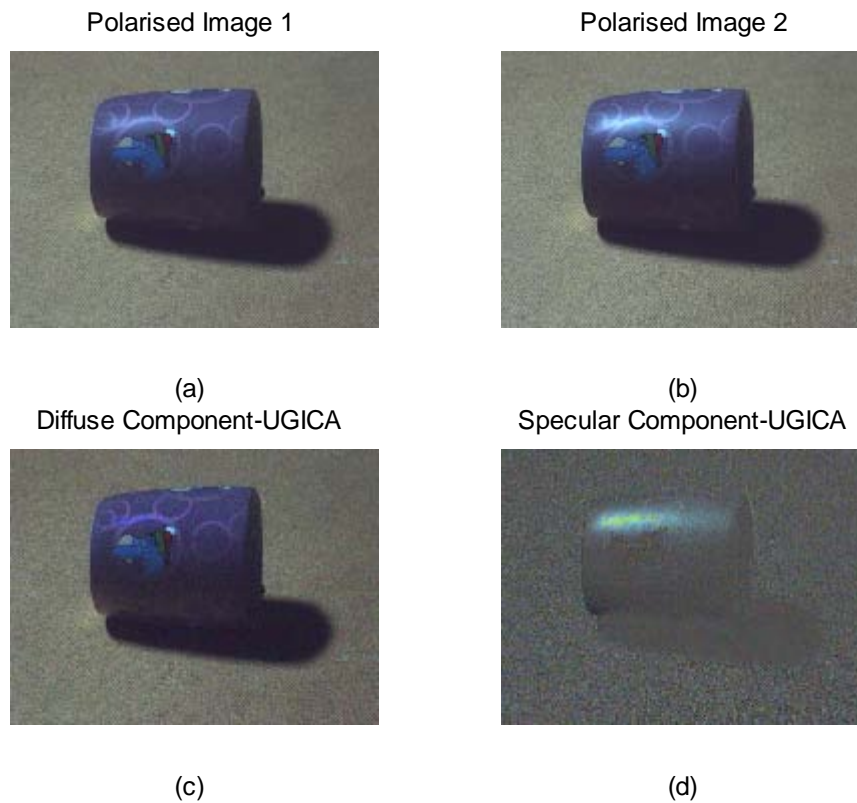


Figure B.18 The specular and the diffuse components extracted from an RGB colour image for the ceramic violet cup illuminated with a light source with a colour temperature of 5500 K using the UGICA technique [28].

Appendix C

Estimates of the Illumination Spectral Power Distribution

C.1 Experiment 1 (Section 5.3.2.1):

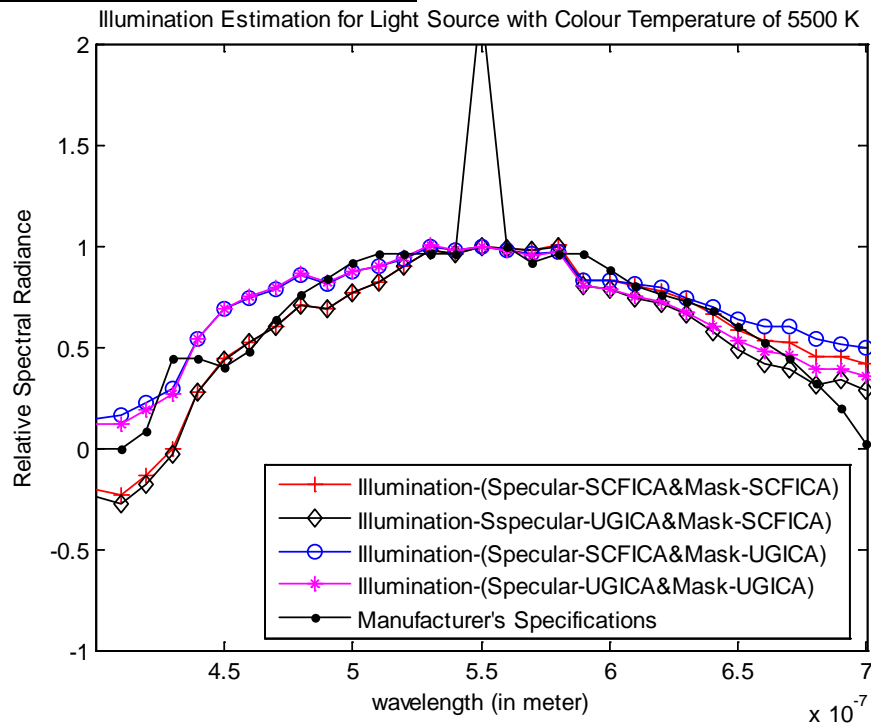


Figure C.1 The four possible illumination estimations using significant specular pixels selected from the two sets of specular components (i.e. extracted using the SCFICA and UGICA techniques), using the two corresponding masks (Mask-SCFICA and Mask-UGICA) interchangeable with each of the two sets, after automatic thresholding for the ceramic violet cup illuminated with a light source of colour temperature of 5500 K.

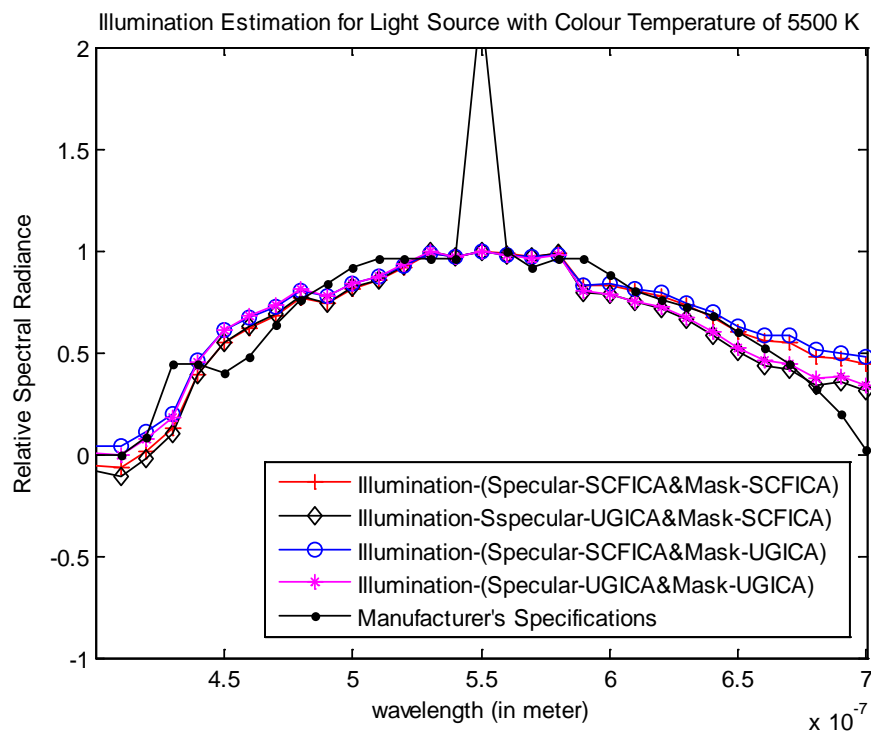


Figure C.2 The four possible illumination estimations using significantly specular pixels selected from the two sets of specular components (i.e. extracted using the SCFICA and UGICA techniques) using the two corresponding masks (Mask-SCFICA and Mask-UGICA) interchangeable with each of the two sets, after empirical thresholding for the ceramic violet cup illuminated with a light source of colour temperature of 5500 K.

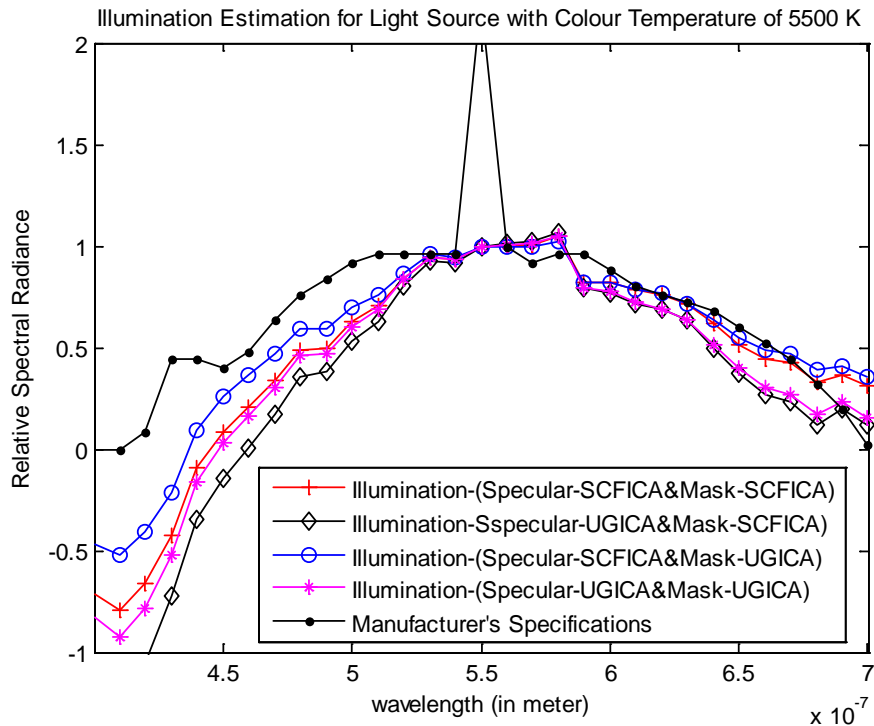


Figure C.3 The four possible illumination estimations using significantly specular pixels selected from the two sets of specular components (i.e. extracted using the SCFICA and UGICA techniques) using the two corresponding masks (Mask-SCFICA and Mask-UGICA) interchangeable with each of the two sets, after automatic thresholding for the plastic green ring illuminated with a light source of colour temperature of 5500 K.

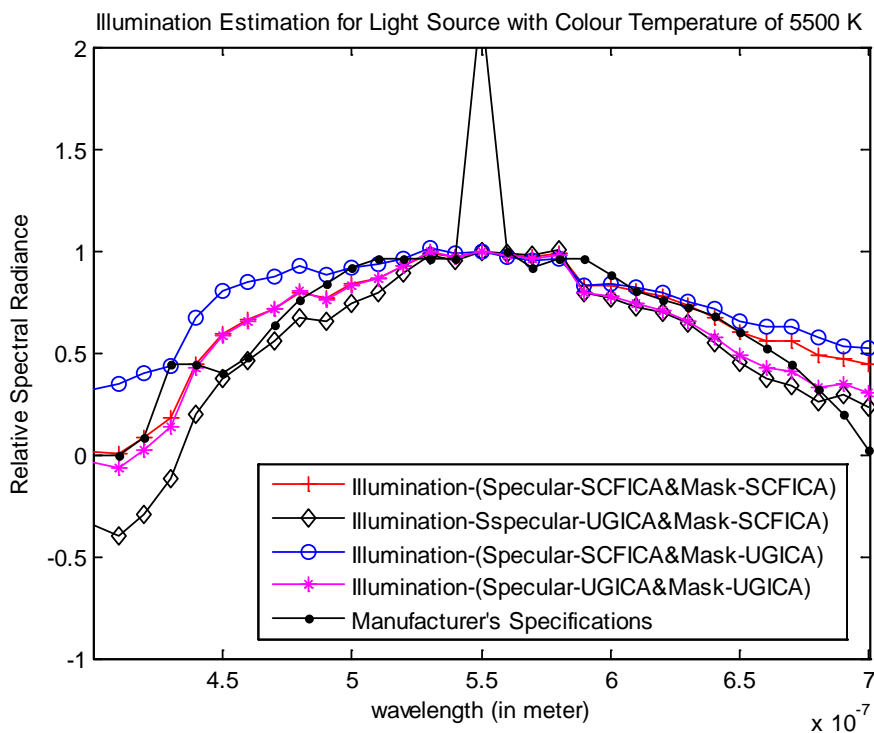


Figure C.4 The four possible illumination estimations using significantly specular pixels selected from the two sets of specular components (i.e. extracted using the SCFICA and UGICA techniques) using the two corresponding masks (Mask-SCFICA and mask-UGICA) interchangeable with each of the two sets, after empirical thresholding for the plastic green ring illuminated with a light source of colour temperature of 5500 K.

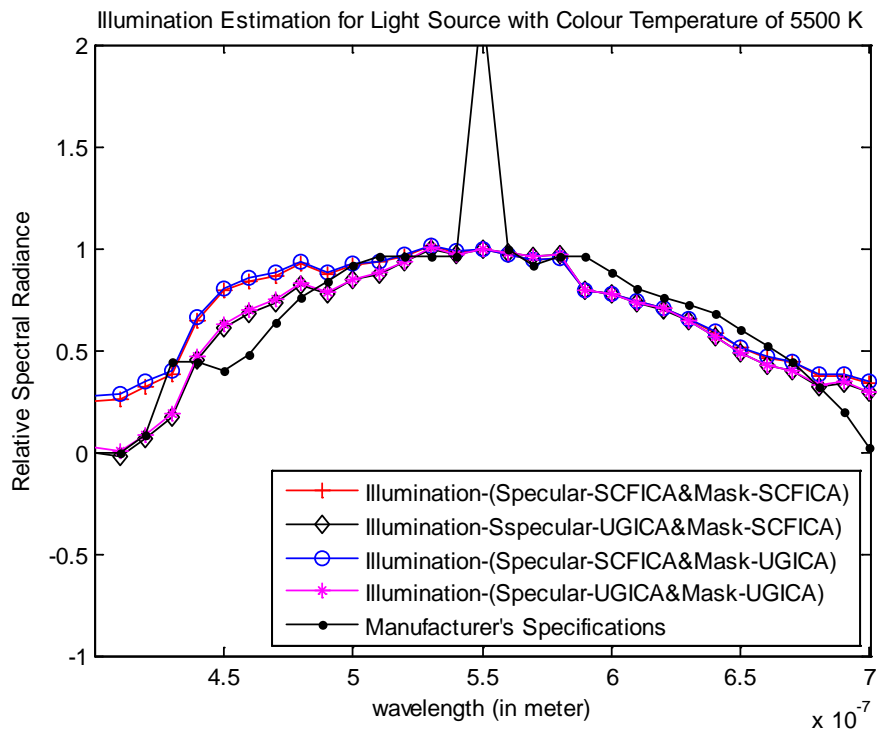


Figure C.5 The four possible illumination estimations using significantly specular pixels selected from the two sets of specular components (i.e. extracted using the SCFICA and UGICA techniques) using the two corresponding masks (Mask-SCFICA and Mask-UGICA) interchangeable with each of the two sets, after automatic thresholding for the red apple illuminated with a light source of colour temperature of 5500 K.

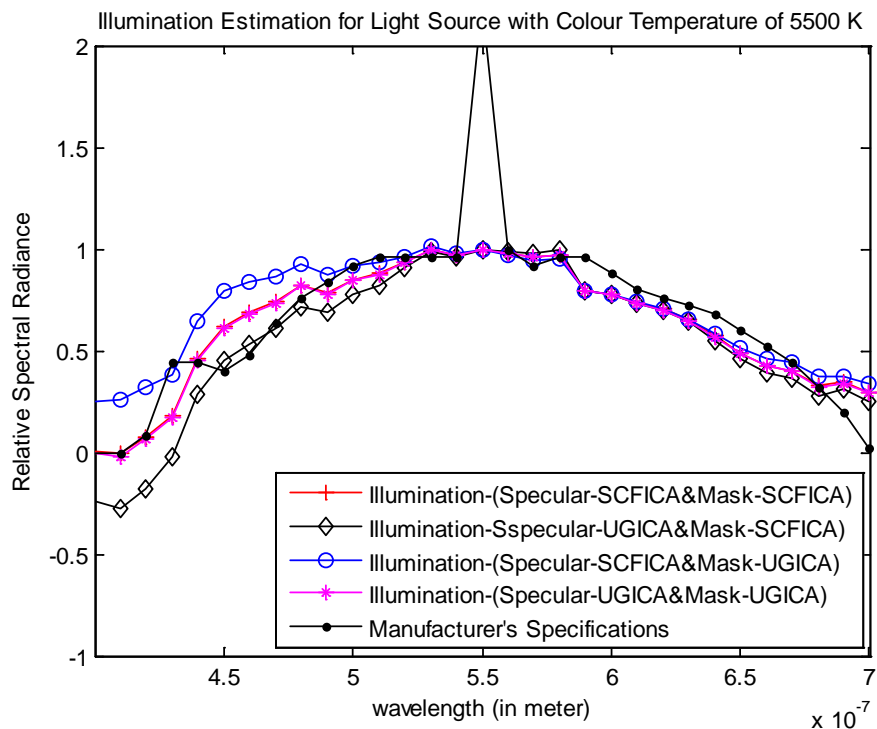


Figure C.6 The four possible illumination estimations using significantly specular pixels selected from the two sets of specular components (i.e. extracted using SCFICA and UGICA techniques) using the two corresponding masks (Mask-SCFICA and Mask-UGICA) interchangeable with each of the two sets, after empirical thresholding for the red apple illuminated with a light source of colour temperature of 5500 K.

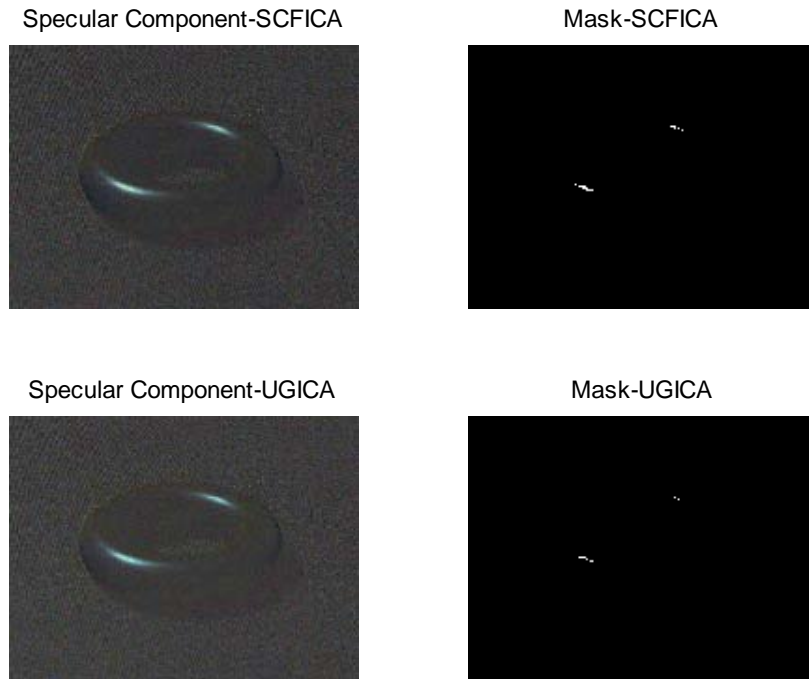


Figure C.7 The two sets of RGB specular components extracted using two blind separation techniques (i.e. SCFICA and UGICA techniques) and the corresponding masks for the plastic blue ring illuminated with a light source of colour temperature of 5500 K, after automatic thresholding.

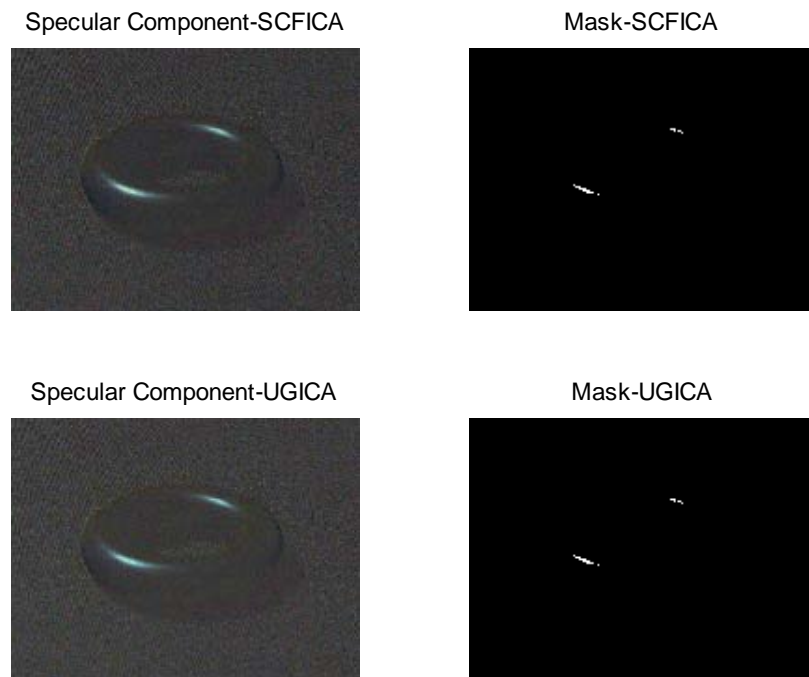


Figure C.8 The two sets of RGB specular components extracted using two blind separation techniques (i.e. SCFICA and UGICA techniques) and the corresponding masks for the plastic blue ring illuminated with a light source of colour temperature of 5500 K, after empirical thresholding.

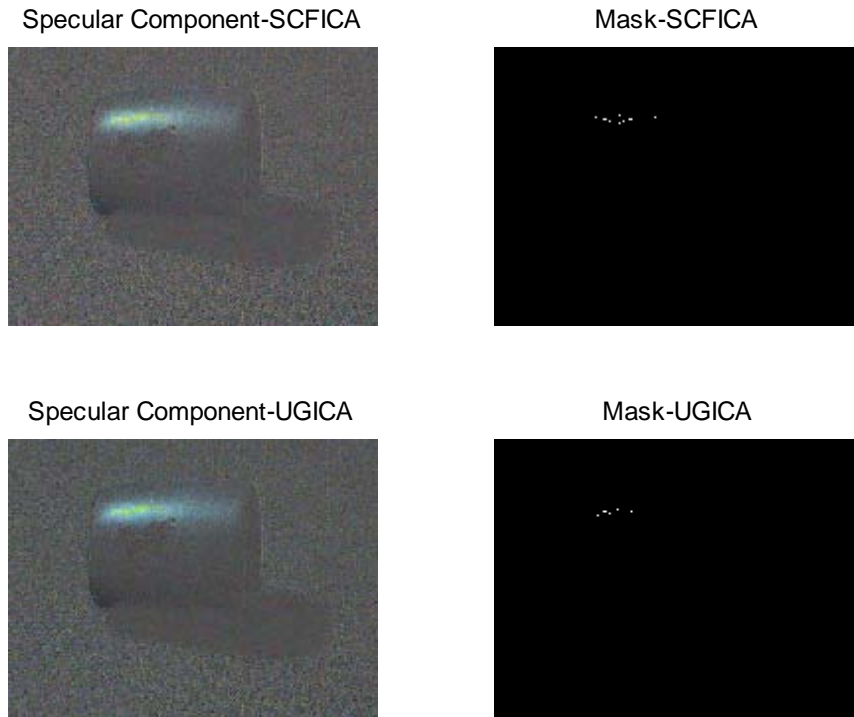


Figure C.9 The two sets of RGB specular components extracted using two blind separation techniques (i.e. SCFICA and UGICA techniques) and the corresponding masks for the ceramic violet cup illuminated with a light source of colour temperature of 5500 K, after automatic thresholding.

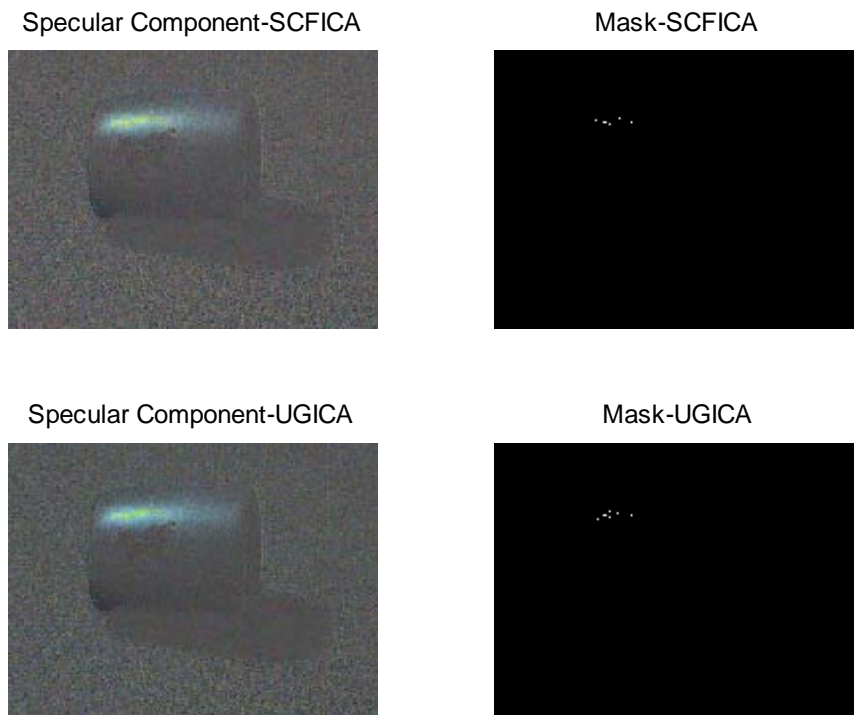


Figure C.10 The two sets of RGB specular components extracted using two blind separation techniques (i.e. SCFICA and UGICA techniques) and the corresponding masks for the ceramic violet cup illuminated with a light source of colour temperature of 5500 K, after empirical thresholding.

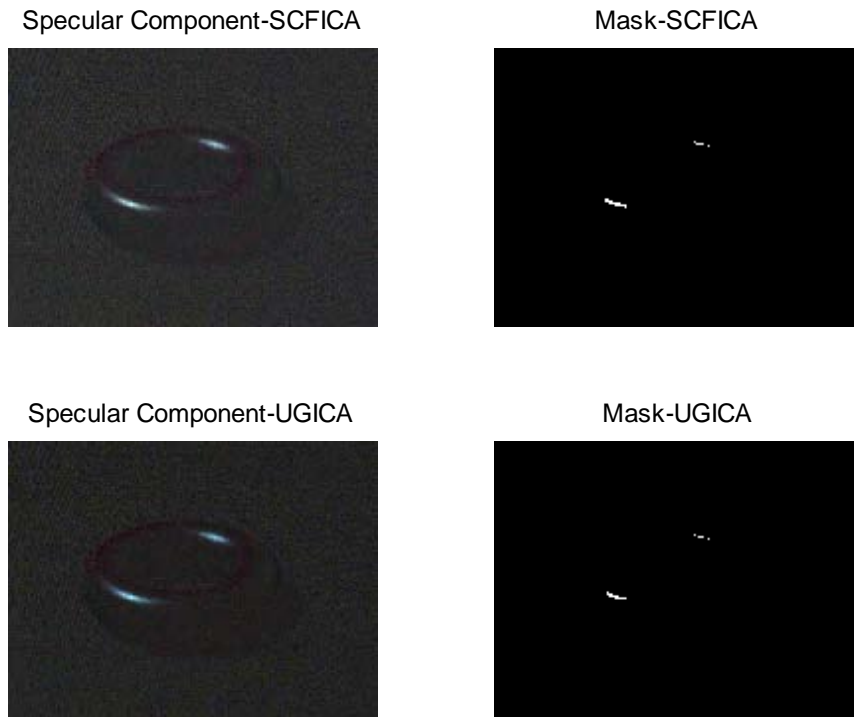


Figure C.11 The two sets of RGB specular components extracted using two blind separation techniques (i.e. SCFICA and UGICA techniques) and the corresponding masks for the plastic green ring illuminated with a light source of colour temperature of 5500 K, after automatic thresholding.

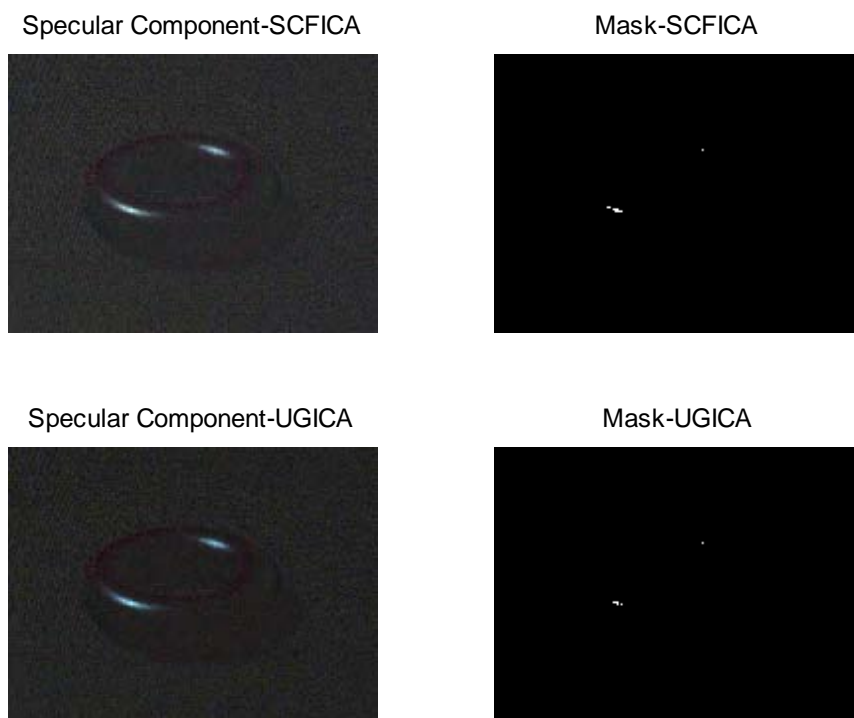


Figure C.12 The two sets of RGB specular components extracted using two blind separation techniques (i.e. SCFICA and UGICA techniques) and the corresponding masks for the plastic green ring illuminated with a light source of colour temperature of 5500 K, after empirical thresholding.

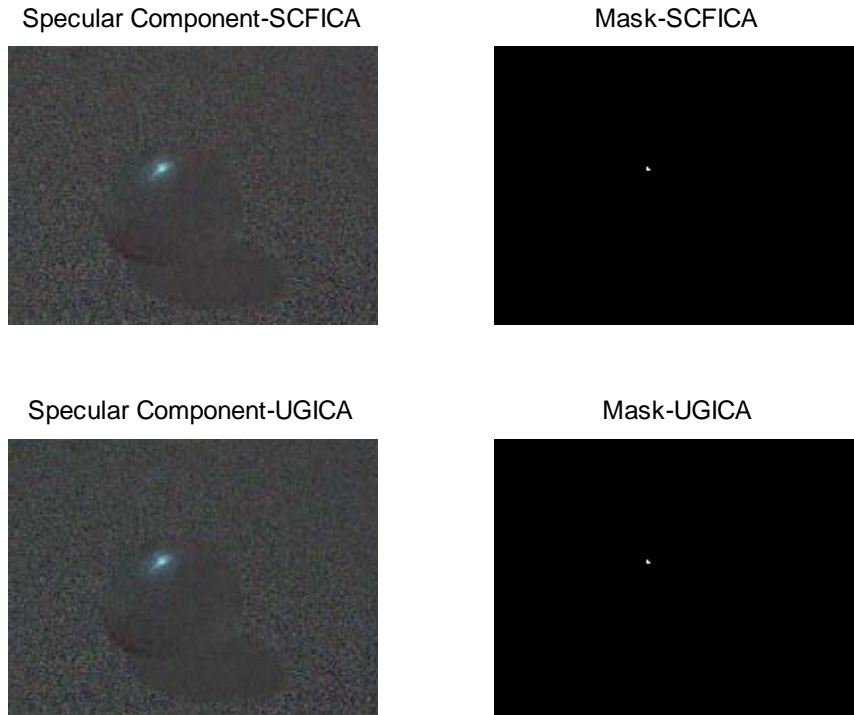


Figure C.13 The two sets of RGB specular components extracted using two blind separation techniques (i.e. SCFICA and UGICA techniques) and the corresponding masks for the red apple illuminated with a light source of colour temperature of 5500 K, after automatic thresholding.

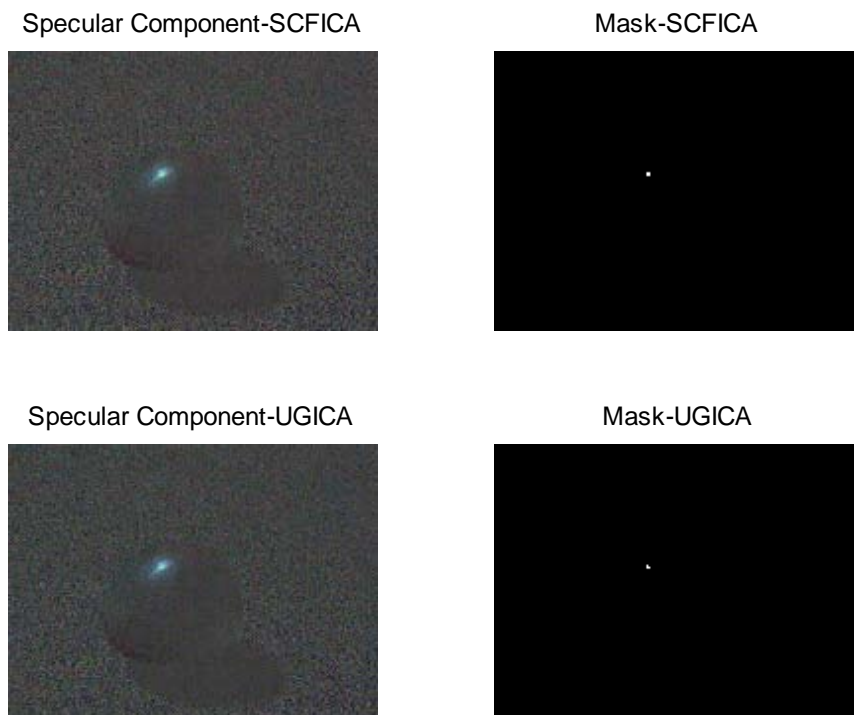


Figure C.14 The two sets of RGB specular components extracted using two blind separation techniques (i.e. SCFICA and UGICA techniques) and the corresponding masks for the red apple illuminated with a light source of colour temperature of 5500 K, after empirical thresholding.

Table C.1 The automatic and the empirical threshold and the corresponding number of pixels in the pixel selection mask for the five examples of objects under an artificial day light source with a colour temperature of 5500 K.

Separation technique	Object	Automatic threshold (number of pixels in mask)	Empirical threshold (number of pixels in mask)
SCFICA	Plastic blue ring	0.59(78)	0.55(252)
	Ceramic violet cup	0.64(127)	0.65(75)
	Plastic green ring	0.51 (307)	0.63 (121)
	Red apple	0.57(51)	0.53(71)
UGICA	Plastic blue ring	0.60(175)	0.52(253)
	Ceramic violet cup	0.60(75)	0.59(96)
	Plastic Green ring	0.45(230)	0.55(59)
	Red apple	0.55(49)	0.54 (51)

Table C.2 Results of the experimental assessment of the effect of: the extraction of the specular image component, and the material of the reflecting object. The table entries represent the RMS error between the illumination spectral power distribution estimated in the experiment and the distribution provided by the manufacturer of the light source with a colour temperature of 5500 K.

Illumination source	Extraction of specular image component		Material of the reflecting object				
	Signal separation	Selection of significantly specular pixels	Plastic blue ring	Ceramic violet cup	Plastic green ring	Red apple	
Colour temperature: 5500 K	Spatially constrained FastICA Technique (SCFICA)	Automatic selection	Mask-SCFICA	16.40×10^{-2}	13.35×10^{-2}	33.78×10^{-2}	16.97×10^{-2}
			Mask-UGICA	26.42×10^{-2}	15.15×10^{-2}	23.67×10^{-2}	18.89×10^{-2}
		Empirical selection	Mask-SCFICA	11.09×10^{-2}	12.80×10^{-2}	12.65×10^{-2}	11.12×10^{-2}
			Mask-UGICA	11.10×10^{-2}	13.43×10^{-2}	20.27×10^{-2}	16.17×10^{-2}
	Umeyama and Godin ICA Techniques (UGICA)	Automatic selection	Mask-SCFICA	17.35×10^{-2}	12.70×10^{-2}	49.51×10^{-2}	11.18×10^{-2}
			Mask-UGICA	27.06×10^{-2}	12.56×10^{-2}	38.56×10^{-2}	11.71×10^{-2}
		Empirical selection	Mask-SCFICA	11.41×10^{-2}	11.55×10^{-2}	18.94×10^{-2}	15.10×10^{-2}
			Mask-UGICA	11.38×10^{-2}	11.12×10^{-2}	11.15×10^{-2}	11.11×10^{-2}
	None	Empirical selection	Mask-SCFICA	20.88×10^{-2}	24.54×10^{-2}	20.53×10^{-2}	24.10×10^{-2}
			Mask-UGICA	21.07×10^{-2}	15.94×10^{-2}	30.04×10^{-2}	19.02×10^{-2}

Table C.3 Results of the experimental assessment of the effect of: the extraction of the specular image component, and the material of the reflecting object. The table entries represent the Median error between the illumination spectral power distribution estimated in the experiment and the distribution provided by the manufacturer of the light source with a colour temperature of 5500 K.

Illumination source	Extraction of specular image component			Material of the reflecting object			
	Signal separation	Selection of significantly specular pixels		Plastic blue ring	Ceramic violet cup	Plastic green ring	Red apple
Colour temperature: 5500 K	Spatially constrained FastICA Technique (SCFICA)	Automatic selection	Mask-SCFICA	2.17×10^{-2}	9.9×10^{-3}	8.00×10^{-2}	5.9×10^{-3}
			Mask-UGICA	6.89×10^{-2}	3.38×10^{-2}	5.82×10^{-2}	1.91×10^{-2}
		Empirical selection	Mask-SCFICA	3.22×10^{-2}	2.0×10^{-3}	8.8×10^{-3}	2.21×10^{-2}
			Mask-UGICA	3.29×10^{-2}	2.40×10^{-2}	3.87×10^{-2}	3.1×10^{-3}
	Umeyama and Godin ICA Techniques (UGICA)	Automatic selection	Mask-SCFICA	9.8×10^{-3}	5.59×10^{-2}	20.13×10^{-2}	2.25×10^{-2}
			Mask-UGICA	4.00×10^{-2}	5.3×10^{-3}	16.88×10^{-2}	1.77×10^{-2}
		Empirical selection	Mask-SCFICA	2.32×10^{-2}	5.08×10^{-2}	8.58×10^{-2}	7.56×10^{-2}
			Mask-UGICA	2.30×10^{-2}	7.0×10^{-3}	4.35×10^{-2}	2.18×10^{-2}
	None	Empirical selection	Mask-SCFICA	14.13×10^{-2}	11.18×10^{-2}	1.48×10^{-2}	1.23×10^{-2}
			Mask-UGICA	14.12×10^{-2}	6.06×10^{-2}	5.59×10^{-2}	8.4×10^{-3}

Table C.4 Results of the experimental assessment of the effect of: the extraction of the specular image component, and the material of the reflecting object. The table entries represent the Mean error between the illumination spectral power distribution estimated in the experiment and the distribution provided by the manufacturer of the light source with a colour temperature of 5500 K.

Illumination source	Extraction of specular image component			Material of the reflecting object			
	Signal separation	Selection of significantly specular pixels		Plastic blue ring	Ceramic violet cup	Plastic green ring	Red apple
Colour temperature: 5500 K	Spatially constrained FastICA Technique (SCFICA)	Automatic selection	Mask-SCFICA	7.20×10^{-2}	1.01×10^{-2}	18.69×10^{-2}	6.79×10^{-2}
			Mask-UGICA	15.03×10^{-2}	7.11×10^{-2}	11.28×10^{-2}	8.34×10^{-2}
		Empirical selection	Mask-SCFICA	8.8×10^{-3}	9.2×10^{-3}	2.69×10^{-2}	8.9×10^{-3}
			Mask-UGICA	1.03×10^{-2}	3.98×10^{-2}	12.15×10^{-2}	6.10×10^{-2}
	Umeyama and Godin ICA Techniques (UGICA)	Automatic selection	Mask-SCFICA	6.10×10^{-2}	4.89×10^{-2}	32.30×10^{-2}	6.3×10^{-3}
			Mask-UGICA	13.54×10^{-2}	3.13×10^{-2}	25.04×10^{-2}	8.6×10^{-3}
		Empirical selection	Mask-SCFICA	1.59×10^{-2}	2.97×10^{-2}	11.33×10^{-2}	8.07×10^{-2}
			Mask-UGICA	1.74×10^{-2}	2.0×10^{-4}	2.13×10^{-2}	1.30×10^{-2}
	None	Empirical selection	Mask-SCFICA	14.56×10^{-2}	15.09×10^{-2}	4.34×10^{-2}	4.38×10^{-2}
			Mask-UGICA	14.71×10^{-2}	8.05×10^{-2}	12.04×10^{-2}	2.45×10^{-2}

Table C.5 Results of the experimental assessment of the effect of: the extraction of the specular image component, and the material of the reflecting object. The table entries represent the angular error (in degrees) between the illumination spectral power distribution estimated in the experiment and the distribution provided by the manufacturer of the light source with a colour temperature of 5500 K.

Illumination source	Extraction of specular image component		Material of the reflecting object				
	Signal separation	Selection of significantly specular pixels	Plastic blue ring	Ceramic violet cup	Plastic green ring	Red apple	
Colour temperature: 5500 K	Spatially constrained FastICA Technique (SCFICA)	Automatic selection	Mask-SCFICA	5.37	3.44	14.75	6.27
			Mask-UGICA	8.97	3.68	9.33	7.08
		Empirical selection	Mask-SCFICA	0.88	2.96	2.58	2.19
			Mask-UGICA	0.77	3.15	5.58	5.92
	Umeyama and Godin ICA Techniques (UGICA)	Automatic selection	Mask-SCFICA	7.07	1.38	23.01	2.41
			Mask-UGICA	10.46	3.31	16.23	3.23
		Empirical selection	Mask-SCFICA	3.16	0.40	5.08	2.89
			Mask-UGICA	3.07	1.35	1.20	2.08
	None	Empirical selection	Mask-SCFICA	6.13	8.36	10.58	11.49
			Mask-UGICA	6.20	3.66	13.49	8.25

C.2 Experiment 2 (Section 5.3.2.2):

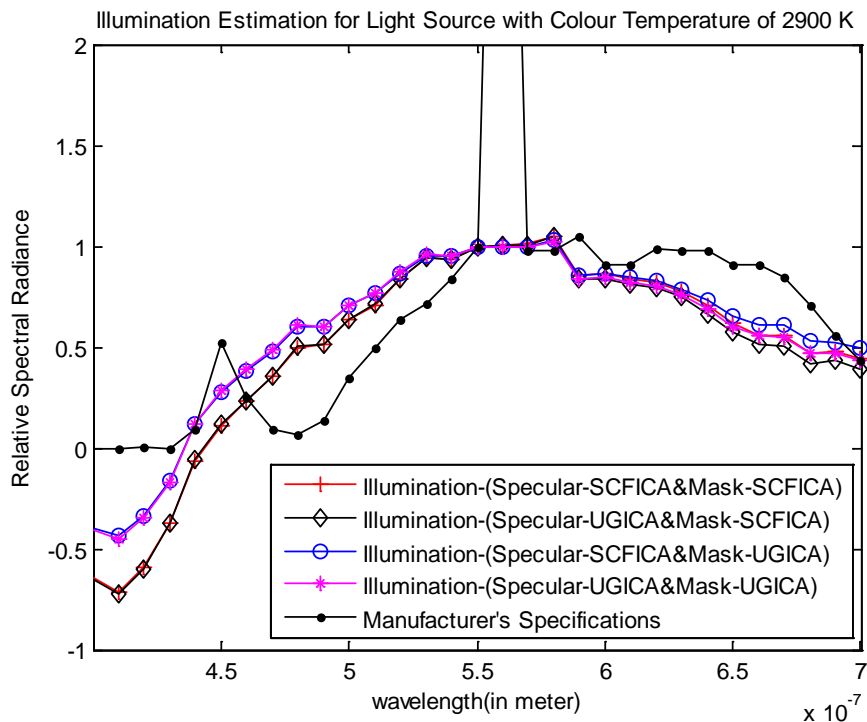


Figure C.15 The four possible illumination estimations using significantly specular pixels selected from the two sets of specular components (i.e. extracted using the SCFICA and UGICA techniques) using the two corresponding masks (Mask-SCFICA and Mask-UGICA) interchangeable with each of the two sets, after automatic thresholding for the ceramic violet cup illuminated with a light source of colour temperature of 2900 K.

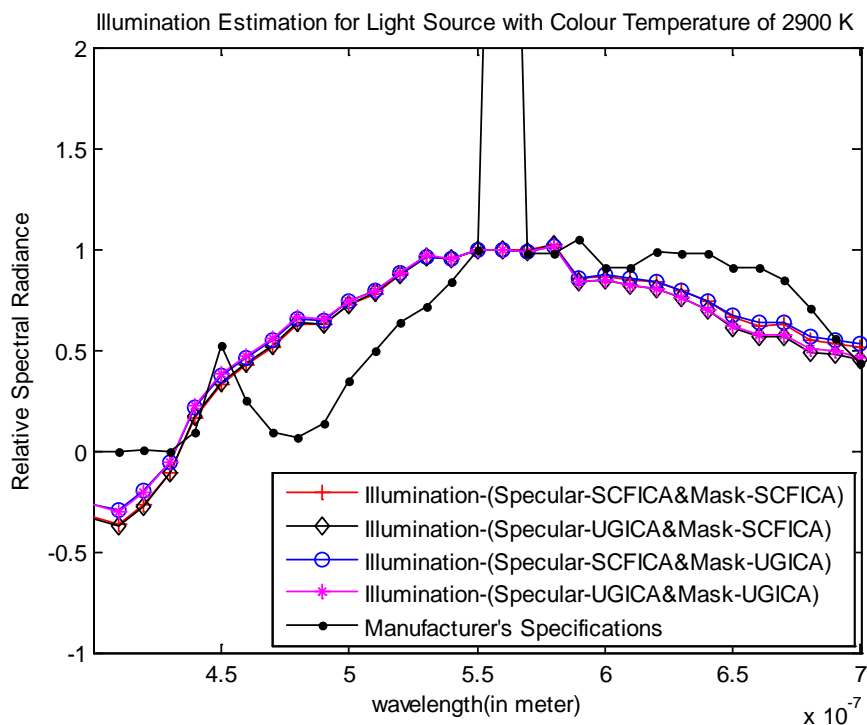


Figure C.16 The four possible illumination estimations using significantly specular pixels selected from the two sets of specular components (i.e. extracted using the SCFICA and UGICA techniques) using the two corresponding masks (Mask-SCFICA and Mask-UGICA) interchangeable with each of the two sets, after empirical thresholding for the ceramic violet cup illuminated with a light source of colour temperature of 2900 K.

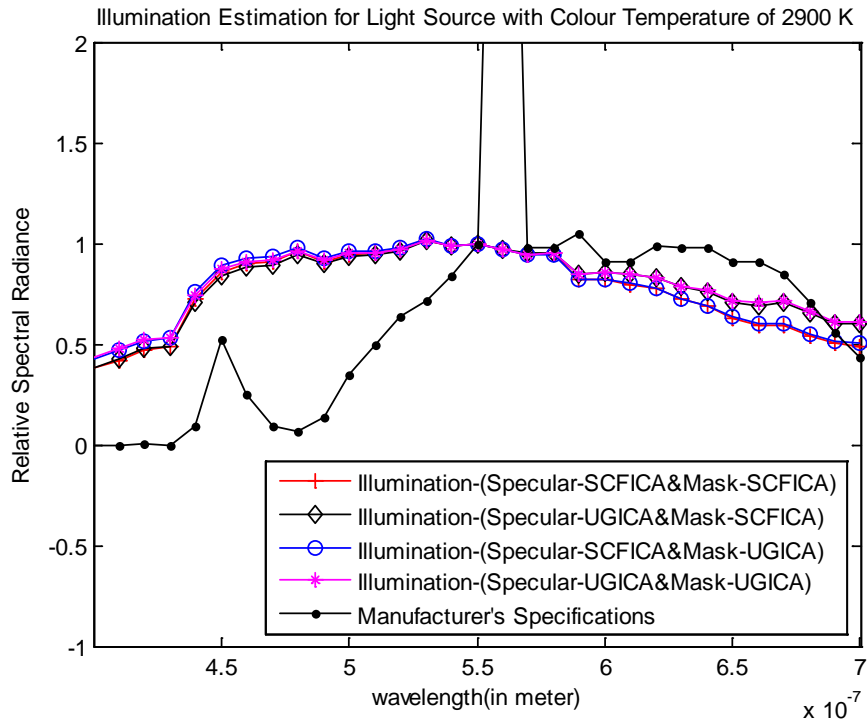


Figure C.17 The four possible illumination estimations using significantly specular pixels selected from the two sets of specular components (i.e. extracted using the SCFICA and UGICA techniques) using the two corresponding masks (mask-SCFICA and mask-UGICA) interchangeable with each of the two sets, after automatic thresholding for the plastic green ring illuminated with a light source of colour temperature of 2900 K.

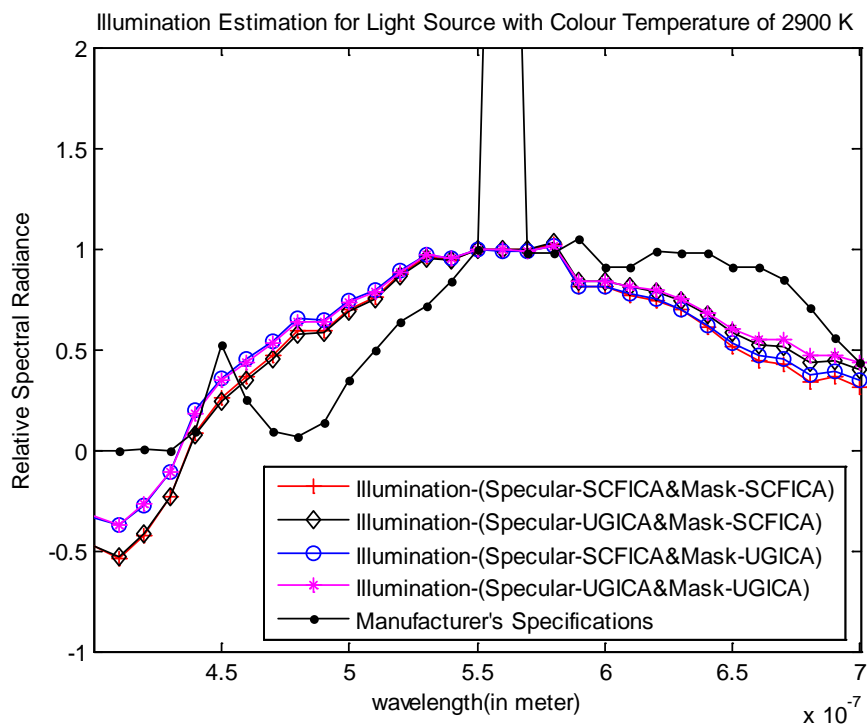


Figure C.18 The four possible illumination estimations using significantly specular pixels selected from the two sets of specular components (i.e. extracted using the SCFICA and UGICA techniques) using the two corresponding masks (mask-SCFICA and mask-UGICA) interchangeable with each of the two sets, after empirical thresholding for the plastic green ring illuminated with a light source of colour temperature of 2900 K.

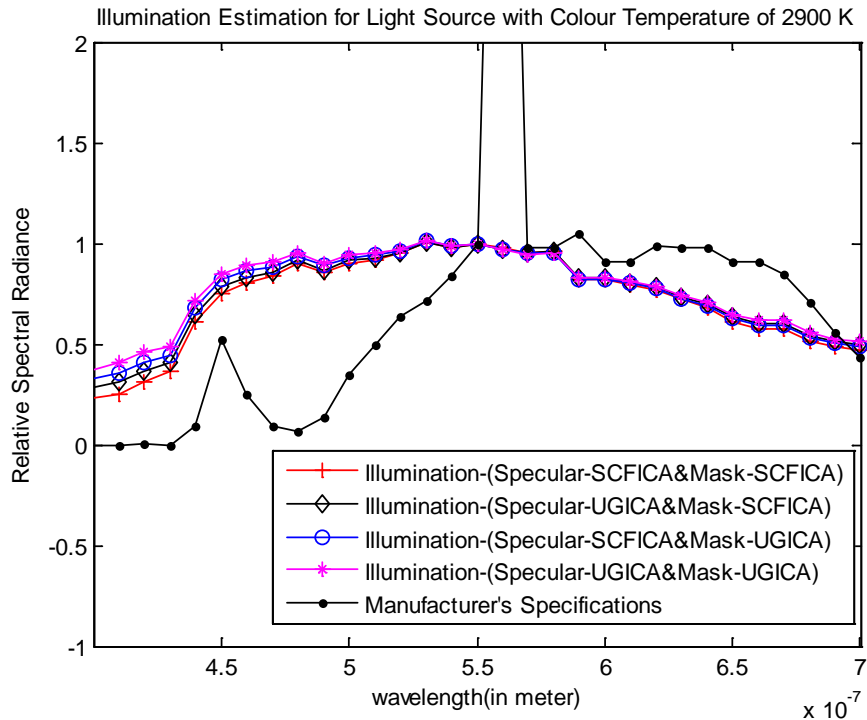


Figure C.19 The four possible illumination estimations using significantly specular pixels selected from the two sets of specular components (i.e. extracted using the SCFICA and UGICA techniques) using the two corresponding masks (Mask-SCFICA and Mask-UGICA) interchangeable with each of the two sets, after automatic thresholding for the green apple illuminated with a light source of colour temperature of 2900 K.

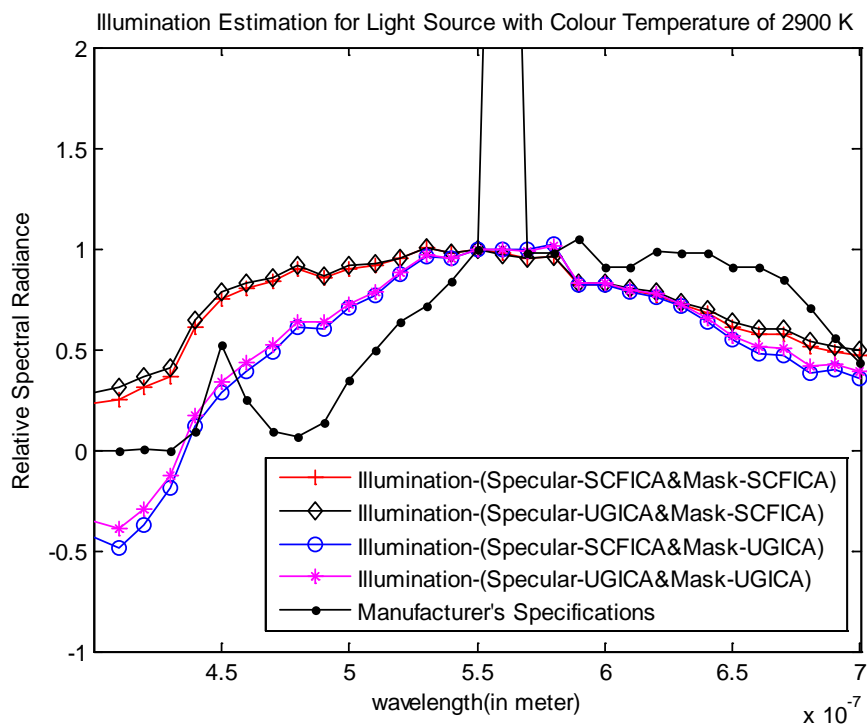


Figure C.20 The four possible illumination estimations using significantly specular pixels selected from the two sets of specular components (i.e. extracted using the SCFICA and UGICA techniques) using the two corresponding masks (Mask-SCFICA and Mask-UGICA) interchangeable with each of the two sets, after empirical thresholding for the green apple illuminated with a light source of colour temperature of 2900 K.

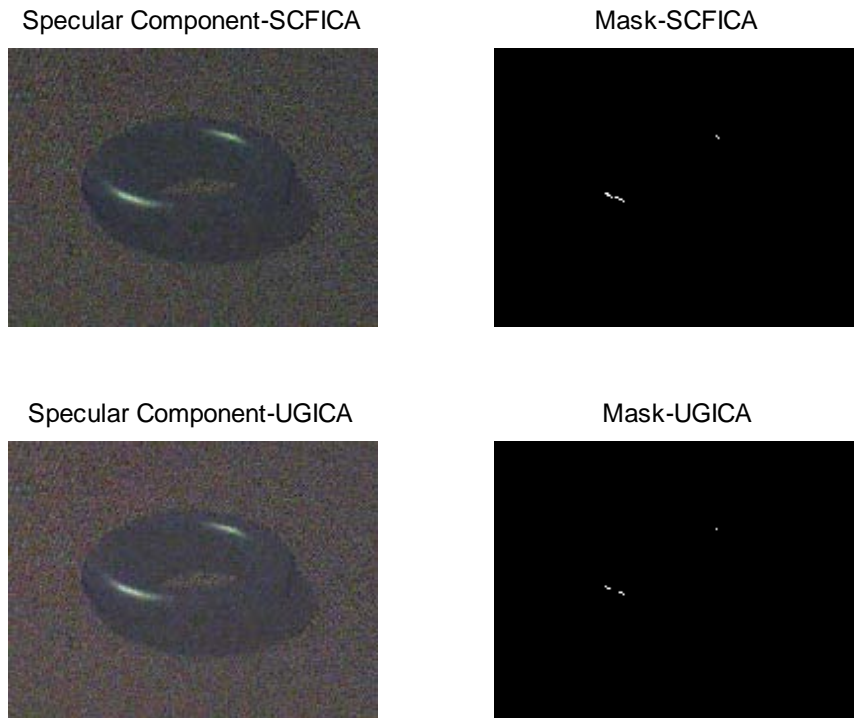


Figure C.21 The two sets of RGB specular components extracted using two blind separation techniques (i.e. the SCFICA and UGICA techniques) and the corresponding masks for the plastic blue ring illuminated with a light source of colour temperature of 2900 K, after automatic thresholding.

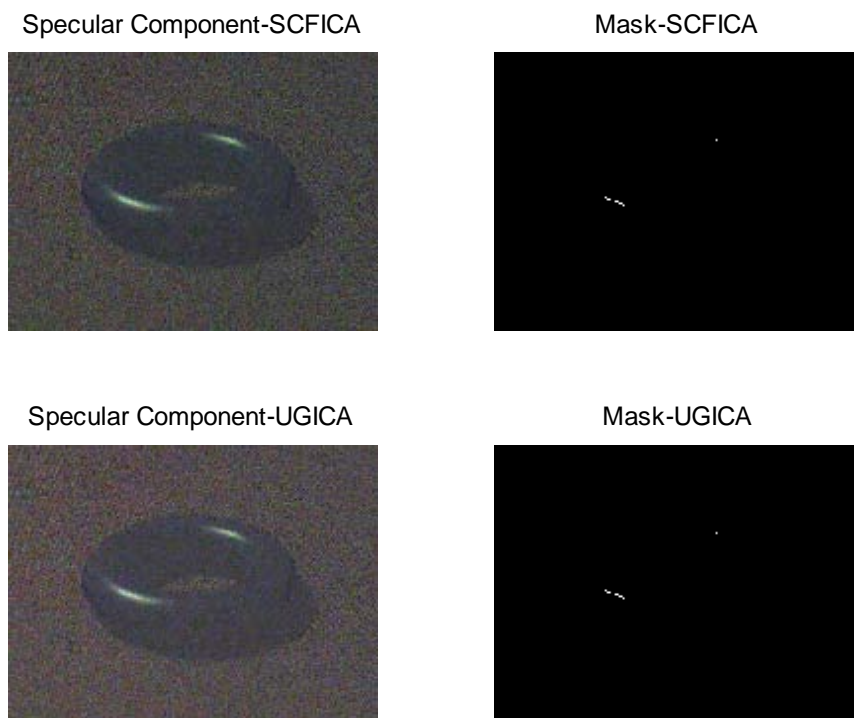


Figure C.22 The two sets of RGB specular components extracted using two blind separation techniques (i.e. the SCFICA and UGICA techniques) and the corresponding masks for the plastic blue ring illuminated with a light source of colour temperature of 2900 K, after empirical thresholding.

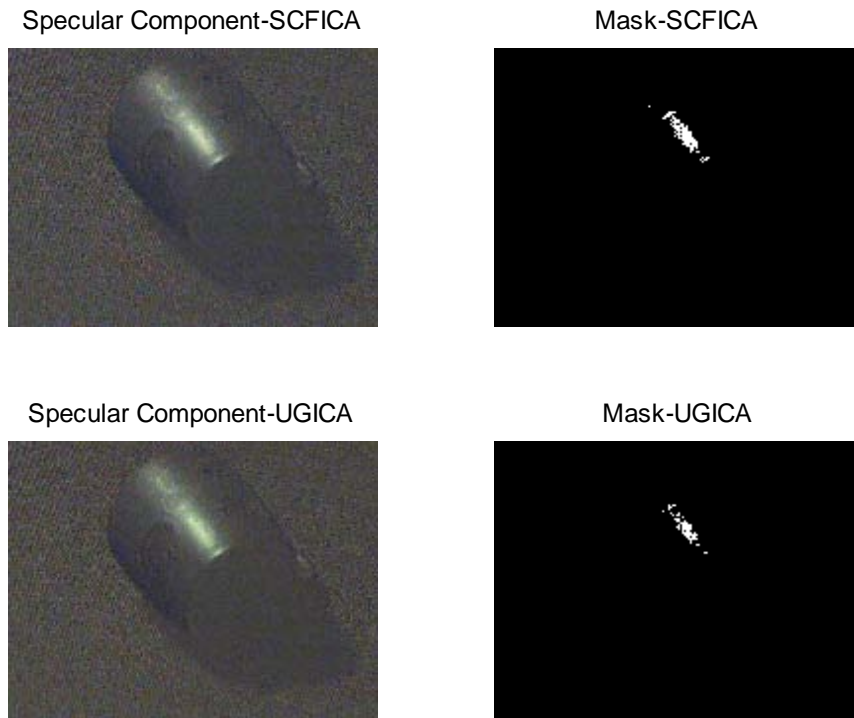


Figure C.23 The two sets of RGB specular components extracted using two blind separation techniques (i.e. the SCFICA and UGICA techniques) and the corresponding masks for the ceramic violet cup illuminated with a light source of colour temperature of 2900 K, after automatic thresholding.

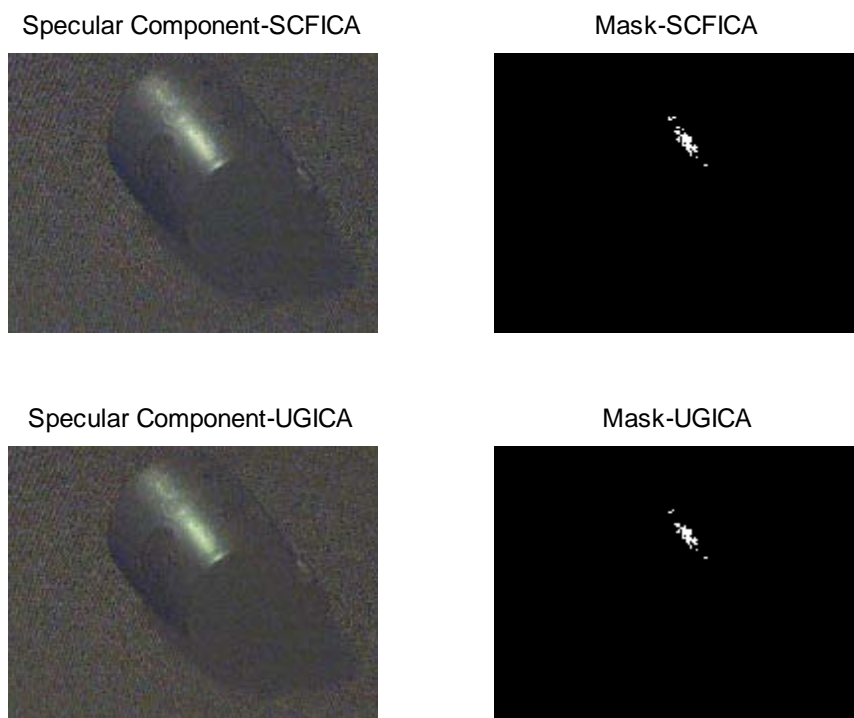


Figure C.24 The two sets of RGB specular components extracted using two blind separation techniques (i.e. the SCFICA and UGICA techniques) and the corresponding masks for the ceramic violet cup illuminated with a light source of colour temperature of 2900 K, after empirical thresholding.

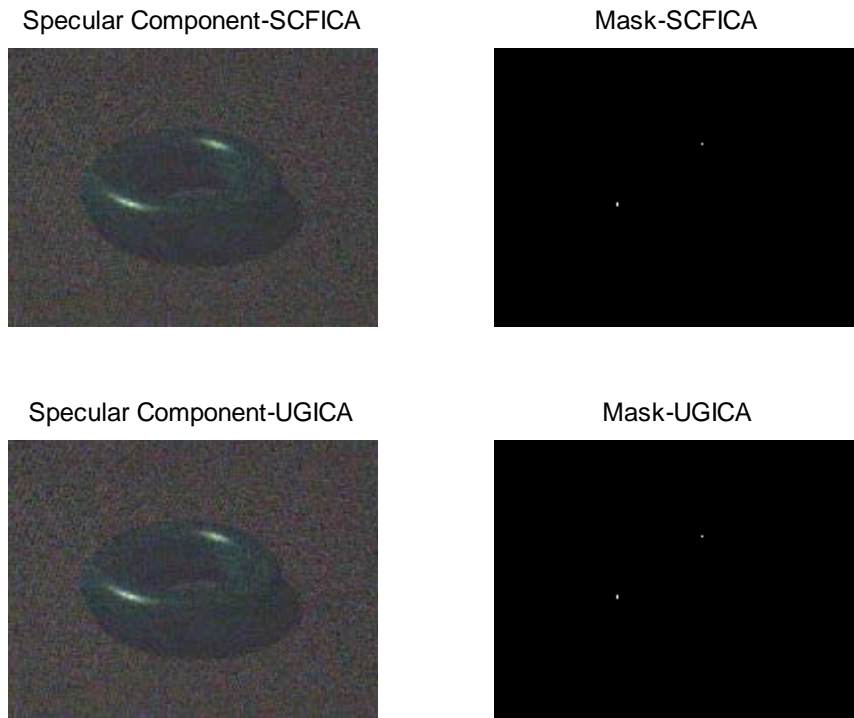


Figure C.25 The two sets of RGB specular components extracted using two blind separation techniques (i.e. the SCFICA and UGICA techniques) and the corresponding masks for the plastic green ring illuminated with a light source of colour temperature of 2900 K, after automatic thresholding.

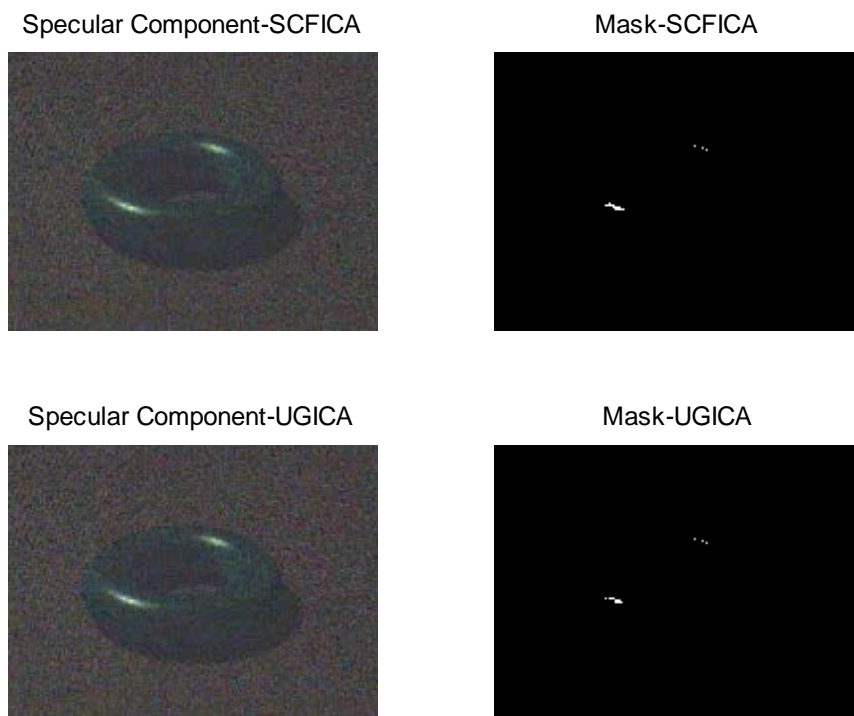


Figure C.26 The two sets of RGB specular components extracted using two blind separation techniques (i.e. the SCFICA and UGICA techniques) and the corresponding masks for the plastic green ring illuminated with a light source of colour temperature of 2900 K, after empirical thresholding.

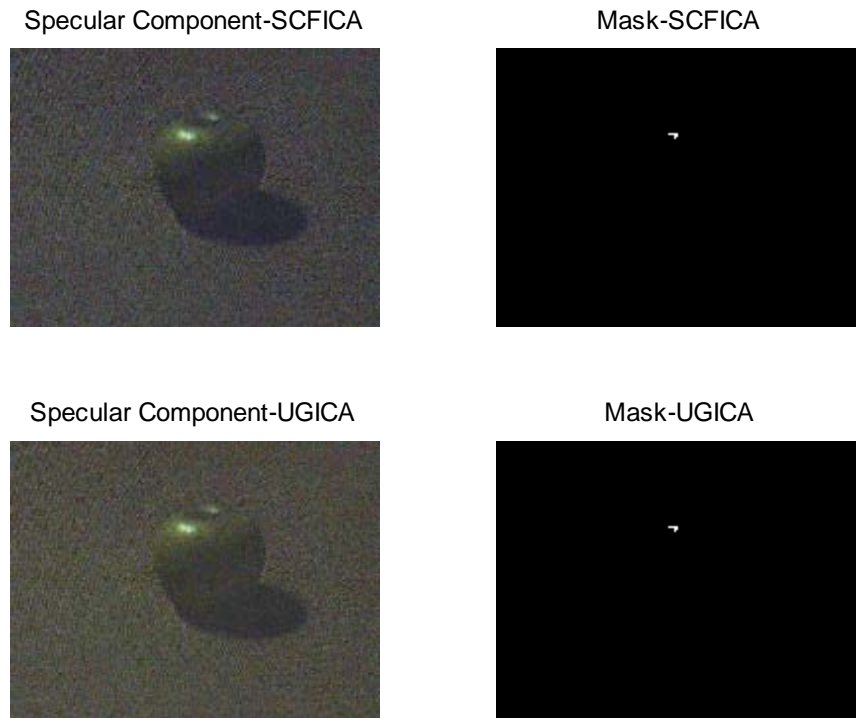


Figure C.27 The two sets of RGB specular components extracted using two blind separation techniques (i.e. the SCFICA and UGICA techniques) and the corresponding masks for the green apple illuminated with a light source of colour temperature of 2900 K, after automatic thresholding.

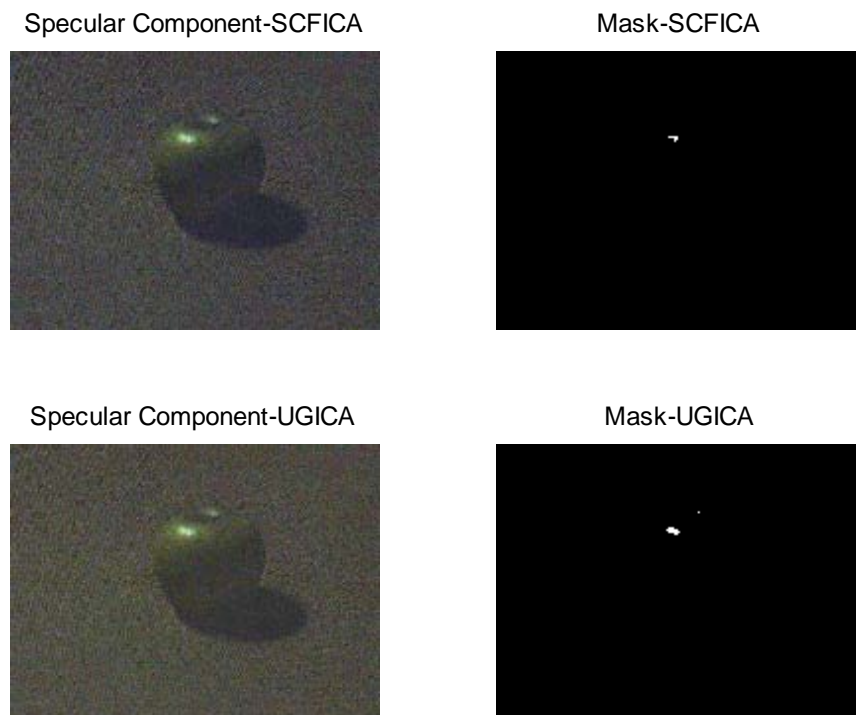


Figure C.28 The two sets of RGB specular components extracted using two blind separation techniques (i.e. the SCFICA and UGICA techniques) and the corresponding masks for the green apple illuminated with a light source of colour temperature of 2900 K, after empirical thresholding.

Table C.6 The automatic and the empirical threshold, and the corresponding number of pixels in the mask for the four examples of objects under an artificial light source with a colour temperature of 2900 K.

Separation technique	Object	Automatic threshold (number of pixels in mask)	Empirical threshold (number of pixels in mask)
SCFICA	Plastic blue ring	0.55(158)	0.58(94)
	Ceramic violet cup	0.58(1359)	0.63(761)
	Plastic green ring	0.65(29)	0.53(200)
	Green apple	0.57(116)	0.48(243)
UGICA	Plastic blue ring	0.68(60)	0.65(113)
	Ceramic violet cup	0.59(862)	0.61(664)
	Plastic green ring	0.72(25)	0.59(164)
	Green apple	0.59(94)	0.49(212)

Table C.7 Results of the experimental assessment of the effect of: the extraction of the specular image component, and the material of the reflecting object. The table entries represent the RMS error between the illumination spectral power distribution estimated in the experiment and the distribution provided by the manufacturer of the light source with a colour temperature of 2900 K.

Illumination source	Extraction of specular image component		Material of the reflecting object				
	Signal separation	Selection of significantly specular pixels	Plastic blue ring	Ceramic violet cup	Plastic green ring	Green apple	
Colour temperature: 2900 K	Spatially constrained FastICA Technique (SCFICA)	Automatic selection	Mask-SCFICA	28.37×10^{-2}	29.12×10^{-2}	41.47×10^{-2}	36.69×10^{-2}
			Mask-UGICA	29.35×10^{-2}	25.16×10^{-2}	43.09×10^{-2}	39.67×10^{-2}
		Empirical selection	Mask-SCFICA	27.82×10^{-2}	24.86×10^{-2}	28.99×10^{-2}	29.30×10^{-2}
			Mask-UGICA	27.67×10^{-2}	24.92×10^{-2}	27.85×10^{-2}	27.70×10^{-2}
	Umeyama and Godin ICA Techniques (UGICA)	Automatic selection	Mask-SCFICA	25.68×10^{-2}	30.04×10^{-2}	40.57×10^{-2}	37.98×10^{-2}
			Mask-UGICA	28.53×10^{-2}	26.05×10^{-2}	42.26×10^{-2}	40.96×10^{-2}
		Empirical selection	Mask-SCFICA	26.28×10^{-2}	25.71×10^{-2}	27.16×10^{-2}	27.67×10^{-2}
			Mask-UGICA	25.73×10^{-2}	25.73×10^{-2}	25.98×10^{-2}	26.82×10^{-2}

Table C.8 Results of the experimental assessment of the effect of: the extraction of the specular image component, and the material of the reflecting object. The table entries represent the median error between the illumination spectral power distribution estimated in the experiment and the distribution provided by the manufacturer of the light source with a colour temperature of 2900 K.

Illumination source	Extraction of specular image component		Material of the reflecting object				
	Signal separation	Selection of significantly specular pixels	Plastic blue ring	Ceramic violet cup	Plastic green ring	Green apple	
Colour temperature: 2900 K	Spatially constrained FastICA Technique (SCFICA)	Automatic selection	Mask-SCFICA	6.0×10^{-3}	8.8×10^{-3}	14.41×10^{-2}	14.41×10^{-2}
			Mask-UGICA	4.84×10^{-2}	4.20×10^{-2}	14.41×10^{-2}	14.41×10^{-2}
		Empirical selection	Mask-SCFICA	1.52×10^{-2}	6.41×10^{-2}	4.8×10^{-3}	5.02×10^{-2}
			Mask-UGICA	1.29×10^{-2}	7.58×10^{-2}	9.4×10^{-3}	5.4×10^{-3}
	Umeyama and Godin ICA Techniques (UGICA)	Automatic selection	Mask-SCFICA	1.72×10^{-2}	3.99×10^{-2}	14.41×10^{-2}	14.41×10^{-2}
			Mask-UGICA	8.94×10^{-2}	3.0×10^{-4}	14.41×10^{-2}	14.41×10^{-2}
		Empirical selection	Mask-SCFICA	6.69×10^{-2}	3.68×10^{-2}	4.0×10^{-3}	3.9×10^{-3}
			Mask-UGICA	6.41×10^{-2}	5.84×10^{-2}	4.42×10^{-2}	3.04×10^{-2}

Table C.9 Results of the experimental assessment of the effect of: the extraction of the specular image component, and the material of the reflecting object. The table entries represent the mean error between the illumination spectral power distribution estimated in the experiment and the distribution provided by the manufacturer of the light source with a colour temperature of 2900 K.

Illumination source	Extraction of specular image component		Material of the reflecting object				
	Signal separation	Selection of significantly specular pixels	Plastic blue ring	Ceramic violet cup	Plastic green ring	Green apple	
Colour temperature: 2900 K	Spatially constrained FastICA Technique (SCFICA)	Automatic selection	Mask-SCFICA	1.21×10^{-2}	1.36×10^{-2}	25.40×10^{-2}	21.22×10^{-2}
			Mask-UGICA	11.64×10^{-2}	6.07×10^{-2}	26.82×10^{-2}	24.00×10^{-2}
		Empirical selection	Mask-SCFICA	7.28×10^{-2}	8.09×10^{-2}	2.3×10^{-3}	1.54×10^{-2}
			Mask-UGICA	5.19×10^{-2}	10.09×10^{-2}	4.13×10^{-2}	1.97×10^{-2}
	Umeyama and Godin ICA Techniques (UGICA)	Automatic selection	Mask-SCFICA	5.90×10^{-2}	2.83×10^{-2}	28.00×10^{-2}	23.07×10^{-2}
			Mask-UGICA	16.07×10^{-2}	4.51×10^{-2}	29.45×10^{-2}	25.72×10^{-2}
		Empirical selection	Mask-SCFICA	11.83×10^{-2}	6.50×10^{-2}	1.83×10^{-2}	1.40×10^{-2}
			Mask-UGICA	9.78×10^{-2}	8.48×10^{-2}	6.28×10^{-2}	4.74×10^{-2}

Table C.10 Results of the experimental assessment of the effect of: the extraction of the specular image component, and the material of the reflecting object. The table entries represent the angular error (in degrees) between the illumination spectral power distribution estimated in the experiment and the distribution provided by the manufacturer of the light source with a colour temperature of 2900 K.

Illumination source	Extraction of specular image component		Material of the reflecting object				
	Signal separation	Selection of significantly specular pixels	Plastic blue ring	Ceramic violet cup	Plastic green ring	Green apple	
Colour temperature: 2900 K	Spatially constrained FastICA Technique (SCFICA)	Automatic selection	Mask-SCFICA	14.73	9.10	24.29	22.41
			Mask-UGICA	18.64	10.71	24.83	23.55
		Empirical selection	Mask-SCFICA	16.83	11.45	14.48	12.92
			Mask-UGICA	16.05	12.24	15.87	13.95
	Umeyama and Godin ICA Techniques (UGICA)	Automatic selection	Mask-SCFICA	12.45	10.54	22.06	22.62
			Mask-UGICA	16.57	12.19	22.61	23.71
		Empirical selection	Mask-SCFICA	14.71	12.93	12.03	13.10
			Mask-UGICA	13.89	13.71	13.44	14.32

C.3 Experiment 3 (Section 5.3.2.3)

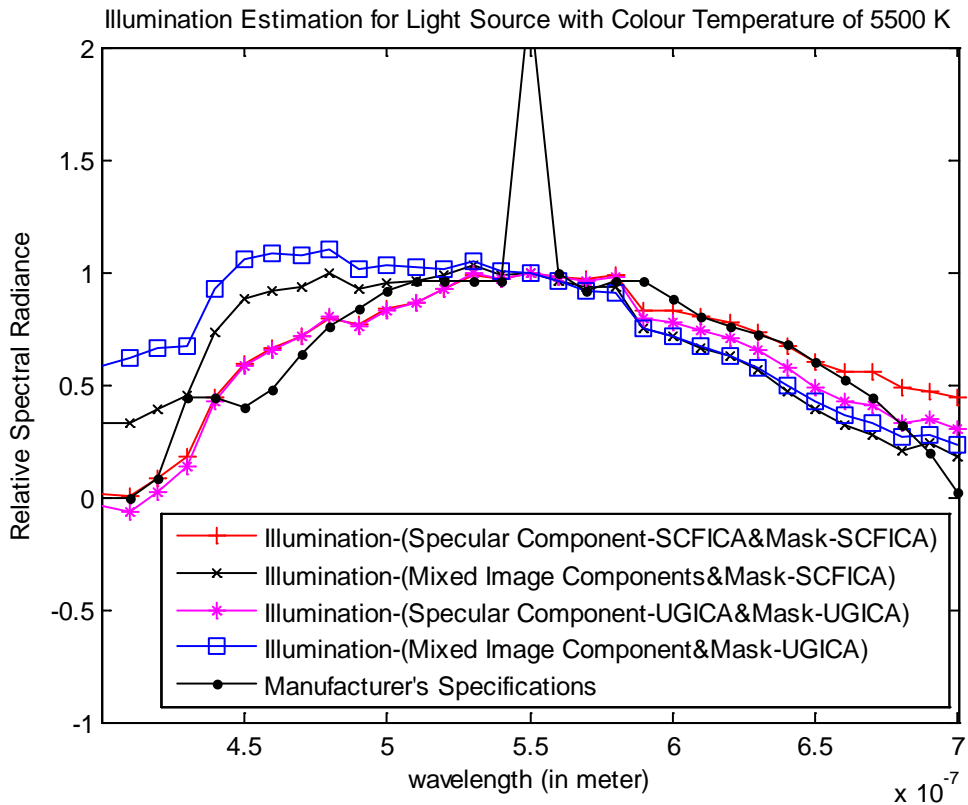


Figure C.29 The illumination estimations from the specular component and mixed image components for the plastic green ring illuminated with a light source of colour temperature of 5500 K using empirical thresholding.

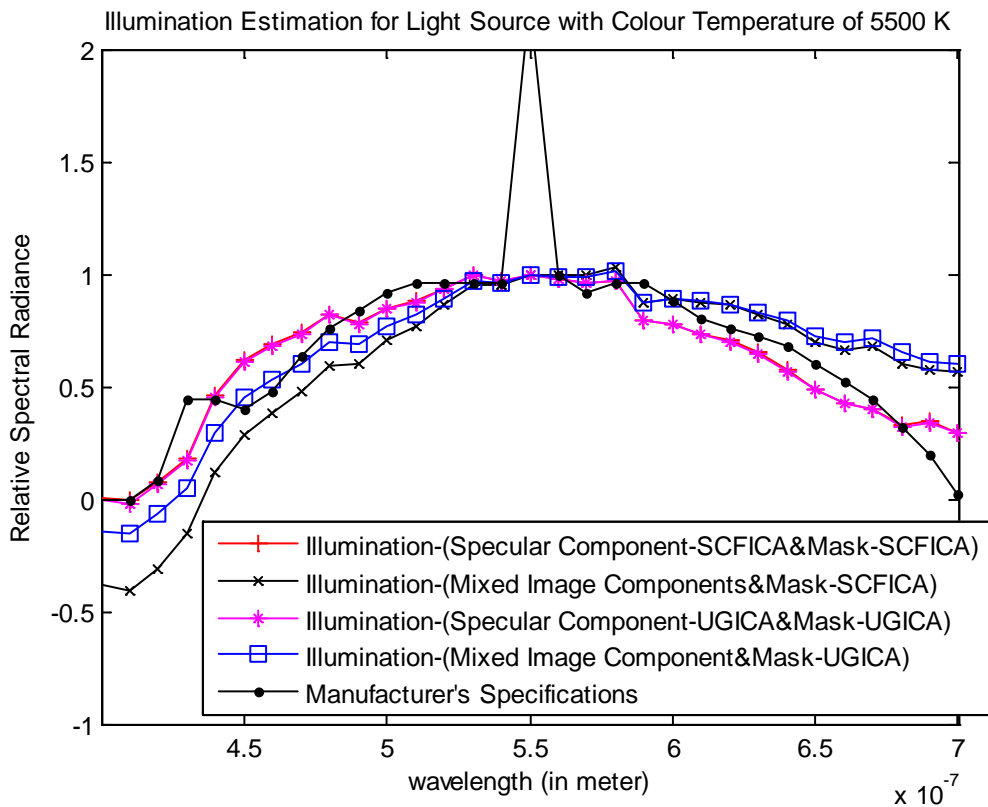


Figure C.30 The illumination estimations from the specular component and mixed image components for the red apple illuminated with a light source of colour temperature of 5500 K using empirical thresholding.

C.4 Experiment 4 (Section 5.3.2.4)

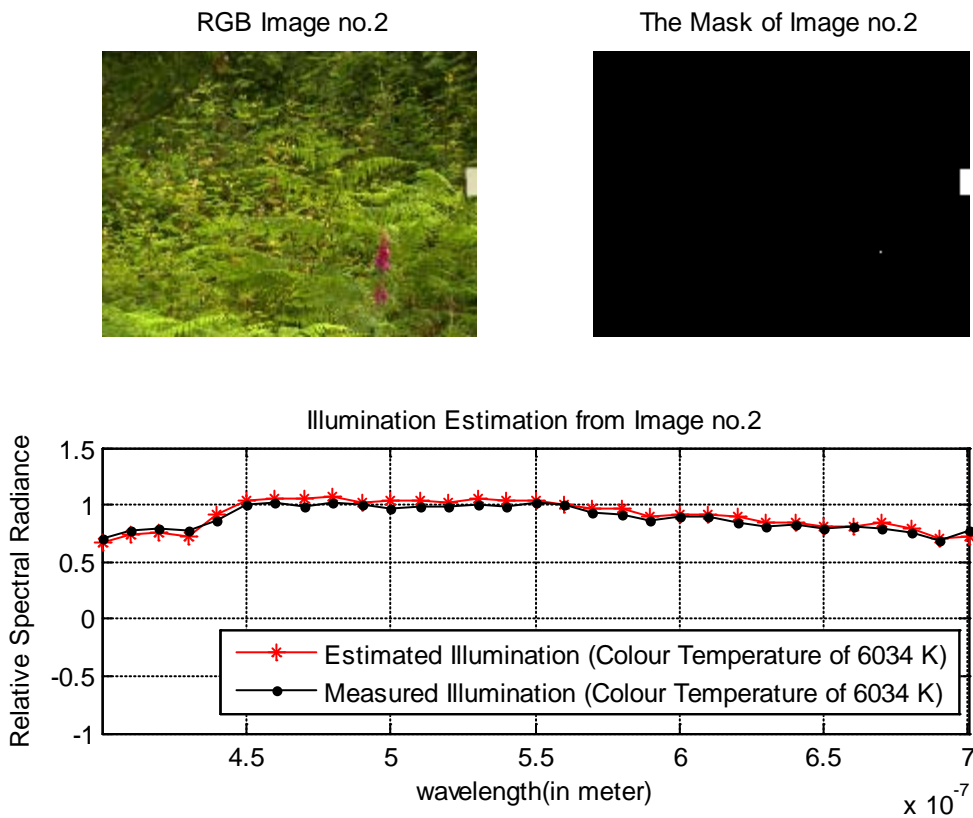


Figure C.31 The illumination estimation from the second image of Foster et al’s data set [181]

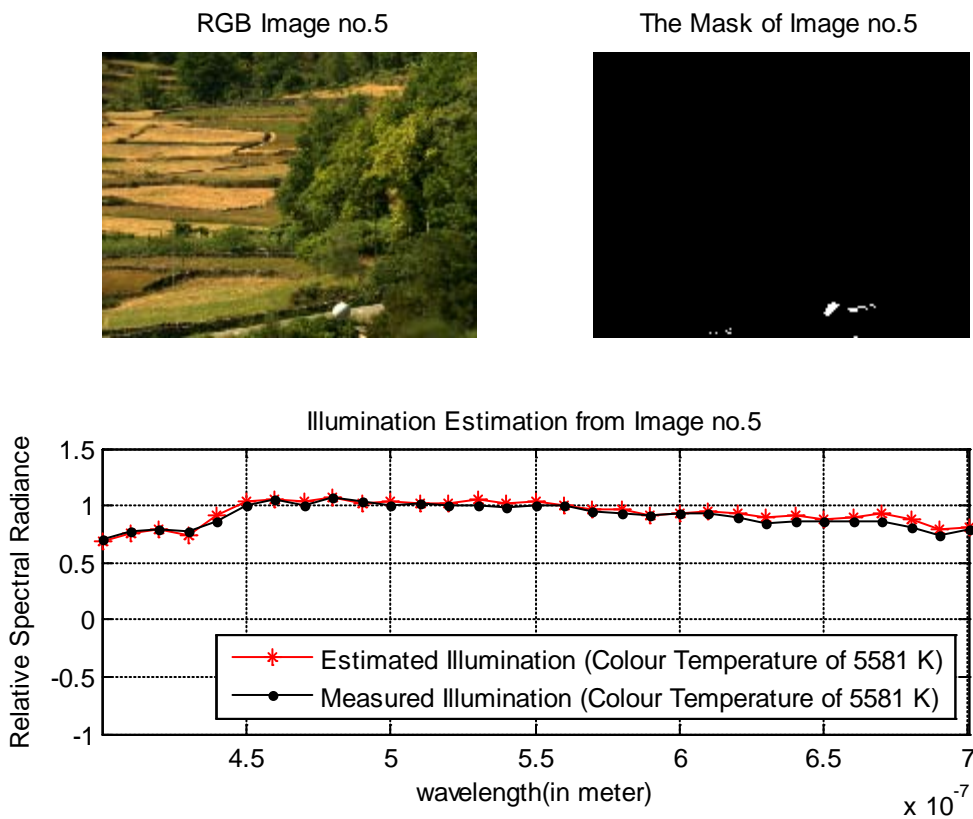


Figure C.32 The illumination estimation from the fifth image of Foster et al’s data set [181].

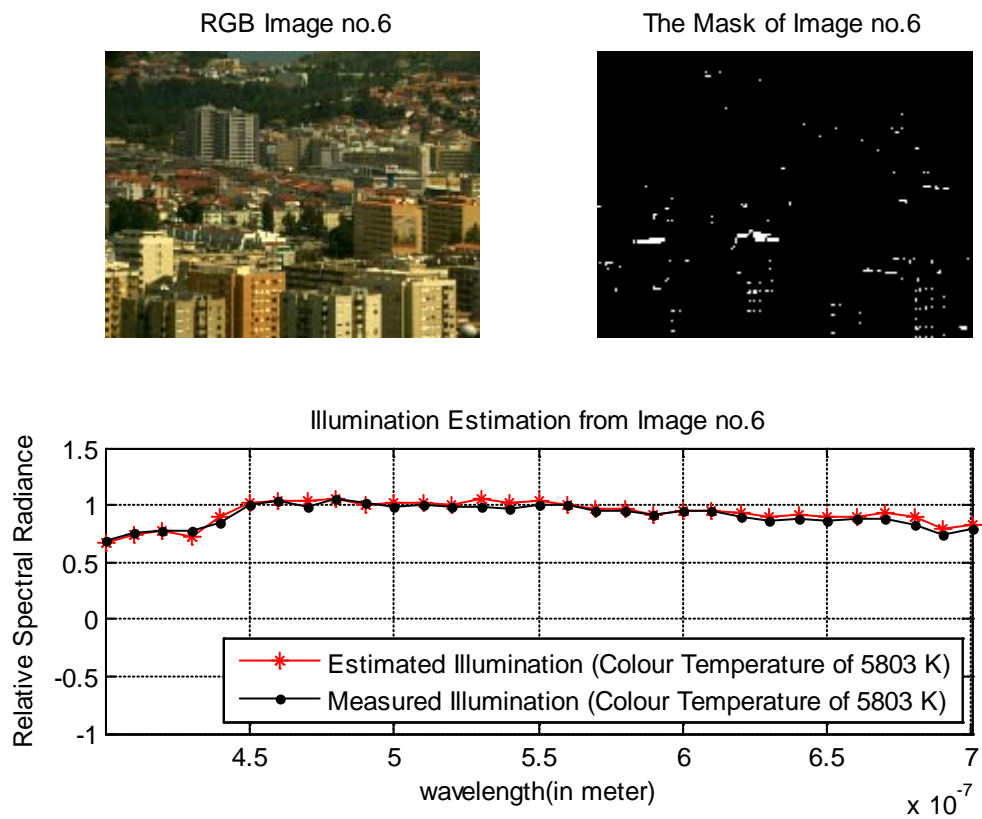


Figure C.33 The illumination estimation from the sixth image of Foster et al’s data set [181].

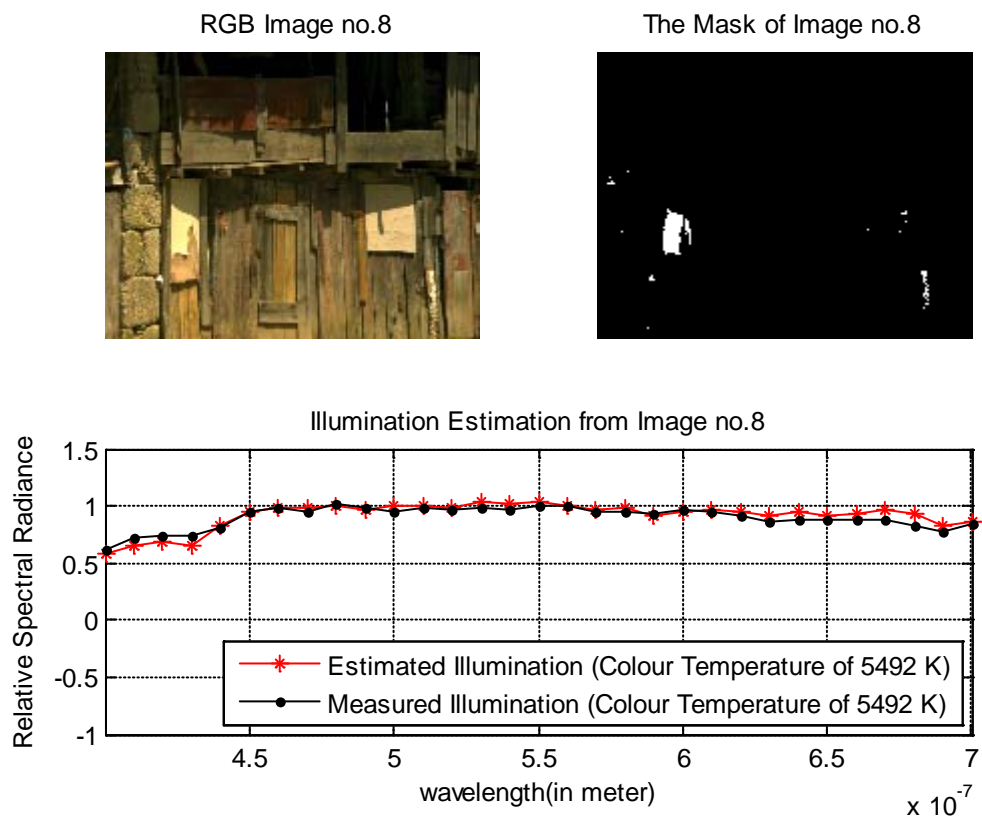


Figure C.34 The illumination estimation from the eighth image of Foster et al’s data set [181]

Appendix **D**

Estimates of Surface Spectral Reflectance

D.1 Experiment 1 (Section 6.2.2.1)

Table D.1 Results of the experimental assessment of the effect of: the extraction of the diffuse image component, the four possible illumination estimates, and the material of the reflecting object. The table entries represent the RMS error between the surface reflectance estimates obtained using the four possible illumination estimates and surface reflectance estimate obtained using the illumination specification provided by the manufacturer of the light source with a colour temperature of 5500 K.

Extraction of diffuse image component Signal separation	The four possible illumination estimates	Material of the reflecting object		
		Plastic blue ring	Ceramic violet cup	Plastic green ring
Spatially constrained FastICA technique (Diffuse -SCFICA)	Illumination-1	8.9×10^{-3}	2.3×10^{-3}	2.02×10^{-2}
	Illumination 2	1.15×10^{-2}	9.46×10^{-2}	6.74×10^{-2}
	Illumination-3	8.6×10^{-3}	1.28×10^{-2}	4.56×10^{-2}
	Illumination-4	1.12×10^{-2}	4.3×10^{-3}	7.2×10^{-3}
Umeyama and Godin ICA technique (Diffuse-UGICA)	Illumination-1	9.6×10^{-3}	4.6×10^{-3}	2.48×10^{-2}
	Illumination 2	1.25×10^{-2}	18.66×10^{-2}	8.37×10^{-2}
	Illumination-3	9.3×10^{-3}	2.61×10^{-2}	5.59×10^{-2}
	Illumination-4	1.22×10^{-2}	9.0×10^{-3}	8.2×10^{-3}

Table D.2 Results of the experimental assessment of the effect of: the extraction of the diffuse image component, the four possible illumination estimates, and the material of the reflecting object. The table entries represent the median error between the surface reflectance estimates obtained using the four possible illumination estimates and surface reflectance estimate obtained using the illumination specification provided by the manufacturer of the light source with a colour temperature of 5500 K.

Extraction of diffuse image component Signal separation	The four possible illumination estimates	Material of the reflecting object		
		Plastic blue ring	Ceramic violet cup	Plastic green ring
Spatially constrained FastICA technique (Diffuse -SCFICA)	Illumination-1	6.3×10^{-3}	2.0×10^{-3}	1.96×10^{-2}
	Illumination 2	8.1×10^{-3}	316×10^{-2}	2.47×10^{-2}
	Illumination-3	5.6×10^{-3}	8.3×10^{-3}	3.75×10^{-2}
	Illumination-4	7.5×10^{-3}	4.2×10^{-3}	6.7×10^{-3}
Umeyama and Godin ICA technique (Diffuse-UGICA)	Illumination-1	6.5×10^{-3}	4.9×10^{-3}	2.35×10^{-2}
	Illumination 2	8.1×10^{-3}	6.25×10^{-2}	3.07×10^{-2}
	Illumination-3	5.9×10^{-3}	1.80×10^{-2}	4.69×10^{-2}
	Illumination-4	7.7×10^{-3}	9.1×10^{-3}	8.1×10^{-3}

Table D.3 Results of the experimental assessment of the effect of: the extraction of the diffuse image component, the four possible illumination estimates, and the material of the reflecting object. The table entries represent the mean error between the surface reflectance estimates obtained using the four possible illumination estimates and surface reflectance estimate obtained using the illumination specification provided by the manufacturer of the light source with a colour temperature of 5500 K

Extraction of diffuse image component Signal separation	The four possible illumination estimates	Material of the reflecting object		
		Plastic blue ring	Ceramic violet cup	Plastic green ring
Spatially constrained FastICA technique (Diffuse -SCFICA)	Illumination-1	7.4×10^{-3}	1.2×10^{-3}	1.91×10^{-2}
	Illumination 2	8.0×10^{-3}	5.97×10^{-2}	3.98×10^{-2}
	Illumination-3	7.1×10^{-3}	1.10×10^{-2}	3.91×10^{-2}
	Illumination-4	7.8×10^{-3}	3.4×10^{-3}	7.1×10^{-3}
Umeyama and Godin ICA technique (Diffuse-UGICA)	Illumination-1	7.7×10^{-3}	3.1×10^{-3}	2.31×10^{-2}
	Illumination 2	8.6×10^{-3}	11.82×10^{-2}	4.91×10^{-2}
	Illumination-3	7.4×10^{-3}	2.31×10^{-2}	4.72×10^{-2}
	Illumination-4	8.3×10^{-3}	7.3×10^{-3}	8.1×10^{-3}

Table D.4 Results of the experimental assessment of the effect of: the extraction of the diffuse image component, the four possible illumination estimates, and the material of the reflecting object. The table entries represent the angular error (in degrees) between the surface reflectance estimates obtained using the four possible illumination estimates and surface reflectance estimate obtained using the illumination specification provided by the manufacturer of the light source with a colour temperature of 5500 K.

Extraction of diffuse image component Signal separation	The four possible illumination estimates	Material of the reflecting object		
		Plastic blue ring	Ceramic violet cup	Plastic green ring
Spatially constrained FastICA technique (Diffuse -SCFICA)	Illumination-1	0.70	0.37	1.68
	Illumination 2	0.93	7.28	5.90
	Illumination-3	0.70	0.79	3.16
	Illumination-4	0.92	0.44	0.36
Umeyama and Godin ICA technique (Diffuse-UGICA)	Illumination-1	0.65	0.69	1.80
	Illumination 2	0.87	8.81	5.69
	Illumination-3	0.65	0.97	3.18
	Illumination-4	0.86	0.70	0.44

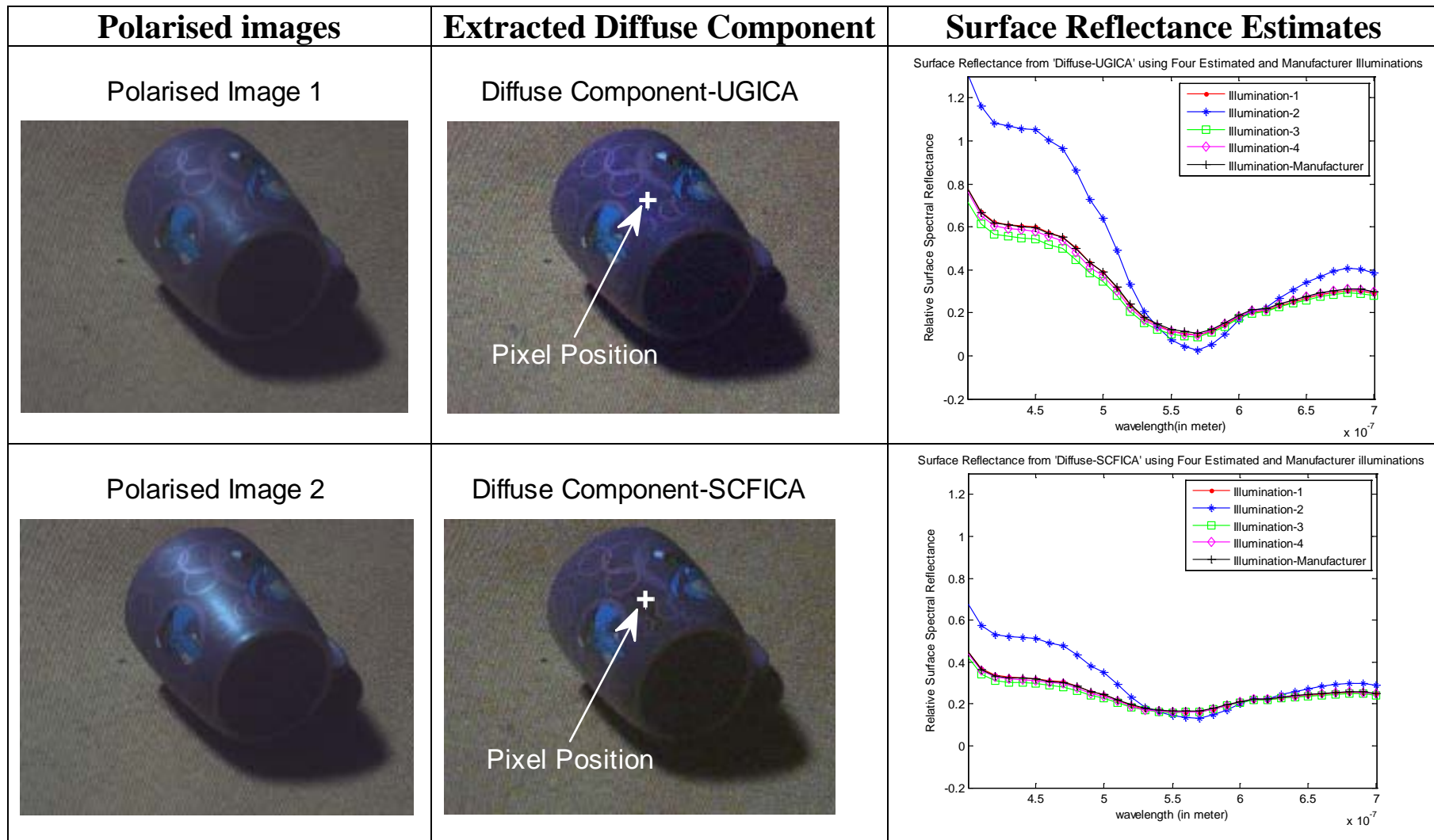


Figure D.1 Illustrative examples of polarised images, two RGB diffuse image components (i.e extracted using two separation techniques), and surface reflectance estimates. These estimates are obtained from each RGB diffuse image component for a pixel located at image position (330, 130) for the ceramic violet cup illuminated by a light source which has a colour temperature of 5500 K, using the four possible illumination estimates and a specification of the illumination provided by the manufacturer of the light source.

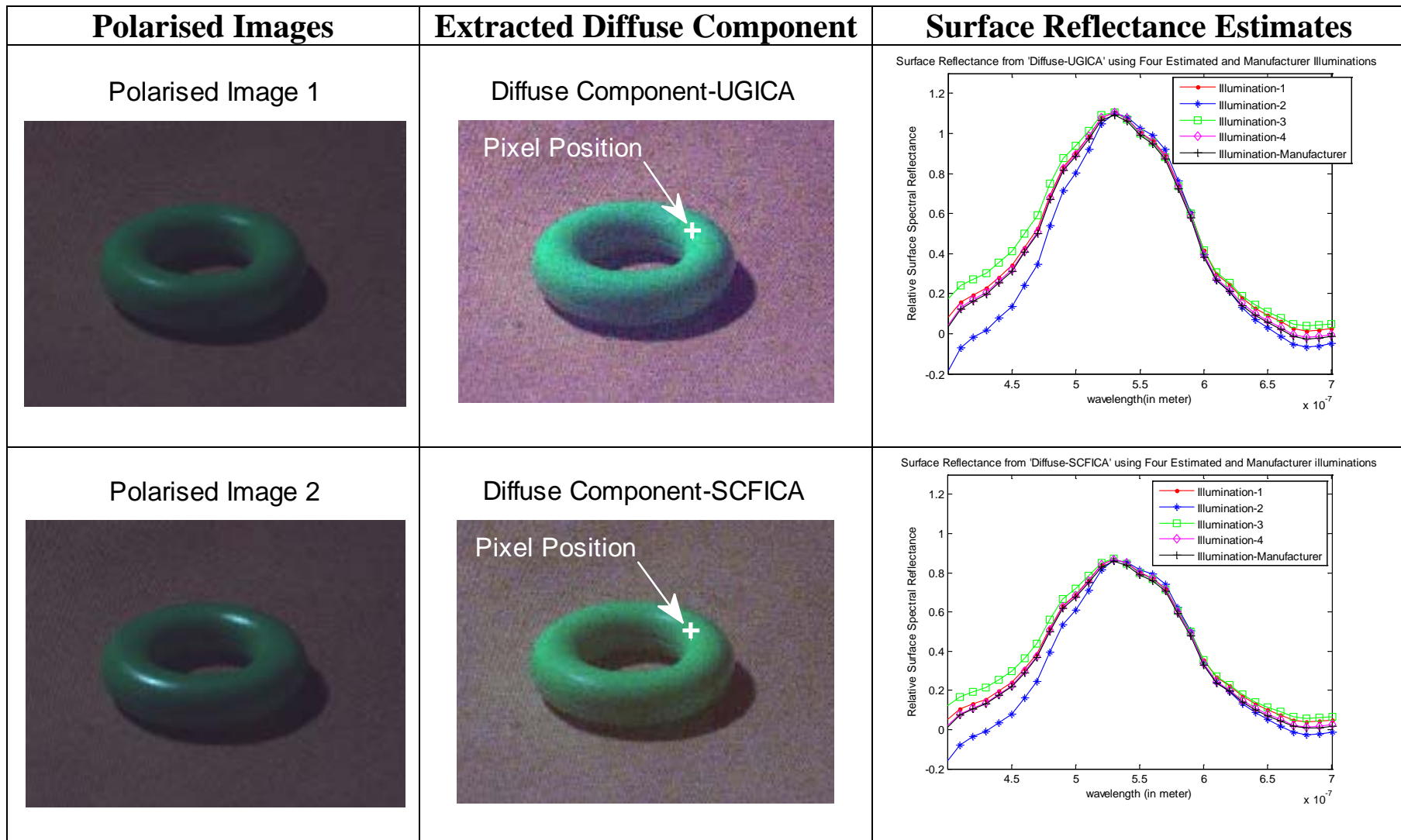


Figure D.2 Illustrative examples of polarised images, two RGB diffuse image components (i.e extracted using two separation techniques), and surface reflectance estimates. These estimates are obtained from each RGB diffuse image component for a pixel located at image position (400,190) for the plastic green ring illuminated by a light source which has a colour temperature of 5500 K, using the four possible illumination estimates and a specification of the illumination provided by the manufacturer of the light source.

Table D.5 Results of the experimental assessment of the effect of: the extraction of the diffuse image component, the four possible illumination estimates, and the material of the reflecting object. The table entries represent the RMS error between the surface reflectance estimates obtained using the four possible illumination estimates and surface reflectance estimate obtained using the illumination specification provided by the manufacturer of the light source with a colour temperature of 2900 K.

Extraction of diffuse image component Signal separation	The four possible illumination estimates	Material of the reflecting object		
		Plastic blue ring	Ceramic violet cup	Plastic green ring
Spatially constrained FastICA technique (Diffuse-SCFICA)	Illumination-1	7.27×10^{-2}	9.61×10^{-2}	3.26×10^{-2}
	Illumination 2	5.40×10^{-2}	9.61×10^{-2}	3.31×10^{-2}
	Illumination-3	4.40×10^{-2}	4.92×10^{-2}	1.58×10^{-2}
	Illumination-4	3.73×10^{-2}	4.98×10^{-2}	1.54×10^{-2}
Umeyama and Godin ICA technique (Diffuse-UGICA)	Illumination-1	7.82×10^{-2}	11.38×10^{-2}	9.16×10^{-2}
	Illumination 2	6.19×10^{-2}	11.37×10^{-2}	9.34×10^{-2}
	Illumination-3	5.59×10^{-2}	5.81×10^{-2}	4.22×10^{-2}
	Illumination-4	5.08×10^{-2}	5.87×10^{-2}	4.16×10^{-2}

Table D.6 Results of the experimental assessment of the effect of: the extraction of the diffuse image component, the four possible illumination estimates, and the material of the reflecting object. The table entries represent the median error between the surface reflectance estimates obtained using the four possible illumination estimates and surface reflectance estimate obtained using the illumination specification provided by the manufacturer of the light source with a colour temperature of 2900 K.

Extraction of diffuse image component Signal separation	The four possible illumination estimates	Material of the reflecting object		
		Plastic blue ring	Ceramic violet cup	Plastic green ring
Spatially constrained FastICA technique (Diffuse-SCFICA)	Illumination-1	3.08×10^{-2}	3.30×10^{-2}	1.59×10^{-2}
	Illumination 2	1.71×10^{-2}	3.52×10^{-2}	1.28×10^{-2}
	Illumination-3	1.33×10^{-2}	1.71×10^{-2}	1.03×10^{-2}
	Illumination-4	8.3×10^{-3}	1.83×10^{-2}	7.9×10^{-3}
Umeyama and Godin ICA technique (Diffuse-UGICA)	Illumination-1	2.68×10^{-2}	3.92×10^{-2}	4.39×10^{-2}
	Illumination 2	1.77×10^{-2}	4.15×10^{-2}	3.58×10^{-2}
	Illumination-3	1.37×10^{-2}	2.02×10^{-2}	2.69×10^{-2}
	Illumination-4	4.9×10^{-3}	2.20×10^{-2}	2.02×10^{-2}

Table D.7 Results of the experimental assessment of the effect of: the extraction of the diffuse image component, the four possible illumination estimates, and the material of the reflecting object. The table entries represent the mean error between the surface reflectance estimates obtained using the four possible illumination estimates and surface reflectance estimate obtained using the illumination specification provided by the manufacturer of the light source with a colour temperature of 2900 K.

Extraction of diffuse image component Signal separation	The four possible illumination estimates	Material of the reflecting object		
		Plastic blue ring	Ceramic violet cup	Plastic green ring
Spatially constrained FastICA technique (Diffuse -SCFICA)	Illumination-1	2.94×10^{-2}	4.79×10^{-2}	2.35×10^{-2}
	Illumination 2	1.50×10^{-2}	4.83×10^{-2}	2.26×10^{-2}
	Illumination-3	5.5×10^{-3}	1.66×10^{-2}	1.27×10^{-2}
	Illumination-4	2.3×10^{-3}	1.72×10^{-2}	1.15×10^{-2}
Umeyama and Godin ICA technique (Diffuse-UGICA)	Illumination-1	2.14×10^{-2}	5.71×10^{-2}	6.36×10^{-2}
	Illumination 2	7.6×10^{-3}	5.76×10^{-2}	6.14×10^{-2}
	Illumination-3	2.6×10^{-3}	2.00×10^{-2}	3.25×10^{-2}
	Illumination-4	9.9×10^{-3}	2.07×10^{-2}	2.94×10^{-2}

Table D.8 Results of the experimental assessment of the effect of: the extraction of the diffuse image component, the four possible illumination estimates, and the material of the reflecting object. The table entries represent the angular error between the surface reflectance estimates obtained using the four possible illumination estimates and surface reflectance estimate obtained using the illumination specification provided by the manufacturer of the light source with a colour temperature of 2900 K.

Extraction of diffuse image component Signal separation	The four possible illumination estimates	Material of the reflecting object		
		Plastic blue ring	Ceramic violet cup	Plastic green ring
Spatially constrained FastICA technique (Diffuse -SCFICA)	Illumination-1	4.33	5.93	2.78
	Illumination 2	3.67	5.86	3.03
	Illumination-3	3.36	3.75	1.05
	Illumination-4	3.05	3.76	1.20
Umeyama and Godin ICA technique (Diffuse-UGICA)	Illumination-1	4.84	6.11	6.03
	Illumination 2	4.32	6.03	6.37
	Illumination-3	4.24	3.85	2.36
	Illumination-4	3.95	3.86	2.45

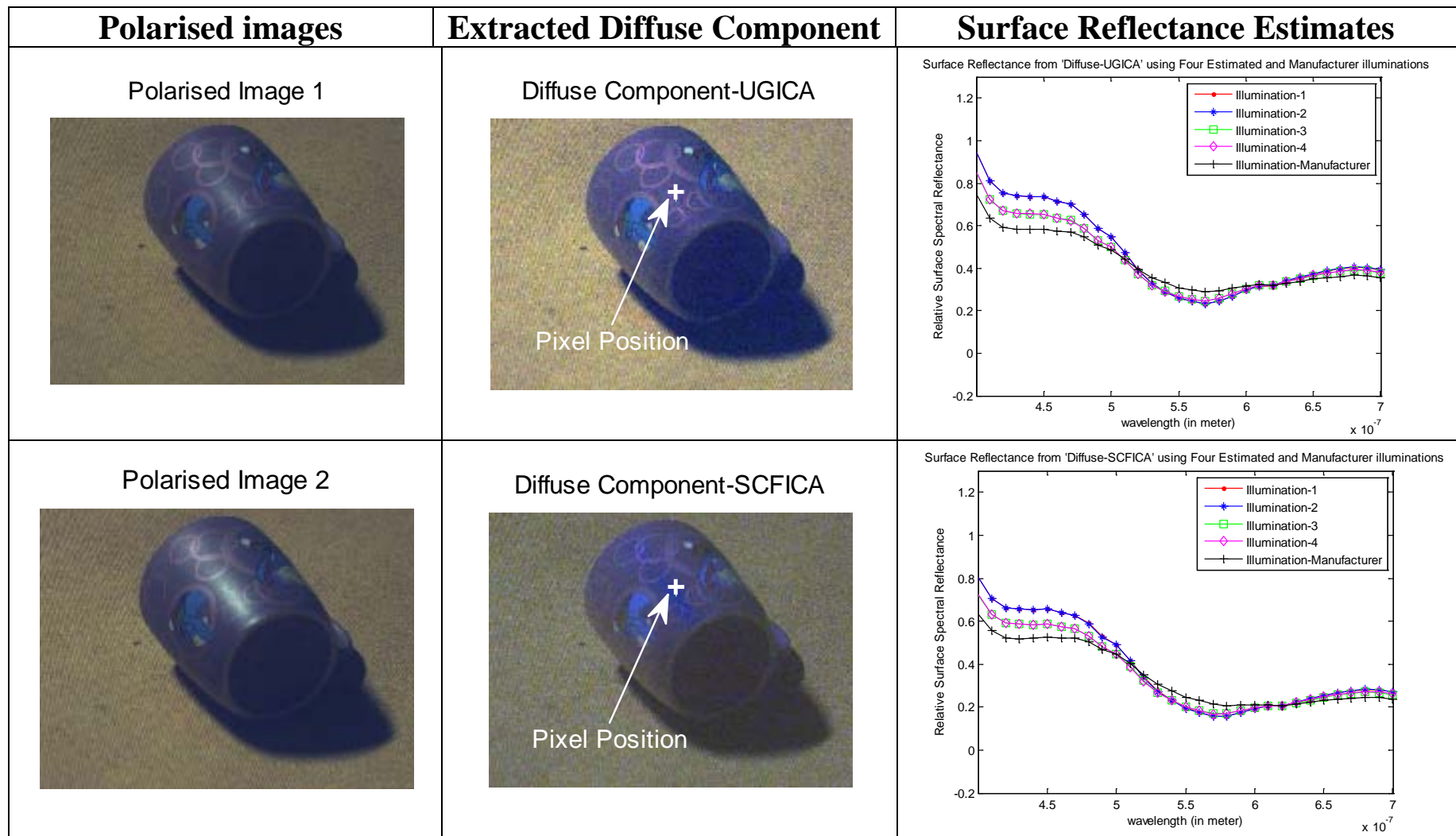


Figure D.3 Illustrative examples of polarised images, two RGB diffuse image components (i.e extracted using two separation techniques), and surface reflectance estimates. These estimates are obtained from each RGB diffuse image component for a pixel located at image position (330,130) for the ceramic violet cup illuminated by a light source which has a colour temperature of 2900 K, using the four possible illumination estimates and the illumination specification provided by the manufacturer of the light source.

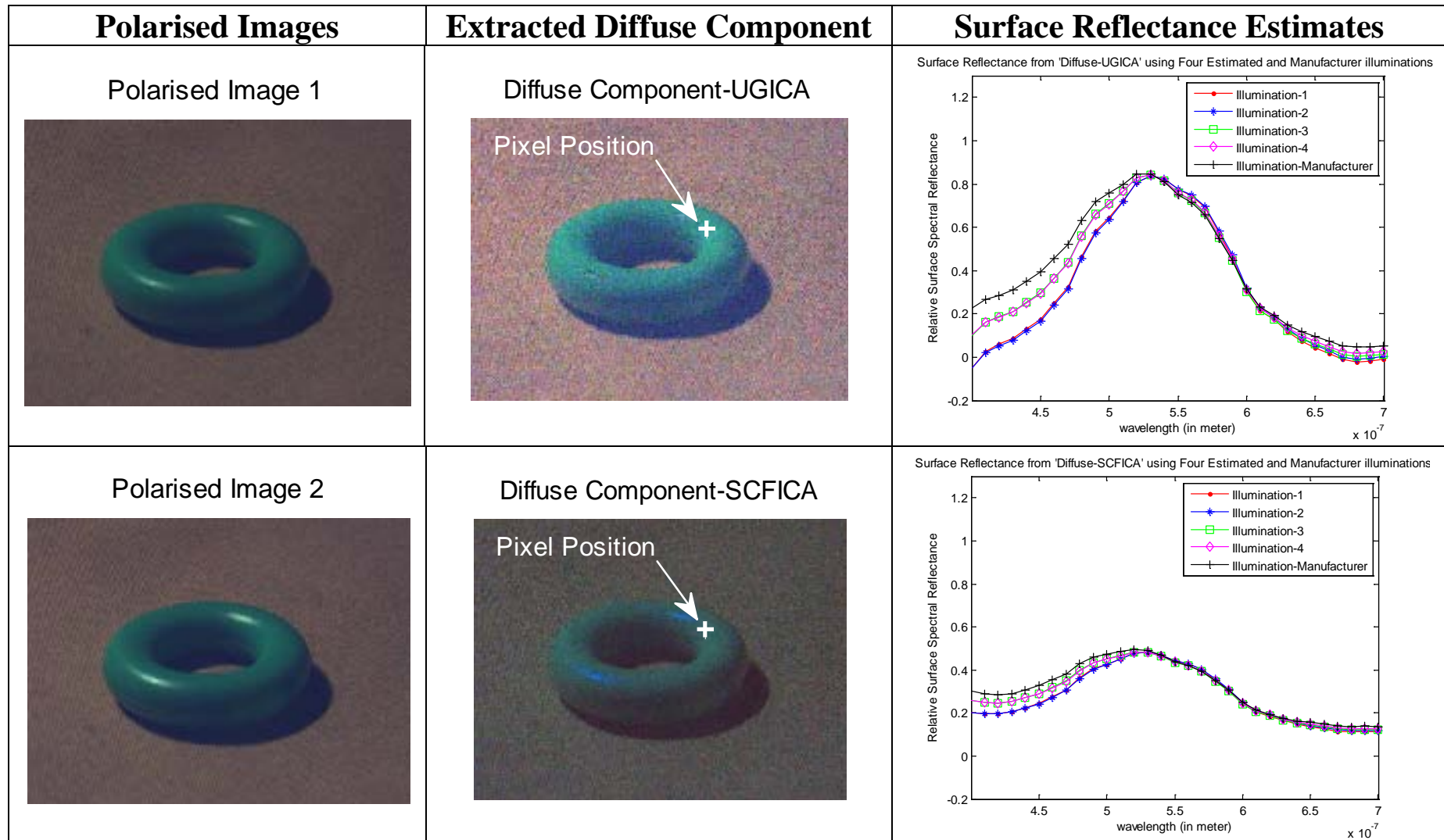


Figure D.4 Illustrative examples of polarised images, two RGB diffuse image components (i.e extracted using two separation techniques), and surface reflectance estimates. These estimates are obtained from each RGB diffuse image component for a pixel located at image position (400, 190) for the plastic green ring illuminated by a light source which has a colour temperature of 2900 K, using the four possible illumination estimates and the illumination specification provided by the manufacturer of the light source.

D.2 Experiment 2 (Section 6.2.2.2)

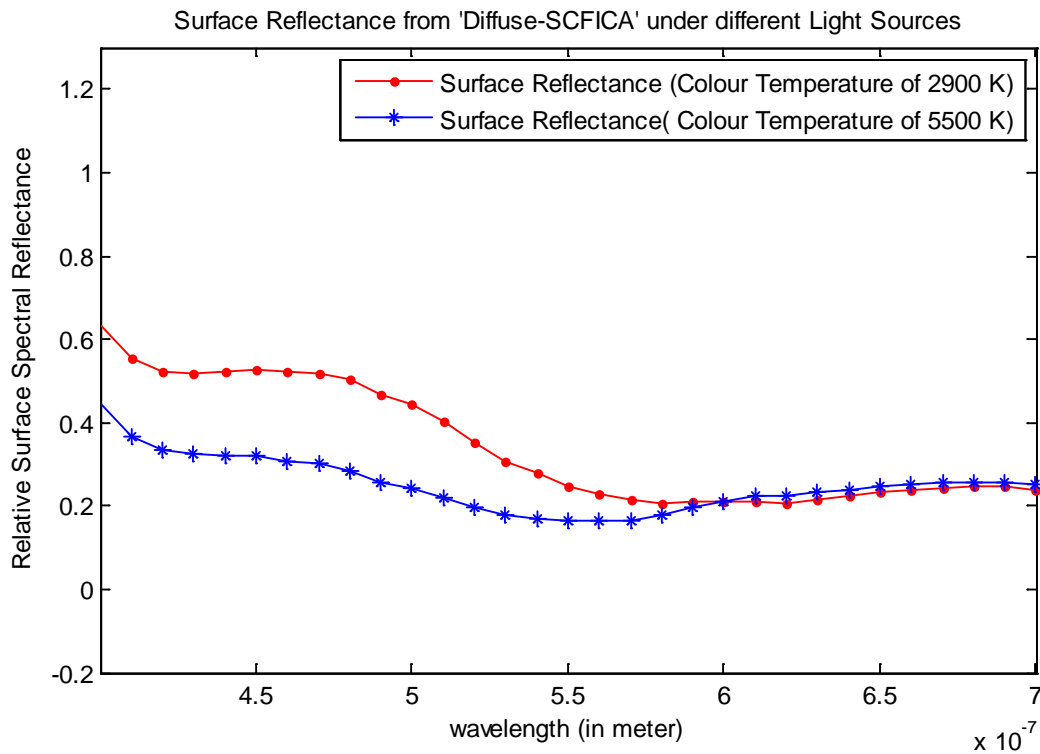


Figure D.5 The surface reflectance, for a pixel located at image coordinates (330, 130), estimated from the 'Diffuse-SCFICA' image component for a ceramic violet cup illuminated by two artificial light sources with different colour temperatures of 2900 and 5500 K.

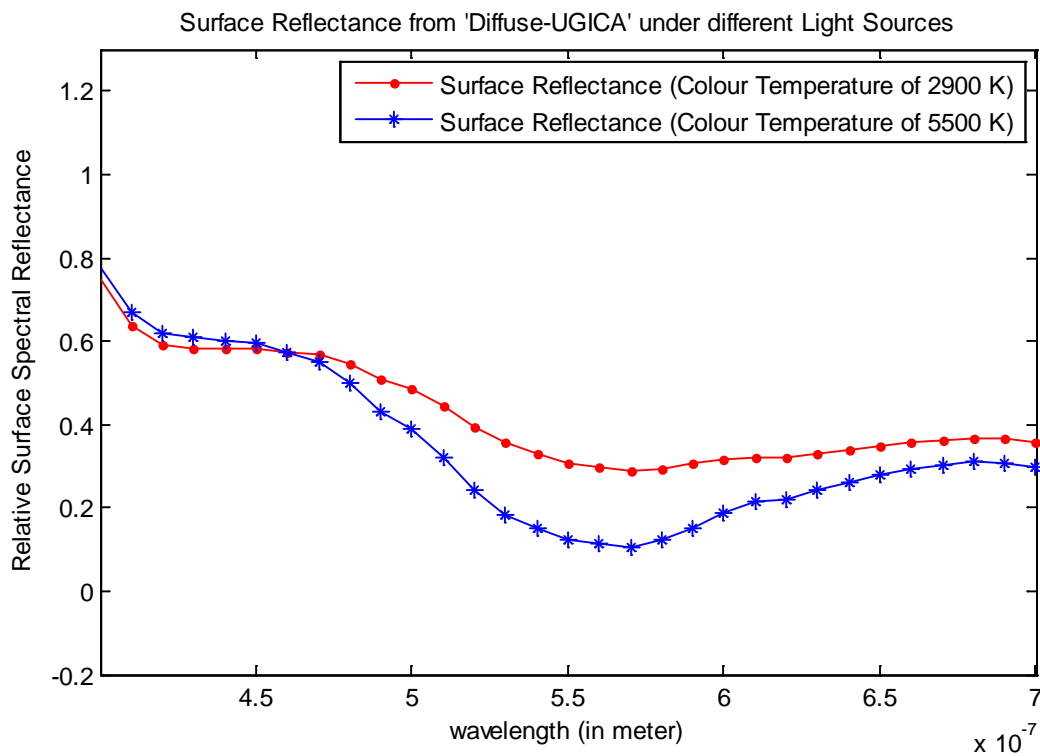


Figure D.6 The surface reflectance for a pixel located at image coordinates (330, 130), estimated from the 'Diffuse-UGICA' image component for a ceramic violet cup, and illuminated by two artificial light sources with different colour temperatures of 2900 and 5500 K.

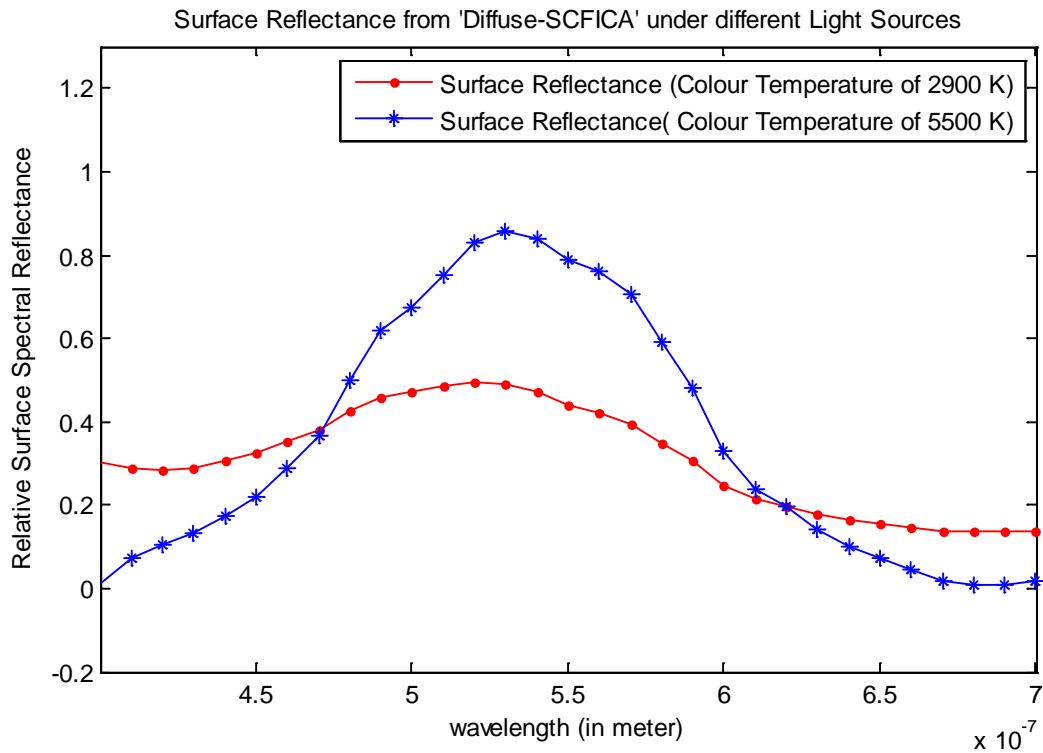


Figure D.7 The surface reflectance, for a pixel located at image coordinates (400, 190), estimated from the 'Diffuse-SCFICA' image component for a plastic green ring illuminated by two artificial light sources with different colour temperatures of 2900 and 5500 K.

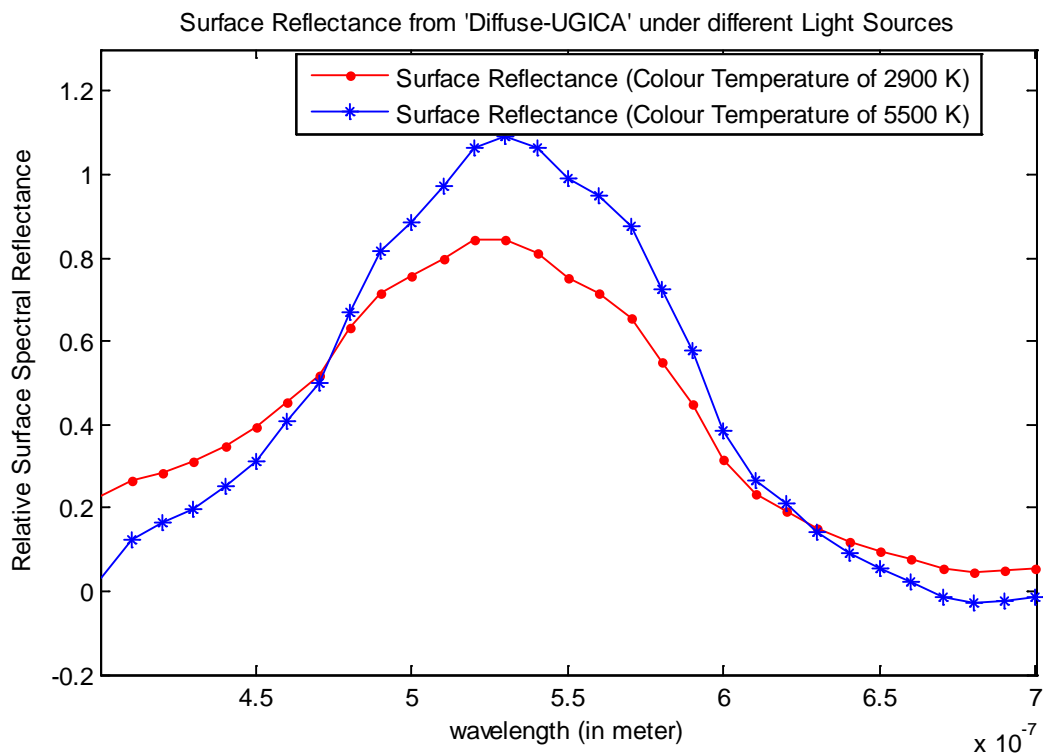


Figure D.8 The surface reflectance for a pixel located at image coordinates (400, 190), estimated from the 'Diffuse-UGICA' image component for a plastic green ring, and illuminated by two artificial light sources with different colour temperatures of 2900 and 5500 K.

D.3 Experiment 3 (Section 6.2.2.3)

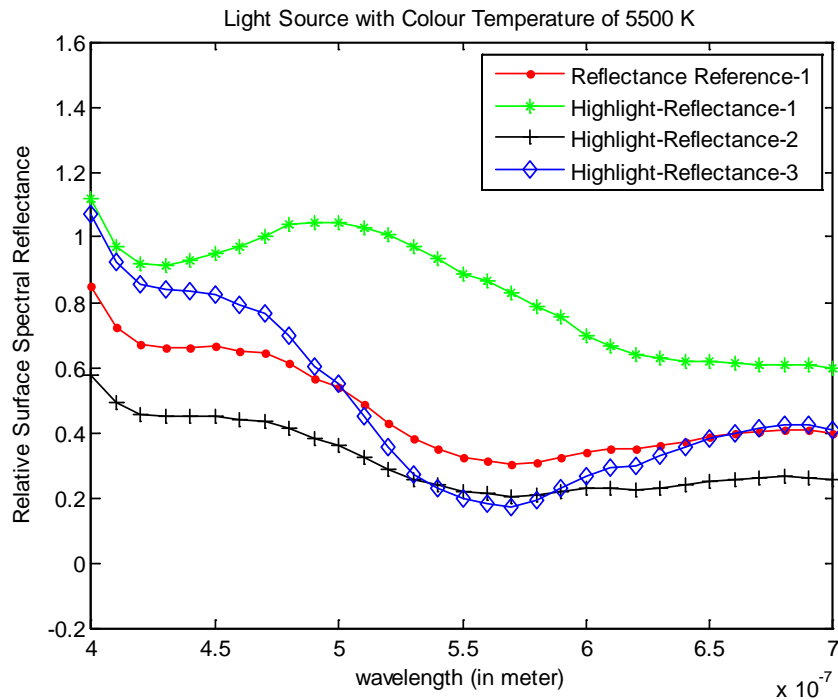


Figure D.9 The surface reflectance (Highlight-Reflectance-1, Highlight-Reflectance-2, Highlight-Reflectance-3) estimated from pixels in image regions which have a strong specular component, shown in comparison to the surface reflectance (reflectance reference-1) estimated from pixels in image regions which have a weak specular component. The test and reference pixels are from images of the ceramic violet cup illuminated by a light source with a colour temperature of 5500 K. The reference pixels are from the polarised image, without extracting the diffuse image component.

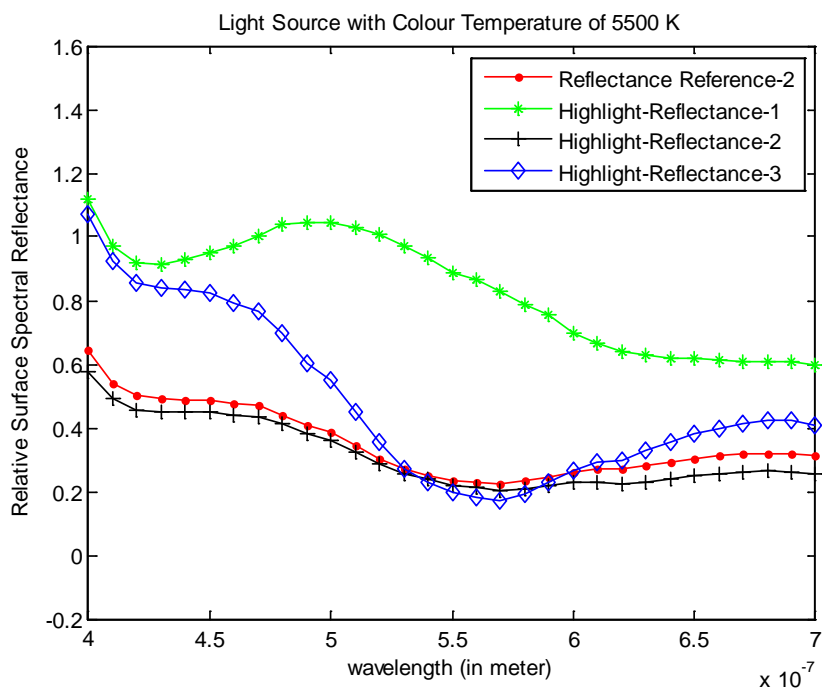


Figure D.10 The surface reflectance (Highlight-Reflectance-1, Highlight-Reflectance-2, Highlight-Reflectance-3) estimated from pixels in image regions which have a strong specular component, shown in comparison to the surface reflectance (reflectance reference-2) estimated from pixels in image regions which have a weak specular component. The test and reference pixels are from images of the ceramic violet cup illuminated by a light source with a colour temperature of 5500 K. The reference pixels are from the diffuse image component-SCFICA.

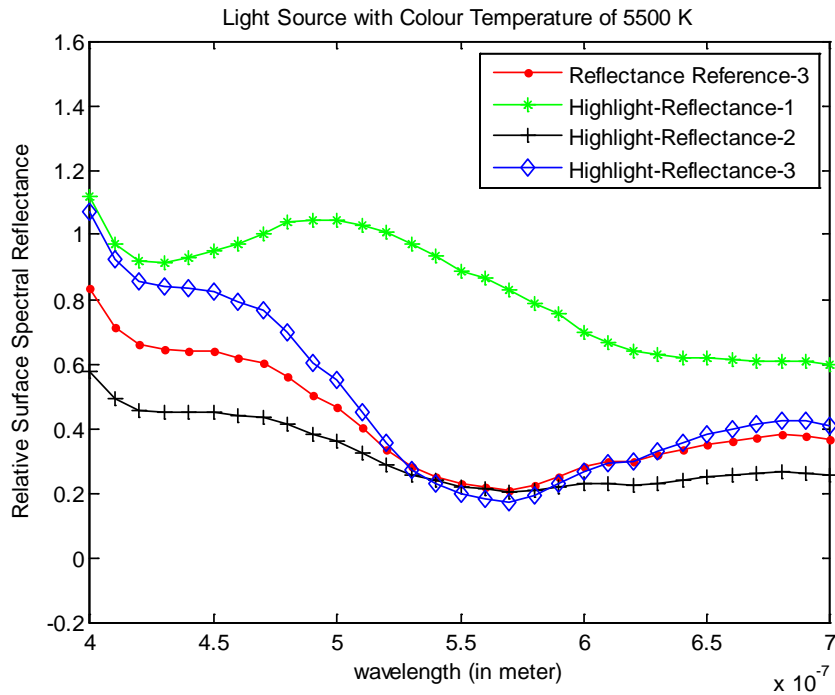


Figure D.11 The surface reflectance (Highlight-Reflectance-1, Highlight-Reflectance-2, Highlight-Reflectance-3) estimated from pixels in image regions which have a strong specular component, shown in comparison to the surface reflectance (reflectance reference-3) estimated from pixels in image regions which have a weak specular component. The test and reference pixels are from images of the ceramic violet cup illuminated by a light source with a colour temperature of 5500 K. The reference pixels are from the diffuse image component-UGICA.

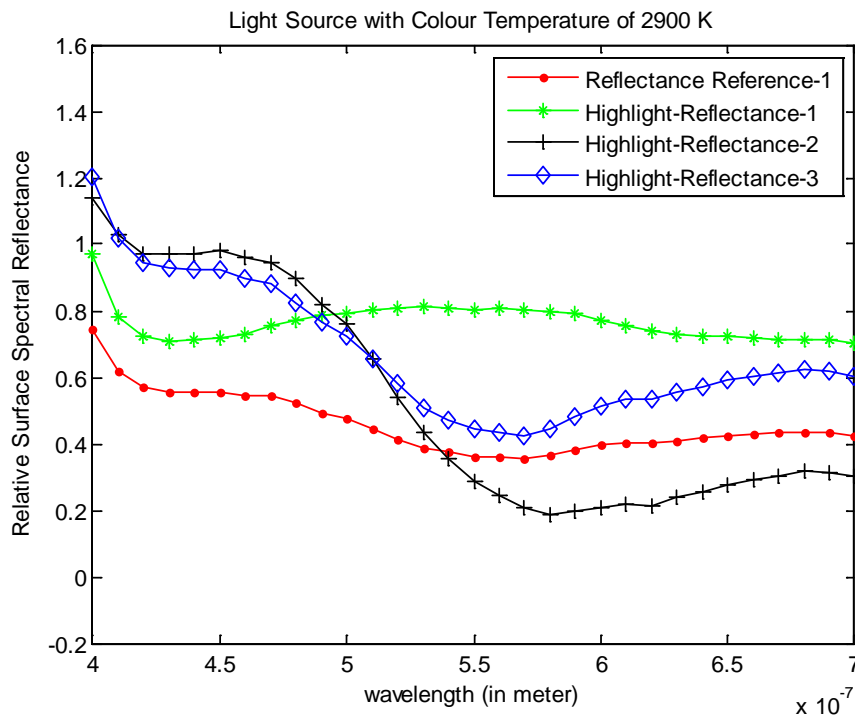


Figure D.12 The surface reflectance (Highlight-Reflectance-1, Highlight-Reflectance-2, Highlight-Reflectance-3) estimated from pixels in image regions which have a strong specular component, shown in comparison to the surface reflectance (reflectance reference-1) estimated from pixels in image regions which have a weak specular component. The test and reference pixels are from images of the ceramic violet cup illuminated by a light source with a colour temperature of 2900 K. The reference pixels are from the polarised image, without extracting the diffuse image component.

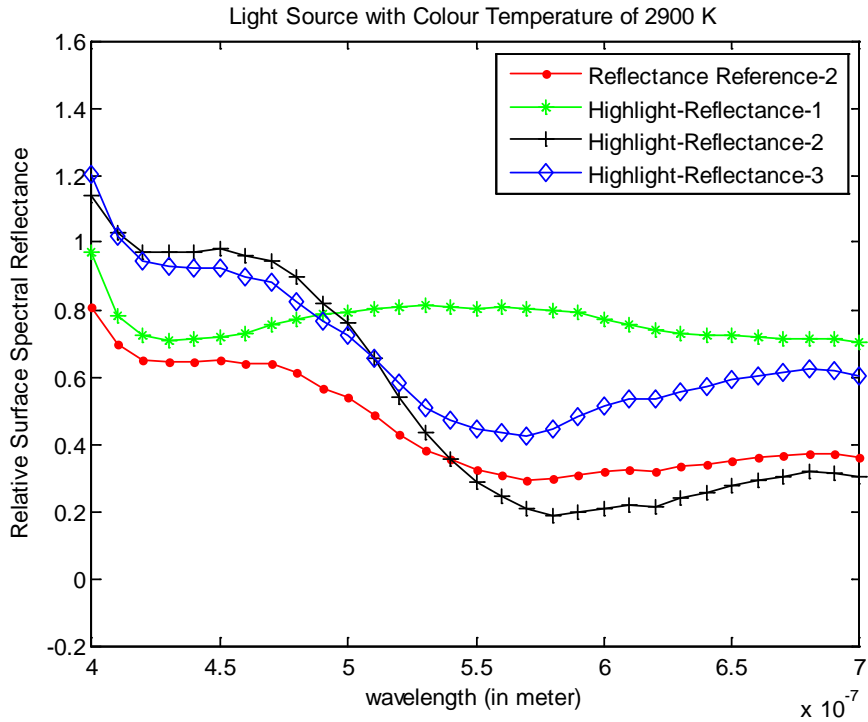


Figure D.13 The surface reflectance (Highlight-Reflectance-1, Highlight-Reflectance-2, Highlight-Reflectance-3) estimated from pixels in image regions which have a strong specular component, shown in comparison to the surface reflectance (reflectance reference-2) estimated from pixels in image regions which have a weak specular component. The test and reference pixels are from images of the ceramic violet cup illuminated by a light source with a colour temperature of 2900 K. The reference pixels are from the diffuse image component-SCFICA.

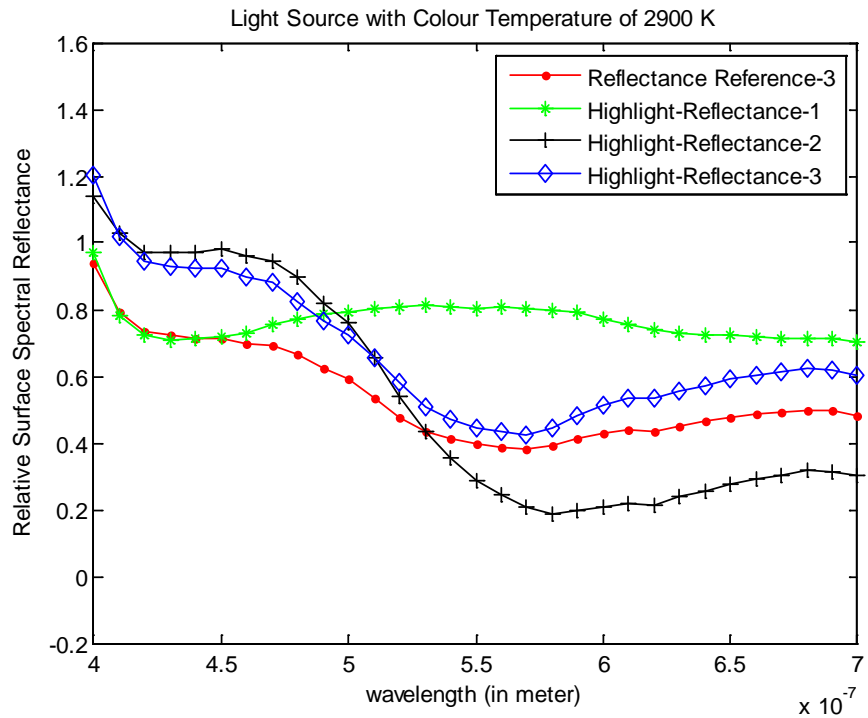


Figure D.14 The surface reflectance (Highlight-Reflectance-1, Highlight-Reflectance-2, Highlight-Reflectance-3) estimated from pixels in image regions which have a strong specular component, shown in comparison to the surface reflectance (reflectance reference-3) estimated from pixels in image regions which have a weak specular component. The test and reference pixels are from images of the ceramic violet cup illuminated by a light source with a colour temperature of 2900 K. The reference pixels are from the diffuse image component-UGICA.

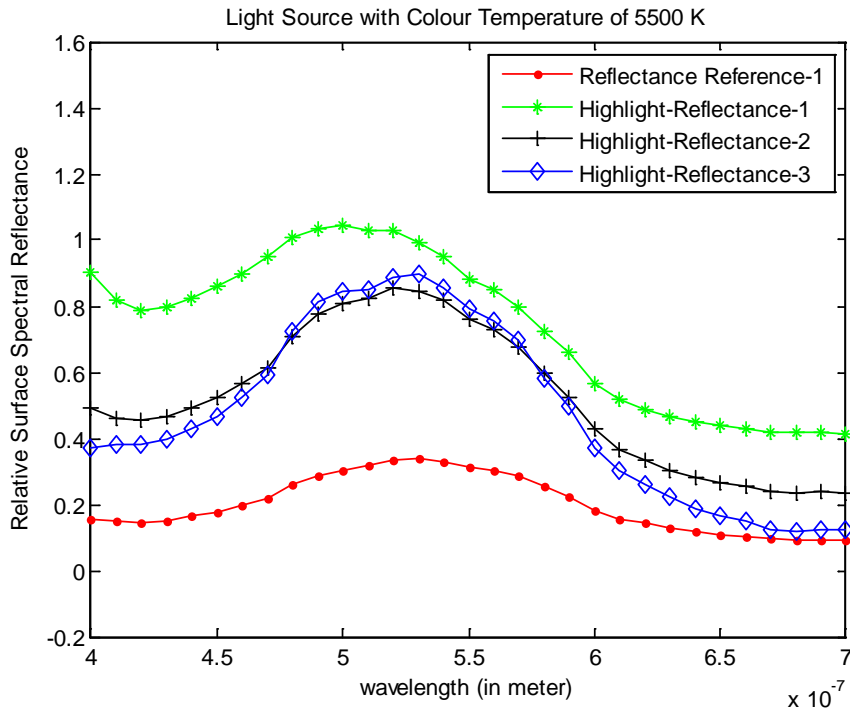


Figure D.15 The surface reflectance (Highlight-Reflectance-1, Highlight-Reflectance-2, Highlight-Reflectance-3) estimated from pixels in image regions which have a strong specular component, shown in comparison to the surface reflectance (reflectance reference-1) estimated from pixels in image regions which have a weak specular component. The test and reference pixels are from images of the plastic green ring illuminated by a light source with a colour temperature of 5500 K. The reference pixels are from the polarised image, without extracting the diffuse image component.

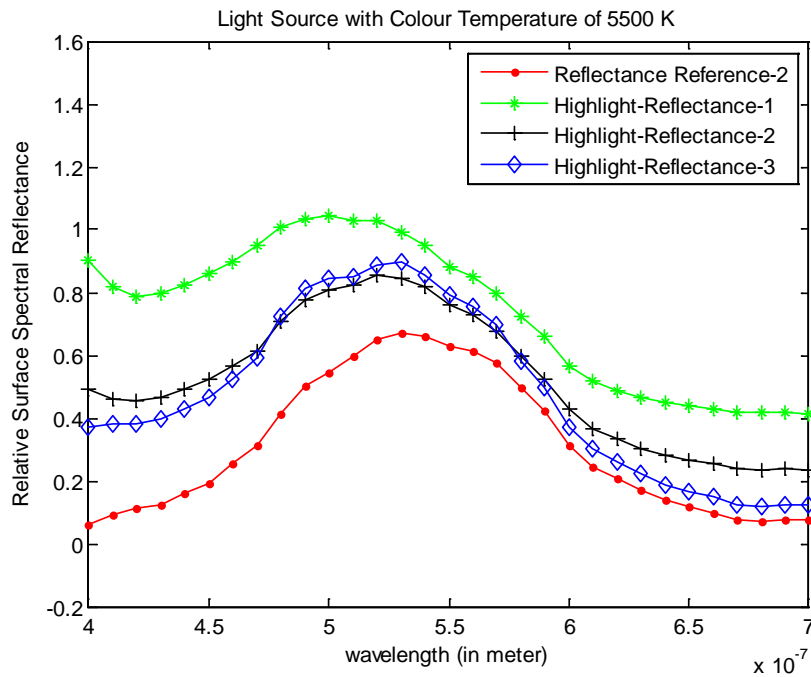


Figure D.16 The surface reflectance (Highlight-Reflectance-1, Highlight-Reflectance-2, Highlight-Reflectance-3) estimated from pixels in image regions which have a strong specular component, shown in comparison to the surface reflectance (reflectance reference-2) estimated from pixels in image regions which have a weak specular component. The test and reference pixels are from images of the plastic green ring illuminated by a light source with a colour temperature of 5500 K. The reference pixels are from the diffuse image component-SCFICA.

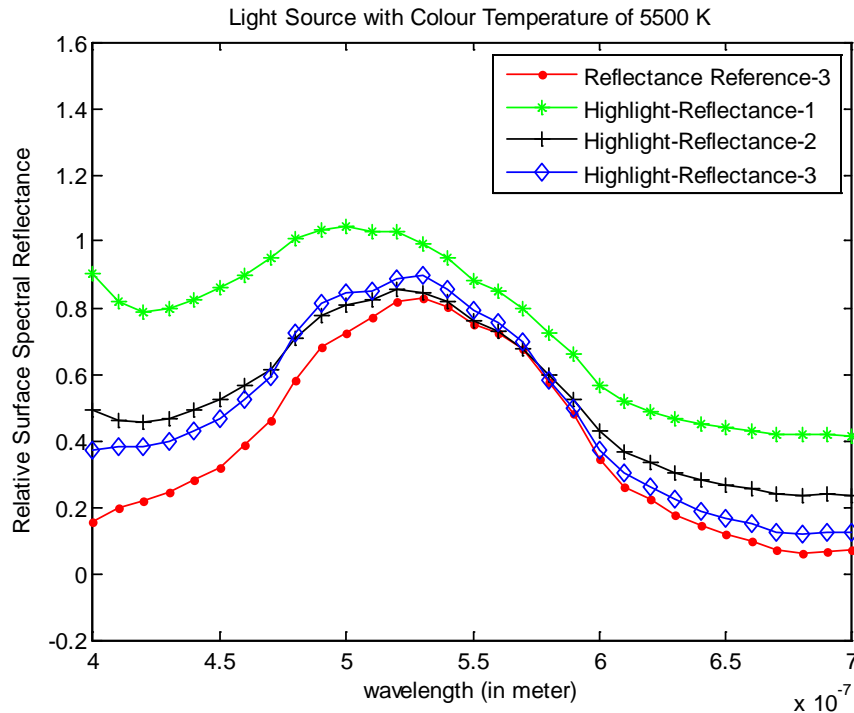


Figure D.17 The surface reflectance (Highlight-Reflectance-1, Highlight-Reflectance-2, Highlight-Reflectance-3) estimated from pixels in image regions which have a strong specular component, shown in comparison to the surface reflectance (reflectance reference-3) estimated from pixels in image regions which have a weak specular component. The test and reference pixels are from images of the plastic green ring illuminated by a light source with a colour temperature of 5500 K. The reference pixels are from the diffuse image component-UGICA.

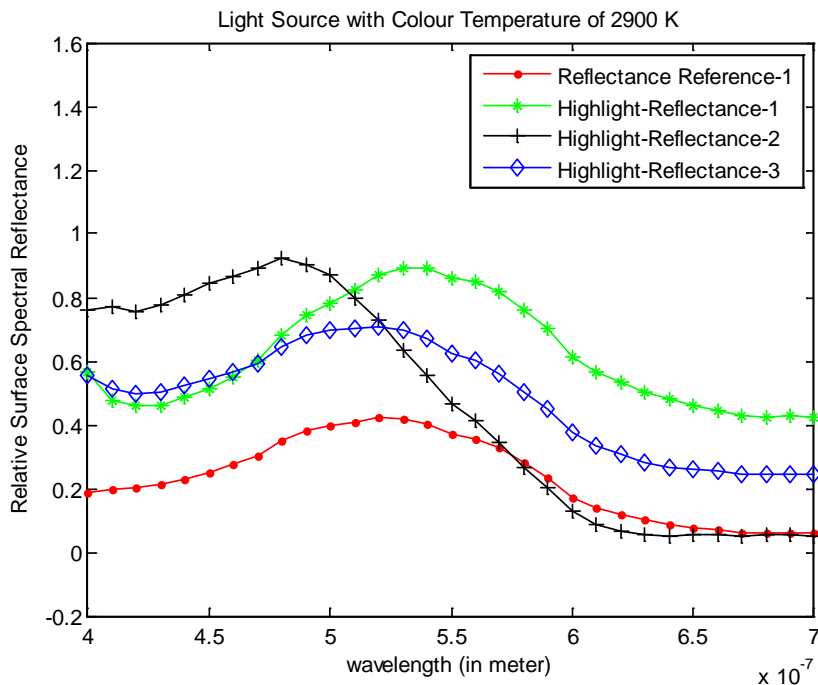


Figure D.18 The surface reflectance (Highlight-Reflectance-1, Highlight-Reflectance-2, Highlight-Reflectance-3) estimated from pixels in image regions which have a strong specular component, shown in comparison to the surface reflectance (reflectance reference-1) estimated from pixels in image regions which have a weak specular component. The test and reference pixels are from images of the plastic green ring illuminated by a light source with a colour temperature of 2900 K. The reference pixels are from the polarised image, without extracting the diffuse image component.

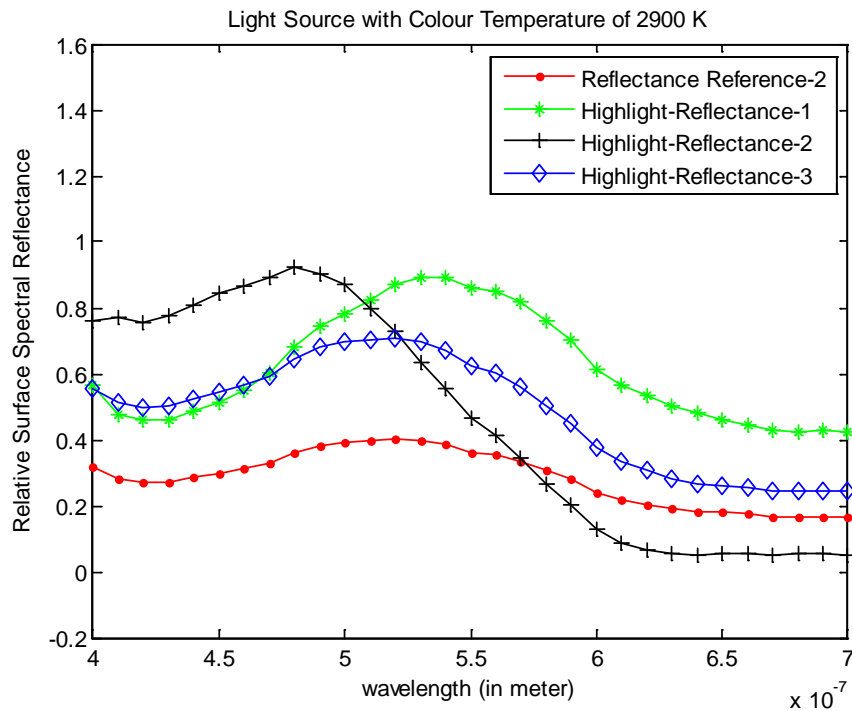


Figure D.19 The surface reflectance (Highlight-Reflectance-1, Highlight-Reflectance-2, Highlight-Reflectance-3) estimated from pixels in image regions which have a strong specular component, shown in comparison to the surface reflectance (reflectance reference-2) estimated from pixels in image regions which have a weak specular component. The test and reference pixels are from images of the plastic green ring illuminated by a light source with colour temperature of 2900 K. The reference pixels are from the diffuse image component-SCFICA.

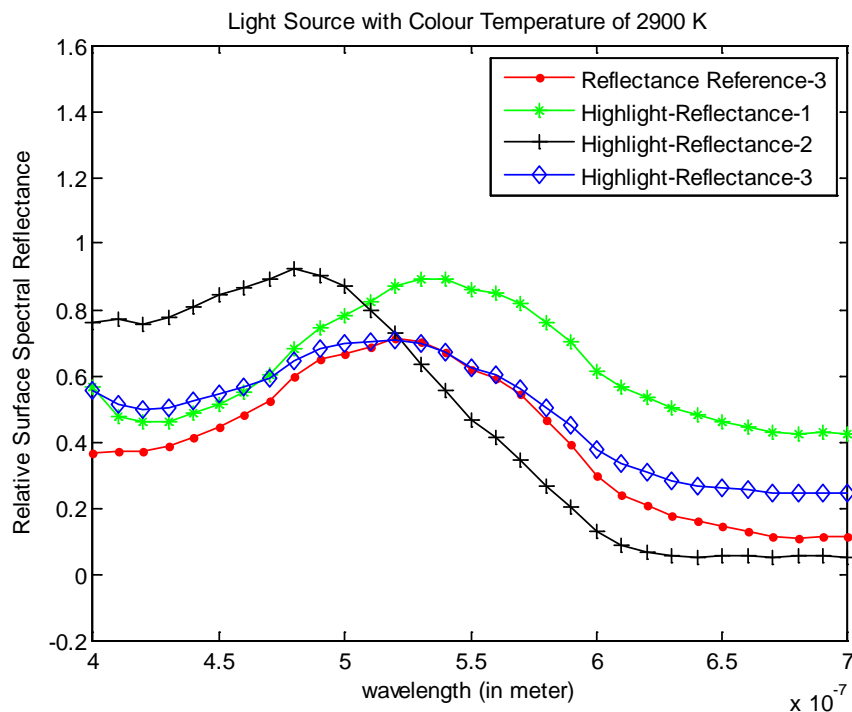


Figure D.20 The surface reflectance (Highlight-Reflectance-1, Highlight-Reflectance-2, Highlight-Reflectance-3) estimated from pixels in image regions which have a strong specular component, shown in comparison to the surface reflectance (reflectance reference-3) estimated from pixels in image regions which have a weak specular component. The test and reference pixels are from images of the plastic green ring illuminated by a light source with a colour temperature of 2900 K. The reference pixels are from the diffuse image component-UGICA.

D.4 Experiment 4 (Section 6.2.2.4)

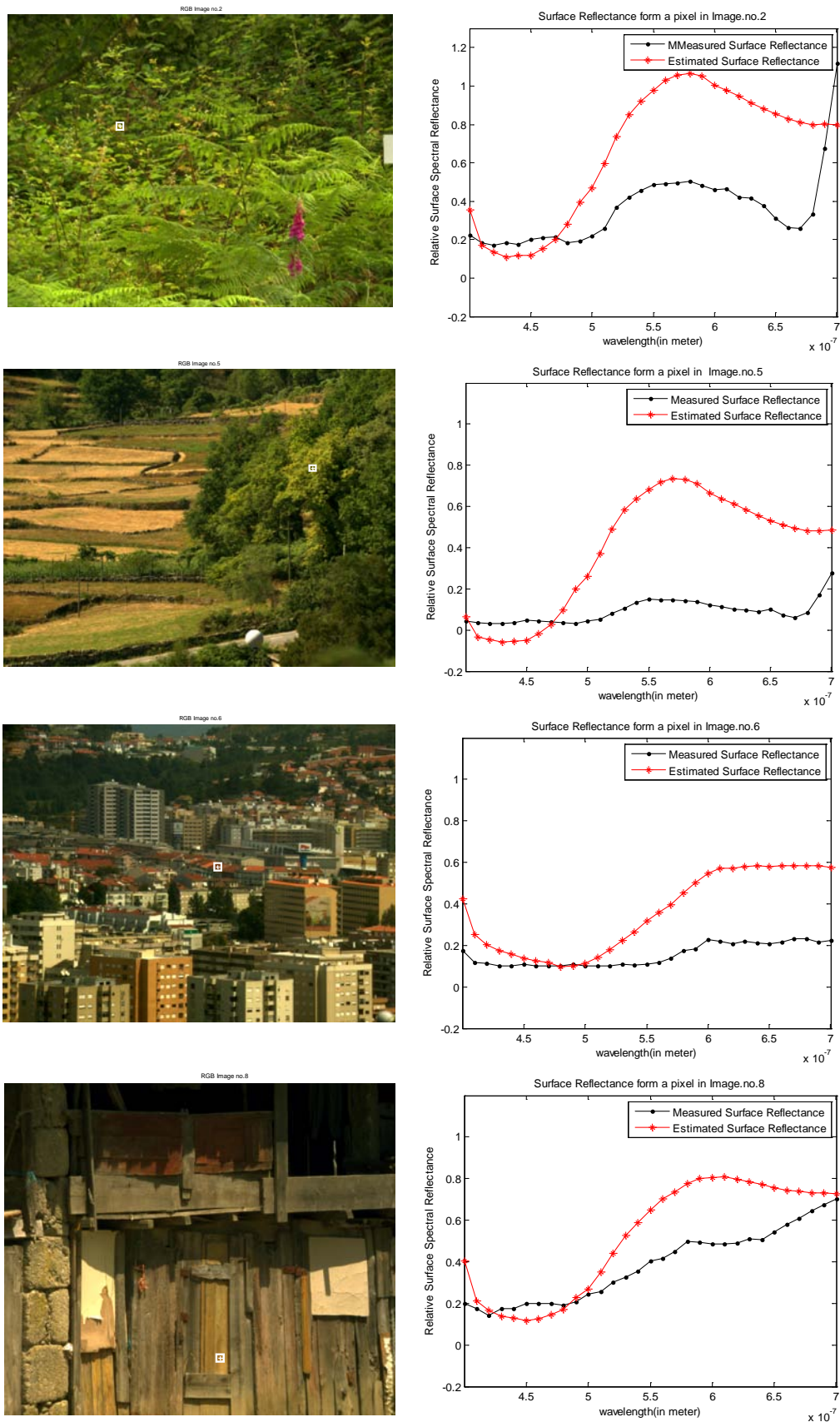


Figure D.21 Illustrative examples for some images of the Foster et al's data set [181], with a white square marker to display the pixel positions at which surface reflectance was estimated. The estimated surface reflectance of that pixel is shown in comparison with the measured surface reflectance.

Appendix **E**

Statistical Significance Tests

In this appendix, the investigation of the statistical significance of measured differences between the experimental results is presented. This investigation was performed using the SPSS statistical software, version 18 [186]. The independent two-sample t-test [186] is used to determine the significance of the results. The independent two-sample t-test is performed to measure the statistical significance of the difference between the means of two independent groups of results. Due to its applicability for a low number of samples ($N < 30$; N - the number of the number of observation samples), the t-test has been considered for assessing the statistical significance of the differences between the experimental results presented in the thesis [187]. The t-test is performed with confidence level of 95%, for all analyses.

The results of the t-test are shown in Tables E.1 to E.7. Each table consists of two parts which are (a) group statistics and (b) the independent samples test. The *group statistics* provide information about the number of samples (N), the mean (M), the standard deviation (Std. Deviation), and the standard error mean (Std. Error Mean) for each of the two independent groups of results. The *independent samples test* shows the results of two different t-test methods which are the 'equal variance t-test' and the 'unequal variance t-test'. These methods are based on the assumption that the variances of the two independent groups of results are equal or unequal, respectively. The equality of the variance is measured by Levene's Test [186]. The result of Levene's Test is presented by an F-value with corresponding significance level (sig). The equal variance assumption is valid when the 'sig' value in the Levene's Test is greater than 0.05 (i.e. for a 95% confidence level t-test) otherwise the unequal variance assumption is applicable. For equal and unequal variance t-test methods there are different formulas used for calculating the t-value (t) and the degree of freedom (df) (provided in Table E.8). The selection between these t-test methods is performed based on the validity of the variance inequality of the two groups of samples. For significant difference in both methods of the t-test, the value of the probability of error (sig. (2-tailed)) has to be less than or equal 0.05 for a 95% confidence level.

Experiment 1 (Section 5.3.2.1):

Table E.1 The improvements in the illumination estimation accuracy compared to the manufacturer’s specification, in terms of GFC, when the empirical threshold is used instead of the automatic threshold for a light source with a colour temperature of 5500 K (Results given in Section 5.3.2.1, Table 5-1).

(a) Group Statistics

	N	Mean	Std. Deviation	Std. Error Mean
Groups empirical_55	16	.98438	.007274	.001819
automatic_55	16	.94513	.064426	.016106

(b) Independent Samples Test

	Levene's Test for Equality of Variances		t-test for Equality of Means						
	F	Sig.	t	df	Sig. (2-tailed)	Mean Difference	Std. Error Difference	95% Confidence Interval of the Difference	
								Lower	Upper
Equal variances assumed	11.052	.002	2.422	30	.022	.039250	.016209	.006147	.072353
Equal variances not assumed			2.422	15.382	.028	.039250	.016209	.004777	.073723

Table E.2 The difference in illumination estimation accuracy compared to the manufacturer’s specification, in terms of GFC, using two sets of specular components (i.e extracted using two different blind separation techniques (SCFICA and UGICA)) for a light source with a colour temperature of 5500 K (Results given in Section 5.3.2.1, Table 5-1).

(a) Group Statistics

	N	Mean	Std. Deviation	Std. Error Mean
Groups scfica_55	16	.97013	.026470	.006617
ugica_55	16	.95938	.065291	.016323

(b) Independent Samples Test

	Levene's Test for Equality of Variances		t-test for Equality of Means						
	F	Sig.	t	df	Sig. (2-tailed)	Mean Difference	Std. Error Difference	95% Confidence Interval of the Difference	
								Lower	Upper
Equal variances assumed	3.477	.072	.610	30	.546	.010750	.017613	-.025221	.046721
Equal variances not assumed			.610	19.801	.549	.010750	.017613	-.026014	.047514

Experiment 2 (Section 5.3.2.2)

Table E.3 The improvements in the illumination estimation accuracy compared to the manufacturer’s specification, in terms of GFC, when the empirical threshold is used instead of the automatic threshold, for a light source with a colour temperature of 2900 K (*Results given in Section 5.3.2.2, Table 5-3*).

(a) Group Statistics

	N	Mean	Std. Deviation	Std. Error Mean
Groups empirical_29	16	.92150	.013023	.003256
automatic_29	16	.89375	.031253	.007813

(b) Independent Samples Test

	Levene's Test for Equality of Variances		t-test for Equality of Means						
	F	Sig.	t	df	Sig. (2-tailed)	Mean Difference	Std. Error Difference	99% Confidence Interval of the Difference	
								Lower	Upper
Equal variances assumed	27.147	.000	3.278	30	.003	.027750	.008464	.004473	.051027
Equal variances not assumed			3.278	20.057	.004	.027750	.008464	.003673	.051827

Table E.4 The difference in illumination estimation accuracy compared to the manufacturer’s specification, in terms of GFC, using two sets of specular components (i.e. extracted using two different blind separation techniques (SCFICA and UGICA)) for a light source with a colour temperature of 2900 K (*Results given in Section 5.3.2.2, Table 5-3*).

(a) Group Statistics

	N	Mean	Std. Deviation	Std. Error Mean
Groups ugica_29	16	.90844	.030232	.007558
scfica_29	16	.90681	.025330	.006333

(b) Independent Samples Test

	Levene's Test for Equality of Variances		t-test for Equality of Means						
	F	Sig.	t	df	Sig. (2-tailed)	Mean Difference	Std. Error Difference	95% Confidence Interval of the Difference	
								Lower	Upper
Equal variances assumed	1.049	.314	.165	30	.870	.001625	.009860	-.018513	.021763
Equal variances not assumed			.165	29.108	.870	.001625	.009860	-.018538	.021788

Experiment 3 (Section 5.3.2.3):

Table E.5 The improvement in the illumination estimation accuracy compared to the manufacturer’s specification, in terms of GFC, when the separated specular component (extracted using two different blind separation techniques (SCFICA and UGICA)) is used the instead of mixed image components, for a light source with a colour temperature of 5500 K (Results given in Section 5.3.2.3, Table 5-5).

(a) Group Statistics

	N	Mean	Std. Deviation	Std. Error Mean
Groups Specular	16	.98438	.007274	.001819
Mixed	8	.95363	.015454	.005464

(b) Independent Samples Test

	Levene's Test for Equality of Variances		t-test for Equality of Means						
	F	Sig.	t	df	Sig. (2-tailed)	Mean Difference	Std. Error Difference	95% Confidence Interval of the Difference	
								Lower	Upper
Equal variances assumed	7.613	.011	6.708	22	.0001	.030750	.004584	.021243	.040257
Equal variances not assumed			5.340	8.588	.001	.030750	.005759	.017627	.043873

Experiment 2 (Section 6.2.2.2)

Table E.6 Comparison between the surface reflectance estimates obtained from the ‘Diffuse-SCFICA’ and ‘Diffuse-UGICA’ image components, for different objects illuminated by two artificial light sources with different colour temperatures of 2900 and 5500 K (Results given in Section 6.2.2.2, Table 6-6 and Table 6-7).

(a) Group Statistics

	N	Mean	Std. Deviation	Std. Error Mean
Groups Surface_ugica_29_55	300	.988662	.0195074	.0011263
Surface_scfica_29_55	300	.961145	.0399745	.0023079

(b) Independent Samples Test

	Levene's Test for Equality of Variances		t-test for Equality of Means						
	F	Sig.	t	df	Sig. (2-tailed)	Mean Difference	Std. Error Difference	95% Confidence Interval of the Difference	
								Lower	Upper
Equal variances assumed	112.803	.000	10.715	598	.0001	.0275170	.0025681	.0224735	.0325605
Equal variances not assumed			10.715	433.766	.0001	.0275170	.0025681	.0224696	.0325644

Experiment 3 (Section 6.2.2.3)

Table E.7 A comparison between the surface spectral reflectance estimated using the diffuse image component and mixed image components (Results given in Section 6.2.2.3, Table 6-10).

(a) Group Statistics

	N	Mean	Std. Deviation	Std. Error Mean
Groups diffuse	36	.976178	.0272738	.0045456
mixed	18	.950411	.0263592	.0062129

(b) Independent Samples Test

	Levene's Test for Equality of Variances		t-test for Equality of Means						
	F	Sig.	t	df	Sig. (2-tailed)	Mean Difference	Std. Error Difference	95% Confidence Interval of the Difference	
								Lower	Upper
Equal variances assumed	.001	.978	3.309	52	.002	.0257667	.0077879	.0101390	.0413943
Equal variances not assumed			3.347	35.176	.002	.0257667	.0076983	.0101411	.0413922

Table E.8 The t-value and the degree of freedom formulas for the equal and unequal variance t-test methods.

	Equal variance t-test method	Unequal variance t-test method
t-value	$t = \frac{M_1 - M_2}{\sqrt{\frac{V_P}{N_1} + \frac{V_P}{N_2}}}$ <p>where</p> $V_P = \frac{(N_1 - 1)V_1 + (N_2 - 1)V_2}{N_1 + N_2 - 2}$	$t = \frac{M_1 - M_2}{\sqrt{\frac{V_1}{N_1} + \frac{V_2}{N_2}}}$
Degree of freedom(df)	$df = N_1 + N_2 - 2$	$df = \frac{\left(\frac{V_1}{N_1} + \frac{V_2}{N_2}\right)^2}{\frac{\left(\frac{V_1}{N_1}\right)^2}{N_1 - 1} + \frac{\left(\frac{V_2}{N_2}\right)^2}{N_2 - 1}}$
<p>where</p> <p>M_1, M_2= the means of groups 1 and 2 respectively</p> <p>V_1, V_2 = the variances of groups 1 and 2 respectively</p> <p>N_1, N_2= the number of observation samples in group 1 and 2, respectively.</p>		

Appendix **F**

Evaluation Formulas

	Formula
Goodness-of-Fit Coefficient	$\text{GFC} = \frac{\sum_{\lambda} S_p(\lambda) \hat{S}_p(\lambda)}{\left(\sum_{\lambda} (\hat{S}_p(\lambda))^2 \right)^{\frac{1}{2}} \left(\sum_{\lambda} (S_p(\lambda))^2 \right)^{\frac{1}{2}}}$ <p>Where S_p, \hat{S}_p are the measured spectral signal and the estimated spectral signal respectively; λ is wavelength and ranges between $\lambda_L=400$ nm and $\lambda_H=700$ nm with step of 10 nm [184].</p>
Root Mean Square Error	$\text{RMSE} = \left(\frac{\sum_{\lambda} (S_p(\lambda) - \hat{S}_p(\lambda))^2}{N_s} \right)^{\frac{1}{2}}$ <p>Where $N_s = \frac{\lambda_H - \lambda_L}{\text{step}} + 1$</p>
Mean Error	$\text{Mean} = \frac{\sum_{\lambda} S_p(\lambda) - \hat{S}_p(\lambda)}{N_s}$
Median Error	Median = middle value of the error values between S_p and \hat{S}_p , which are sorted in order of magnitude[187].
Angular Error	$\text{A.E} = \text{Cos}^{-1} \left(\frac{\boldsymbol{\rho} \hat{\boldsymbol{\rho}}^T}{\ \boldsymbol{\rho}\ \ \hat{\boldsymbol{\rho}}\ } \right)$ <p>Where $\boldsymbol{\rho}$ represent a vector that contains values of the measured signal in the the R , G, B space, $\boldsymbol{\rho} = [\rho_R \ \rho_G \ \rho_B]$; $\hat{\boldsymbol{\rho}}$ is a vector which contains values of the estimated signal, $\hat{\boldsymbol{\rho}} = [\hat{\rho}_R \ \hat{\rho}_G \ \hat{\rho}_B]$ [3].</p>

Appendix **G**

List of Publications

1] Waleed K.Badawi, Claude Chibelushi, Mohammad Patwary, and Mansour Moniri
“Specular-based Illumination Estimation Using Blind Signal Separation Techniques”
submitted to IET Image Processing Journal.

2] Waleed K.Badawi, Claude Chibelushi, Mohammad Patwary, and Mansour Moniri
“Surface Spectral Reflectance Recovery Using Blind Signal Separation Techniques”
submitted to IET Image Processing Journal.